APPLICATION OF THE LATCHING CONTROL ON A WAVE ENERGY CONVERTER

Milad Shadman

Tese de Doutorado apresentada ao Programa de Pós-graduação em Engenharia Oceânica, COPPE, da Universidade Federal do Rio de Janeiro, como parte dos requisitos necessários à obtenção do título de Doutor em Engenharia Oceânica.

Orientadores: Segen Farid Estefen
Claudio Alexis Rodríguez Castillo

Rio de Janeiro
Agosto de 2017

APPLICATION OF THE LATCHING CONTROL ON A WAVE ENERGY CONVERTER

Milad Shadman

TESE SUBMETIDA AO CORPO DOCENTE DO INSTITUTO ALBERTO LUIZ COIMBRA DE PÓS-GRADUAÇÃO E PESQUISA DE ENGENHARIA (COPPE) DA UNIVERSIDADE FEDERAL DO RIO DE JANEIRO COMO PARTE DOS REQUISITOS NECESSÁRIOS PARA A OBTENÇÃO DO GRAU DE DOUTOR EM CIÊNCIAS EM ENGENHARIA OCEÂNICA.

Examinada por:

_____
Prof. Segen Farid Estefen, Ph.D.

_____
Prof. Claudio Alexis Rodríguez Castillo, D.Sc.

_____
Prof. Edson Hirokazu Watanabe, Ph.D.

_____
Prof. Carlos Antônio Levi da Conceição, Ph.D.

_____
Prof. Marcelo Igor Lourenço de Souza, D.Sc.

_____
Prof. Osvaldo Ronald Saavedra Mendez, D.Sc.

RIO DE JANEIRO, RJ - BRASIL
AGOSTO DE 2017

Shadman, Milad

Application of the latching control on a wave energy converter/ Milad Shadman. – Rio de Janeiro: UFRJ/COPPE, 2017.

XXIV, 235 p.: il.; 29,7 cm.

Orientador: Segen Farid Estefen

Claudio Alexis Rodríguez Castillo

Tese (doutorado) – UFRJ/ COPPE/ Programa de Engenharia Oceânica, 2017.

Referências Bibliográficas: p. 224-235.

1. Energia das ondas. 2. Otimização geométrica. 3. Controle *latching*. 4. Modelo *wave-to-wire*. I. Estefen, Segen Farid *et al*. II. Universidade Federal do Rio de Janeiro, COPPE, Programa de Engenharia Oceânica. III. Título.

I dedicate my thesis to my parents Siavash and Jamileh, because I owe it all to them.

For their endless love, support and encouragement.

Acknowledgements

To my dear sister Armaghan; thank you for your special support during my thesis.

To my fiancée, Gabi, and her parents, Flavio and Helena: Thank you for your unconditional supports.

To my advisor Prof.Segen Farid Estefen, because of his continuous support of my thesis, his patience and motivation. Thank you professor for encouraging my research and for allowing me to grow as a research scientist.

To Prof.Carlos Antônio Levi da Conceição, Prof.Marcelo Igor Lourenço de Souza and my co-advisor Prof.Claudio Alexis Rodríguez Castillo, because of their insightful comments and guidance during the thesis work.

To my dear friends Izabel Nogueira and Prof.Miguel Angel Celis Carbajal because of their supports in providing the sea characteristics data and developing the hydrodynamic simulation code, respectively.

To Wittlin family because of their support and encouragement.

To my dear friend Mohammad Mohseni because of his sincere friendship and his helpful advices, especially in the preparation of my final presentation.

To CAPES for the D.Sc. scholarship and FURNAS through ANEEL (Brazilian Electrical Energy Agency) R&D program for the financial support.

To LTS (laboratório de tecnologia submarina) technicians and staff for their support.

"*There are no incurable diseases, Only the lack of will.*

There are no worthless herbs, Only the lack of knowledge."

Avicenna, Persian polymath (c.980-1037)

Resumo da Tese apresentada à COPPE/UFRJ como parte dos requisitos necessários para a obtenção do grau de Doutor em Ciências (D.Sc.)

CONTROLE LATCHING APLICADO A UM CONVERSOR DE ENERGIA DAS ONDAS

Milad Shadman

Agosto/2017

Orientadores: Segen Farid Estefen
Claudio Alexis Rodríguez Castillo

Programa: Engenharia Oceânica

Inicialmente, propõe-se o desenvolvimento de um processo de otimização para determinar as dimensões ótimas de um conversor de energia da onda (CEO) de tipo *point absorber*. A metodologia é baseada em simulações no domínio da frequência e um método de análise estatística chamado "planejamento de experimentos". Em seguida, utilizando os resultados preliminares, uma abordagem é adotada com base em uma série de análises no domínio do tempo para determinar as dimensões ótimas do CEO, utilizando controle *latching* com intervalo de travamento fixo. O objetivo é determinar as dimensões ótimas de um sistema que absorve máxima potência na faixa de ondas predominantes do mar local. Além disso, é desenvolvido um modelo numérico do tipo *wave-to-wire*, para a análise de desempenho do dispositivo de conversor de energia de onda proposto pela COPPE/*Seahorse* nas condições de mar próximo da costa do Rio de Janeiro. O código é modificado para modelar um sistema de geração da energia elétrica (*power take-off*), que consiste em uma caixa de engrenagem e um gerador rotativo. Adicionalmente, propõe-se um controle *latching* adaptado, baseado nas características do dispositivo, com o objetivo de otimizar a produção de energia elétrica. Os resultados são comparados com o dispositivo sem a aplicação do sistema de controle.

Abstract of Thesis presented to COPPE/UFRJ as a partial fulfillment of the requirements for the degree of Doctor of Science (D.Sc.)

APPLICATION OF THE LATCHING CONTROL ON A WAVE ENERGY CONVERTER

Milad Shadman

August/2017

Advisors: Segen Farid Estefen
Claudio Alexis Rodríguez Castillo

Department: Ocean Engineering

Initially, an optimization process is proposed to determine the optimum dimensions of a control-free point absorber wave energy converter (WEC). The methodology is based on frequency domain simulation of the WEC oscillations and a statistical analysis method called “design of experiment” (DOE). Then, using the preliminary results, an approach based on a series of time domain analyses is adapted to obtain the optimum dimensions of a point absorber controlled by a constant-delay latching. The optimization goal is to maximize both WEC absorbed power and absorption bandwidth when providing a natural period close to the predominant wave periods of the sea site. In addition, a wave-to-wire numerical model is developed to address the performance of the COPPE/Seahorse device in the nearshore Rio de Janeiro. The code is adapted to model a specific PTO system consisting of a gearbox and a rotational generator. An adapted constant-delay latching control aiming at the optimization of the WEC power generation is proposed and the results are compared to the control-free model.

Contents

List of Figures

List of Tables

Chapter 1

1. Introduction

1.1 Overview

Climate change is one of the main concerns of the 21st century. The transformation of the current energy systems may help to avoid its most sever impacts. Renewable energy sources have a huge potential to diminish the emissions of greenhouse gases from the combustion of fossil fuels and consequently to fade climate change. By a proper implementation of the renewable energy sources, they can contribute to social and economic development, to energy access, to a secure and sustainable energy supply, and to a diminution of negative impacts of energy provision on the environment and human health [1].

Ocean waves, with a global theoretical potential of about $32000\ TWh/year$, are a huge resource of energy [2]. A global technical potential of $500\ GW$ is estimated for the wave energy, considering an efficiency of 40% for the wave energy converters which are installed near coastlines with a wave energy transfer of more than $30\ kW/m$ [3]. Brazil with about $7500\ km$ coastline has one of the longest national coastlines in the world. The main wave energy potential of the Brazil is located in the Northeastern, Southeastern and Southern regions of the country with an estimated theoretical potential of about $87\ GW$ [4].

The device that capture the ocean wave energy and convert it in a desirable form of energy is called "wave energy converter" (WEC). Until now, more than a hundred patents have been presented to harness the ocean wave energy, however, they can be divide into three categories, based on their operation principles; *a) oscillating water columns (OWC), b) oscillating bodies* and *c) overtopping devices* [5]. They can also be categorized as the *onshore*, *nearshore* and *offshore* devices based on the distance of their installation local from coast. The oscillating bodies can be surface or submerged heaving oscillators, submerged surge oscillator or a surface oscillator with rotational joints that capture the wave motion in any direction. A heaving point absorber (PA) is a surface oscillating body type WEC. It consists of a semi-submerged floater at the water surface connected to a power take-off (PTO) system. The PTO system captures the vertical movement of the oscillator result from the incoming wave forces and converts it into desirable form of energy. The main challenge of the WEC technology is its cost. For a PA, the cost increases with its size. Therefore, the optimal dimensions of a WEC can help to have an economic system. Furthermore, several control methods have been developed to improve the performance of the PAs. One of these control systems is latching control. It increases the

efficiency of a heaving PA by locking (latching) the oscillator when its heave velocity vanishes and releasing (unlatching) it at a certain time allowing a resonance condition between oscillator and incoming waves. Since latching control makes changes in the system characteristics, the optimum dimensions of a system controlled by latching may be different to a control-free system. The subject of this thesis is firstly, development of an optimization process to determine the optimum dimensions of a PA controlled by latching and secondly, improvement of the power generation of a wave energy converter proposed by COPPE/UFRJ through the application of a latching control adapted to the wave converter characteristics.

1.2Motivations and objectives

The WEC technology is still pre-commercial and the main barrier that hinders its commercialization is its high cost. The cost of the WEC increases with its size. Therefore, the geometrical optimization of a WEC may has a significant role in its design process. In the other hand, the efforts to design more economic systems have begun since mid-1970s. When control methods presented to maximize the energy conversion. In some earlier researches, the geometry optimization of the WECs have been usually performed for the systems without taking into account control strategy in any way, or the control strategy was considered, but the focus lied on merely power absorption maximization without considering the absorption bandwidth of the system and other practical requirements such as the high level of the PTO damping, floater mass, forces and etc. Optimizing WEC size aiming maximization of the power generation within the dominant energetic wave frequency range of the real sea, specifically in the regions with predominant wave periods beyond 7 second, may lead to a quite non-practical solution due to the large body dimensions and prohibitively high costs. Latching control is a suboptimal control method that tunes WEC oscillation period to the sea predominant wave periods by locking the system during the certain time intervals along its oscillation. Therefore, the natural period of WEC must be adjusted to a period well under the predominant sea waves resulting a smaller floater size. Applying latching control results in changes in the system characteristics and, consequently, it affect the optimum dimensions of the system. In this work, an optimization process was proposed considering the nearshore Rio de Janeiro as the location to install the WEC. Firstly and as a preliminary approach, the optimum dimensions of a control-free point absorber were

determined by running a few simulations in the frequency domain and using the design of experiment (DOE) method. Secondly, based on the preliminary results, a practical approach was adapted to find the optimum dimensions of a point absorber controlled by latching, based on a series of time domain analyses. The optimization process goal is to determine the optimum dimensions of a point absorber controlled by latching that absorbs the maximum power in the largest range of the predominant wave frequencies. It leads that the system performs as close as possible to its design limits during a significant percentage of its lifetime. As a case study, the performance of a wave energy converter proposed by COPPE/UFRJ, called "COPPE nearshore WEC", is analyzed. The specific characteristics of the PTO system degrade the positive effect of the application of the latching control. Therefore, a latching control adapted to the specific characteristics of the device, is proposed to improve the power generation.

1.3Thesis chapters

- **Chapter 2:** This chapter presents an overall review of the wave energy conversion technology. It is divided into four main sections regarding the wave energy potential, technology concepts, control strategies and geometrical optimization. Different aspects such as the global and Brazilian wave energy potential, energy conversion technologies, global status and device deployment are addressed. The control strategies which have been applied to improve the performance of the wave energy converters since 1974, are presented. Additionally, the last section of this chapter presents a review of the deployed geometry optimization method of the WEC.
- **Chapter 3:** The motion of a fluid can be described by the equation of continuity together with the Navier-Stokes equations. These equations are based on the conservation of mass and conservation of momentums respectively. The principle of Computational Fluid Dynamics (CFD) codes is based on the Navier-Stokes equations. Generally, Navier-Stokes equations are difficult and time-consuming to solve because of the coupled system of non-linear partial differential equations. Hence, some assumptions are often introduced to facilitate the analyses. In this thesis, the frequency domain analyses have been performed by AQWA ANSYS based on linear potential theory. The considered assumptions are; irrotational flow, the fluid is non-viscous, incompressible and without surface tension effect.

In this chapter, based on these assumptions, some principles of hydrodynamics theory for wave conversion are described. However, there several references that provide further elaboration and more details such as [6,7].

- **Chapter 4:** A methodology for the geometrical optimization of control-free wave energy converters (WEC) based on statistical analysis methods and the hydrodynamics of the system in the frequency domain is presented in this chapter. The optimization process has been applied to a one-body point absorber for a nearshore region of the Rio de Janeiro coast. The sea characteristics have been described using a five-year wave hindcast and are based on a third generation wind wave model WAVEWATCH III. The optimization procedure is performed based on the resultant wave spectrum and joint probability distribution. The aim is to determine the WEC that absorbs the maximum energy into the largest range of frequencies with the closest possible natural period to the predominant wave periods of the sea site. The optimized geometry of the WEC is determined by running a few simulations in the frequency domain and using the design of experiment (DOE) method. The software ANSYS-AQWA is used for the hydrodynamic diffraction analysis, and the DOE method is applied through the Minitab software to determine the optimized geometry. The two primary advantages of the proposed optimization method are the reduced computational time and the possibility of performing parametric analyses for the WEC geometry.
- **Chapter 5:** In this chapter, a practical approach, through the series of time domain analyses, is adapted to find the optimum dimensions of a point absorber controlled by latching based on the preliminary geometrical optimization results of chapter 3. To achieve this, a wave-to-wire model for a heaving point absorber is developed. A pure damper was used as power take-off (PTO) system and the sea site characteristics of the nearshore Rio de Janeiro, Brazil were considered for the simulations. The PTO damping effect on power generation and the maximum absorbed power and its variation over the range of predominant wave periods were addressed in order to obtain the buoy with the best performance. The annual energy production of the selected buoy is also presented based on two approaches for the latching control.
- **Chapter 6:** This chapter addresses the performance of the wave energy converter proposed by the COPPE/UFRJ , called “COPPE nearshore WEC”, that is the

second generation of the Brazilian WEC to be installed near to the Rio de Janeiro coastline. It can be categorized as a nearshore surface point absorber. The PTO system is a combination of a gearbox and a rotational generator system that is used in the wind turbine industry. This chapter addresses the performance of the WEC with and without the application of a constant-delay latching (CDL) control. It is shown that, because of the specific characteristics of the device, the application of the CDL control cannot improve the WEC performance efficiently. Therefore, an alternative CDL control adapted to the specific characteristics of the device is proposed to improve the power generation. The annual energy production (AEP) calculation of the device is performed and the results are compared to the control-free model.

- **Chapter 7:** This chapter presents the main conclusions of the thesis work as well as the ideas to be pursued for future research.

Chapter 2

2. Literature review

2.1 Ocean renewable energy potential

2.1.1 Introduction

The ocean renewable energy sources can be divided into five categories.

- **Waves**, which are derived from the transfer of the kinetic energy of the wind to the upper surface of the ocean
- **Tidal energy,** which can be divided into two subdivision:
  - **Tidal range (tidal rise and fall),** which are derived from the gravitational forces of the earth-moon-sun system;
  - **Tidal currents,** which are the water flow resulting from the filling and emptying of coastal regions as a result of the tidal rise and fall;
- **Ocean currents,** which are derived from wind-driven and thermohaline ocean circulation;
- **Ocean thermal energy conversion (OTEC),** which is derived from the temperature differences between solar energy stored as heat in upper ocean layers and colder seawater, generally below 1000 m
- **Salinity gradients (osmotic power),** which is derived from salinity differences between fresh water and ocean water at river mouths.

To discuss the global potential of the ocean renewable energy resources, it is important to define the type of potential that is considered. Krewitt et al [8] distinguished and defined five types of potentials.

- **Theoretical potential**: is the highest level of potential and only considers the restrictions with respect to natural and climatic parameters.
- **Geographical potential**: there are often geographical restrictions that reduce the theoretical potential. The geographical potential is the theoretical potential limited by the resources at geographical locations that are suitable.
- **Technical potential**: technical limitations such as conversion efficiencies, electrical energy storage challenges etc., may reduce the geographical potential resulting in the technical potential.
- **Economic potential**: the economic potential is the technical potential at cost levels considered competitive with other energy sources.

- **Market potential**: the market potential is the total amount of renewable energy that can be implemented in the market considering the demand for energy, the competing technologies, the costs and subsidies of renewable energy sources and etc.

It should be noted that, up to now, relatively few assessments have been conducted on the technical potential of the various ocean energy sources and such potentials will vary based on the future technology development.

The World Energy Assessment presented a total theoretical potential of over 2 million (TW·h). $yr^{-1}$for global ocean energy resource (excluding wind) [9], however, its technical potential range was estimated to have a range from about 2000 (TW·h)·yr^{-1} to 92 000 (TW·h)·yr^{-1} [8][10]. The technical potential of offshore wind energy is estimated by Krewitt et al [8] to be about 16 000 (TW·h)·yr^{-1} by 2050. Charlier and Justus [11] estimated the theoretical tidal energy potential (including both tidal stream and tidal range) to be 26 000 (TW·h)·yr^{-1}, of which about 8800 (TW·h)·yr^{-1} is in shallow coastal basins; though much lower technical potential is anticipated [8][10]. The theoretical wave energy potential is about 32 000 (TW·h)·yr^{-1} [2], with a technical potential of about 5600 (TW·h)·yr^{-1} [8]. The ocean renewable energy resource potential is dominated by ocean thermal energy conversion (OTEC), with a theoretical potential of about 44 000 (TW·h)·yr^{-1} [12]. Ocean salinity gradients have an estimated technical potential of about 1650 (TW·h)·yr^{-1} [13].

2.1.2 Wave energy potential

Waves most commonly are formed from fetch: a region where the wind is blowing in a prominent direction for some region of space. The wind blowing over the sea transfers some energy to water, due to the air-sea interaction. The resulting waves store this energy as potential energy (in the mass of water displaced from the mean sea level) and kinetic energy (in the motion of water particles). The size and period of the resulting waves depend on the amount of transferred energy, which is a function of the wind speed, the length of time the wind blows (order of days) and the length of ocean over which the wind blows (fetch). Waves are very efficient at transferring energy, and can travel long distances over the ocean surface beyond the storm area and are then classed as swells [14][15]. The most energetic waves on earth are generated between 30º and 60º latitudes by extra-tropical storms [1]. One of the richest nations in terms of potential for wave

energy is the UK, where wave energy devices are estimated to be able to contribute more than 50 TWh/yr [16].Wave energy availability typically varies seasonally and over shorter time periods, with seasonal variation typically being greater in the northern hemisphere. Annual variations in the wave climate are usually estimated by the use of long-term averages in modelling, using global databases with reasonably long histories [1]. Figure 2-1, presented by Huckerby et al in 2011 [17], illustrates the global offshore average annual wave power distribution. It can be seen that the largest power levels occur off the west coasts of the continents, where the most energetic winds and greatest fetch areas occur. The theoretical wave energy potential is about 32 000 $(TW \cdot h) \cdot yr^{-1}$ [2], roughly twice the global electricity supply in 2008 (16800 TWh/yr or 54 EJ/yr). It should be noted that this figure illustrates the theoretical potential of global wave energy which will be reduced by geographical, technical and economical considerations.

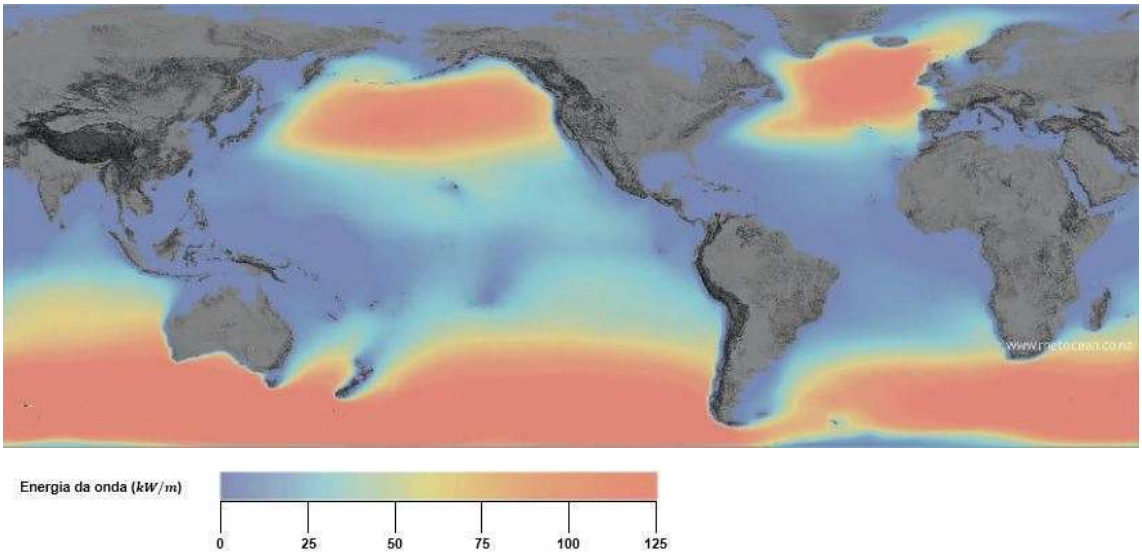

Figure 2-1- Global annual mean wave power distribution [17]

Morket et al [2] computed the regional distribution of the theoretical potential of the global wave energy resource which is limited to deep water off the coastline bounding each ocean basin. Lewis et al [1] illustrated the Morket results for the areas where theoretical wave power $P \geq 5\ kW/m$ and latitude $\leq 66.5°$, table 2-1.

Table 2-1- Regional theoretical potential of wave energy

Region	TWh/yr (EJ/yr)
Western and Northern Europe	2800 (10,1)
Mediterranean Sea and Atlantic Archipelagos	1300 (4,7)
North America and Greenland	4000 (14,4)
Central America	1500 (5,4)
South America	4600 (16,6)
Africa	3500 (12,6)
Asia	6200 (22,3)
Australia, New Zealand and pacific Islands	5600 (20,2)

Sims et al (2007) [10] estimated a global technical potential of 500 GW (~16 EJ/yr) for wave energy. They assumed wave energy converters with 40% efficiency which are installed near coastlines with wave climate of >30 kW/m. Krewitt et al (2009) [8] reported a technical wave energy potential of 20 EJ/yr.

2.2 Wave energy conversion technology

2.2.1 Introduction

Currently, the global development status of ocean energy technologies ranges from the conceptual and pure R&D phases to the prototype and demonstration phase, and only tidal range technology can be considered mature [1]. There are a large number of concepts and technologies for ocean wave energy conversion, but they restricted to the pre-commercial phase. Over the past decades, the oil and gas industry and the other marine industries have made significant advances in the field of materials, constructions, corrosion, submarine cable and communications, which may help the ocean energy technologies in its way to commercialization.

2.2.2 Concepts

To date, many wave energy conversion techniques with different operating principles have been patented in different countries. These technologies can be divided into different categories based on the main variables which include [1]:

- The method of wave interaction with respective motion includes heaving, surging and pitching
- Water depth which can be deep, intermediate or shallow water
- Distance from the shore which includes onshore, nearshore and offshore

The process of generating electricity from ocean waves can be split into three principal stages, including primary, secondary and tertiary conversion stages [18]. It can be applied to characterize the wave energy converter (WEC) devices. The primary interface subsystem represents the wave-body interaction, which delivers the mechanical power to the next stage. the wave converters that do not use the direct-drive technologies to generate electricity need an intermediate subsystem as a secondary stage for short-term storage and power processing i.e. hydraulic systems in [19][20]. The tertiary conversion uses electromechanical and electrical processes. The system that receive the mechanical power and deliver electricity is called power take-off (PTO) system. Serious academic attention to the wave energy conversion began in the early 1970 with the oil and gas crises. |Based on the international towing tank conference (ITTC, 2017) final report, more than 100 wave power pilot projects have been launched over the past few years. Moreover, more than 1000 patents have been registered since [21], [22], [23], [5]. Utility-scale electricity production form wave energy require array of wave energy converters that from a wave farm. The wave energy systems can be classified in different ways. Falcao [5] classified the WECs based on the principle of operation. As it is illustrated in figure 2-2, the first column shows the genus, the second and third columns are the classification of the WECs based on the location of installation and mode of operation respectively.

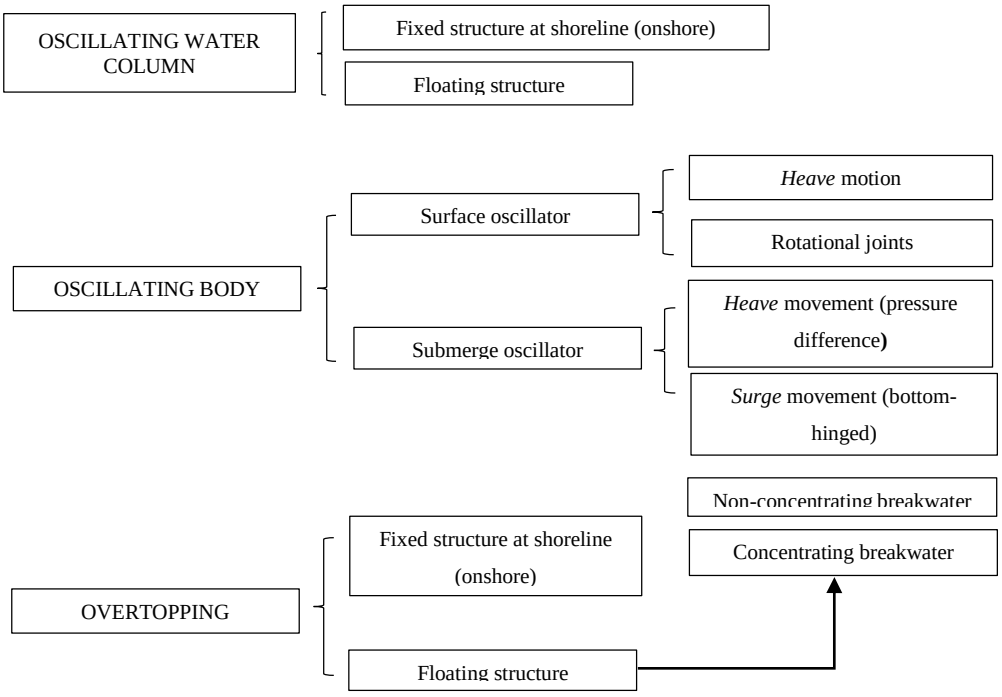

Figure 2-2- Wave energy technologies: classification based on principles of operation [5]

Furthermore, the WECs sometimes can be categorized based upon their dimension and orientation as attenuator, point absorber and terminator. Attenuators lie parallel to the predominant wave direction and 'ride' the waves, point absorbers are floating or submerged devices which have small dimension relative to the incident wavelength and terminators devices have their principle axis perpendicular to the predominant wave direction [24].

2.2.2.1 Oscillating water column

Oscillating water columns (OWC) are wave energy converters that utilize wave motion to induce varying pressure levels between the air-filled chamber and the atmosphere [5][25]. It consists of an air-filled chamber with two open ends, one to the water and another connected to the atmosphere via an air turbine coupled with an electrical generator, figure 2-3. As the water level goes up, the trapped airflow force the turbine to spin and drive an electrical generator. When the water level goes down the airflow reverses and fills the chamber. The turbine rotates in both directions, because of either its design or variable-pitch turbine blades. An OWC device can be installed above the breaking waves as a fixed structure; it can be a bottom-mounted structure that locates nearshore or a floating structure moored in relatively deep waters.

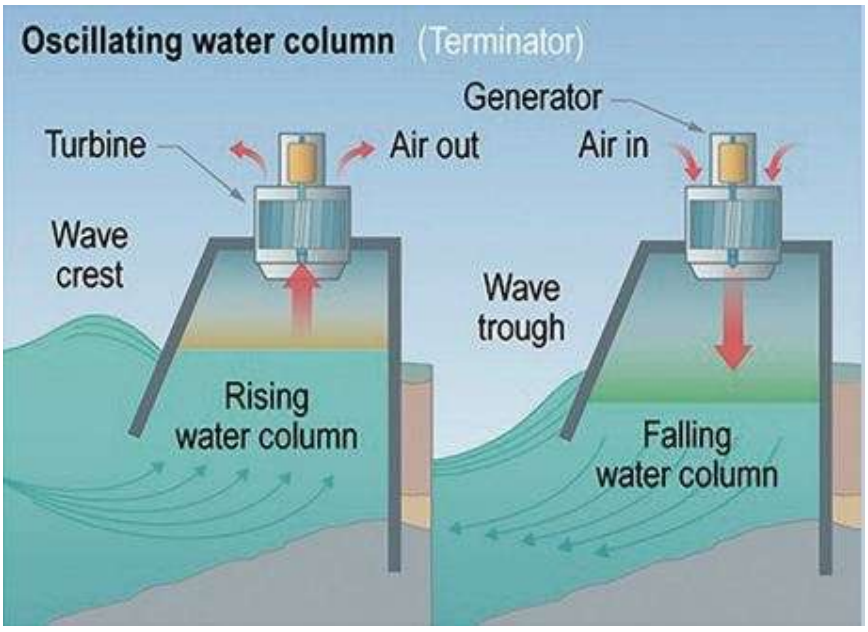

Figure 2-3- Oscillating water column [26]

2.2.2.2 Oscillating body systems

Oscillating-body (OB) WECs generate power through an oscillatory motion between two body, figure 2-4-a,b or between one body and a fixed reference point, figure 2-4-c,d,e. The OBs can be surface or fully submerged oscillators. A “point absorber” is a surface or submerged oscillator that have small dimension relative to the incident wavelength with an oscillatory motion in one or two degrees of freedom. This motion can be a relative motion between two bodies (two-body point absorber) figure 2-4-a, or the reaction of the buoy to the seabed, figure 2-4-c. Dimension of the efficient buoys are very small comparing to the predominant wavelength of the sea site (up to 5 to 10% of the predominant wavelength [27]. Some OB WECs are fully submerged and work based on the changes in hydrodynamic pressure on the device. This type of devices are typically installed nearshore and moored to the seafloor by the chains and cables, or are mounted directly, figure 2-4-d. Another type of the oscillatory surface WEC utilizes angularly articulating (pitching) buoyant bodies, which are connected to each other, figure 2-4-b. The alternating rotational motions of the joints drive the PTO system to generate electricity. Currently each device has 120 m long with buoys of 3.5 m diameter [22]. Finally, the hinged devices that place on the seafloor in nearshore regions and extract the energy of the horizontal surge motion of the incoming waves, figure 2-4-e.

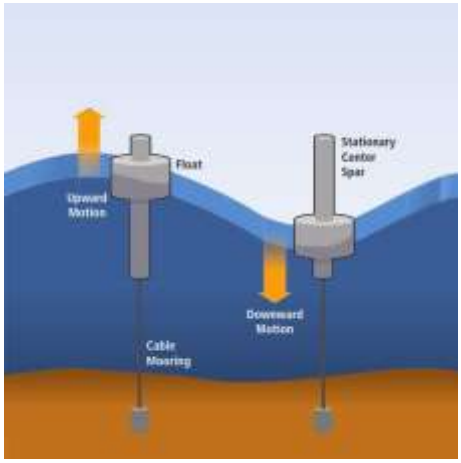

a)

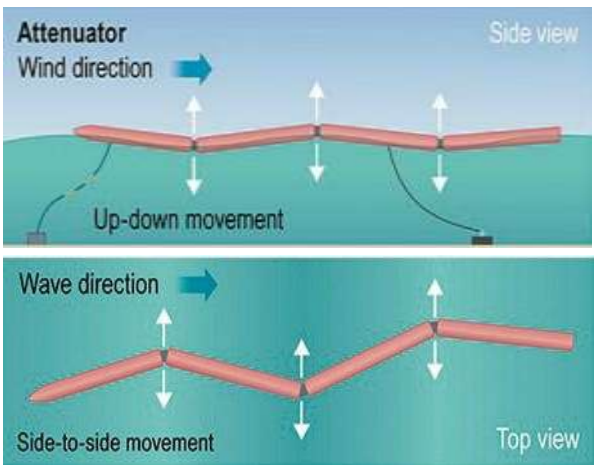

b)

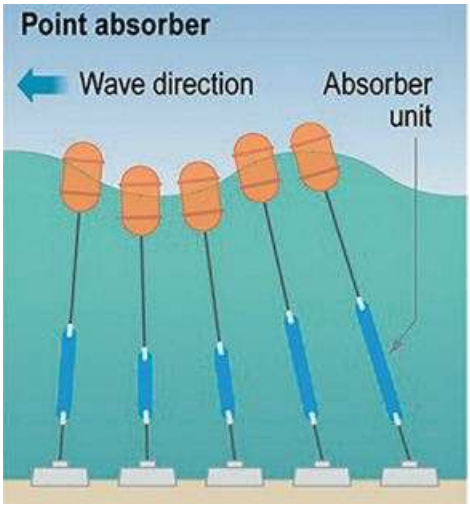

c)

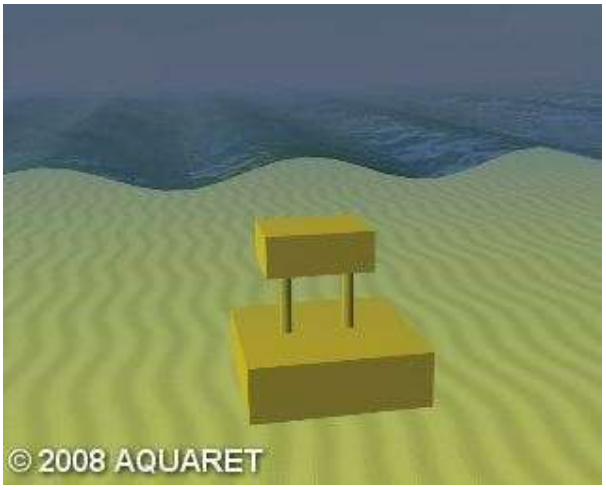

d)

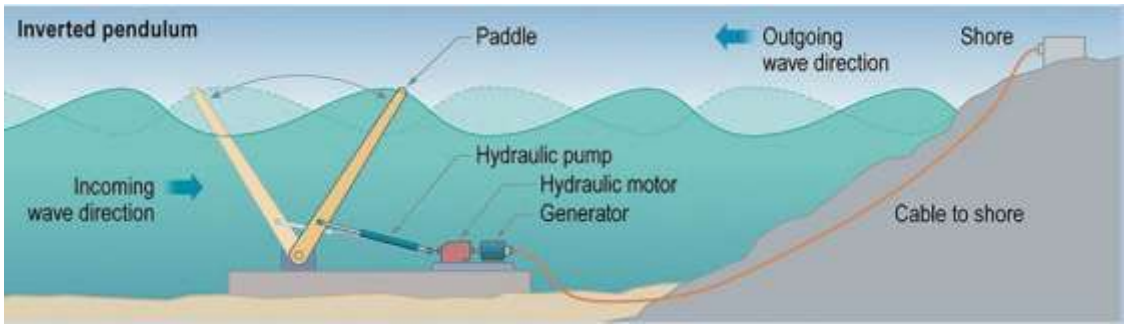

e)

Figure 2-4 - Oscillating body wave energy converters, a) (designed by National Renewable Energy Laboratory (NREL)), b, c and e) [26] and d) (EMEC)

2.2.2.3 Overtopping devices

Overtopping devices utilize the surging waves to collect water into a reservoir (sometimes via a concentrating collector) above the mean water level, figure 2-5 [5]. The collected water then drain down to the sea via a conventional low-head hydraulic turbine. These devices can be offshore floating systems or installed on shoreline or man-made breakwaters [1].

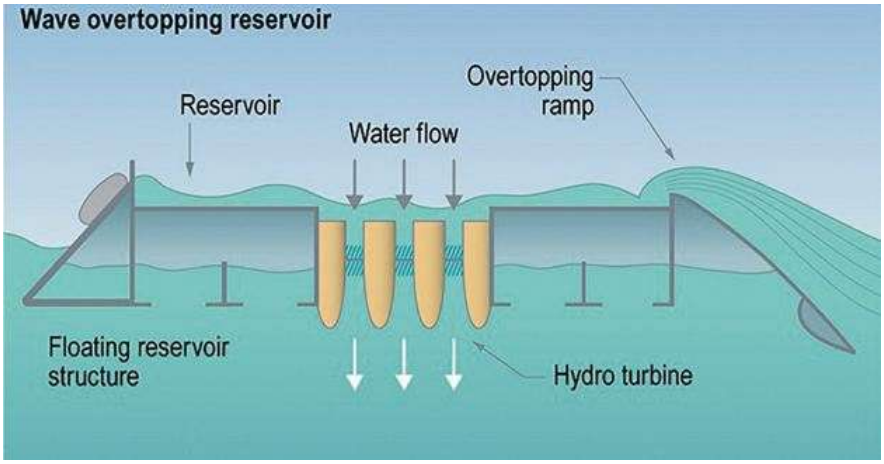

Figure 2-5- overtopping device [26]

2.2.2.4 Power take-off (PTO)

PTO systems convert the delivered kinetic energy, airflow or water flow by the WEC device into a useful form of energy, usually electricity. There are different types of PTOs which have been adapted for different WEC devices, e.g. pneumatic, hydraulic, direct drive, etc. A complete description of these systems can be found in [18][28]. The varying wave climate in a real sea may degrade power quality from a single device, so in practice, some methods like short-term energy storage or PTO resistance control may be required to smooth energy production. The cumulative energy generation of an array of wave energy devices will be smoother than the energy production of a single device, therefore arrays of wave energy devices are likely to be common . An efficient electrical energy generation is intensely depended on the advance control systems [1].

2.2.3 Global status

The worldwide installed capacity of ocean energy technologies, except offshore wind, was just about 530 MW, by the end of 2013 [29]. The most of this capacity come from the La Rance, 240 MW (France) and Sihwa, 254 MW (Republic of Korea) tidal range barrages. The technologies of other ocean energy sources are still at the conceptual , R&D or demonstrative prototype stages [1], however, a global commercial application is expected for the wave and tidal current in the near to medium future [29]. Figure 2-6, which is provided by IRENA 2014 [29], illustrates the ocean energy technologies` maturity level, using the so-called technology readiness level (TRL) scale. It should be

noted that, the other parameters such as manufacturability and economic performance of each technology, also influence their short-term development prospect. The tidal current and wave energy attracted significant global interests and it is confirmed by the huge number of prototype deployments and sea trials that has recently done (100 kW nameplate power capacity or greater) [29]. Since 1960s, when the first commercially tidal range barrage was built in France, there has only been a single large tidal range project (Sihwa, South Korea), while the cumulative capacity of the prototypes of the tidal current and wave energy is less than of a single tidal barrage project. Considering this fact, we can infer that the tidal range could not attract the interests comparing to other pre-commercial ocean energy technologies. So, the wave energy and tidal current can be considered as the promising ocean energy sources to be commercialized at a near or mid-term. Table 2-2 illustrates short-term development attractiveness of the ocean energy technologies, except offshore wind. As it can be seen, wave and tidal current energy technologies are the options with the most attractions.

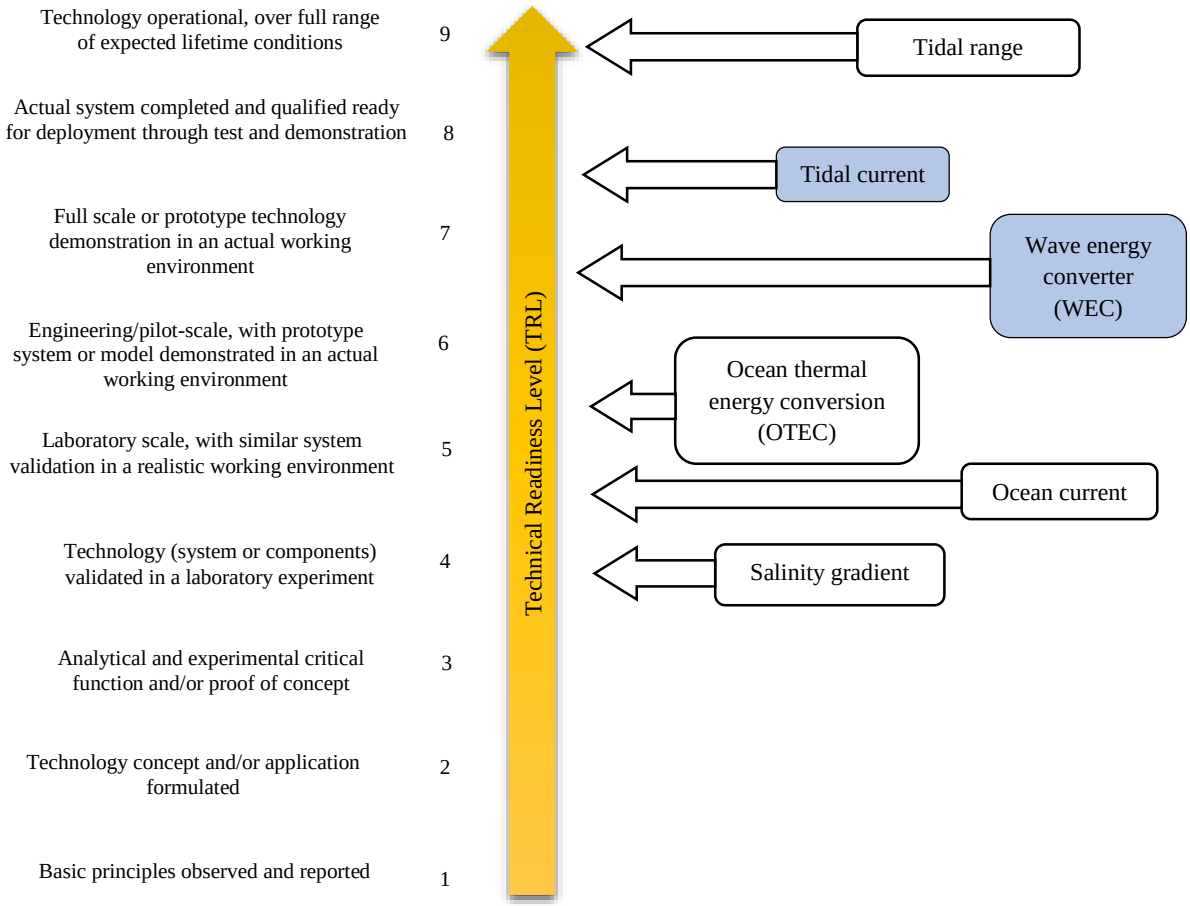

Figure 2-6- Technical readiness level of the ocean energy sources [21] (based on the DNV GL data, 2014)

Table 2-2 - Short-term development attractiveness of ocean energy technologies [21] (based on the DNV GL data, 2014)

	Technology readiness level (TRL)	Global site/resource availability	Level of industrial involvement	Financial investment interest	Relative attractiveness
Salinity gradient					
Ocean current					
OTEC					
Wave energy					
Tidal current					
Tidal range					

High	Moderate	Low

2.2.4 Global deployment

After the oil crisis in 1973, the investments on the wave energy by the governments started and the wave energy technology began to develop. Many concepts of wave converters have been presented and tested during past decades, but until late 2016, there was no commercial WEC in operation. It is common to test the small-scale models of WEC devices (1:15 to 1:50) in wave-tanks and laboratories before the prototype testing in the open-sea [1]. The half or full scale testing is necessary for the pre-commercial stage of development. Recently, the pre-commercial testing of trial individual WECs and small arrays have been started and is expected to grow faster through this decade [28]. Figure 2-7 depicts the geographical distribution of the WECs prototype deployment with a minimum capacity of 100 kW, for the period of the beginning of the 21th century to the end of 2013 [29]. As it is illustrated, Portugal and the UK are the countries with major contribution. Figure 2-8 illustrates the breakdown of the wave energy technology types which is presented by the IRENA in 2014 [21]. 36 known active, commercial (i.e.non-university) WEC technology developers, from 13 different countries have been considered. The trend of developers are to offshore floating devices. Point absorbers have been studied and tested more than other types and as it can be seen, direct-drive and hydraulic PTO systems have more contribution comparing to other types of PTO systems.

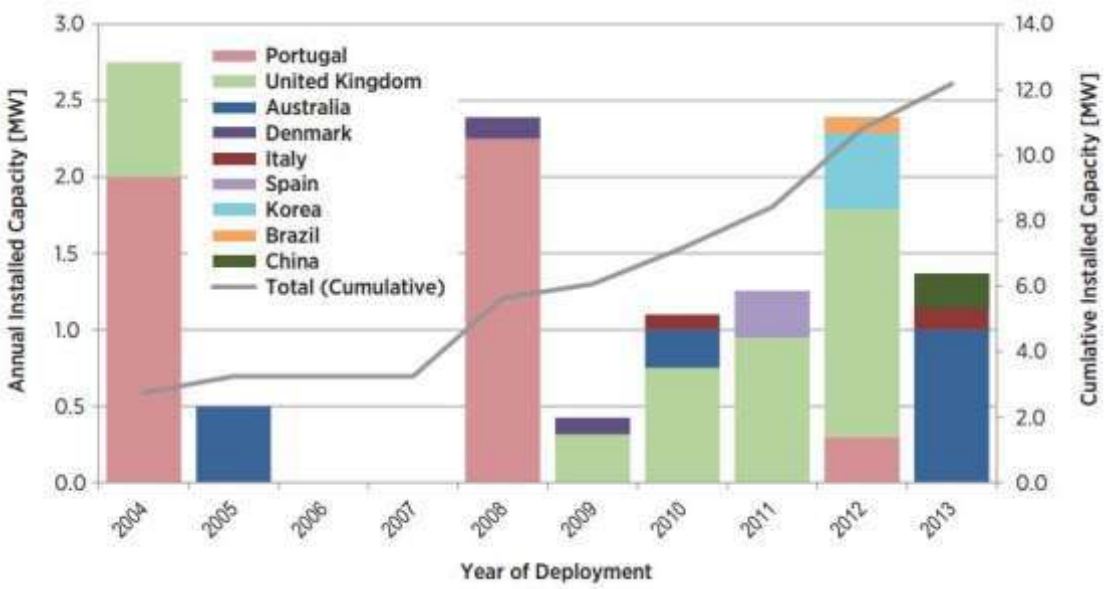

Figure 2-7- Summary of wave energy prototype deployment (with a minimum capacity of 100 kW) until the end of 2013 [29] (based on the DNV GL data, 2014)
Note: As some units were removed after testing or failed during the trial effort, cumulative capacity deployed does not represent total installed capacity until that date.

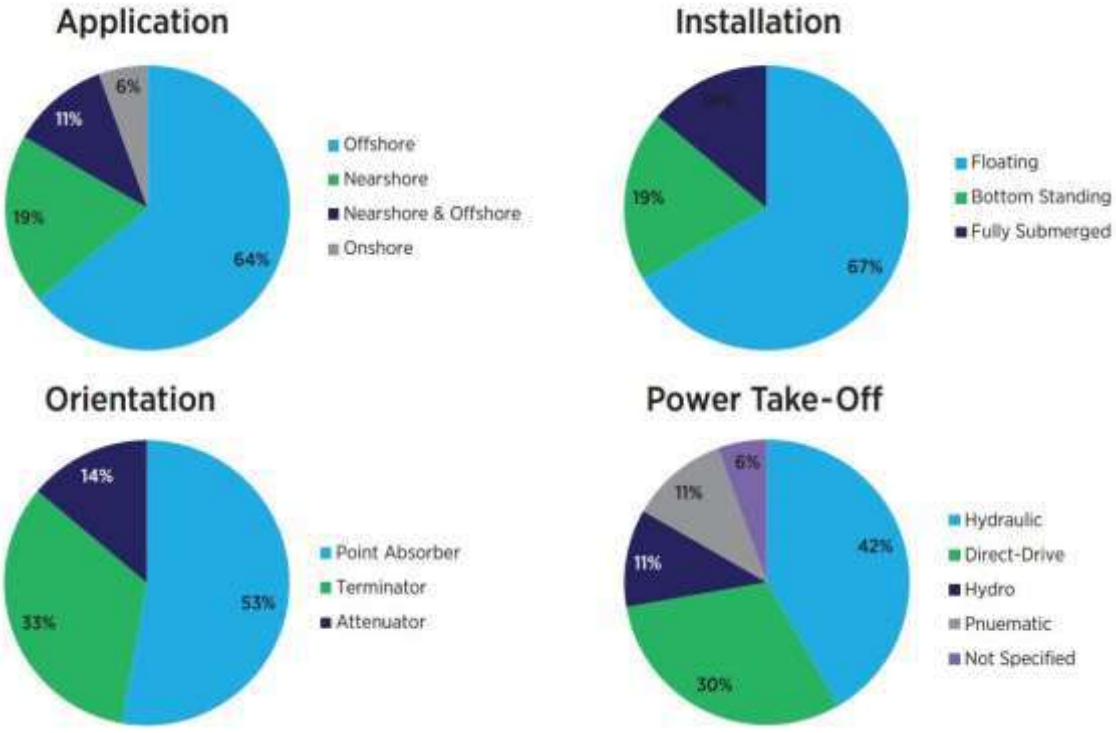

Figure 2-8- Breakdown of the wave energy technology devices [21] (based on analysis of data from DNV GL (2014))

2.2.5 Prototypes

As it is explained in the section 2.2.2, the technologies for extracting the wave energy is divided into three categories based on the principle of their operation. Figure 2-9

illustrates the classification of the wave energy devices, which have been deployed in different regions, based on the principle of their operation.

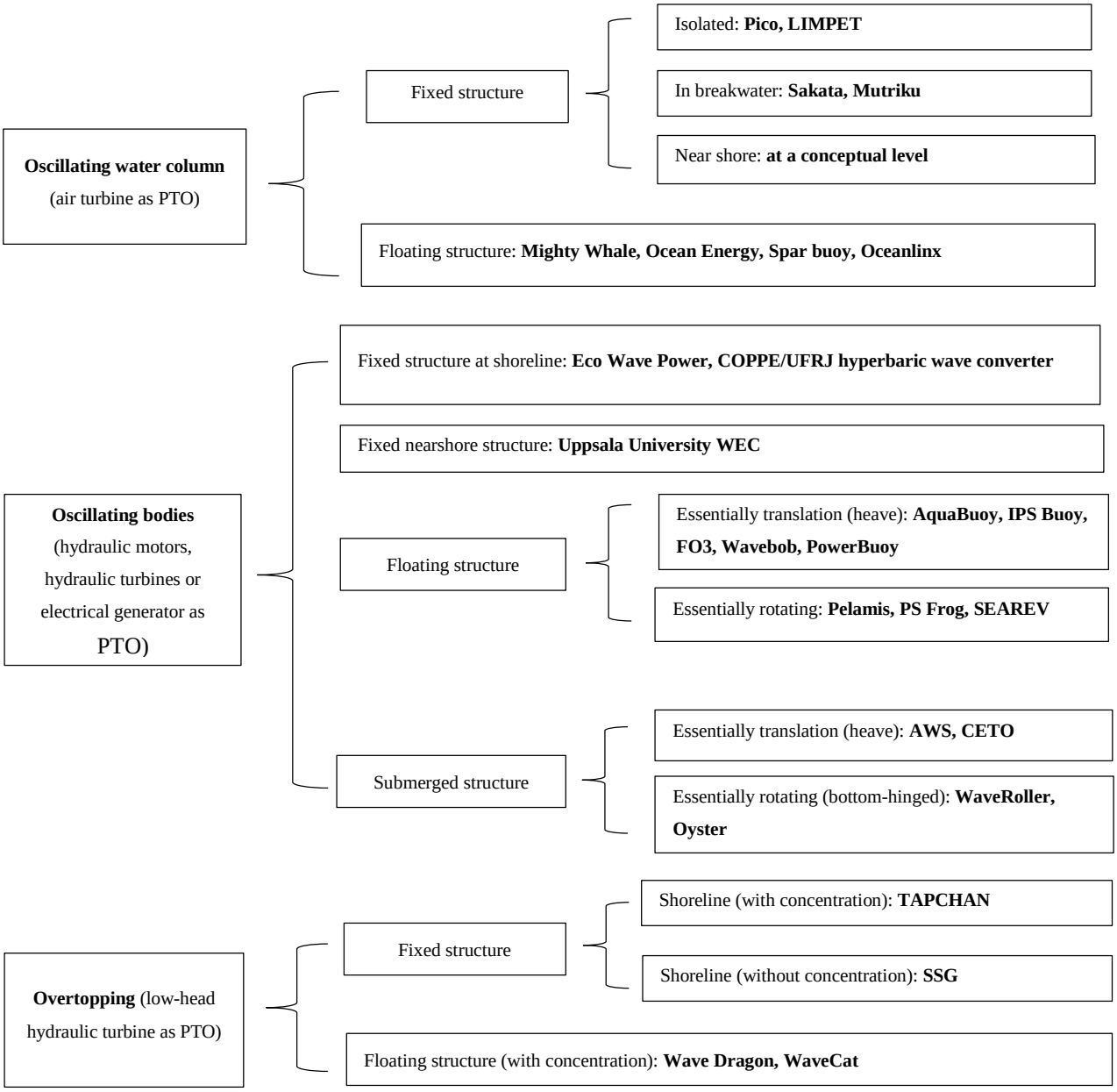

Figure 2-9- Wave energy technologies, modified based on [21] [30][5]

CETO5 is the commercial name of a submerged oscillating body WEC, figure 2-10. A wave farm consists of three units of CETO 5 (The Perth wave energy project), which are connected to the power grid, were installed in the Garden Island, Western Australia and operated for a year. CETO5[1] was also tested to drive a wave powered reverse osmosis desalination plant. In late 2015, another wave farm was installed on the Swedish west coast[2], with connection to the national grid, figure 2-11 . The Swedish WEC is a surface oscillating body that was proposed by the Uppsala University[3] [31]. Both projects were installed in the relatively shallow water (<50 m) and their PTO system is located under the water surface. They plan to commercialize their power plants through the next two or three years.

Figure 2-10- CETO5 wave energy converter[1]

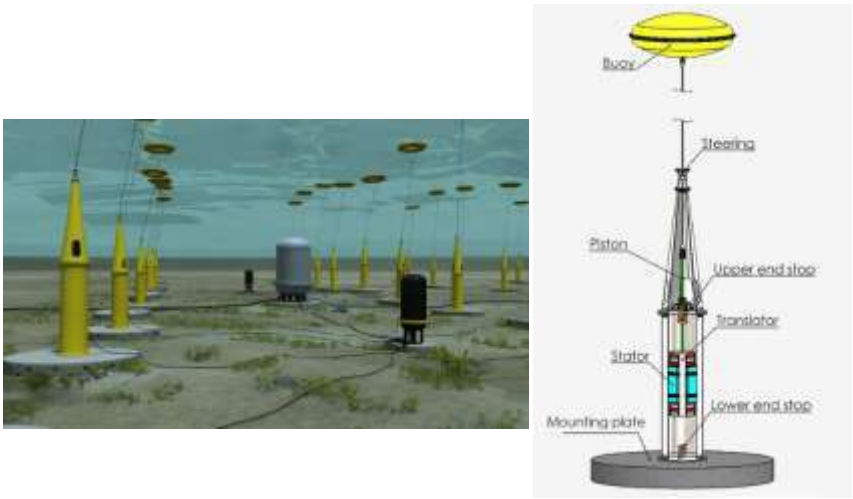

Figure 2-11- The Swedish wave energy converter[2]

[1] http://carnegiewave.com/

[2] www.seabased.com

[3] http://www.teknik.uu.se/electricity/research-areas/wave-power/wave-power-concept/

Some representative of oscillating water column devices are: GreenWave (Scotland;UK); Mutriku (Basque Country/Spain); Mighty Whale [32] (Japan) the OE Buoy [33] (Ireland/|Denmark), Spar buoy [34]; Oceanlinx (patented by Oceanlinx company: PCT/AU2009/001128); Pico Plant (Azores/Portugal) [25] and Viot Hydro Wavegen's LIMPET (Scotland/UK) [35] [36][29][1]. Figure 2-12 shows the Mutriku power plant, which was installed in 2011 in Spain.

Figure 2-12- Mutriku´s power plant (source: http://www.eve.eus)

Except CETO and Uppsal University devices, which have been installed and demonstrated as wave arrays in a pre-commercial stage, the 750 kW Pelamis Wavepower is the most maturely developed oscillating-body device. It has been tested in Scotland and deployed in Portugal and it was sold as part of a commercial demonstration project [1]. Some representative devices of oscillating-body system: the PowerBuoy of Columbia Power Technologies, Oyster (Scotland) [37], Seatricity (Cornwall), WaveRoller (Finland), Wave Star (Denmark), Wavebob, (Ireland) and the Brazilian hyperbaric wave converter [20,38][1,29,36]. Figure 2-13 shows some examples of the oscillating-body WECs. Overtopping converters can be floating or fixed structures. Wave Dragon and WavePlane are two Danish overtopping prototype deployed at sea. The Seawave Slot-Cone generator (Norway) and WaveCat (Spain) are the representative of the overtopping with fixed and floating structure respectively. Figure 2-14 illustrates the WaveCat and Wave Dragon overtopping devices.

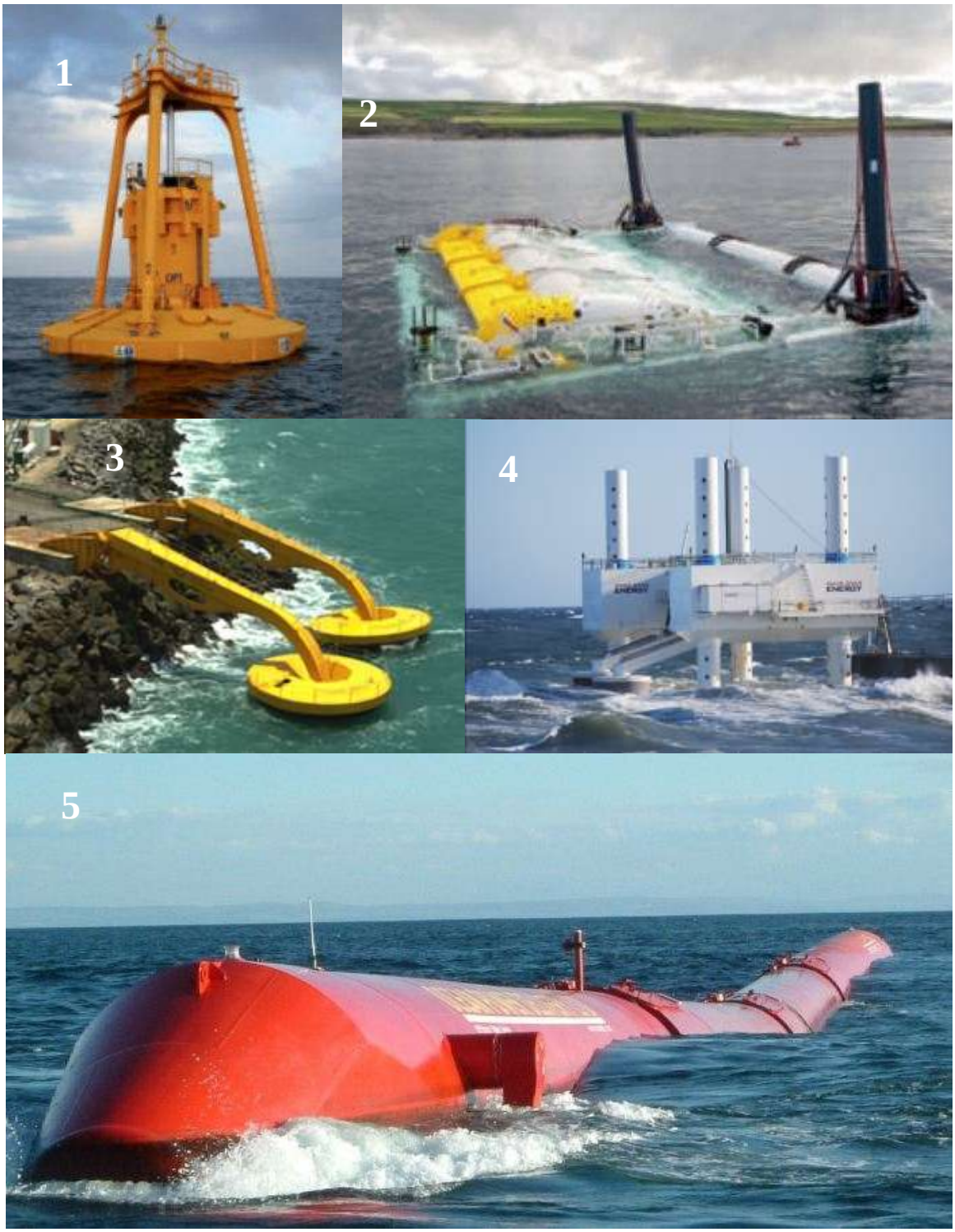

Figure 2-13- Oscillating-body WECs, (1): PowerBuoy (Ocean Power Technologies Inc.), (2): Oyster (Aquamarine Power), (3): Brazilian hyperbaric wave converter (COPPE/UFRJ), (4): Wave Star (Wave Star AS, photo by: MPE, www.panoramio.com), (5): Pelamis (Pelamis Wavepower)

Figure 2-14- Floating overtopping devices: left; WAVECAT [39] , right; Wave Dragon (Wave Dragon AS)

2.3 WEC control strategies

2.3.1 Reactive control

Generally, it can be said that a good wave absorber must be a good wave-maker [40]. Hence, in order to absorb wave energy it is necessary to displace water in an oscillatory manner and with correct phase (timing). A two-dimensional symmetrical system oscillating in one mode can, at most, absorbs half of the incident wave energy [41][42][43]. Almost all incident energy can be absorbed if the two-dimensional system is sufficiently non-symmetric, as for instance the Salter Duck (1974) [44]. For an axi-symmetrical wave-absorbing device oscillating in one degree of freedom, the maximum power that can be absorbed, equals the incident wave power associated with a wave front of width one wavelength divided by 2π [45][41][42][46]. The maximum absorbed power is less than indicated here if the wave is so high that the required oscillation amplitude exceeds the maximum specified value of the oscillation amplitude as selected when designing the absorber. The importance of resonance is that it ensures that the oscillating velocity is in phase with the excitation force. For sinusoidal waves off resonance, or for real non-sinusoidal waves, it is more complicated to attain optimum conditions for maximizing the energy output. Already during the mid-1970s it was proposed independently by Salter [47] and by Budal [48],[49], to apply control engineering for optimizing the oscillatory motion of a wave energy converter (WEC) in order to maximize the energy output. For the practical implementation, it was proposed to use a controllable power take-off device, for instance a combined generator and motor. In this way, the optimum conditions of the oscillation may be achieved by allowing a certain reactive power to be handled in an optimum way in order to maximize the active power. Reactive

control leads the motion of the body to fulfill two conditions. The first one states that the oscillating velocity of the body must be in phase with the excitation force on the body. This happens naturally when the wave frequency equals the natural frequency of the body, but one must act on the body when it is not the case in order to respect it. This is known as phase control. The second condition is called the optimum amplitude condition. If the amplitude is unconstrained, this condition is that the resistive load B of the PTO must be equal to the hydrodynamic damping coefficient at the incident wave frequency. In case of optimum control, continuous control can be achieved by acting on the parameters of the PTO in order to respect these two conditions. For this reason the term "reactive control" has been used by Salter (1979) [47], as an alternative to the term "phase control". In principle, the knowledge about the future wave is required for such a control strategy. If the oscillation amplitude is not restricted "optimum amplitude and phase control" may be regarded to as "complex-conjugate control" which was presented by Nebel (1992) [50]. For instance, Perdigão and Sarmento [51] presented a solution for approximating the complex conjugate control applied to an oscillating water column. Beirão [52] and Gieske [53] investigated the application of reactive control strategy on Archimedes wave swing (AWS).

2.3.2 Latching control

In order to avoid the necessity of reversing the flow of energy through the power take-off device, Budal (1978-1980) proposed [40],[54][55], that approximate optimum phase control may be conveniently achieved by latching the wave absorber in a fixed position during certain intervals of the oscillation cycle. This kind of controller that do not involve reactive power flow may be classified as "resistive bang-bang controllers" [56][57]. It was soon realized [55] , that in order to apply discrete control (latching) it is necessary to predict an irregular wave some distance into the future, a time of the order of a quarter or a half of the natural period of the wave-absorbing oscillator. With this method, which was proposed independently also by Guenther et al. (1979) [58], and by French (1979) [59], the energy conversion is somewhat sub-optimal, at least for the case of non-restricted oscillation amplitude. Latching consists of locking the motion of the body at the instant when its velocity vanishes at the end of one oscillation, and waiting for the most favorable instant to release the body. The instant of latching is imposed by the dynamics of the body itself (i.e. vanishing velocity); thus, the control variable is simply the duration of the

latching phase, or equivalently the instant of release. This mode of control, applied to the heave motion of the buoy, was proposed by Budal and Falnes in regular [40][55] waves and further investigated experimentally by Budal et al. [60] in irregular waves (1978-1982). They considered a spherical buoy, figure 2-15, which can perform heaving oscillation relative to strut joined to an anchor on the seabed. The buoy is supplied with latching means for optimum phase control and with an air turbine for power take-off. They assumed that the excitation force was known sufficiently far in the future for the real sea. They used a Kalman filter for wave prediction and for the provision of unlatching signals based on the measured signals of the local wave.

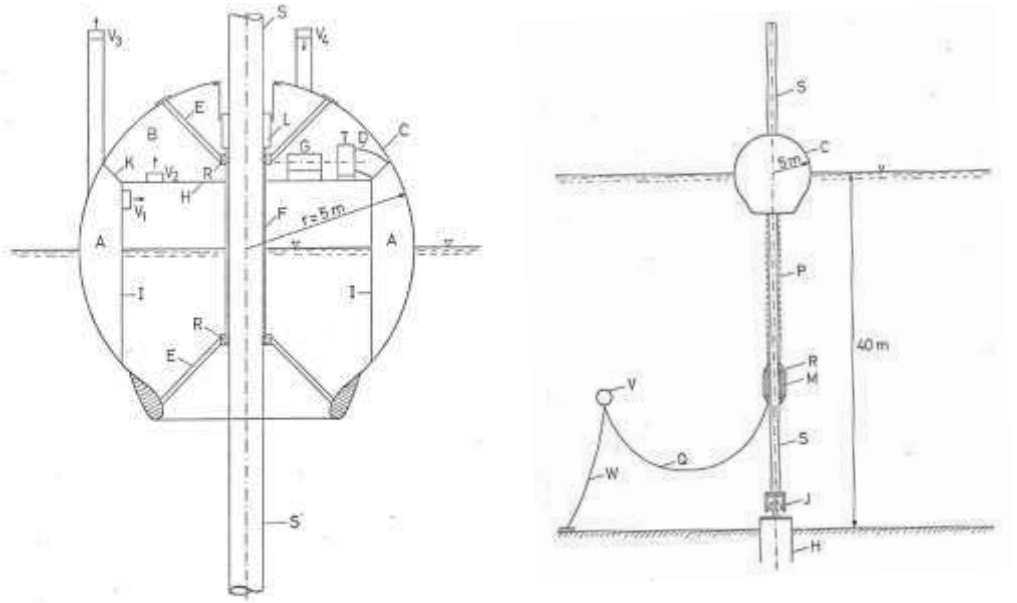

Figure 2-15- The Norwegian wave-power project [60]

Note: the hull of the buoy C has a spherical shaped with an opening to the sea at its lower end. I and A are the cylindrical wall and the buoyance chamber respectively. The horizontal deck H and the conical wall K separate another chamber B. The concentric cylinder F is fixed at its upper end and lower end to the hull of the body by means of rod E. The cylinder is provided with rollers R at its ends rolling on a vertical, cylindrical strut S connected to the sea floor through a universal joint J and an anchor H. the clamping mechanism L can lock the otherwise freely floating buoy to the strut. The turbine T is connected between chambers B and A by means of the tube D. the buoy is equipped with four non-return air valves V_1 - V_4. A concentric, streamlined mass M, moveable along the strut by means of rollers R, is connected to the buoy through cables P. The mass assures that the strut has an equilibrium upright position. The electrical cable from the generator passes along the cables P, via the flexible cable Q to the buoyant body V and along the mooring cable W to the sea floor [60].

Iversen (1982) [18] presented a numerical method for estimating the power absorbed from an irregular wave by means of a phase-controlled (latching) body with a limited amplitude. One of the basic simplifications in his model was the sinusoidal approximation. The velocity was prescribed, having a sinusoidal shape and not calculated in detail. Thus, the hydrodynamical damping, the damping from the power generator and the frequency dependence of the added mass were neglected. The accuracy of the numerical method depends on the accuracy of estimating the excitation force coefficient. One important numerical result of the Iversen's work was that the exact value of the natural period of the buoy, T0, has a rather small influence on the amount of absorbed power. The only restriction is that has to be below a certain limit in order to avoid any significant reduction in the number of strokes.

Greenhow et al (1984) [61] applied the latching control on a terminator type of wave energy converter (he called it the 'clam') with a wells turbine as the power take-off system, figure 2-16. In 1997, Greenhow and White [62] presented a mathematical model of the transient motion of a floating body wave energy device (a point absorber), including memory effect and infinite added mass, in regular wave and a finite water depth. They showed that the use of the full memory model combined with the latching strategy is essential. To demonstrate how inclusion of memory terms affects latching strategies, they considered the efficiencies for a definite geometry tuned at a certain period of oscillation, with and without memory effect for both situation of with and without latching. For the case without latching system, the results were very similar, but, in contrast, the results were remarkably different for the case of using latching system.

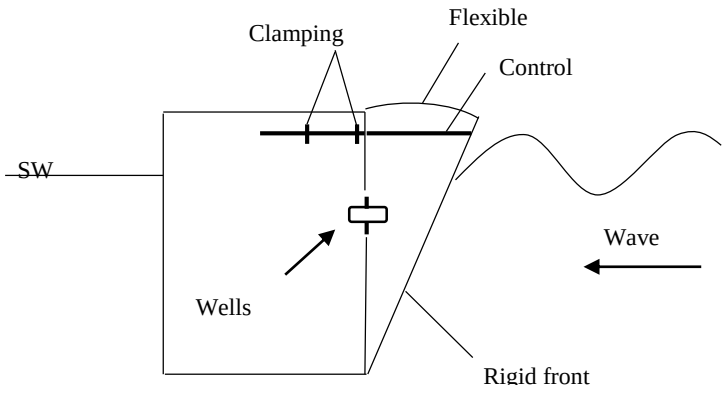

Figure 2-16- A generic model of "CLAM" wave energy converter [61]

Eidsmoen (1995) [63] simulated a tight-moored heaving-buoy wave energy converter controlled by a latching system. Later (1996), he applied the same control system on a slack-moored wave energy converter, consisting of a semi-submerged heaving buoy moving relative to a submerged plate, figure 2-17 [64] . In both cases, a high-pressure hydraulic machinery was proposed for energy production and latching control which is based on the future wave information prediction. An actively controllable valve in the machinery was used to obtain the largest possible power production, and limit the excursion of the buoy, in order to protect the hydraulic machinery. In addition, an end-stop device was provided as a safety measure, in case the control fails to limit the excursion. The time-domain mathematical models were developed for the systems in both sinusoidal and irregular waves. As a comparison of two devices, tight versus two-body slack-moored, it was observed that for the tight-moored device the hydraulic system worked satisfactory, and the output power increased very rapidly with the wave height for small wave heights. For the slack-moored device, it was observed that keeping the submerged plate in the desired mean position was a problem. In the other hand, the power dissipation by the non-linear drag force of the submerged plate was large and they were not able to produce the same rapid increase in the power production for small wave heights as with tight-moored WEC. It should be noticed that, to calculate the drag force on the submerged plate, a relatively simple model had been used in the Eidsmoen's works and more precise model of drag force is important for the development of this kind of WEC. A duration curve was presented, which shows the percentage of the year that the mean power production is above a certain level. The power production should be close to the year average during a large fraction of the year, so that the power output is smooth. The power output from the slack-moored device was not as smooth as the power output from a tight-moored device with control, but more smooth than the power output from a tight-moored device without control.

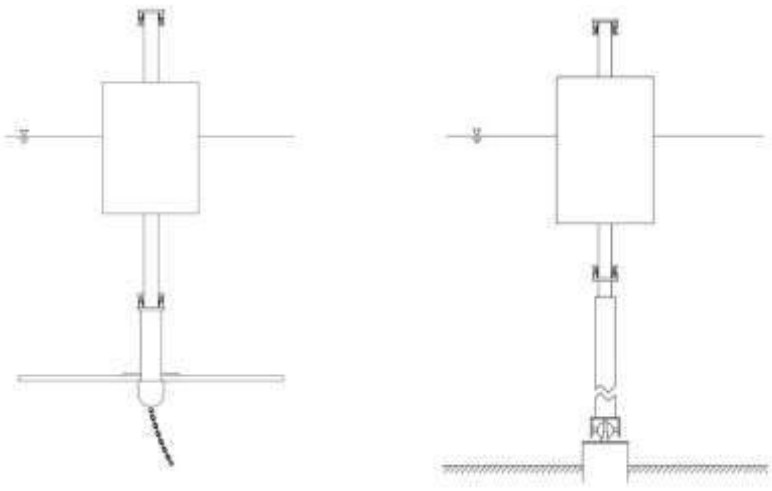

Figure 2-17- Slack-moored (left) and tight-moored (right) heaving-buoy wave- energy converters [64][63]

Korde (2001) [65] investigated the application of the latching control on an alternative floating wave energy converter in deep water. He utilized an on-board, actively controlled motion-compensated platform as a reference (‘active reference’) for power absorption and latching. Then he compared the results of this active reference to a sea-bottom-fixed reference device. Pneumatic cylinders equipped with open/close valves were used here for latching and power absorption. Time-domain simulations were carried out in small-amplitude regular and irregular waves. For the irregular wave case, the exciting force was assumed to be known far enough into the future. As a result, it was found that the energy absorbed by the active reference system was somewhat less than, but comparable to, that observed with the sea-bottom reference. The author suggested that an alternative to the PTO system and some improvement in the algorithm for the evaluating the optimal control may result in greater energy absorption in both cases (fixed and active references). Hals et al (2002) [66] presented a quantitative discussion and comparison of reactive control versus latching phase control. They assumed a heaving semi-submerged sphere as a WEC in regular wave. The linear theory was applied and an ideal (100% efficient) linear hydraulic pump was considered as the PTO system. To have a more realistic results and based on the practical and economical consideration, the heave excursion of the sphere was restricted to not exceed a certain value. They concluded that although the latching control has the drawback that somewhat less average power is produced, as compared with reactive control, a very important advantage, however, is that reversed energy flow through the device is not needed, and then the ratio between maximum

instantaneous and average power is less excessive than with reactive control. Hence, the conversion-efficiency requirement of the power take-off device is less strict.

Bjarte-Larsson et al (2002) [67] carried out a set of experimental tests in a wave channel in order to investigate the application of latching control on an oscillating water column (OWC), which previously presented by Lillebekken et al (2000) [68]. Later in 2005 [69] , they also tested a heaving axi-symmetric floating body, which was controlled by latching, in a wave channel. The same hydraulic PTO system was used for converting the energy. They found that the latching control results in a significant increase in the performance of the both devices, the OWC and heaving axi-symmetric floating body, for the sub-resonant frequencies.

Babarit et al (2005) [70] compared three latching control strategies for a heaving wave energy device in irregular waves. They investigated semi-analytically the latching control applied to a mechanical oscillator, and numerically three strategies of latching control for a point absorber wave energy converter oscillating in the heave mode only. They compared a strategy aiming at the maximization of the amplitude of the motion of WEC with a strategy aiming at the maximization of the absorbed energy and a strategy aiming at the keeping velocity and excitation force in phase. It was found that in random waves, the control strategy aiming at maximizing the amplitude of the motion gives approximately the same results as strategy aiming at keeping velocity and excitation force in phase. In regular waves, the former one (the strategy aiming at maximizing the absorbed energy) is the most efficient. Moreover, they found that the need for prediction of the future excitation force remains bounded by the natural period of the system.

Falcão (2007) [19][71] developed a method of applying latching control without necessity of predicting the wave excitation (none-predictive method). The device was a heaving floater equipped with a PTO consisting of a high-pressure hydraulic circuit and a gas accumulator, figure 2-18. The body was kept fixed at the instant of zero velocity of the floater until the hydrodynamic force applied on the body exceeded the resisting force due to the gas pressure difference between low-pressure (LP) and high-pressure (HP) accumulators [71]. This critical hydrodynamic force was estimated based on the two control parameters which were weakly dependent on significant wave height, but (for best results) should be adjusted to match the sea state wave period. Theoretically, a great gain was found in absorbed energy by the device due to the large unrealistic oscillations. This may imply very large forces to keep the body fixed prior to its release. Such forces are

likely to exceed the practical limits of the hydraulic PTO system. He suggested that a special braking system may be required.

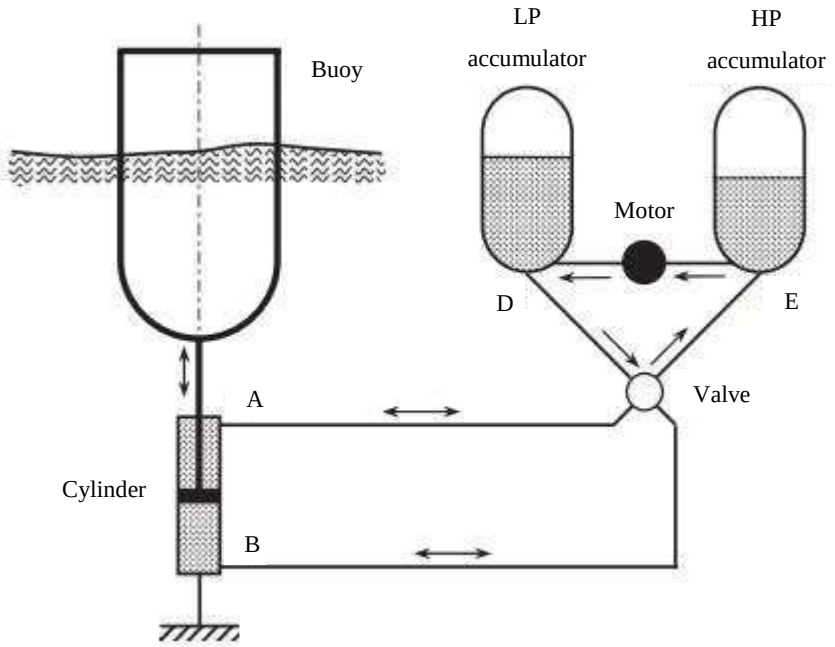

Figure 2-18- Schematic representation of the WEC presented by Falcão [19]

Lopes et al (2009) [72] experimentally verified, this system. Based on the Falcão system, the Hydraulic PTO pressure measurement was utilized as input to the controller, but this did not work in the investigated system due to non-negligible high-frequency pressure oscillations inside the hydraulic chamber during the latched interval. Four different irregular sea state were run, and the results showed that the investigated latching control enables the capture width to increase by a factor of 2.5 or more.

An alternative way for controlling the hydraulic PTO system, which is called "Declutching" had been presented by Babarit et al in 2009 [73]. Declutching is achieved by uncoupling the PTO and the floater system, a simple by-pass valve for the hydraulic PTO system, at discrete instants, which is determined by the optimal control method. They applied an iterative scheme based on their previous work [74] to compute the optimal control algorithm. As they concluded, this method can be difficult to implement in practice because of the necessity of the knowledge of the future of the excitation force, which requires prediction of the incoming wave. However, theoretically, it was found that

using declutching can improve the power absorption by the WEC. Clement et al (2011) [75] theoretically investigated a three-state control strategy which is the combination of the latching and declutching control methods. They called it latching-operating-declutching (LOD) control. It was shown that any of these methods can be applied with great benefit, not only to mono-resonant WEC oscillators, but also to bi-resonant and multi-resonant systems (like SEAREV [76]). The LOD method speared to give far better results than each method individually. It was found that the declutching control enhances the power of latching in this combination, especially for long waves, and its performance is less sensitive to the PTO damping coefficient. Nevertheless, the challenge of practical implementation of these methods in the real world is remained because of the required knowledge of the future of the wave excitation force.

Sheng et al (2014) [77] [78] presented a none-predictive method for applying latching control on an oscillating cylinder in heave direction. They simply calculated the latching duration, as half of the subtraction of the incident wave period and the natural period of the oscillating body, similar to the Falnes´ proposal [55] in which the unlatching of the device occurs at the instant of $T_0/4$ (T_0 is the natural period of the oscillator) ahead of the next ´peak excitation´ in regular waves. It can be seen that, the future information of the excitation force is necessary in irregular waves. In this none-predictive method, the latching duration is decided merely by the characteristics period(s) of the waves due to the facts that the wave spectrum can be much forecast correctly well ahead of the time or obtained from the sea measurement [77]. Then, three characteristic wave periods were considered for calculating the latching duration; first period is the modal period, Tp, and other two periods are the mean period, T0 , and the energy period, Te . They used a constant latching duration, based on a given spectrum and characteristic period, for the specified sea state, regardless of the difference in the individual waves in the wave train. The results showed that, theoretically, by applying this latching method the wave energy conversion may be increased. They also concluded that the latching duration for the irregular waves is best calculated based on the energy period and increasing or decreasing the latching duration slightly, may reduce power production significantly [78].

2.4 Geometry optimization of WEC

Structural and shape optimization techniques have been used for the seakeeping of ships and minimizing the dynamic response of moored vessels. Clauss and Brik

[79][80][81][82] developed numerous automated optimization procedures for the hydrodynamic shape optimization of offshore structure hulls. Advanced parametric design algorithms, numerical analyses of wave-body interactions, and formal multi-objective optimizations were integrated into a computer aided design system that produced hull shapes with high seakeeping quality. They studied different structures, including gravity base structures, tension leg platforms, caisson semisubmersibles and semisubmersibles with minimum downtime. Elchahal et al [83] used a density distribution process to perform a structural optimization of floating breakwaters and developed an optimization procedure based on genetic algorithms. A case study of a breakwater appearing in a port's construction far from shore has been considered.

Wave energy conversion technology is still in the pre-commercial stage. The cost of a wave energy converter (WEC) increases with its size; therefore, the geometry optimization of the system has a significant role in the design process to have an economically feasible system. The first step of the design process for a WEC is to develop a conceptual design that is appropriate for the reference resource site. Once the concept design is completed, a detailed device design can be developed using a combination of numerical modeling tools and model scaled tests. In contrast to the optimization process of offshore platforms, breakwaters etc., where the objective is to improve the seakeeping ability by minimizing the motion of the structure, an oscillating-body type WEC is designed to oscillate in the range of sea predominant frequencies allowing maximum motion amplitudes to produce more power. Until now, different works have been presented for geometry optimization of a PA. Vantorre et al [84] presented an optimization study of a point absorber with controllable inertia through linear frequency domain analyses and experimental tests for the Belgian coastal area of the North Sea. The geometry of the heaving buoy, PTO damping and supplementary inertia are considered as variable parameters to optimize the absorption system. For a given shape, the optimal values of the supplementary inertia and PTO damping were determined in function of the buoy waterline radius to maximize the power absorption while limiting the probability of slamming. Sjokvist et al [85] applied a frequency domain approach to optimize a heaving point absorber, with a pure damper as PTO system, for the Lysekil test site in Sweden. The objective of the optimization was to determine the buoy dimensions that maximize its heaving velocity for that sea state and a certain PTO damping. To attain this, several runs with different diameters and drafts were performed for three different PTO damping. Goggins and Finnegan [86] presented a frequency domain analyses applied to a heaving

axisymmetric point absorber to determine its optimum shape and radius. They use the Atlantic marine energy test site (AMETS) as a design location. The optimization goal was to maximize the extracted energy over an appropriate frequency range. The term significant velocity, previously defined by Clauss and Brick [79], proportional to the dynamic heave velocity response, was employed as the objective function. The optimum shape and radius that yields the maximum significant velocity for the input wave energy spectrum were chosen as the optimum geometric configuration. The process was applied on five different shapes with radius in the range of 1 to 25 meters. Several studies have also investigated the geometrical optimization process for other WEC concepts. For instance, Kramer and Frigaard [87] used the boundary element method to optimize wave reflectors by exploring their orientation and angle to increase the wave energy absorption for the wave energy converter Wave Dragon. Genetic algorithms have been used by Babarit and Clement [88] and McCabe [89] to the shape optimization of the SEAREV device, which is based on a pendulum that is placed in a closed buoy actuated by the swell through excitation forces [90], and a surging wave energy collector, respectively. The SEAREV optimization process goals were to maximize the absorbed power and minimize the costs. The objective of the shape optimization of the surging wave energy collector was to maximize the mean power, the ratio of the mean power to the characteristic length of the device shape, and the ratio of the mean power to the displaced volume of the collector.

Kurniawan and Moan [91] used a multi-objective optimization algorithm to determine the optimal geometry of a wave absorber oscillating about a fixed submerged horizontal axis. They used two objective functions to be minimized, which were the ratios of the submerged surface to the maximum absorbed power and the maximum reaction force to the maximum absorbed power. Geometric configurations of uniform simple cross-sectional shapes were considered, and for each configuration, the body dimensions as well as the submergence of the rotation axis were the variables to be optimized.

It is shown, later in this thesis, that, for the local sea with the energetic wave periods beyond 5 or 6 seconds, determining a WEC which will resonate within the dominant energetic wave frequency range of the real sea to absorb the maximum possible energy may lead to a quite non-practical solution due to the body large dimensions and prohibitively high costs. Efforts to design more economic systems have started since mid-1970s. Different control methods have been presented to maximize energy conversion e.g. [74][56][92]. The mentioned geometrical optimization works have been performed

for control-free WECs (the WECs without taking into account control strategy in any way), and the objective circumscribed the problem into maximizing the energy production. Since applying control forces on the system may result in changes in its characteristics, geometrical optimization processes that consider such effects is required. Recently, Garcia-Rosa et al [93] addressed the effect of three different control methods on the geometry optimization of a cylindrical PA. They applied an optimization process to determine the buoy dimensions (diameter and draught) that maximize the average absorbed power.

Chapter 3

3. Theoretical background

3.1 Introduction

The motion of a fluid can be described by the equation of continuity together with the Navier-Stokes equations. These equations are based on the conservation of mass and conservation of momentum respectively. The principle of Computational Fluid Dynamics (CFD) codes is based on the Navier-Stokes equations. Generally, the Navier-Stokes equations are difficult and time-consuming to solve because of the coupled system of non-linear partial differential equations. Hence, some assumption are often introduced to facilitate the analyses. In this thesis, the frequency domain analyses have been performed by ANSYS-AQWA, hydrodynamic diffraction analyses system, which is based on linear potential theory. The considered assumptions are; the fluid is non-viscous, irrotational, incompressible and without surface tension effect. In this chapter, based on these assumptions, some principles of hydrodynamics theory are described. However, there several literatures that provide further elaboration and more details such as [6,7].

3.2 Wave energy transport

The Airy theory or small amplitude wave theory is assumed to describe the energy transport by waves. Following the expressions presented in Journee's book "Offshore Hydrodynamics" [6], As it is shown in figure 3-1, considering a Virtual vertical plane $A\acute{A}$ perpendicular to the direction of the wave propagation, the work done by the fluid passes through the plane element with unit width and height of dz can be expressed as follow:

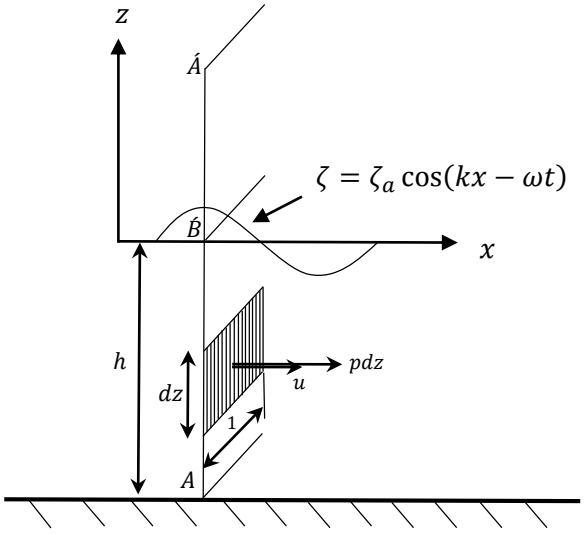

Figure 3-1– Wave energy transport [6]

$$dW = \{p.1.dz\}.\{u.dt\} \tag{3.1}$$

The power is the average work done over one period, T (considering linearization):

$$\bar{P} = \overline{W} = \frac{1}{T}\iint p.u.dz.dt \tag{3.2}$$

By neglecting the contribution of the upper part, $\acute{B}\acute{A}$:

$$\bar{P} = \frac{1}{8}\rho g H^2.\frac{c}{2}.\left(1 + \frac{2kh}{\sinh 2kh}\right) \tag{3.3}$$

Where $c = \omega/k$ is the phase velocity and $c_g = \frac{c}{2}.\left(1 + \frac{2kh}{\sinh 2kh}\right)$ is the wave group velocity, which is the velocity of the wave energy transport. The wave group velocity in deep and shallow water is equal to $c/2$ and c, respectively [6].
k is the wavenumber and is defined as:

$$k = \frac{2\pi}{\lambda} \tag{3.4}$$

Where λ is the wavelength derived from the dispersion relation [6] and can be expressed as:

$$\lambda = \frac{g}{2\pi}.T^2 \qquad \text{deep water} \tag{3.5}$$

$$\lambda = T.\sqrt{gh} \qquad \text{shallow water} \tag{3.6}$$

3.3 Energy density spectrum

The real sea surface changes continuously with time without repeating itself. Nevertheless, it is possible to represent the irregular sea surface using a linear superposition of a series of sinusoidal waves. Suppose an irregular wave record, $\zeta(t)$ that is sampled at a large number, N, intervals, Δt. The wave elevation (a time history of the

wave elevation during a sufficient long period,) of a long–crested irregular sea propagating in one direction can be expressed using Fourier series analysis as follow [6]:

$$\zeta(t) = \sum_{n=1}^{N} \zeta_{an} \cos(k_n x - \omega_n t + \varepsilon_n) \tag{3.7}$$

where:

N : is the number of components

ζ_{an} : is the wave amplitude component (m)

k_n : is the wave number component (rad/s)

ω_n : is the circular frequency component (rad/s)

ε_n : is the random phase angle component (rad)

A wave spectrum is used to represent the density distribution of the sea waves at a certain sea site and can be described by the following expression:

$$S_\zeta(\omega_n).\, d\omega = \frac{1}{2}{\zeta_{an}}^2 \tag{3.8}$$

The relationship between the wave energy spectrum and the waves can be explained better through the figure 3-2. The irregular wave history is transformed into the frequency domain as the sum of a large number of regular wave components, each with its own frequency, amplitude and phase. Calculating the $\frac{1}{2}{\zeta_{an}}^2/\Delta\omega$ value for each wave component on the ω-axis gives the wave energy spectrum $S_\zeta(\omega)$. The phases are random and usually can be discarded.

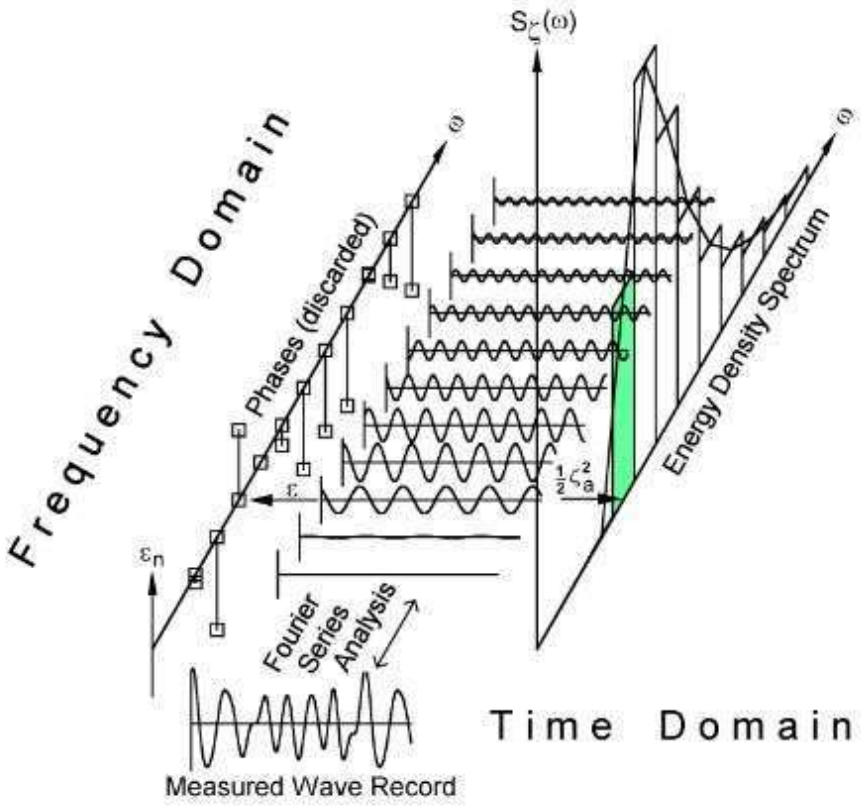

Figure 3-2 – Wave record analysis [6]

The most suitable spectrum is a measured wave spectrum at the local sea. However, the theoretical spectrum models that are based on the fetch, wind and other meteorological conditions of the site can be used as an alternative [7]. The mathematical spectrum models are generally based on one or more parameters, e.g., significant wave height, wave period, shape factors, etc. the most common single parameter spectrum is the Pierson-Moskowitz (1964) model which is based on the significant wave height or wind speed. The commonly used models with two parameters are Bretschneider (1969), Scott (1965), ISSC (1964) and ITTC (1966). JONSWAP wave spectra presented by Hasselman et al [94] is a five-parameter spectrum, but usually three of them are held constant [7]. It is used in this thesis, to analyze the wave converter device in irregular sea. The Joint North Sea Wave Project (JONSWAP) is an extensive measurement program, which was carried out along a line extending over 100 miles into the North Sea from Sylt Island, in 1968 and 1969. By considering a one directional wave propagation, the following definition of a Mean JONSWAP wave spectrum is advised by the 17th ITTC in 1984 for fetch-limited situation:

$$S_{\varsigma}(\omega) = \frac{320H_{1/3}^2}{T_p^4}\omega^{-5}exp\left\{\frac{-1950}{T_p^4}\omega^{-4}\right\}\gamma^A \quad (3.9)$$

in which:

$\gamma =$ is considered to be equal to 3.3

$$A = exp\left\{-\left(\frac{\frac{\omega}{\omega_p}-1}{\sigma\sqrt{2}}\right)^2\right\}$$

$\omega_p = \frac{2\pi}{T_p}$ is the circular frequency at spectral peak,

σ is a step function of ω. Its value for $\omega < \omega_p$ and $\omega > \omega_p$ is equal to 0.07 and 0.09, respectively.

$H_{1/3}$ is the significant wave height, defined as the average of the highest 1/3 of the waves in the record.

T_p is the peak period defined as the wave period with highest energy.

3.4 Wave-body interaction

3.4.1 Frequency domain analysis

A rigid body that is freely floating in waves has six degrees of freedom: three translational and three rotational degrees of freedom, figure 3-3.

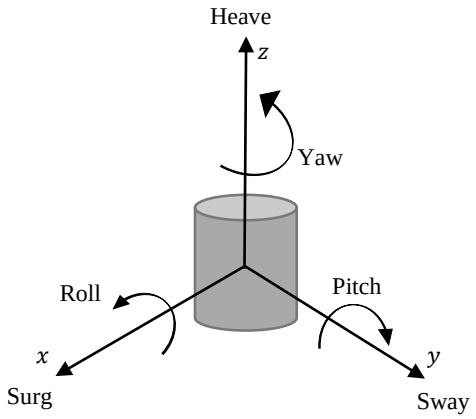

Figure 3-3 – Six degrees of freedom of a free-floating rigid body

- Surge: horizontal, longitudinal motion along the x-axis.
- Sway: horizontal, transverse motion along the y-axis.
- Heave: vertical motion along the z-axis.
- Roll: angular motion about the x-axis.
- Pitch: angular motion about the y-axis.
- Yaw: angular motion about the z-axis.

The motions of some structures are restricted to fewer degrees of freedom. For instance, the point absorber that is considered in this thesis is restrained to heave mode only.

In a real sea, the responses (motions) of a floating structure result from random waves with a known wave spectrum have an irregular behavior. Because of the simplicity of the analysis, the motions of an offshore structure are calculated in frequency domain. Then, the structure responses in an irregular sea can be obtained by making use of a superposition of these results at a range of frequencies [7]. Due to the linear behavior, the different ratios between the motion amplitudes and the wave amplitudes and also the phase shifts between the motions and the waves are constant at each frequency [6].

The dynamics of rigid bodies and fluid motions are governed by the combined actions of different external forces and moments as well as by the inertia of the bodies themselves [6]. Considering the linear theory, the resultant motion can be obtained as a superposition of the motion of the body in still water and the forces on the restrained body in waves. Figure 3-4 illustrates the superposition of the hydromechanical and wave loads considering two assumptions as follows:

1- Hydromechanical forces and moments that are induced by the harmonic oscillations of the rigid body, moving in the undisturbed surface of the fluid.
2- Wave exciting forces and moments that are generated by incoming waves applied on the restrained body.

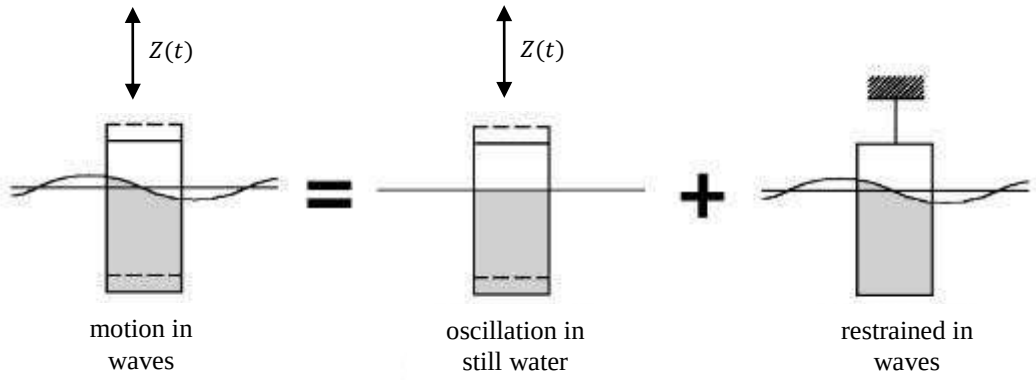

Figure 3-4 – Superposition of the hydromechanical and wave loads [6]

Based on the Newton`s second law:

$$\rho \nabla . \ddot{z} = F_h + F_w \tag{3.10}$$

where ρ is the density of the water, ∇ is the body displacement volume, F_h and F_w are the hydro mechanical and exciting wave force in the z-direction.

3.4.1.1 Hydromechanical forces

Imagine a free decay test in still water. The cylinder is released after applying a vertical displacement. The resultant motion dies out freely. The vertical motions of the cylinder can be determined by the mass of the cylinder and the hydromechanical loads on it. Applying the Newton's second law, the linear equation of the heave motion can be expressed as:

$$m\ddot{z} = F_h \tag{3.11}$$

$$F_h = -a\ddot{z} - b\dot{z} - cz \tag{3.12}$$

$$(m + a)\ddot{z} + b\dot{z} + cz = 0 \tag{3.13}$$

where z is the vertical displacement, $m = \rho A_w d$ is the solid mass of the cylinder, A_w is the water plane area, d is the cylinder draft at rest, a is the hydrodynamic mass coefficient

or added mass ($\frac{Ns^2}{m} = kg$), b is the hydrodynamic damping coefficient $\left(\frac{Ns}{m} = \frac{kg}{s}\right)$ and $c = \rho g A_w$ is the linear restoring spring coefficient ($\frac{N}{m} = \frac{kg}{s^2}$). The waves generated from the vertical oscillation of the cylinder transport its energy, and will damped as the oscillation fades. In a linear system, and by neglecting the viscosity, this so-called wave damping $b\dot{z}$ is proportional to the velocity of the cylinder [6]. The other term of the hydromechanical forces is $a\ddot{z}$ that is the reaction of the water particle resulting from the given acceleration of the cylinder. In contrast to the hydrodynamic damping, this term does not dissipate energy and manifests itself as a standing wave system near to the oscillator. The added mass and damping coefficients may be calculated experimentally or analytically. More details about these methods are provided in [6,7].

3.4.1.2 Wave exciting forces

Considering the second condition of the right hand side of the figure 3-4, the cylinder is restrained in waves, and the objective is to measure the vertical loads of the waves. Assuming the hydrodynamic linear theory the wave pressure on the bottom of the cylinder ($z = -d$) can be determined from the linearized Bernoulli Equation as follow:

$$\begin{aligned} &= -\rho \frac{\partial \Phi}{\partial t} - \rho g z \\ &= \rho g \zeta_a e^{-kd} \cos(\omega t - kx) + \rho g d \end{aligned} \tag{3.14}$$

The vertical force, considering a uniform distribution of the pressure on the bottom of the cylinder, is:

$$F = \{\rho g \zeta_a e^{-kd} \cos(\omega t) + \rho g d\}. \frac{\pi}{4} D^2 \tag{3.15}$$

This expression represents the wave exciting force assuming that the diameter of the cylinder is small relative to the wavelength ($KD < 0.5$). It implies that the incident waves upon arriving at the structure do not undergo significant scattering or diffraction, therefore the effect of diffraction of waves from the surface of the cylinder can be neglected [7][95].

The first part of this force that results from the integration of the wave pressure on the body in an undisturbed wave is called the Froude-Krylov force. This force can be rewritten as:

$$F_{FK} = c.\zeta^* \tag{3.16}$$

in which:

$$c = \rho g \frac{\pi}{4} D^2$$

$$\zeta^* = e^{-kd}.\zeta_a \cos(\omega t) \qquad \text{deep water} \tag{3.17}$$

where c is the spring coefficient and ζ^* is the reduced or effective wave elevation [6].

3.4.2 Time domain analysis

The hydromechanical reaction forces and moments, due to time varying ship motions, can be described using the classic formulation given by Cummins (1962) [96]. Considering the hydrodynamic linear theory assumption, the equation of motion for a floating object in waves can be expressed as follow:

$$(M + A).\ddot{x}(t) + \int_{-\infty}^{t} B(t-\tau).\dot{x}(t).d\tau + C.x(t) = X(t) \tag{3.18}$$

where:

$\ddot{x}(t)$: is the translational (or rotational) acceleration at time t (m/s^2)

$\dot{x}(t)$: is the translational (or rotational) velocity at time t (m/s)

$x(t)$: is the translational (or rotational) displacement at time t (m)

M : is the solid mass or mass moment of inertia (kg)

A : is the hydrodynamic (or added) mass coefficient (kg)

$B(t), B(\tau)$: are the retardation functions (Ns/m)

C : is the spring coefficient from body geometry (N/m)

$X(t)$: is the external load at time t (N)

t, τ : are time (s)

Assuming a linear restoring (hydrostatic) spring coefficient. The coefficients A and B can be found through a method which was presented by Ogilvie [97], as follows (a detailed description of the mathematics can be found in [6,97]):

$$B(\tau) = \frac{2}{\pi}.\int_0^\infty b(\omega).\cos(\omega\tau).d\omega \tag{3.19}$$

$$A = a(\omega) + \frac{1}{\omega}.\int_0^\infty B(\tau).\sin(\omega\tau).d\tau \tag{3.20}$$

where $a(\omega)$ and $b(\omega)$ are the frequency-dependent hydrodynamic mass and damping coefficients with units of $(\frac{Ns^2}{m} = kg)$ and (Ns/m) respectively. The expression for A is valid for any value of ω. For $\omega = \infty$, the expression becomes:

$$A = a(\infty)\ , \qquad \text{infinit added mass} \tag{3.21}$$

Assuming a linear first order wave force, the right hand side of the Eq.(3.18) can be calculated using the superposition principles by summing the frequency domain characteristics of the first order wave loads and the wave spectrum as follow:

$$X_\omega(t) = \sum_{n=1}^{N} \left(\frac{X_{\omega an}}{\zeta_{an}}\right).\zeta_{an}\cos\left(\omega_n t + \varepsilon_n + \varepsilon_{X_\omega\zeta_n}\right) \tag{3.22}$$

in which:

$X_\omega(t)$: is the wave load (N)

N : is the number of frequencies

ω_n : is the wave frequency (rad/s)

$\frac{X_{\omega an}}{\zeta_{an}}$: is the transfer function of wave load (N/m)

$\varepsilon_{X_\omega\zeta_n}$: is the phase shift of wave load (rad)

ε_n : is the phase shift of wave (rad) which is randomly chosen between 0 and 2π

Knowing the hydrodynamic coefficients and the wave force, the equation of motion, Eq.(3.18), can be integrated to obtain the responses in time domain.

Chapter 4

4. Geometrical optimization of a control-free point absorber in frequency domain

4.1 Introduction

This chapter presents a geometry optimization methodology, as a preliminary approach, applied on a control-free one-body point absorber, considering the nearshore region of Rio de Janeiro, Brazil as the sea site. The WEC consists of a floating cylinder (with diameter D and draft L), which reacts against the seabed with an ideal pure damper as the PTO system (PTO stiffness is zero), figure 4-1. The optimization process has been developed through linear hydrodynamic frequency domain analyses and the design of experiments (DOE) approach. Minitab [98] is used to apply the DOE and perform statistical analysis of the optimization process. The frequency domain analysis of the system hydrodynamics is performed using ANSYS-AQWA [99]. The diameter and draft of the floating cylinder (buoy) are considered as the geometrical parameters to be optimized. The objective of the optimization process is to determine the buoy that absorbs the maximum wave energy over the largest range of frequencies for the site's prevailing waves. The presented methodology can be applied to geometrical optimization of different types of wave energy converters. To understand the requirements (objectives) that should be satisfied in order to obtain the optimum buoy, it is necessary to know the principles of the wave absorption by a wave energy system. The next section describes wave absorption by a control-free heaving point absorber.

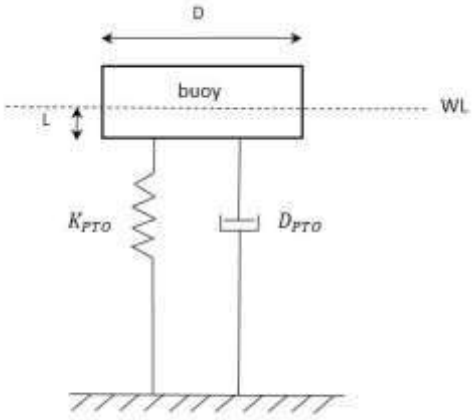

Figure 4-1 - Generic point absorber with a PTO system ($K_{pto} = 0$) in reference to the seabed

4.2 Wave absorption by a heaving point absorber

4.2.1 Optimum oscillation

As it is defined by Falnes [100], "absorbing wave energy for conversion means that energy has to be removed from the waves". It occurs when an oscillating body radiated waves that interfere destructively with the incoming waves. It is shown in [41–43] that a symmetrical body oscillating in one mode of oscillation (i.e. *heave*) is able to absorb only 50% of the wave energy.

To have an optimum absorption, two following conditions should be satisfied; optimum phase and optimum amplitude [40]. The optimum phase condition for an oscillating body in heave direction occurs when it is in resonance with the waves. It means that the oscillation velocity of the body is in phase with the wave excitation. The optimum amplitude condition can be satisfied through an optimum value of the power take-off (PTO) resistive load. The next section describes the expressions presented by Falnes [100] in frequency domain for calculating the maximum absorption by a point absorber.

4.2.2 Maximum absorbed power

Figure 4-2 illustrates a generic heaving point absorber connected to the seabed through a PTO system. The idealized PTO provides the required stiffness (spring coefficient) K_{PTO} and damping (mechanical resistance) D_{PTO}. Let us consider an incident wave applying on the buoy as the external sinusoidal force. The buoy responds to the incident wave force by oscillating with a velocity u (velocity in heave direction). Applying the complex representation of a harmonic oscillation presented by Falnes [100] and assuming the linear theory, the dynamic equation of the floating body coupled with a PTO system can be expressed as:

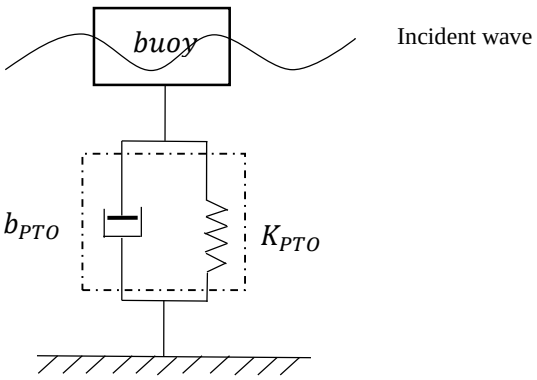

Figure 4-2 - Generic model of a heaving point absorber connected to the seabed through a PTO system

$$\left[i\omega(m + a_{33}) + b_{33} + \frac{C_{33}}{i\omega}\right]\hat{u}_3 = \widehat{F}_{e,3} - \widehat{F}_{PTO} \tag{4.1}$$

where m is the mass of the buoy, a_{33}, b_{33} and C_{33} are the added mass, hydrodynamic damping coefficient and stiffness coefficient, respectively. $\hat{u}_3$ is the complex velocity amplitude; $\widehat{F}_{e,3}$ is the complex amplitude of the excitation force for heave motion; $\widehat{F}_{PTO}$ is the complex amplitude of the PTO force and ω is the wave circular frequency. The PTO force can be written as [100]:

$$Z_{PTO}\hat{u}_3 = \widehat{F}_{PTO} \tag{4.2}$$

Where $Z_{PTO} = b_{PTO} + k_{PTO}/i\omega$ is the PTO impedance (considering that the PTO consists of stiffness and damping).

Then the equation 4.1 can be rewritten as:

$$\left\{i\omega(m + a_{33}) + b_{33} + \frac{C_{33}}{i\omega} + b_{PTO} + \frac{k_{PTO}}{i\omega}\right\}\hat{u}_3 = \widehat{F}_{e,3} \tag{4.3}$$

or:

$$\left\{(b_{33} + b_{PTO}) + i\left[\omega(m + a_{33}) - \frac{C_{33} + k_{PTO}}{\omega}\right]\right\}\hat{u}_3 = \widehat{F}_{e,3} \tag{4.4}$$

Thus the solution is obtained as:

$$\hat{u}_3 = \frac{\widehat{F}_{e,3}}{(b_{33} + b_{PTO}) + i\left[\omega(m + a_{33}) - \frac{C_{33} + k_{PTO}}{\omega}\right]} \tag{4.5}$$

The time-average absorbed power by the PTO system can be calculated as:

$$\bar{P} = \frac{b_{PTO}}{2}|\hat{u}_3|^2 \tag{4.6}$$

Substituting the $\hat{u}_3$ applying equation (4.5) gives:

$$\bar{P} = \frac{\left(\frac{b_{PTO}}{2}\right)\left|\widehat{F}_{e,3}\right|^2}{(b_{33} + b_{PTO})^2 + \left(\omega(m + a_{33}) - \frac{C_{33} + k_{PTO}}{\omega}\right)^2} \tag{4.7}$$

It is shown in [100] that the optimum PTO damping can be obtained using $\partial\bar{P}/\partial b_{PTO} = 0$. As the result:

$$b_{PTO,opt} = \left\{{b_{33}}^2 + \left[\omega(m + a_{33}) - \frac{C_{33} + k_{PTO}}{\omega}\right]^2\right\}^{1/2} \tag{4.8}$$

Thus, the maximum absorbed power at each frequency can be calculated by substituting the optimum b_{PTO} in the Eq.(4.6) as follow:

$$\bar{P}_{max} = \frac{1}{4}\frac{\left|\widehat{F}_{e,3}\right|^2}{b_{33} + \left\{{b_{33}}^2 + \left[\omega(m + a_{33}) - \frac{C_{33} + k_{PTO}}{\omega}\right]^2\right\}^{\frac{1}{2}}} \tag{4.9}$$

The optimum value of the PTO damping satisfies the optimum amplitude condition. Another requirement that must be fulfilled is the optimum phase, which is satisfied when the oscillation velocity phase is equal to the phase of the wave excitation. As it described by Falnes, it is occurred when the ratio between the complex amplitudes $\widehat{u}_3$ and $\widehat{F}_{e,3}$ is a real [100]. Therefore, the optimum phase condition can be expressed as follow:

$$\omega(m + a_{33}) - \frac{C_{33} + k_{PTO}}{\omega} = 0 \tag{4.10}$$

Applying the optimum phase and amplitude condition the maximum absorbed power can be expressed as:

$$\bar{P}_{MAX} = \left|\widehat{F}_{e,3}\right|^2 / (8b_{33}) \tag{4.11}$$

This expression shows that the maximum absorbed power by a symmetric point absorber occurs at the resonance frequency applying a PTO damping equal to the corresponding hydrodynamic damping of the oscillating body in that frequency.

4.3 Optimization process

4.3.1 Methodology approach

From the previous section (section 4.2), we know that the optimum buoy needs to satisfy three principle requirements as follow:

1- Buoy heave natural frequency, which should be within the prevailing sea wave frequencies to guarantee the maximum energy absorption.
2- Resonance bandwidth, which is defined as the frequency interval where the buoy mechanical power exceeds half of the maximum value; to guarantee the maximum frequency range of absorption.
3- Maximum mechanical power which is required to be maximum.

A methodology has been developed to find a set of geometrical parameters (factors) to optimize the point absorber in relation to the mentioned three primary requirements (responses). A simple wave energy converter is used as the WEC system for the optimization study. The wave energy converter is a generic heaving PA of a cylinder (buoy) with a diameter D and a draft L, as illustrated in figure 4-1. The point absorber is

a single body device with reference to the seabed. The analyses are carefully defined to consider the requirement that the WEC device has to absorb the maximum energy in the largest range of wave frequencies. The optimization process is a combination of hydrodynamic analysis in frequency domain and design of experiment (DOE) method as a statistical analysis. Figure 4-3 illustrates the optimization process. As indicated, the first step in the optimization process is to provide information regarding the sea characteristics of the site where the WEC will be installed, e.g., significant wave height, mean period and water depth (or bathymetry, for shallow water cases). The second step, which is called "immature determination", is the definition of the upper and lower bounds for the buoy diameter and draft. Within these bounds, a set of geometrical parameters are obtained for the buoy. The third step is to compute the primary WEC requirements, what we call "responses" in this study, (heave natural frequency, resonance bandwidth and maximum mechanical power) in the frequency domain and apply the DOE method. In the next step, which is called "mature determination", the results of the previous steps are analyzed, and the optimized buoy geometries are selected based on the statistical analyses results, which will be explained later. In contrast to the methodologies that have been presented so far (see section 2.4), due to the application of the DOE method as a statistical analysis, a few runs (13 runs) must be performed to optimize the responses. It should be noted that for the optimization with more than two geometrical parameters, the number of required runs could be slightly increased. Furthermore, the graphical results of the statistical analyses such as contour and surface plots offer a broad view of the optimization problem domain that give us the ability of discussing and comparing the effect of all the possible sets of geometrical parameters on the responses.

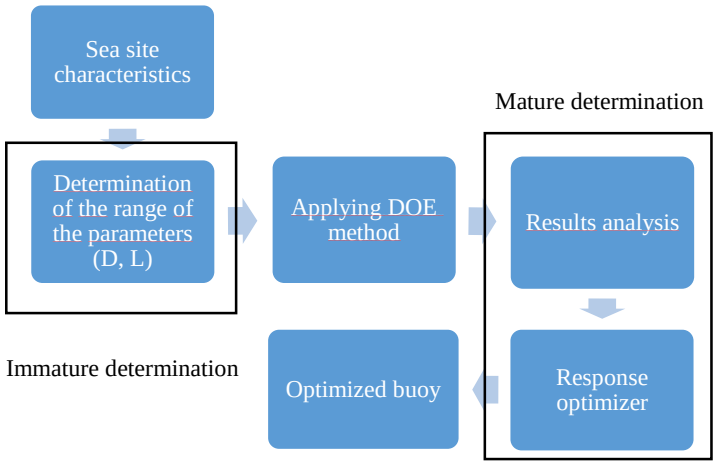

Figure 4-3 - Geometry optimization process of the WEC

4.3.2 Sea characteristics

The information on the wave climate is obtained by either *in situ* measurements or numerical modeling. Third generation spectral wave models have emerged as a reliable tool for forecasting and hindcasting ocean conditions. The use of these models in hindcast mode allows for an assessment of the global wave climate [101] and the energy resources [102–104]. The wave power assessment along the Brazilian coast has been discussed in several studies [105,106]. To describe the nearshore wave climate on the Rio de Janeiro coast, a wave hindcast for five years was developed [107] with the third generation wind wave model WAVEWATCH III (WW3) version 3.14 [108] using the NCEP's Climate Forecast System Reanalysis (CFSR) wind database [109].

The wave statistics on the Rio de Janeiro coast are presented in terms of their joint probability distribution (JPD) in Figure 4-4, which indicates the probability of both a significant wave height and a wave peak period occurring for a given location. There is a dominance of peak periods between 7 - 9 seconds for a Hs between 0.5 and 1 meter with occurrence of 17.3%. Furthermore, the majority of waves have a height of less than 2 meters, and only 2.2% of the waves are more than 3 meters in height. The predominant waves have periods between 7 and 13 seconds with an occurrence of 86%. The average significant height was $Hs = 1.33\,m$, and the wave peak period was $Tp = 9.7\,s$. The average wave energy spectrum based on the wave hindcast is illustrated in Figure 4-5. The primary spectral characteristic determined from the average spectrum is the presence of large amounts of energy at a frequency between 0.14 and 0.076 Hz (7.14 and 13.16 s). The peak of this average spectrum was 0.0908 Hz (11 s).

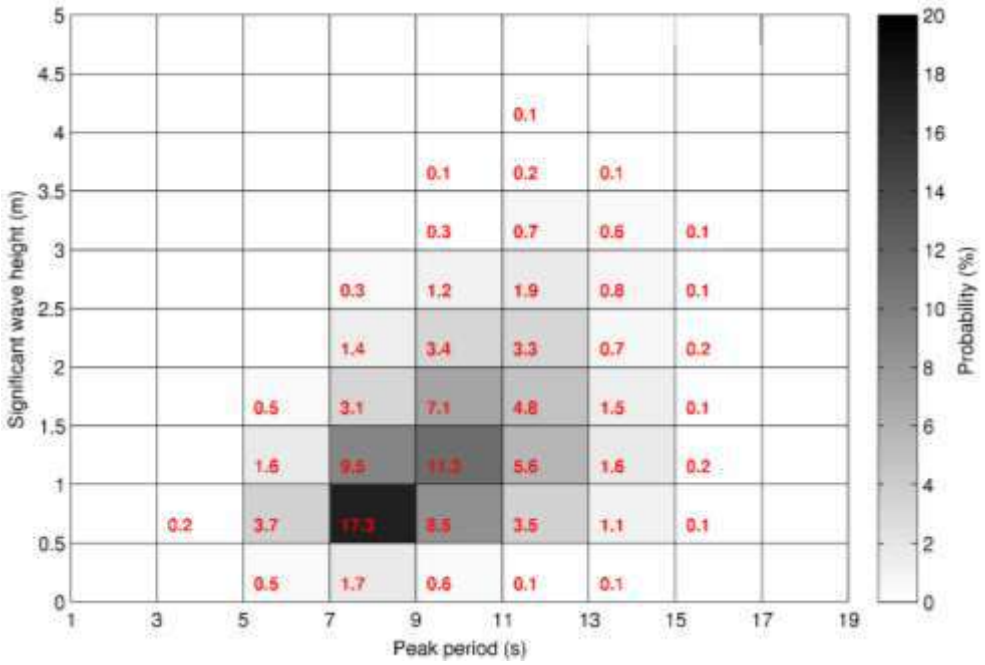

Figure 4-4- Joint Probability Distribution (%) for the nearshore region of Rio de Janeiro [107]

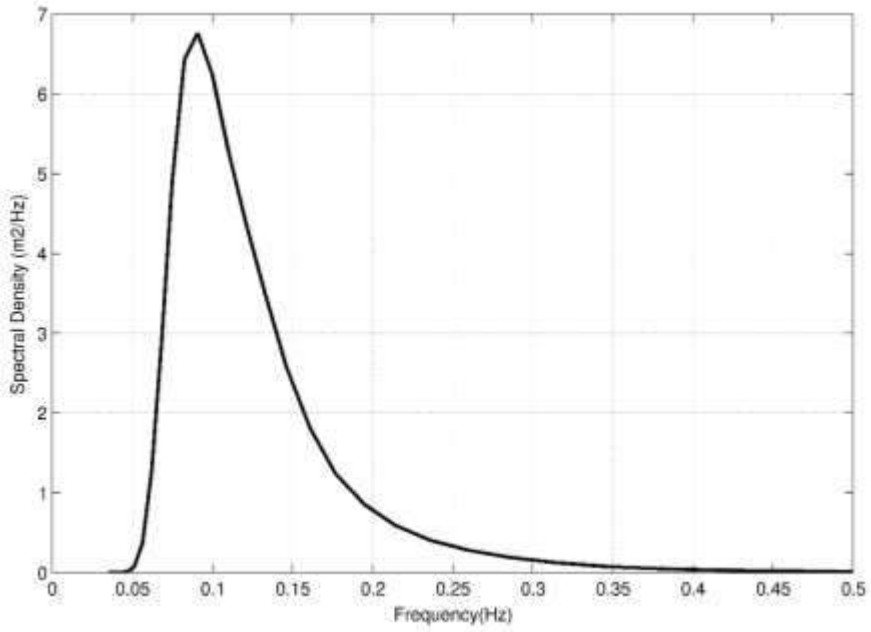

Figure 4-5 - Average spectral density (m²/Hz) based on the hindcast from 2006 to 2010 for the nearshore region of Rio de Janeiro [107]

The total stored energy, *E*, in a wave per unit area of sea surface in terms of the significant wave height (*Hs*) can be computed directly from the hindcast data as follows [6]:

$$E = \frac{\rho g {H_s}^2}{16} \tag{4.12}$$

where ρ is the density of the fluid; and g is the acceleration due to gravity. The wave power level, P, per width unit in a wave in terms of the significant wave height (Hs) and the energy period (Te) can be given as follows:

$$P = \frac{\rho g^2 {H_s}^2 T_e}{64\pi} \tag{4.13}$$

The measured sea states are often specified in terms of the significant wave height Hs and either the peak period Tp or the mean period Tz. The energy period Te is rarely specified and must be estimated from other variables. When the peak period Tp is known, one potential approach can be assumed as follows:

$$T_e = \alpha T_p \tag{4.14}$$

where the coefficient α depends on the frequency spectrum model, which was assumed to be equal to 1 [110]. Eq.(4.13) is a deep water approximation and has been used in this study to describe the wave power for the nearshore region of Rio de Janeiro. By considering an average significant height, $Hs = 1.33\, m$, and a wave energy period, $Te = Tp = 9.7\, \boldsymbol{s}$, for the sea site and applying Eq.(4.13), the resultant wave power level per unit width is approximately 8.5 kW/m.

Figure 4-6 illustrates a combined scatter and energy diagram to visualize the composition of the wave energy resource in terms of wave heights and periods. The numerical values represent the probability of occurrence of a combination of significant wave heights and peak period in percentage. The peak period and significant wave height are divided into intervals of 2 s and 0.5 m, respectively. Color scale represents annual wave power level (in $MWh/m\ year$). As it shown, the most energetic waves have significant wave heights between 1.5 m and 2.0 m with peak periods between 9 s and 11 s, which represents only 7.1% of the total number of waves per year.

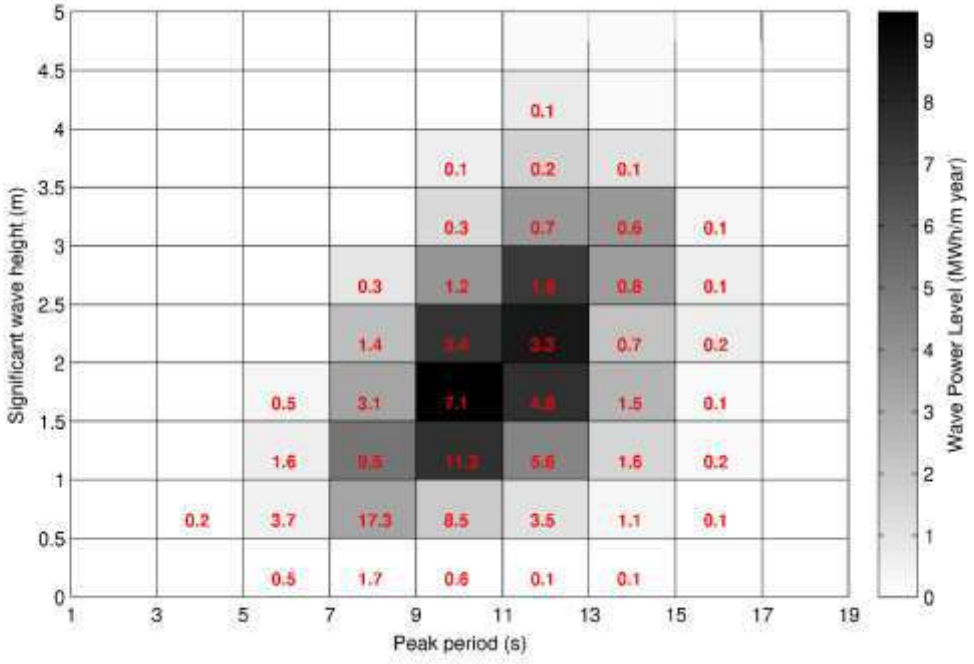

Figure 4-6 - Combined scatter and energy diagram: the colors denote the annual wave power level (MWh/m year), and the numbers indicate the probability occurrence per year (%) in terms of significant wave height and peak period [107]

4.3.3 Immature determination

As mentioned in previous sections, the optimization of the buoy starts by an immature determination, which includes the definition of the upper and lower bounds for its diameter and draft, $D1$ and $L1$, respectively. These bounds should satisfy two design premises. The first one is associated with the maximum amount of power that the buoy can absorb from incident waves, and the second one is related to the maximum buoy response in heaving due to the incident waves. Evidently, both premises are related to the

waves' characteristics, specifically the range of predominant wave periods at the WEC's installation site.

4.3.3.1 Upper and lower bounds of the diameter

The first premise requires that the maximum possible energy available from the incident wave is absorbed by the buoy. The fundamental quantity employed to evaluate the WEC performance is "capture width' or "absorption width". At a given frequency this is defined to be the ratio of the total mean power absorbed by the oscillating body to the mean power per unit crest waves width of the incident wave train, where mean refer to the average value per wave period for regular waves or per energy period for irregular waves [111]. Capture width has the dimension of length, however, sometimes the non-dimensional capture width, which is the ratio of the capture width to the width of the device, may be used to assess its performance. The maximum energy that may be absorbed by a heaving axisymmetric body equals the wave energy transported by the incident wave front of width equal to the wavelength divided by 2π [41,42,45]. The maximum capture width L_{max} can be defined as follows:

$$L_{max} = \lambda/2\pi \tag{4.15}$$

Then, the maximum wave power P_{max} absorbed by a heaving axisymmetric body can be given as follows:

$$P_{max} = JL_{max} \tag{4.16}$$

where J is the energy flux per unit wave crest width. For linear deep water waves, according to Eq.(3.3) for energy transport of waves and Eq.(3.5) for the wavelength, we can obtain:

$$J = \rho g^2 T H^2/32\pi \tag{4.17}$$

Where ρ is the water density, T and H are the period and height of the regular wave. If the capture width is divided by the device's width (e.g., the buoy diameter, $D1$), we can

obtain the non-dimensional or relative capture width, C_{wr}, which, for successful devices, should satisfy (recommended by Twidell and Weir) [112] the expression as follows:

$$C_{wr} = \frac{L_{max}}{D_1} \geq 3 \tag{4.18}$$

Based on Eq.(4.18) and knowing that the predominant wave periods for the nearshore region of Rio de Janeiro are between 7 s and 13 s, the upper bound of $D1$ can be established for both limits: for the 7 s wave, $D1 \leq 4\ m$, and for the 13 s wave, $D1 \leq 14\ m$. Additionally, there is a practical rule for a point absorber used as a WEC, presented bay Falnes [27], that recommends that the point absorber diameter should preferably be in the range of 5% to 10% of the prevailing wavelength. For the nearshore region of Rio de Janeiro, the prevailing wavelength corresponds to the wave peak period ($Tp = 9.7\ s$); thus, the recommended range for the buoy diameter, according to Falnes' recommendation, would be $7 \leq D1 \leq 14\ m$. The upper value is in good agreement with the one obtained from the wave capture width consideration for the 13 s wave. However, there is a disagreement between the lower bound of the Falnes recommendation and the bound given by the capture width for the 7 s wave. Although the capture width suggests buoy diameters smaller than 4 m, the practical rule recommends buoy diameters exceeding 7 m. For the optimization process, it is desirable to cover a wider range of buoy diameters; hence, the bounds for $D1$ will be taken as $4 < D1 < 14\ m$.

4.3.3.2 Upper and lower bounds of the draft

Once the lower and upper bounds of $D1$ are defined, the draft of the buoy may be determined. Now, the second design premise for the buoy will be used, i.e., the range of heave natural periods of the buoys should match the range of predominant wave periods of the WEC installation site. Assuming a one degree-of-freedom free-floating body the buoy heave natural frequency ω_{n3} can be given as follows:

$$\omega_{n3} = \sqrt{\frac{\rho g A_{wp}}{M + A_{33}}} \tag{4.19}$$

where A_{wp} is the buoy water plane area, which is a function of the buoy diameter ($D1$); M is the mass of the buoy based on the submersed volume (i.e., $D1$ and $L1$); and A_{33} is the added mass coefficient, which can be calculated at this preliminary stage as follows [113]:

$$A_{33} = 0.167\rho D_1^3 \tag{4.20}$$

To trigger the buoy resonance motions, Eq.(4.19) should be set equal to the incident wave frequency. For the sea site's prevailing wave periods (7 to 13 s) and the range of buoy diameters obtained in Section 4.3.3.1 (4 to 14 m), a set of values for the buoy draft ($L1$) that causes the buoy to resonate within a range of prevailing waves was determined, as indicated in table 4-3.

Table 4-1- Resonant buoys (the cell colors are used to identify the magnitude of the draft)

$Lmax$ (m)	λ (m)	Period (s)	14	13	12	11	10	9	8	7	6	5	4	Diameter, D1 (m)
6.2	39.0	5.0	3.2	3.4	3.7	3.9	4.1	4.3	4.5	4.7	4.9	5.1	5.4	Draft, L1 (m)
8.9	56.2	6.0	6.0	6.2	6.4	6.6	6.8	7.0	7.2	7.5	7.7	7.9	8.1	
12.2	76.5	7.0	9.2	9.4	9.6	9.8	10.1	10.3	10.5	10.7	10.9	11.1	11.3	
15.9	99.9	8.0	12.9	13.1	13.4	13.6	13.8	14.0	14.2	14.4	14.6	14.8	15.0	
20.1	126.5	9.0	17.2	17.4	17.6	17.8	18.0	18.2	18.4	18.6	18.9	19.1	19.3	
24.8	156.1	10.0	21.9	22.1	22.3	22.5	22.7	22.9	23.1	23.4	23.6	23.8	24.0	
30.1	188.9	11.0	27.1	27.3	27.5	27.7	27.9	28.2	28.4	28.6	28.8	29.0	29.0	
35.8	224.8	12.0	32.8	33.0	33.2	33.4	33.7	33.9	34.1	34.3	34.5	34.7	35.0	
42.0	263.9	13.0	39.0	39.2	39.4	39.7	39.9	40.1	40.3	40.5	40.7	40.9	41.0	

Within each table cell, the value of the draft is listed for several buoy diameters that satisfy the maximum capture width condition for a given wave period to make the buoy resonate during heaving. The cell colors are used to identify the magnitude of L_1 (green for smaller values and red for the larger ones) so that the corresponding upper and lower bounds for L_1 can be easily established:$3 < L1 < 42\,m$. Nevertheless, because this range is excessively wide, a few additional considerations should be noted to narrow the limits for $L1$. Based on the typical linear responses of a mass-spring-damper system under harmonic external excitation, a few preliminary conclusions may be stated regarding the responses in waves for a point absorber. As illustrated in figure 4-7, the vertical axis represents the heave RAO of an oscillating cylinder in regular waves and the horizontal

one shows the ratio of the wave frequency to the cylinder natural frequency. Three frequency area for the heave response of the oscillating cylinder to the regular waves can be distinguished.

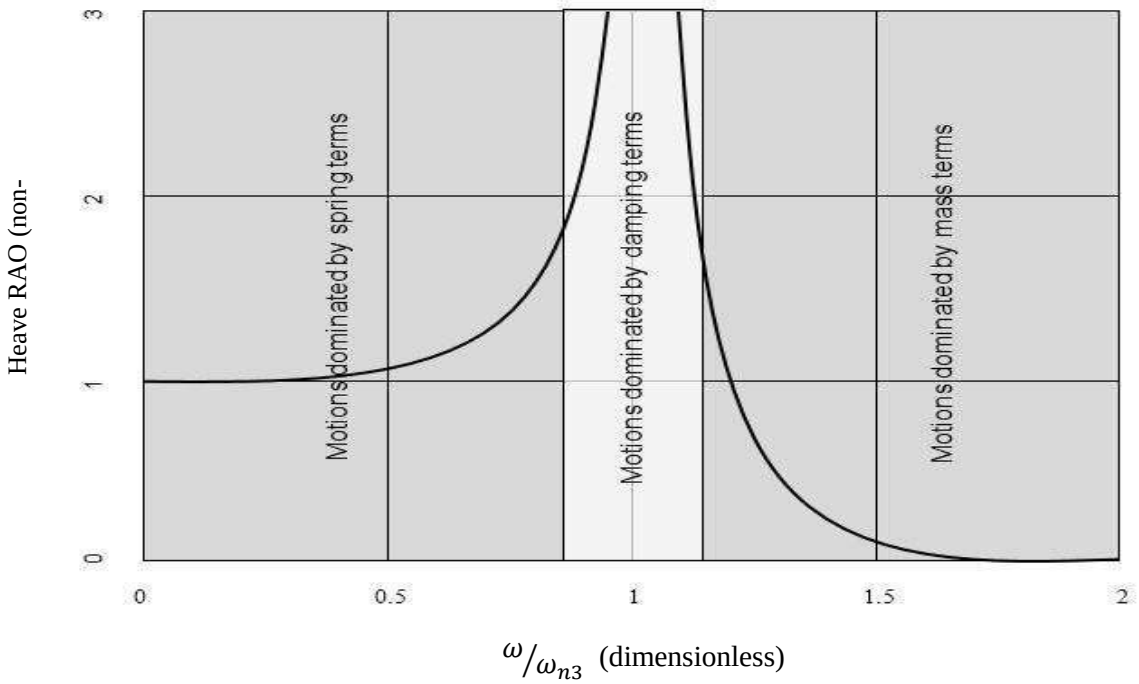

Figure 4-7 – heave motion behavior of an oscillating cylinder in frequency domain [6]

In the resonance region, ${\omega_{n3}}^2 \approx \frac{\rho g A_{wp}}{M+A_{33}}$, the body responses are dominated by damping term, and the responses can achieve relatively large amplitudes when the damping is small. In the low-frequency region, ${\omega_{n3}}^2 \ll \frac{\rho g A_{wp}}{M+A_{33}}$, the body responses are dominated by the restoring spring term. At very low frequencies, the wavelength is large when compared to the horizontal length (diameter) of the buoy, and it will "follow" the waves, upwards and downwards. In the high frequency region, ${\omega_{n3}}^2 \gg \frac{\rho g A_{wp}}{M+A_{33}}$, the buoy responses are dominated by mass, which indicates that the waves "lose" their influence on the behavior of the buoy; there are several wave crests and troughs within the horizontal length (diameter) of the buoy [6]. From the above statement, it can be concluded that to harness the wave energy for a wider range of wave periods, it is desirable to design a buoy whose natural period is tuned with the lowest prevailing wave period (or perhaps, less) so that it works in the resonance region for the shorter wave

lengths (lower wave periods) and "follows" the waves for the longer waves (higher wave periods). Thus, the region where the waves "lose" their influence is minimized. In conclusion, to guarantee a wider operational wave scenario for the WEC, shorter natural periods should be selected. Therefore, from table 4-3, we can select heaving natural periods between 5 and 7 s such that the limits for $L1$ can be updated to $3 < L1 < 12\ m$. Table 4-4 summarizes the upper and lower bounds for D_1 and L_1, as determined from the previous sections.

Table 4-2 – Upper and lower bounds for the buoy's geometrical parameters

	Lower bound	Upper bound
$D1\ (m)$	4	14
$L1\ (m)$	3	12

4.3.4 Applying DOE method

The design of experiments (DOE) is a systematic technique for studying any situation that involves a response that varies as a function of one or more independent variables. The DOE can address complex problems where more than one variable may affect a response (or a set of responses) and two or more variables may interact with each other. The technique provides answers to specific questions on the behavior of a system requiring an optimum number of experimental observations.

In this thesis, so far a range of primary dimensions has been defined for the WEC: $4 < D1 < 14\ m$ and $3 < L_1 < 12\ m$. Theoretically, an infinite number of solutions is possible. The main task is to determine the optimal solution without having to perform a large number of simulations. In fact, by applying the DOE method, it is possible to study the performance of hundreds of buoys in the mentioned range using just a few computer runs (13 buoys), as indicated in Table 4-5.

Table 4-3 – The determined buoy by DOE to be analyzed (the designed experiments)

	1	2	3	4	5	6	7	8	9	10	11	12	13
$D1\ (m)$	5.46	14	9	4	9	12.5	5.5	9	9	9	9	12.5	9
$L1\ (m)$	10.68	7.5	7.5	7.5	7.5	4.3	4.3	7.5	12	7.5	7.5	10.7	3

Each process has inputs that determine the behavior of a system as well as outputs that are produced by the process. The objective of doing an experiment (or "computer simulation" in this thesis) is to determine how the inputs affect the outputs. The goal of engineering experimentation is to learn how to control the process inputs to generate the desired outputs. The process inputs are called "factors" or "variables" whereas the process outputs are called "responses". The primary advantages of using DOE method can be stated as follows:

- Screening the factors to determine which are important for explaining the process variation (this is more applicable when the number of factors is more than 3),
- Understanding how factors interact and drive the process,
- Finding the factor settings that produce optimal process performance,
- Decreasing the number of experiments or runs and time-saving.

There can be several experiments designed for a specified number of design variables; however, the extreme designs that encompass all of the others are called "screening experiments" and "response surface experiments". Screening experiments are used when the objective is the study of a large number of design variables to determine the most important ones rather than the interactions between pairs of variables. The response surface experiments are capable of providing the primary effects of the variables, factors interactions and terms to measure the curvature induced in the response by each design variable [114]. Hence, the response surface method (RSM) is applied to use the sequence of designed experiments to obtain an optimal response or combination of responses.

As it was discussed in the section 4.3.1, three principle requirements must be satisfied to have an optimum, or almost optimum, wave absorption in a certain range of wave frequencies. Accordingly, the optimum control-free buoy must be designed to have a natural frequency close to the peak frequency of the sea site spectrum, a sufficiently wide resonance bandwidth to absorb the predominant wave frequencies and the maximum energy absorption. By considering a certain natural frequency as the goal, the response variable is defined as the combination of the maximum absorbed power and resonance bandwidth which provides a heaving point absorber that absorbs the maximum energy within the broadest range of frequencies. The resonance bandwidth is defined as the frequency interval in which the absorbed power is more than half of its maximum value.

4.3.5 The point absorber modeling in frequency domain by ANSYS AQWA

4.3.5.1 Introduction

The wave energy converter simulations, in time domain or frequency domain, usually rely on the application of boundary element methods (BEM), which is also referred as boundary integral equation methods (BIEM) or panel methods. In contrast to the finite element method (FEM), where the fluid volume is discretized, in the boundary element method the numerical discretization is applied on the boundary of an object. Different BEM codes, e.g. WAMIT, AQUADYN, NMIWAVE, ACHILD3D etc., have been developed to analyze the wave energy devices [4, 5, 6, 7, 10, 11, 19].

ANSYS AQWA is another software that provides an engineering toolset for the investigation of the effects of wave, wind and current on floating and fixed offshore and marine structures in both frequency and time domain. Like WAMIT (and other BEM codes), ANSYS AQWA uses boundary element method to find diffraction and radiation velocity potentials. Excitation forces, added mass and damping matrices, as well as wave field pressure, velocity, and surface elevation can be determined by solving the diffraction and radiation velocity potential fields. In this thesis, the AQWA Hydrodynamic Diffraction feature is used to calculate the primary hydrodynamic coefficients required for undertaking the time domain analysis.

4.3.5.2 ANSYS AQWA inputs

A geometry must be attached to the Aqwa hydrodynamic diffraction feature in order to perform a hydrodynamic analysis. The geometry can be modeled in the ANSYS DesignModeler application which is a parametric feature-based modeler. As an example, figure 4-8 shows a buoy with diameter of 6 m and draft of 1.5 m, modeled in ANSYS. As it is illustrated, the submersed part is separated from the upper part by the waterline.

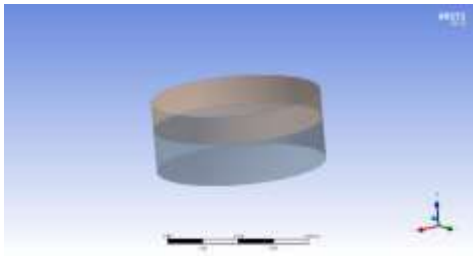

Figure 4-8 – The buoy with diameter of 6 m and draft of 1.5 m, modeled in ANSYS DesignModeler

After attaching the geometry to the hydrodynamic system, the required inputs for a frequency domain analysis including, water depth, center of gravity of the object, radii of gyrations, wave heading angles, range of wave frequencies, meshing etc., must be provided. Figure 4-9 shows the 3-D meshed geometry of the buoy.

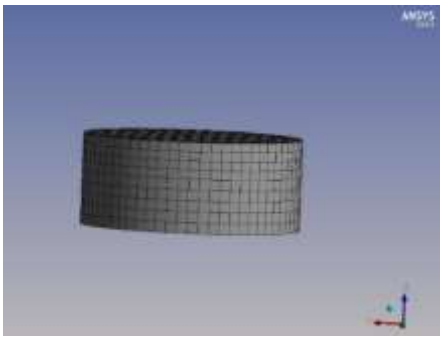

Figure 4-9 – The 3D meshed geometry of a buoy with diameter of 6 m and draft of 1.5 m,

Once the meshed model is created and the inputs are provided the diffraction and radiation analysis can be performed to calculate the wave forces, structure responses as well as the hydrostatic analysis.

4.3.5.3 Equation of motion

In the preliminary hydrodynamic modeling of the WECs, it is typically assumed that the hydrodynamic forces of the floating body in waves are those obtained from the linear diffraction theory, i.e., viscous effects are neglected and only potential forces are considered. Because the primary mechanism for the energy extraction of the proposed point absorber is the heave motion, at this preliminary stage, only the heave motion of the floater will be considered. Thus, the motion equation can be given as follows:

$$(M + A_{33})\ddot{x}_3 + B_{33}\dot{x}_3 + C_{33}x_3 = \mathrm{F}_3(\mathrm{t}) \tag{4.21}$$

where M is the mass of the system; A_{33}, B_{33} and C_{33} are the added mass matrix, hydrodynamic damping matrix and hydrostatic matrix, respectively, in the heave direction; and F_3 is the external force (diffraction + Froude-Krylov) on the body in the heave direction. It should be noted that the external forces may include, in addition to the wave excitation forces and mooring, other forces, such as mechanical forces (e.g., power take-off forces).

4.3.5.4 Power take-off (PTO)

A PTO system should be integrated in the WEC modeling to calculate the wave energy conversion. Although it is not completely realistic, a simple pure damper model is used here to represent the power take-off mechanism (PTO stiffness is equal to zero). The stiffness and control forces may be included in later stages. The constant damping of the PTO system is assumed to be frequency independent and is applied in the heave direction. The PTO force that is applied on the buoy in the heave direction can be expressed as follows:

$$F_{PTO} = D_{PTO}\dot{x}_3 \tag{4.22}$$

where D_{pto} is the PTO damping coefficient. After applying the PTO force, the equation of motion for the system can be given as follows:

$$(M + A_{33})\ddot{x}_3 + B_{33}\dot{x}_3 + C_{33}x_3 = \mathrm{F}_3 + F_{PTO} \tag{4.23}$$

According to Falnes [100], a maximum amount of energy can be captured if the power take-off mechanical damping is equal to the radiation damping of the point absorber at resonant frequency (see section 4.2.2). Under these assumptions, the PTO damping will be equal to that of the point absorber at resonance. The expression for the absorbed mean power ($\overline{\mathrm{P_{pto}}}$) of a heaving point absorber under harmonic motion can be given as follow:

$$\overline{\mathrm{P_{pto}}} = \frac{1}{2}\mathrm{D_{pto}}\omega^2|\mathrm{X_3}|^2 \tag{4.24}$$

where ω is the wave frequency; and X_3 is the heave motion amplitude of the buoy.

4.3.5.5 Results

The results of the frequency domain analysis of the buoy (diameter of 6 m and draft of 1.5 m) including hydrodynamic damping and added mass coefficients, displacement in heave direction as well as Froude-Krylov and diffraction forces are shown in figure 4-10 and 11.

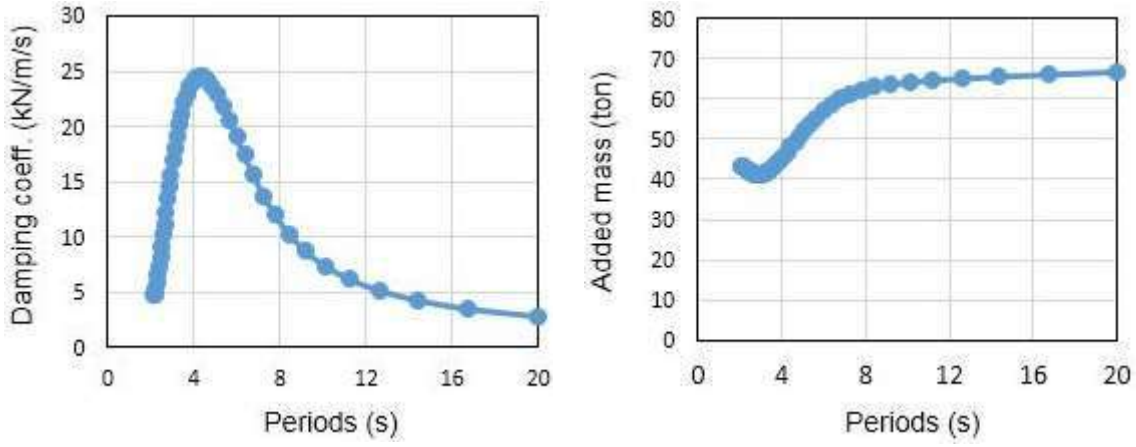

a) b)

Figure 4-10 – a) Hydrodynamic damping coefficient, b) Added mass coefficients

Figure 4-11-a illustrates the wave excitation forces with and without considering the diffraction effects (see section 3.4.1.2). Figure 11-b shows the displacement RAO of the buoy in heave direction with and without considering the effect of PTO system. A PTO applies a force on the system in the opposite direction of the velocity to absorb its kinetic energy and produces electricity or other desired form of energy. Therefore, in the case of heaving point absorber, the presence of PTO system results in a smaller heave amplitude, specifically in the resonance range.

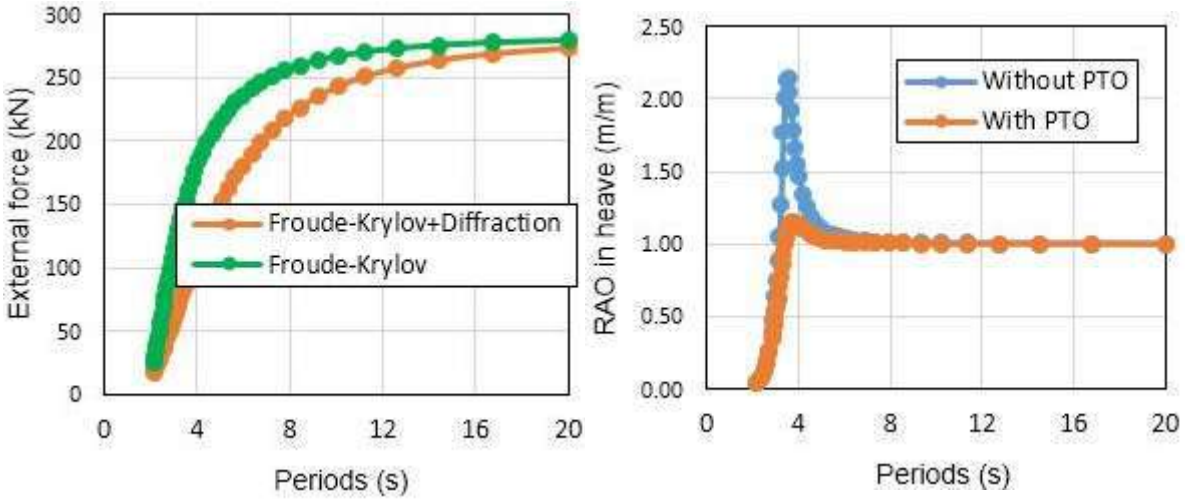

a) b)

Figure 4-11 – a) Froude-Krylov and diffraction forces, b) Displacement RAO in heave direction

Finally, the mechanical power (absorbed power) of the buoy is calculated applying a constant damping for PTO (D_{PTO}) equal to the hydrodynamic damping at resonant frequency. Figure 4-12 shows the mechanical power curve versus the wave periods. The natural period, the maximum mechanical power and the resonance bandwidth, which is the period interval where the buoy mechanical power exceeds half of the maximum value, can be determined as illustrated in the figure.

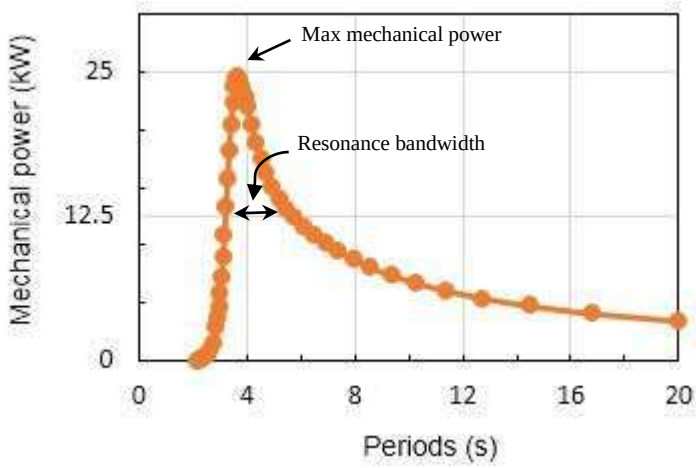

Figure 4-12 – Absorbed power by a heaving buoy with a constant PTO damping equal to the hydrodynamic damping at the resonant frequency.

The frequency domain analyses are performed for 13 buoys presented by the Minitab through the DOE method. Table 4-6 shows the factors and responses for these buoys.

Table 4-4 – Input factors and responses required by DOE method using Minitab

	Factors		Responses		
	$D1\ (m)$	$L1\ (m)$	Max mechanical power (kW)	Resonance bandwidth (s)	Natural period (s)
1	5.46	10.68	323.80	0.23	7.08
2	14	7.5	293.73	1	6.87
3	9	7.5	233.58	0.56	6.30
4	4	7.5	143.38	0.2	5.97
5	9	7.5	233.58	0.56	6.30
6	12.53	4.32	166.63	1.49	5.54
7	5.46	4.32	107.87	0.41	4.84
8	9	7.5	233.58	0.56	6.30
9	9	12	577.91	0.4	7.80
10	9	7.5	233.58	0.56	6.30
11	9	7.5	233.58	0.56	6.30
12	12.53	10.68	437.93	0.69	7.54
13	9	3	99.11	1.3	4.74

4.3.6 Statistical analysis results; mature determination

Thus far, the range of factors was determined based on the sea site characteristics and the principle conditions applied using the DOE method. In this step, the statistical analysis results are discussed, and the final buoys are determined based on the resultant contour and surface plots.

4.3.6.1 Diameter and draft interaction

After analyzing the designed experiments in Minitab, the results are illustrated by the contour plots in Figure 4-13. The contour plots give us the ability of screening the interactions of the geometrical parameters (factors) and their effects on the resonance bandwidth (RB), maximum power (MP) and natural period (NP) as the responses. In Figure 4-13, the horizontal and vertical axes represent the diameter (D1) and draft (L1) in the predefined ranges that have been determined in the immature determination step. The colored solid and dotted lines show the responses. The green, red and blue represent the maximum power, resonance bandwidth and natural period.

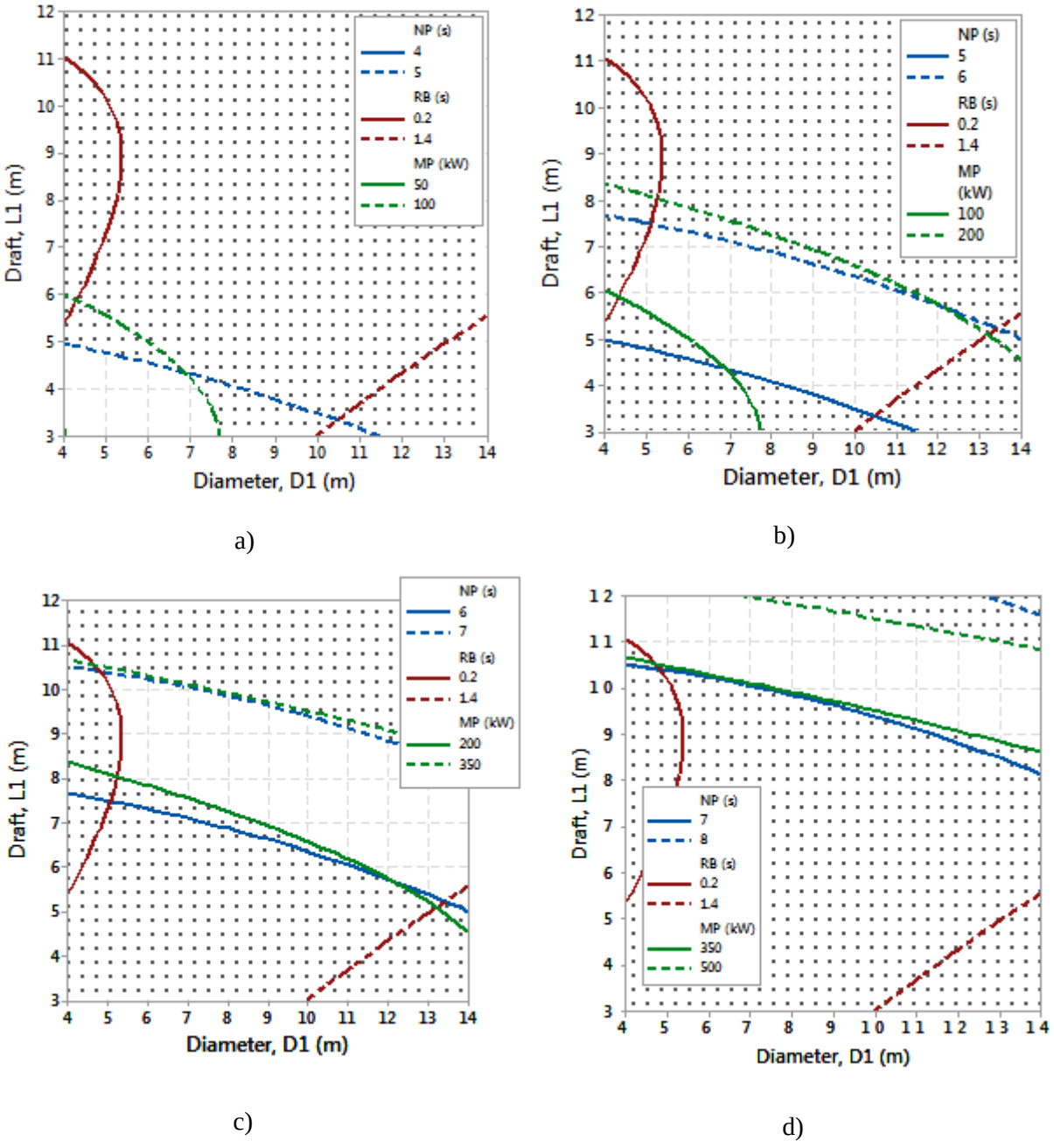

Figure 4-13 - Contour plots of the geometrical parameters (draft and diameters) in meter and the maximum power (MP in kW), resonance bandwidth (RB in second) and natural period (NP in second)

A maximum and a minimum value of 1.4 s and 0.2 s are respectively considered for the resonance bandwidth based on the frequency domain analyses and DOE results. It means that, the buoys which are located on the solid red line ($RB = 0.2\ s$) have the lowest resonance bandwidth comparing to the others implying that its performance capability is good close to the natural period but poor elsewhere. Moving away from this zone towards the maximum resonance bandwidth line ($RB = 1.4\ s$, dotted red line), the buoys with the

capability of absorbing wider range of wave periods are achievable. It is more evident in figure 4-14, where the effect of changing the geometrical parameters on the responses are depicted separately. Figure 4-14-a shows that the buoys with the smallest drafts and largest diameter provide the widest resonance bandwidth. Back to the figure 4-13, the white area in each figure shows the buoys $(D1, L1)$ bounded by the certain response values. For instance, in Figure 4-13-c, the buoy with the diameter of 9 m and draft of 8 m is located in the white area. It means that the buoy $(9, 8)$ has a natural period between 6 and 7 s with a maximum power of approximately 200 kW at its resonance period. By observing the contour plots of figure 4-14-a and c, it seen that the maximum resonance bandwidth and the maximum power do not occur at the same region. The larger diameters with relatively small drafts ($L1 < 6\ m$) provide a good resonance bandwidth while the maximum energy absorption is achievable in the same diameter range with larger drafts ($L1 > 10\ m$). However, it should be kept in mind that the maximum power in the present methodology is the energy absorption at the buoy natural period. On the other hand, Figure 4-14-b shows that the highest possible natural period provided by a buoy inside the geometrical parameter range is 8 s. It implies that a very large buoy, outside the specified range of diameters and drafts, is required to satisfy the resonant condition for the sea site energetic waves, which are between 9 and 11 s (see figure 4-6) . This is a challenge for the local seas with predominant wave periods beyond 6 or 7 s.

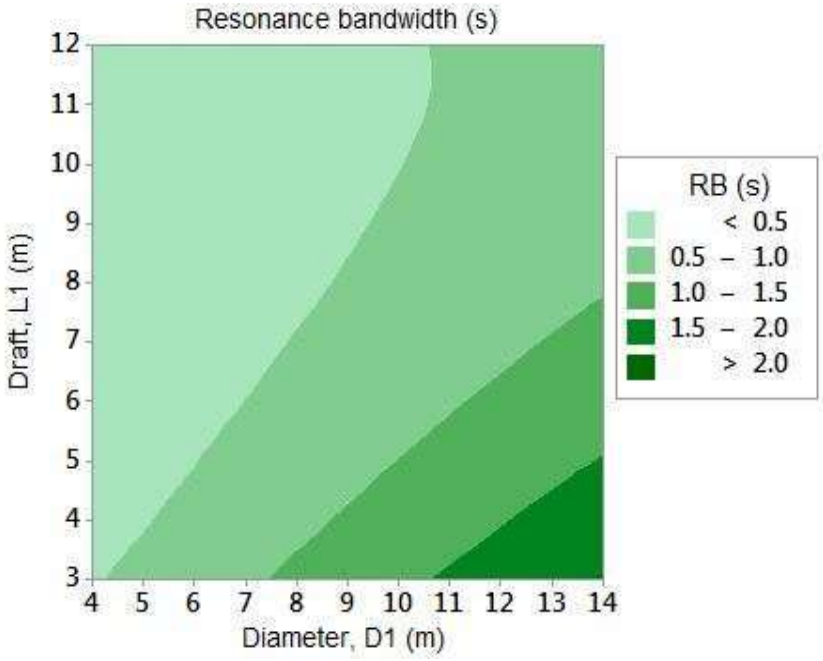

a)

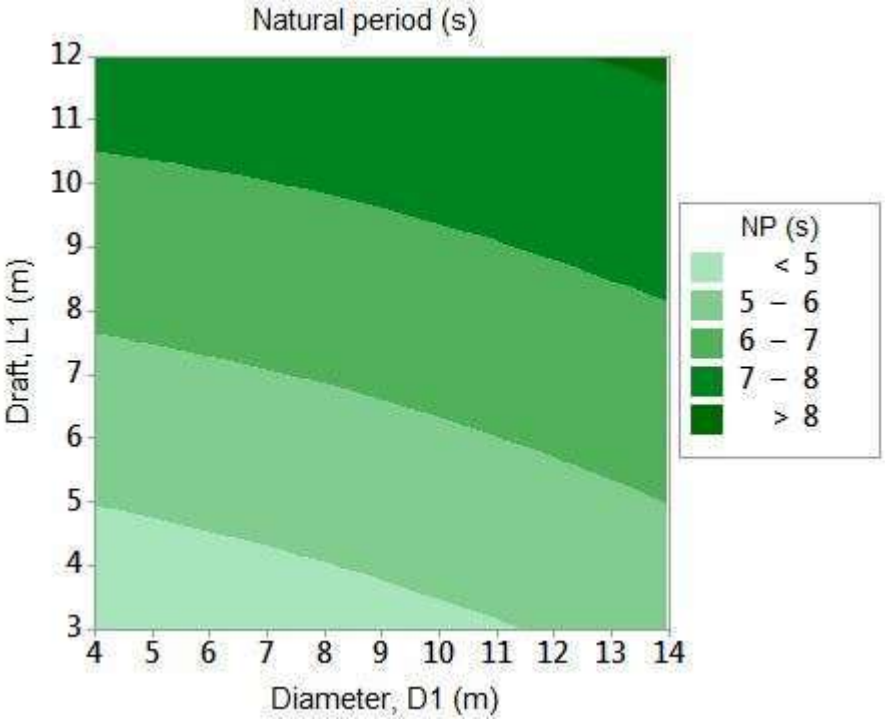

b)

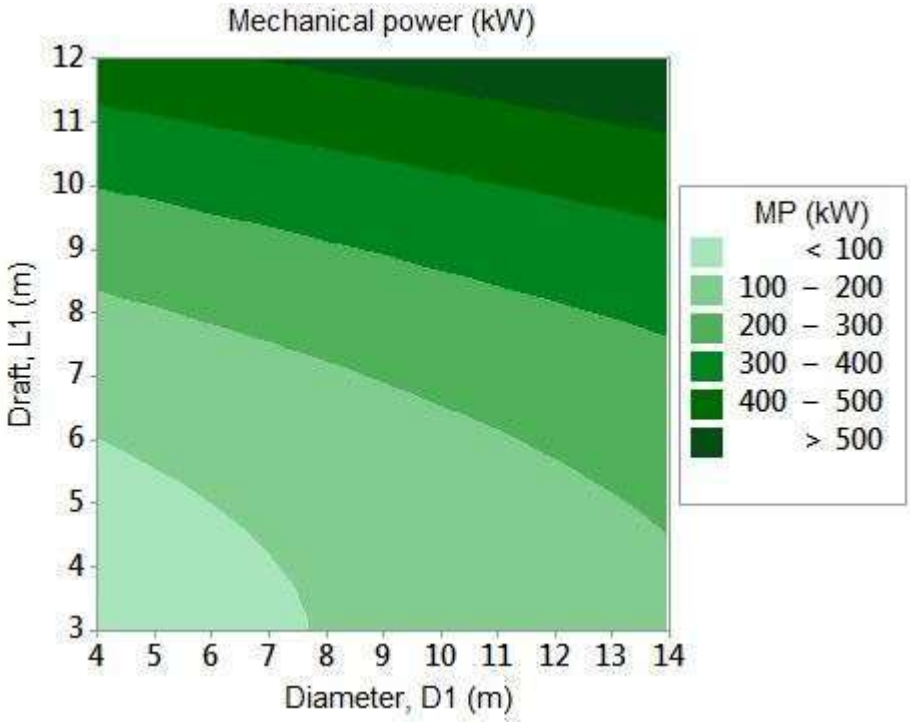

c)

Figure 4-14 - Contour plots of the geometrical parameters (draft and diameters) in meter versus a) resonance bandwidth (RB in second), b) natural period (NP in second) and c) the maximum power (MP in kW)

Figure 4-15 shows some frequency domain analyses for different buoys selected from figure 4-13 to provide a better understanding of the interaction of the geometrical parameters and their effects on the responses. For this reason, an arbitrarily selected buoy of diameter 11 m and draft 5 m is considered. To observe the effect of both diameter and draft, the simulations are performed for the buoys with a constant diameter and varying drafts and vice-versa. A constant PTO damping is applied to maximize the energy absorption. The vertical and horizontal axes represent the maximum mechanical power and wave periods, respectively.

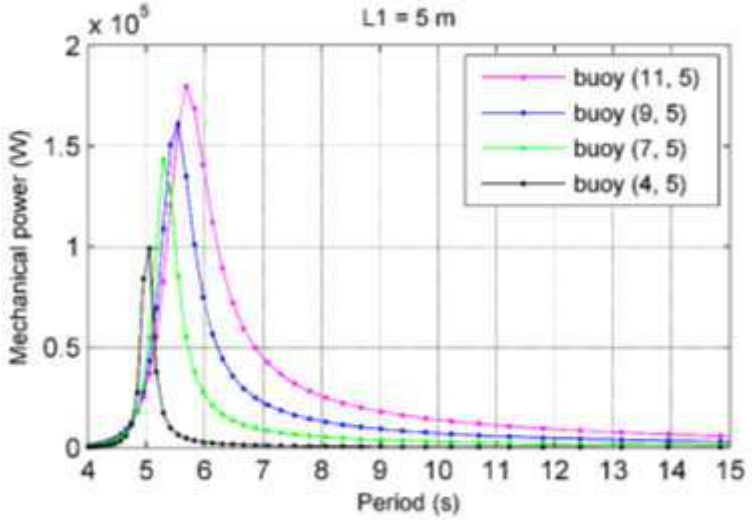

a)

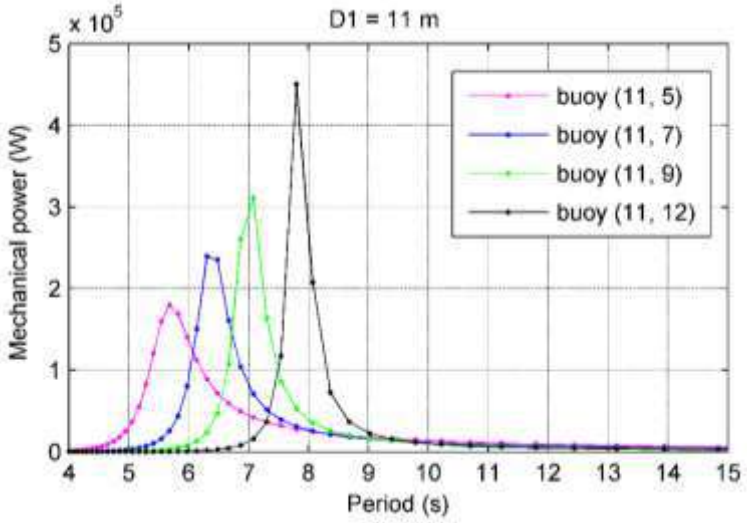

b)

Figure 4-15 - Mechanical power vs wave periods; a) Different diameters with a fixed draft; and b) Different drafts with a fixed diameter

Figure 4-15-a illustrates the effect of changing diameters for a constant draft. As can be seen, larger diameter improves the buoy performance by increasing the maximum power, natural period and resonance bandwidth. This is based on theoretical analyses for an unconstrained system. In practice, there are some limitations regarding the cost, PTO forces, mooring etc. that restrict the buoy diameter increase. Furthermore, increasing the diameter results in better absorption in low-frequency region (periods higher than the natural period) while letting the absorption in high-frequency region unchanged. It may be a desirable effect for the sea regions that are dominated by large wave periods. Figure 4-15-b shows the influence of the draft in the performance of the buoy. Increasing the draft leads to a higher maximum power and natural period but a lower resonance bandwidth. As seen, as the buoy draft increases the power curve narrowed leading to a short resonance bandwidth. It means that the buoys with larger drafts provide high natural periods and absorb a significant amount of energy in its resonant condition. It is observed that, quantitatively, the effect of the draft is more significant than that of diameter. For instance, the maximum power increase of 13% is reached for a diameter increase of 2 meters (considering buoy $(7, 5)$ and buoy $(9, 5)$ in Figure 4-15-a), while this value is about 20% for the same increment in draft (considering buoy $(11, 7)$ and buoy $(11, 9)$ in Figure 4-15-b). Therefore, it should be noted that modifying the draft values can significantly influence the point absorber performance. The contour plots enable us to understand the problem better and identify the limits by providing a broad view of its domain. The next section describes the process of selecting the optimum buoy.

4.3.6.2 Optimum diameter and draft

Surface plots can also illustrate the interaction of geometrical parameters to analyze the statistical results. Figure 4-16 shows the surface plot of the maximum mechanical power and resonance bandwidth versus buoy diameter and draft. As seen, the buoy with the maximum mechanical power, buoy $(14, 12)$, has a relatively low resonance bandwidth whereas the buoy with the maximum resonance bandwidth, buoy $(14, 3)$, has a low mechanical power. Therefore, considering figure 4-16, to guarantee the sufficiently wide resonance bandwidth, the values lower than half of the maximum (maximum value equal to 2 s) are discarded. It should be noted that, this is a relative resonance bandwidth, in other words, the modified range provides the buoys that have a larger resonance bandwidth values when comparing to the other buoys in the main range. Then, the

modified geometrical parameter range is achieved, $8 < D_1 < 14\,m$ and $3 < L_1 < 6\,m$.

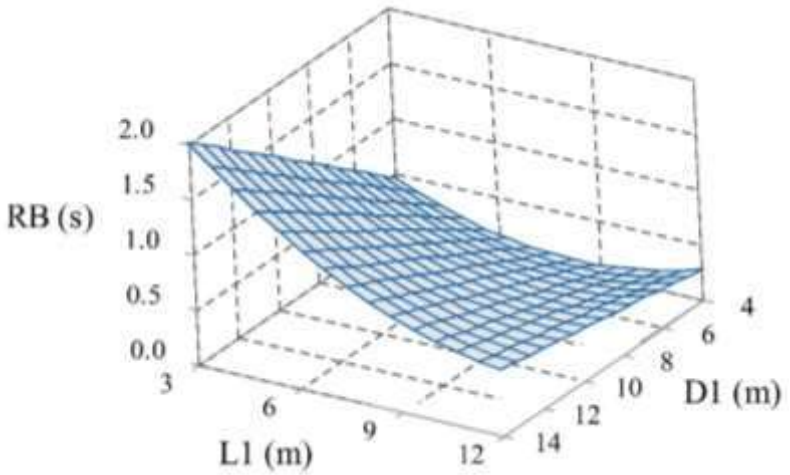

a)

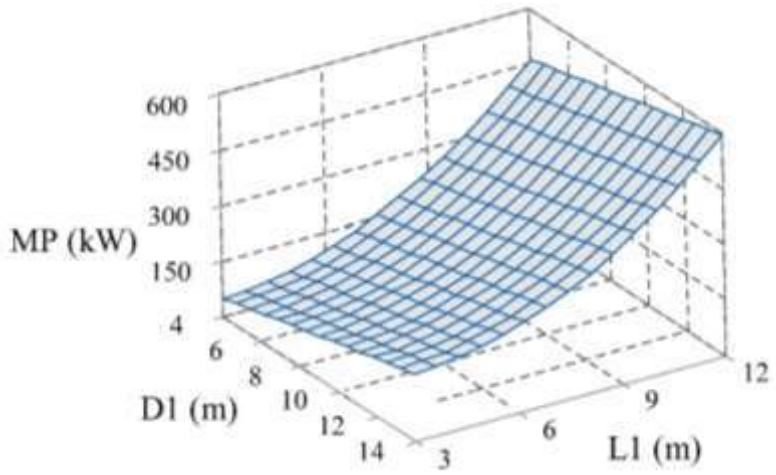

b)

Figure 4-16 - Surface plot of the a) resonance bandwidth, RB (s) and b) the maximum mechanical power, MP (kW) vs. buoy diameter and draft

The optimized buoy in this range is determined using the Minitab response optimizer [98]. This feature helps identify the combination of geometrical parameters that jointly optimize the resonance bandwidth and maximum power. In this study, the objective is to obtain a system that works as close as possible to the prevailing wave periods while

absorbing the maximum possible energy in a relatively wide range of the sea dominant waves. By considering the modified range of the factors resulted from figure 4-16, buoy $(14, 6)$ has the largest values of diameter and draft, providing the highest natural period $(6\ s)$. This resonance period is selected as a target for the response optimization process. The maximum mechanical power and resonance bandwidth are set to satisfy the maximum values. Eventually, the response optimizer numerically determines the buoy that satisfies the optimization requirements. Under these conditions, $13.5\ m$ diameter and $5\ m$ draft are determined for the optimized buoy. Figure 4-17 shows the response optimizer window in Minitab. The joint optimization must satisfy the requirements for all the responses in the set, which here is the maximization of the combination of the resonance bandwidth and maximum power considering a target value for the natural period. This is measured by the composite desirability D. The composite desirability assesses how well a combination of input variables ($D1$ and $L1$) satisfies the goals defined for the responses. Figure 4-17, illustrates the interactions between the factors and the responses. The curves show the changes of each response as a function of the corresponding factor. The blue dashed line illustrates the position of the response value on each curve. For instance, the value of the maximum resonance bandwidth for a buoy with a fixed draft of $\approx 5\ m$ is approximately $1.5\ s$ which is the ending point of the diameter curve, where $D_1 \approx 13.5\ m$. The red values on the top show the optimum set of the factors predicted by the response optimizer inside the lower and upper bound range. The composite desirability curves are illustrated for each factor separately. Decreasing the diameter with a fixed draft results in decreasing the composite desirability. For the case of varying draft with a fixed diameter, either decreasing and increasing the draft value, $L_1 \approx 5\ m$, result in a lower composite desirability. For instance, in the case of moving the draft red line to the right, increasing the draft value, the natural period value moves away from its target, $6\ s$, the resonance bandwidth value decreases and the maximum mechanical power value increases. As the result, the composite desirability decreases. Additionally, by observing the inclination of the curves, it can be inferred that the natural period and the maximum mechanical power are more sensitive to the changes in draft than diameter. For the resonance bandwidth the effect of draft and diameter has the same rate but in the opposite direction.

As indicated in figure 4-25, to verify the numerical optimization result, a set of runs with buoys in the range of $8 < D_1 < 14\,m$ and $3 < L_1 < 6\,m$ are performed in AQWA/ANSYS, and the results are compared to those from the optimization results.

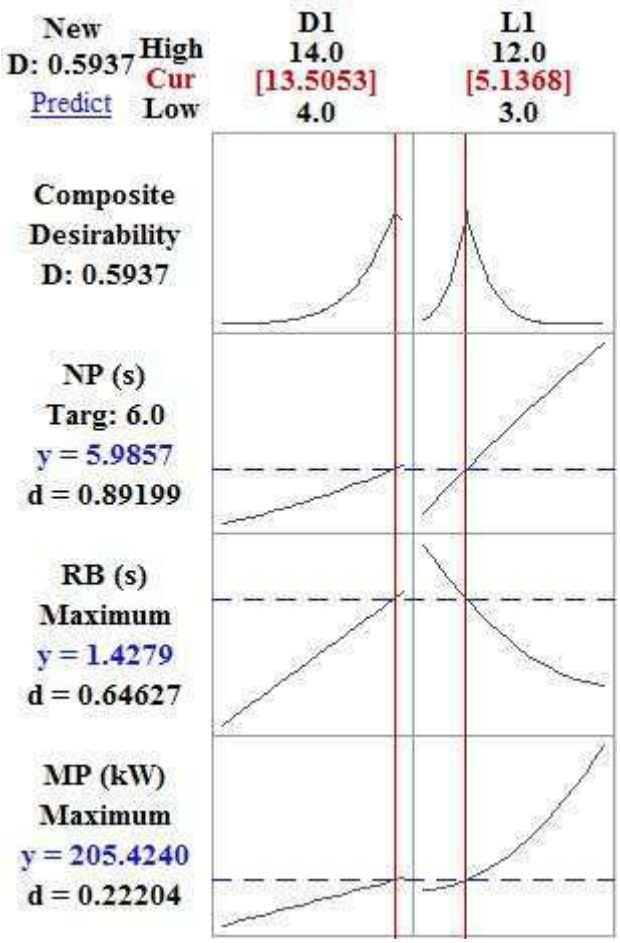

Figure 4-17 – The response optimizer window of Minitab showing the optimum set of the geometrical parameters

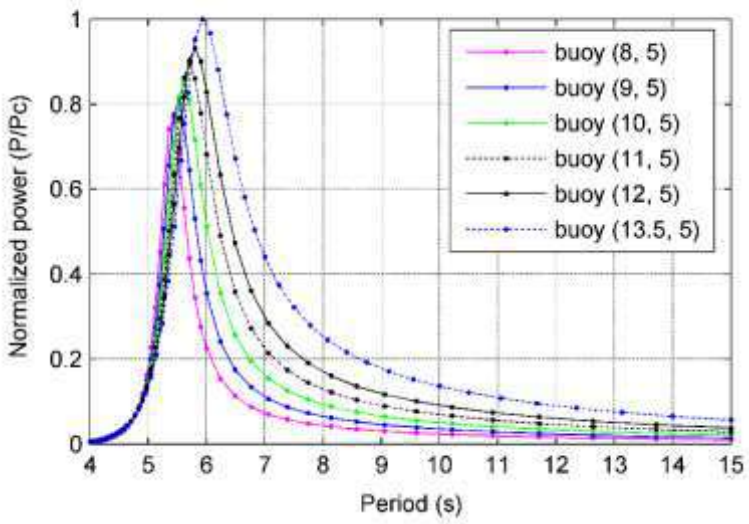

a)

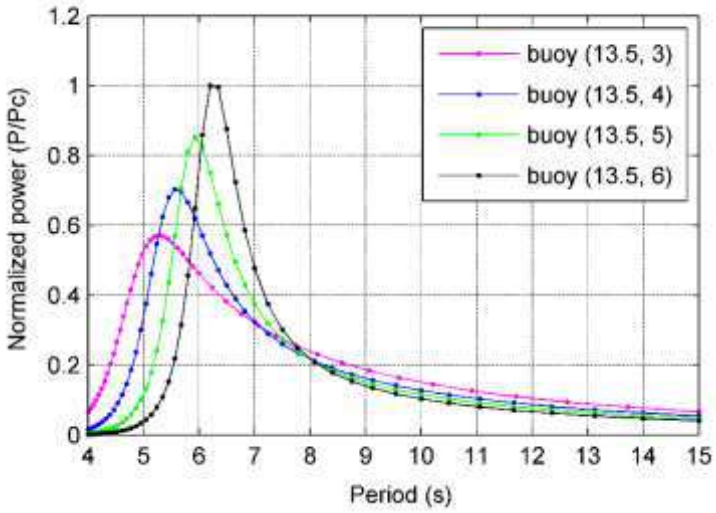

b)

Figure 4-18 - Normalized mechanical power vs period for a) different diameters with the same draft; b) Different drafts with the same diameter

Figure 4-18 illustrates the captured mechanical power for the buoy over the range of period between 4 and 15 s. The vertical axis represents the normalized mechanical power. The power values are divided by P_c, which is the maximum mechanical power of buoy (13.5, 5) and buoy (13.5, 6) in figures 4-18-a and b, respectively. It can be seen that,

as expected, decreasing the diameter in figures 4-18-a results in a decrease in the maximum mechanical power, resonance bandwidth and resonance period, which implies that a diameter of 13.5 m is the best selection in the range. This result is in accordance with the result of the numerical optimization. In figures 4-18-b, buoy $(13.5, 5)$ is compared with other buoys with different drafts in the range of 3 to 6 m. The results are the same as those discussed in figures 4-13 to 17. Increasing the draft leads to a buoy with a higher maximum mechanical power, narrower resonance bandwidth and a higher resonance period. Conversely, decreasing the draft results in a lower maximum mechanical power, wider resonance bandwidth and lower resonance period. However, an important issue that must be considered during the optimization of the buoy dimensions is the performance of the buoy over the range of prevailing wave periods at the sea site. As indicated in figures 4-18-b and considering buoy $(13.5, 3)$, it can be seen that although this buoy has the lowest maximum mechanical power and resonance period, it captures more power over the sea site prevailing wave periods (between 7 and 13 s) when compared to the dimensions of other buoys. In figures 4-18-b, the differences between the captured power graphs in the range of predominant wave periods are not significant; however, selecting a buoy with a smaller draft results in a few benefits, such as lower cost and lower system loads due to a lighter weight system, which consequently results in increasing the efficiency of the system. Thus, a buoy with a diameter of 13.5 m and a draft of 3 m is selected as the optimized buoy for the mentioned nearshore sea site of Rio de Janeiro. It is observed that for sea regions, such as the nearshore region of Rio de Janeiro, with predominant wave periods greater than 7 s, the challenge is to have a control-free point absorber with a resonance bandwidth tuned to the prevailing wave range. In our study, the one-body point absorber that can meet this requirement is a large buoy close to the geometrical parameters boundaries. Practically, this type of system results in several challenges related to the cost, slamming, water depth consideration, proper PTO system, etc.

4.4 Conclusion

In this chapter, the objective is to present a methodology for the geometric optimization of WECs based on a series of frequency domain analyses and a statistical analysis method known as Design of Experiments (DOE). The optimization process is applied to the preliminary design of a one-body point absorber with an axisymmetric floating cylinder

for the nearshore region of Rio de Janeiro. The complex representation of the governing equations which were adapted by Falnes [100] are described in order to model the system in frequency domain. An ideal pure damper is considered as PTO and the energy absorption is calculated for different wave frequencies. First, the local sea characteristics has been described through a five-year wave hindcast (2006-2010) based on a third generation wind wave model WAVEWATCH III. The results indicated a predominant wave period range between 7 and 13 s with an energy period $T_e = 9.7$ s , as well as an average significant height of $H_s = 1.33$ m. Based on these results, the calculated wave power level per width unit is approximately 8.5 kW/m. Then, the optimization procedure is applied in two principle steps, immature and mature determination. The lower and upper bounds of the geometrical parameters are determined in the first step based on the practical recommendations regarding the ratio of the point absorber diameter to the predominant wavelength and the non-dimensional capture width. In the second step, after considering a set of frequency domain analyses and the design of experiments method, the WEC's geometrical parameters (diameter and draft) are determined to achieve a system that absorbs the maximum energy over a wide range of wave periods. In other words, a set of geometrical parameters (factors) are determined to maximize the response, which is a combination of the maximum absorbed power and the resonance bandwidth of the buoy, considering a target natural period.

The results include the contour and surface plots of the factors interactions. The effects of different sets of diameter and draft on the maximum mechanical power, resonance bandwidth and natural period of the buoy were determined. The lower and upper bounds of the geometrical parameters are further modified based on the resonance bandwidth requirement. Considering the modified domain of the diameter and draft, the maximum buoy natural period is $T = 6$ s, which corresponds to the buoy with a diameter 14 m and draft 6 m. Consequently, this period is considered as a satisfactory target natural period for the optimization process. The response optimizer, which is a feature of Minitab, is used to numerically determine the best set of geometrical parameters that jointly maximize the maximum power and resonance bandwidth. The numerical results of the response optimizer are then verified by a series of frequency domain analyses and, eventually, the buoy with diameter $D1 = 13.5\ m$ and draft $L1 = 3\ m$ is selected as the optimized control-free buoy for the design sea site.

Applying DOE method as a statistical analysis combined with the frequency domain hydrodynamic analysis provide a wide picture of the optimization problem domain, and the possibility of observing the effects of different variables on the optimization process objective. Furthermore, a considerable amount of CPU time is saved by performing only a few runs for the optimization process. The proposed methodology can be applied to the other types of wave converters with different geometrical properties.

It is observed that none of the buoys inside the defined upper and lower bounds can provide a natural period and resonance bandwidth tuned to the sea site predominant wave range. This is observed as the primary challenge for the nearshore region of Rio de Janeiro that have prevailing wave periods beyond $7\ s$. Applying control methods may help to reduce the dimensions and improve the system performance. The next chapter is dedicated to the improvement of the point absorber by investigating the application of a specific "constant-time latching" control method through a series of time-domain simulations.

Chapter 5

5. Application of a “constant-delay latching control” on a heaving point absorber wave energy converter

5.1 Introduction

Waves are a generous source of clean and renewable energy still waiting for a proper technology to become a fully useful energy resource. In the last decades, global climate changes and more recently the rocketing oil price risings helped putting pressure on pursuing efficient wave energy converters and innovative devices. So far, one of the most promising concepts under technical and economic evaluation is the point absorbers (Pas). In the case of PA, previous investigations have shown the smaller the oscillating body is, the higher will be its efficiency. A body oscillating in water generates waves. A large body and a small body may produce equally large waves since the smaller one oscillates with larger amplitude. Such a feature may be well explored to extract energy from sea waves [115]. However, geometry optimization process is required to achieve an efficient system. At present, the geometry optimization of the WECs have been usually performed for the systems without taking into account control strategy in any way [88,89,91,116–118]. The objective circumscribed the problem into maximizing the energy production as well as absorption bandwidth in the sea predominant wave range. Only then, the solution applied control methods to increase the efficiency of the system. As observed in the chapter 3, determining a WEC that will resonate within the dominant energetic wave frequency range of the real sea to absorb the maximum possible energy may lead to a quite non-practical solution due to the body large dimensions and prohibitively high costs. Recently, Garcia-Rosa et al [93] addressed the effect of three different control methods on the geometry optimization of a cylindrical PA. They applied an optimization process to determine the buoy dimensions (diameter and draught) that maximize the average absorbed power.

Efforts to design more economic systems have started since mid-1970s. Different control methods have been presented to maximize energy conversion e.g. [56,74,92] .One of these control methods is “latching” which was originally proposed by Budal and Falnes [55]. Latching control is a suboptimal control method that tunes WEC oscillation period to the sea predominant wave periods by locking the system during some time intervals along its oscillation. Therefore, the natural period of WEC must be adjusted to a period well under the predominant sea waves. Consequently, the optimized dimensions of a WEC under latching control will be different from the dimensions obtained by optimization of a control-free device.

There are many either numerical or experimental works investigating latching control methodology on wave energy converters. Most of these works feature heaving point absorbers. Latching control systems can be divided into two distinct categories: predictive [55,61,63–65,70,119] and non-predictive [71,77] ."Predictive" and "non-predictive" refer to the necessity or not of predicting the wave exciting force to apply the latching control methodology. Among the available methodologies, a very simple one is the non-predictive latching control method presented by Sheng et al [77]. They simply calculated the latching duration, using the half of the difference between wave period and the natural period of the floater. This would be similar to the Falnes' proposal [55] who unlatches the device at the instant $T_0/4$ ahead of the next ´peak excitation´ in regular waves (where T_0 is the natural period of the oscillator) . In Sheng et al´s method, the latching duration is defined merely by the wave energy period, with no need of tuning based on the wave excitation force prediction. In real seas, the wave spectrum can be forecast based on the local sea measurements and it usually changes each two or three hours.

This chapter discusses a practical approach, through a series of time domain analyses based on the preliminary geometrical optimization described in chapter 3, to address the effect of applying latching control on the optimum dimensions of a heaving point absorber for a specific sea site (nearshore Rio de Janeiro - Brazil). Due to the practical approach chosen here, the non-predictive latching methodology as presented by Sheng et al [77] is applied. Based on the results of the optimization process in chapter 3, four different control-free buoy geometries were selected. Then, the application of the latching control (presented by Sheng et al) on different oscillating buoys are quantitatively investigated for both regular and irregular waves. The latching duration was determined based on the energy period of the local sea state. The hydrodynamic coefficients are calculated through AQWA ANSYS and a FORTRAN code is developed for the time-domain simulation using the linear hydrodynamic theory. The performance of the oscillators under latching control are then compared considering the potential effects of the hydrodynamic damping coefficients on the energy output and the annual energy production (AEP) matrix of the optimum buoy.

5.2 Practical difficulties

As a preliminary approach, chapter 3 adapts a frequency domain analysis, to identify the optimum geometry of a cylindrical buoy to be installed in a nearshore area of Rio de

Janeiro – Brazil. Figure 5-1 shows a part of results from the applied methodology. Figure 5-1 illustrates the buoys maximum mechanical power (green lines), resonance bandwidth (red lines) and the natural period (blue lines) in the range of $4\ m \leq D_1 \leq 14\ m$ and $3\ m \leq L_1 \leq 12\ m$. The optimization process maximized the mechanical power and resonance bandwidth (defined as the period interval in which buoy maximum mechanical power exceeds half of its maximum value) of a control-free oscillator with a natural period taken as close as possible to the sea site predominant waves (see section 4.3.6). A buoy with 13.5 m diameter and 3 m draft was found to be the optimized buoy. The practical difficulty is that the predominant wave period is beyond 7 seconds and as it shown in figure 5-1-b, only large buoys could meet such a requirement. For instance, a 7 s natural period buoy requires a 14 m diameter by 8m draught cylinder. Larger WEC requires larger excursion, velocity, PTO capacity etc, imposing greater investment costs.

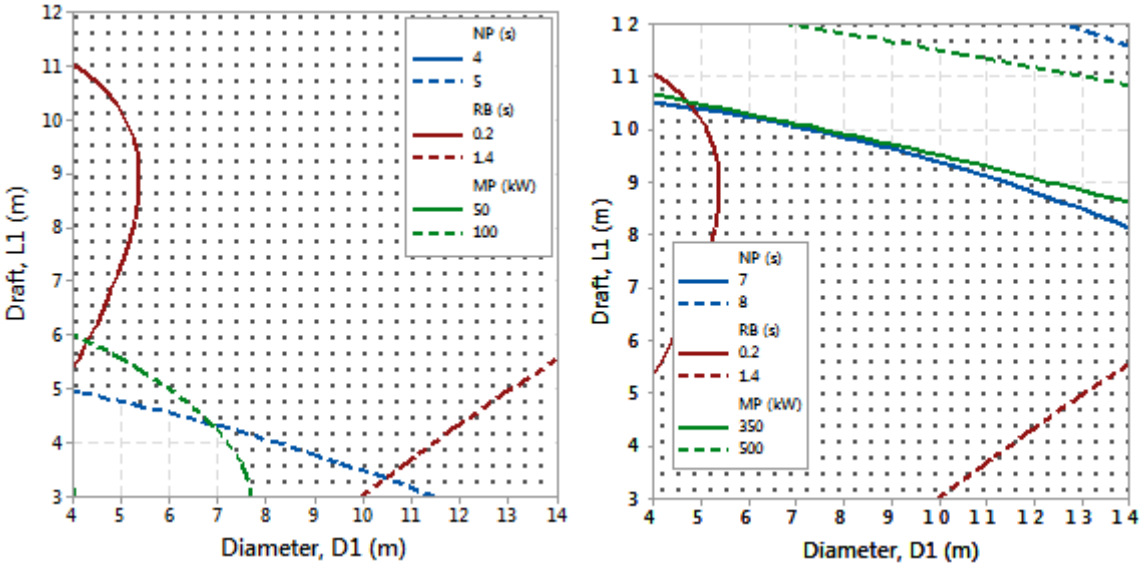

Figure 5-1- Contour plots of the geometrical parameters (draft and diameters) in meter and the maximum power (MP in kW), resonance bandwidth (RB in second) and natural period (NP in second)

Local waves are presented in terms of the joint probability distribution (JPD) in figure 4-4, indicating the probability of simultaneous occurrence of given significant wave height and wave peak period. Ocean data from the site (nearshore Rio de Janeiro – Brazil) indicate predominant wave periods laying between 7 and 13 seconds (about 86%). From figure 4-4, the average values: significant height: $H_s = 1.33\ m$; and wave peak period: $T_p = 9.7\ s$. Figure 4-6 shows the annual wave power per unit width (in MWh/m) and its probability of occurrence (see section 4.3.2). The figures within the graphs indicate the

probability of occurrence of given sea state (in %), defined by the pair: significant wave height and peak period. The most energetic waves represent only 7.1 % for the range from 9 to 11s and 3.3% for the range from 11 to 13s of the total occurrence of waves.

Results from figure 5-1, allow for tuning the oscillating buoy natural period to the lower bound of the predominant wave period range $T = 7\ s$. In figure 5-1-b, the buoys located on the solid blue line have the natural period equals to 7 s . Three buoys: b_1 (4, 10.5), b_2 (9, 9.5) and b_3 (14, 8) were selected and had their behavior investigated along the solid blue line ($NP = 7\ s$). At resonant condition, three buoys generate approximately the same mechanical power, ($MP \approx 350\ kW$). Therefore, to maximize the ratio of the absorbed power to cost, it makes a lot of sense to choose the smallest buoy (or rather, as had been anticipated by Falnes [120]: "small is beautiful): b_1 buoy $= 132\ ton$ instead of :$b_2\ buoy = 604$ ton; and $b_3 buoy\ = 1231$ ton (buoy weight considers ballast weight at their static equilibrium). On the other hand, the effect of the resonance bandwidth on the mechanical power is very relevant. Referring to the figure 5-1-b, the buoy b_1 features the narrowest resonance (see also figure 4-14-a). It implies that the selected buoy presents high energy absorption only at the resonant period and low absorption at the other wave periods. Latching control, therefore, may be considered as an alternative to improve energy absorption within a broader range of wave periods. Latching control could make smaller buoys competitive with larger ones. It may achieve even better power absorption performance than resonant (larger) buoys. Buoys dimensions selection took into consideration the lowest bound of the predominant wave period (see figure 4-4), $T = 5\ s$, which was considered as the target for natural period matching. As illustrated in figure 5-1-a, the blue line represents all the buoys with the natural period equals to 5 s (diameter: $4 \leq D_1 \leq 11.5$ and draught, $3m \leq L_1 \leq 5m$). Therefore, four buoys b1 (4, 5), b2 (6, 4.5), b3 (8, 4) and b4 (11.5, 3), (buoy ($diameter\ (m), Draught\ (m)$)) which are located on this blue line, were selected to investigate the effect of latching control and optimization process.

5.3 Latching control concept

The principle of the latching control is to hold the floater motion at the instant that velocity vanishes and release it at the next favorable condition. As a result, the floater velocity is forced to be in phase with the wave excitation force. As proposed by Budal and Falnes [55], the method of latching to achieve optimum phase is applicable to wave

periods above the resonant period. Figure 5-2, inspired by Budal et al [60], illustrates the latching concept, where curve **a** represents the elevation of the water surface due to the sinusoidal incident wave of period T. If the body diameter were much smaller than the wavelength, curve **a** could be thought as the wave exciting force representation. Curve **b** is the vertical displacement of heaving body with large enough mass to make the natural period equals to the wave period. Curve **c** shows the vertical displacement of a body with smaller mass and hence shorter natural period T_0 ($T_0 < T$), controlled by latching. Considering a time interval: $0 < t < T$, as shown in figure 5-4, at a certain instant t_l, when the heave motion of **c**, reaches its maximum positive excursion and velocity vanishes, the body motion is locked by the latching mechanism, until an instant t_u when unlatching occurs. When heave motion reaches its maximum negative excursion (at the instant t'_l), latching occurs again until the next unlatching time t'_u. The resonant body with larger mass is tuned to the incident wave while the body with smaller mass needs a time lag of $(T - T_0)$ seconds to follow the incident wave. Therefore, in each wave cycle there are two, approximately $(T - T_0)/2$ intervals during which the floater motion is prevented. Therefore, the unlatching of the body happens at $T_0/4$ s before the next maximum of the wave exciting force:

$$latching\ duration = \frac{(T - T_0)}{2} \tag{5.1}$$

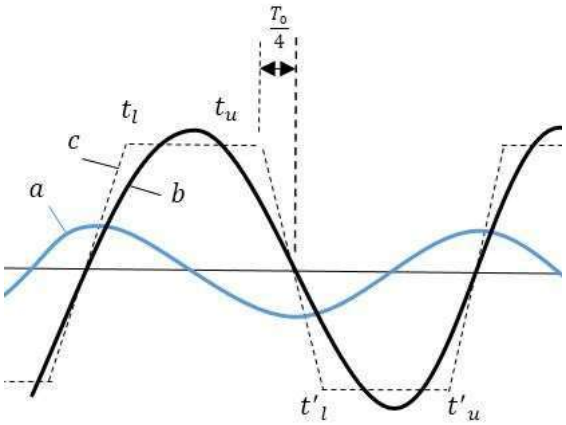

Figure 5-2 - Latching and unlatching: a) Elevation of the water surface due to the sinusoidal incident wave, b) Resonant Vertical Displacement ; c) Non Resonant Vertical Displacement (with natural period smaller than wave period)

In real seas, latching control needs predictive wave data, imposing difficulties to its practical application. Sheng et al [77] proposed an alternative approach without the necessity of predicting waves. In this method, a characteristic period of the sea spectrum substitutes the monochromatic period used in regular waves to calculate the latching duration. Here, in the present thesis, the latching duration was calculated based on the energy period of the sea spectrum, as defined by Eq.5.1, and it is fixed for each sea state. For this reason, this type of latching control method could be named as "constant-delay latching control".

5.4 Mathematical model

The mathematical model features a cylindrical heaving point absorber (diameter: D and draught: d), figure 5-3. An idealized (100% efficiency) pure damper, D_{PTO}, is considered for the PTO mechanism to convert absorbed energy. The PTO works in a single heave motion mode. A latching mechanism holds up the buoy at the maximum heave displacement and releases it after a predefined time interval (latching duration). The dynamic equation (Newton´s Second Law application) for a simple point absorber in heave direction include the latching force and PTO effect:

$$(M + A)\ddot{X}_3(t) = F_{e,3}(t) + F_{r,3}(t) + F_{h,3}(t) + F_{PTO}(t) + F_{Latching}(t) \qquad (5.2)$$

where:

M: is the mass of the buoy;

$\ddot{X}_3$: is the buoy acceleration in heave direction;

$F_{e,3}(t)$: is the excitation force (the force the incoming wave imparts on the buoy in heave direction);

$F_{r,3}(t)$: is the radiation force (the force the floating buoy creates by moving and thus radiating waves, in heave direction);

$F_{h,3}$: is the hydrostatic force in heave direction;

F_{PTO} and $F_{Latching}$: are the forces due to the PTO and latching system, respectively.

The hydrodynamic reaction forces (and moments), due to time varying floater motions, can be described using the classic formulation given by Cummins (1962) [96] .Ogilvie

(1964) [97] proposed a simplified way to calculate time domain parameters via frequency domain calculation.

By applying Cummins approach, the Eq.(5.2) can be rewritten to present the equation of motion of a generic single degree of freedom point absorber with latching control and a linear PTO system ($K_{PTO} = 0$), as follow:

$$\left(M + A_{33}(\infty)\right)\ddot{X}_3(t) = F_{e,3}(t) - \int_{-\infty}^{t} f_{r,33}(t-\tau)\dot{X}_3(\tau)d\tau - C_{33}X_3(t) - b_{PTO}\dot{X}_3(t) + F_{latching}(t) \quad (5.3)$$

where:

$A_{33}(\infty)$: is the added mass at infinite wave frequency in heave direction (see section 3.6.2);

$F_{e,3}(t)$: is calculated (via Eq.(5.4) [100]) by the convolution integral of the water surface elevation, $\eta(t)$, with the non-causal excitation impulse response function, $f_e(t)$;

$F_{r,3}(t)$: is calculated by the convolution integral of the radiation impulse response function, $f_{r,3}(t)$ (via Eq.(5.5));

$F_{h,3}(t)$: is the restoring force (via Eq.(5.6)). C_{33} is the linear restoring (hydrostatic) spring coefficient, in the heave direction. F_{PTO}, with $K_{PTO} = 0$, calculated via Eq.(5.7) (see section 4.2.2). b_{PTO} is the damping of the PTO device.

$$F_e(t) = \int_{-\infty}^{\infty} \eta(\tau) f_e(t-\tau)d\tau \quad (5.4)$$

$$F_r(t) = \int_{-\infty}^{t} f_r(t-\tau)\dot{X}(\tau)d\tau \quad (5.5)$$

$$F_{h,3} = C_{33}X_3(t) \quad (5.6)$$

$$F_{PTO} = D_{PTO}\dot{X}(t) \quad (5.7)$$

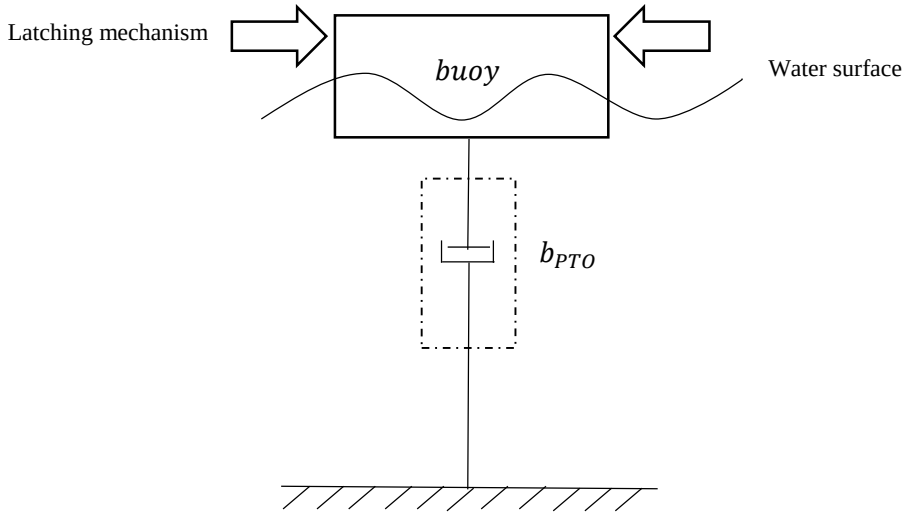

Figure 5-3- Single point absorber with a pure damper as PTO system fixed at seabed

The floating cylinder was assumed to have a linear behavior, neglecting any nonlinearities including effects from currents, wind etc.

The latching mechanism could be imposed by either the PTO system or any other mechanism (like mechanical brakes etc.). The latching force will be zero during oscillation until buoy velocity becomes zero or very small (latching moment). The latching mechanism holds the buoy displacement and keep it still during latching. The required latching force to keep the buoy locked can be expressed as:

$$F_{latching} = -F_{e,3}(t) + \int_{-\infty}^{t} f_{r,33}(t-\tau)\dot{X}_3(\tau)d\tau + C_{33}X_3(t) \tag{5.8}$$

During latching, PTO force becomes zero, while memory effect term still exists due to the previous velocity effects. Once Eq.(5.3) is solved, the average produced power can be calculated as:

$$\bar{P} = \frac{1}{T}\int_0^T b_{PTO} \times \dot{X}_3{}^2(t)\, dt \tag{5.9}$$

where: T is the total simulation time.

5.5 Hydrodynamic coefficients computation

AQWA ANSYS is used to calculate the hydrodynamic parameters of each buoy. No PTO damping is considered at this step and the buoy is freely oscillating in pure heave only. Figure 5-4-a and b show buoys added mass and hydrodynamic damping coefficients. When $\omega \rightarrow \infty$, added mass assumes the following values: buoy b1 = 16 ton; Buoy b2 = 52 ton; Buoy b3 = 120 ton; and b4 = 335 ton. The maximum hydrodynamic damping coefficient occurred at $\omega = 1.047\ rad/s$ with the values: Buoy b1 = 2.2 kN/m/s; Buoy b2 = 10.2 kN/m/s; Buoy b3 = 30.4 kN/m/s; and b4 = 121.3 kN/m/s. Figure 5-5 illustrates the excitation force applied on the buoys, corresponding to the sum of diffraction and Froude-krylov forces (see section 4.3.5).

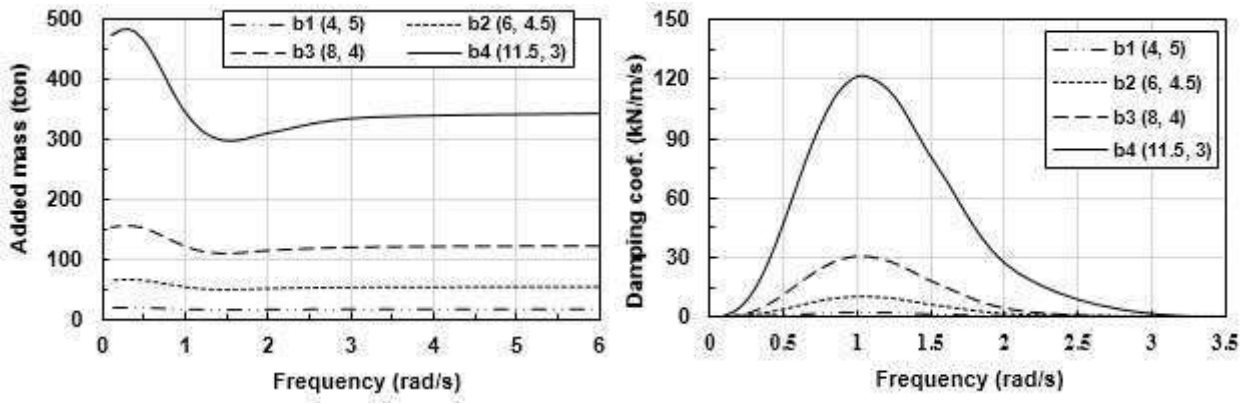

a) b)

Figure 5-4- Added mass and hydrodynamic damping coefficient for the oscillating buoys

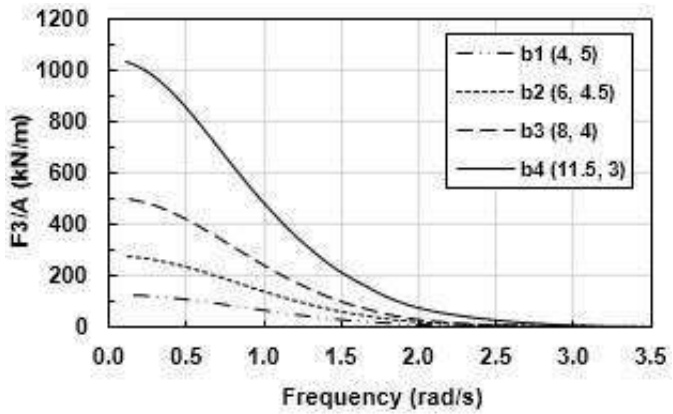

Figure 5-5- Excitation forces (Froude-Krylov + Diffraction) acting on the oscillating buoy

5.6 PTO control methods

5.6.1 Introduction

For the PTO optimal and control technologies, different optimal strategies have been studied till now. The analytical formulations of wave energy absorption which were presented by Falnes [100], is used in order to describe these methods. Following the expression given by Falnes, the dynamic equation for a floating body, in frequency domain, has a form as (see section 4.2.2):

$$\left[i\omega(m + a_{33}) + b_{33} + \frac{C_{33}}{i\omega}\right]u_3 = f_3 \tag{5.10}$$

Where m is the mass of the device, a_{33}, $b_{33}$and C_{33} are the added mass, hydrodynamic damping coefficient and the stiffness coefficient, respectively; u_3 the complex velocity amplitude; f_3 the complex excitation force amplitude for heave motion and ω the wave circular frequency. The PTO considered here is linear with the acceleration, velocity and motion of heave [100]:

$$F_{PTO} = -\left[a_{PTO}\ddot{X}_3(t) + b_{PTO}\dot{X}_3(t) + k_{PTO}X_3(t)\right] \tag{5.11}$$

Where $X_3(t)$ is the time-dependent heave motion, a_{PTO}, b_{PTO} and k_{PTO} are the linear coefficients of the PTO additional mass, PTO damping and PTO spring coefficient. Ideally, the PTO can be used as a device for energy extraction as well as a control device. To maximize the wave energy conversion, the PTO device is needed to be controlled so that the power take-off devices would have abilities to control the device as well as to convert energy from the moving body. Mathematically, it can be understood that the power take-off system will apply an external force on the oscillating body, and the mathematical expression of the force can be made as the linear terms of the acceleration, velocity and motion, given by Eq.(5.11). The average power extraction by the power take-off system is calculated as (see section 4.2.2):

$$\bar{P} = \overline{F_{PTO}(t).U_3(t)} = \frac{1}{2}Re(f_{PTO}.{U_3}^*) \tag{5.12}$$

Where * denotes the conjugate, overbar the average value over time and $U_3(t)$ is the time –dependent velocity. In analytical form, the average captured power can be given:

$$\bar{P} = \frac{1}{2}\frac{b_{PTO}|f_3|^2}{(b_{33}+b_{PTO})^2 + \left[\omega(m+a_{33}+a_{PTO}) - \frac{c_{33}+k_{PTO}}{\omega}\right]^2} \tag{5.13}$$

5.6.2 Optimum PTO damping (OPD)

As Falnes explained in [40], for a point absorber which oscillates in only one direction (heave as instance) the maximum power generation in the frequency domain can be achieved at the resonance frequency and it occurs when the PTO damping is equal the hydrodynamic damping. However, it does not guarantee the maximum power at the other frequencies. Considering a pure damper as PTO system ($k_{PTO} = 0,\ a_{PTO} = 0$), the analytical formula for the average captured power in each frequency can be expressed using Eq.(5.13) as follow:

$$\bar{P} = \frac{1}{2}\frac{b_{PTO}|f_3|^2}{(b_{33}+b_{PTO})^2 + \left[\omega(m+a_{33}) - \frac{c_{33}}{\omega}\right]^2} \tag{5.14}$$

Where m is the mass of the device, a_{33}, b_{33} and C_{33} are the added mass, hydrodynamic damping coefficient and the stiffness coefficient, respectively; f_3 the complex excitation force amplitude for heave motion and ω the wave circular frequency. Consequently, the optimized damping can be calculated as explained in section 4.2.2 as follow:

$$b_{PTOoptimized} = \left\{b_{33}^2 + \left[\omega(m+a_{33}) - \frac{C_{33}}{\omega}\right]^2\right\}^{\frac{1}{2}} \tag{5.15}$$

It is evident that the optimized PTO damping is frequency dependent, and this hinder its practical implementation. It can be said that it is the required PTO damping to maximize the power conversion in each frequency. Figure 5-6 shows the optimized damping, which has been calculated by the Eq.(5.15), and the hydrodynamic damping for each buoy. As it was expected (see section 4.2.2), two curves meet each other at the resonance frequency that proves that the value of hydrodynamic damping at resonance frequency maximize

the power production in that frequency. The values of optimized damping in higher and smaller frequencies are largely different from the hydrodynamic damping values.

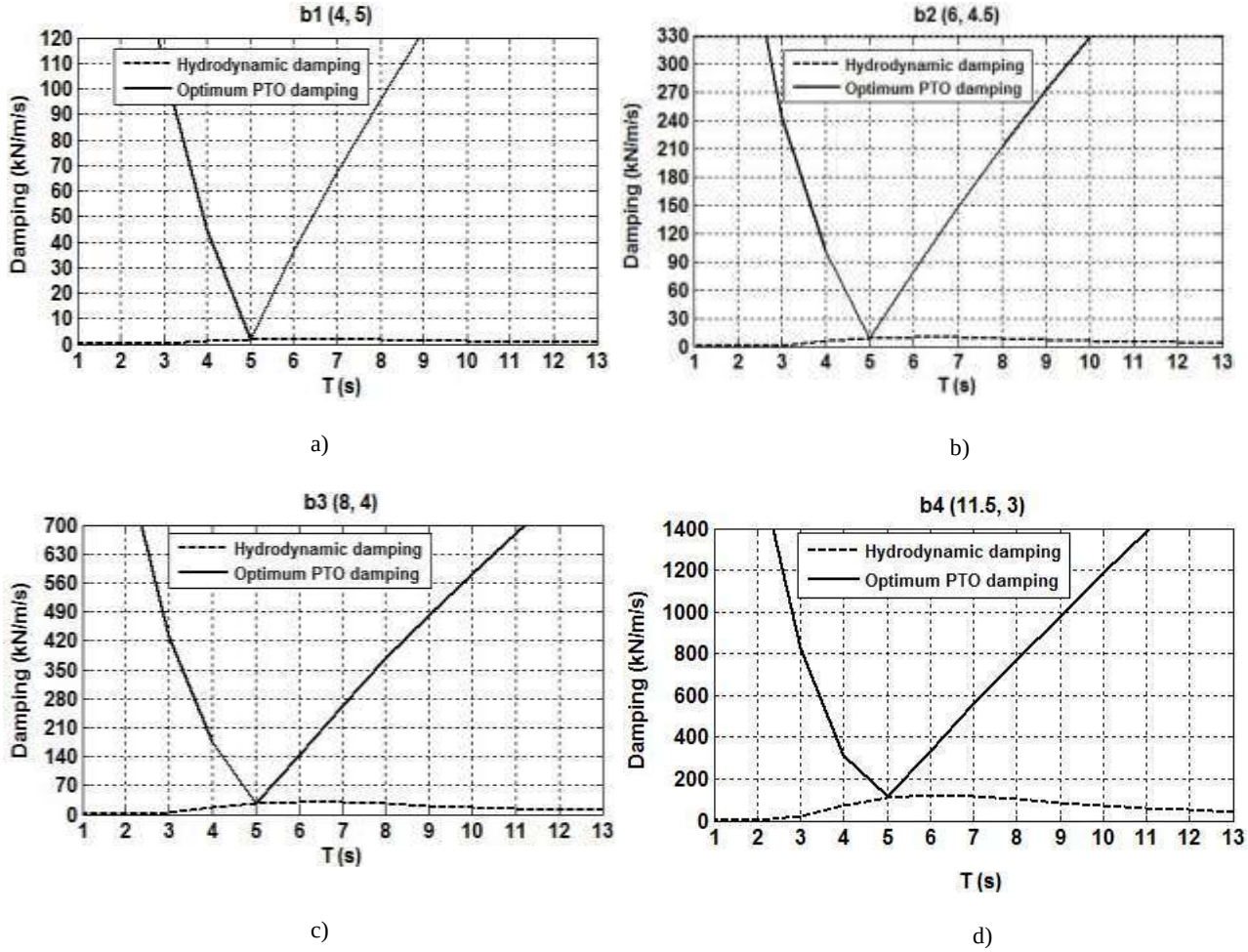

Figure 5-6 - Comparison of hydrodynamic coefficient and optimized PTO damping for each buoys, a) b1(4, 5), b) b2(6, 4.5), c) b3(8, 4) and d) b4(11, 3.5)

5.6.3 Constant PTO damping (CPD)

In this case, which may be considered as the simplest PTO control method, the pure damper is tuned to a constant damping to produce maximum wave energy conversion at a specified frequency. It is common to tune the PTO damping to the hydrodynamic damping at resonance frequency.

$$b_{PTO} = b_{33} \qquad \text{at the resonance frequency} \qquad (5.16)$$

Then, the absorbed power can be calculated via Eq.(5.14). Figure 5-7 shows the application of the CPD method on the buoys for different PTO damping levels. The concept of capture width, which is the ratio of the total average power absorbed by the

oscillating body to the mean power per unit crest waves width of the incident wave train at a given frequency, is used to illustrate the performance of the buoys. The capture width for the regular waves can be given as follow:

$$L = \bar{P}/(\rho g^2 T H^2/32\pi) \qquad \text{(deep water)} \qquad (5.17)$$

where the average power is calculated via Eq.(5.14) and the denominator is the wave energy flux of regular waves in deep water (see section 3.2). A significant wave height of $2\,m$ is considered for these analyses. The maximum capture width of a heaving axisymmetric body can be calculated as follow:

$$L_{max} = \lambda/2\pi \qquad (5.18)$$

which is the theoretical maximum capture width of a heaving axisymmetric body. As it is seen in figures 5-7- a to d, the maximum capture width is achieved at the resonance frequency, where the PTO damping is equal to the hydrodynamic damping. Larger and smaller values of PTO damping can not provide the same level of absorbed power at the resonance frequency. Adjusting the PTO damping to the smaller values results in smaller absorbed power and narrower bandwidth. In the other hand, the larger values increase the absorption bandwidth in both higher and lower frequencies. However, the absorbed power at the resonance frequency slightly decrease with the PTO damping increase. Comparing the buoy's graphs, it can be inferred that the capture width growth rate for the lower frequencies (lower than the resonance frequency) are more significant for the larger buoys. For instance, considering the performance of the b (4, 5) and b4 (11.5, 3) at the frequency of $\omega = 1\,rad/s$ ($T = 6.3\,s$), in the case of buoy b1, the capture width has a growth of about 20% for 200% increase of PTO damping while this value is about 60% for the same increase of PTO damping of buoy b4. It can be concluded that a slightly larger values for PTO damping may lead to a better absorption specially in the region of frequencies lower than the buoy resonance frequency. This issue should be considered for the local sea with the predominant wave periods beyond the heaving PA natural period.

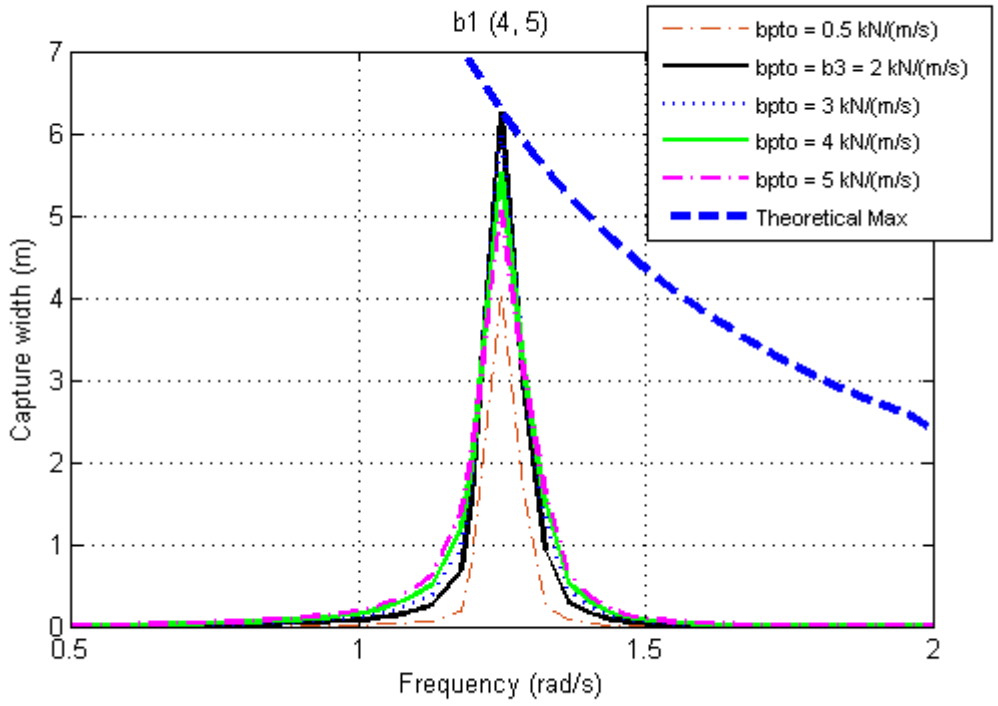
b1 (4, 5)
bpto = 0.5 kN/(m/s)
bpto = b3 = 2 kN/(m/s)
bpto = 3 kN/(m/s)
bpto = 4 kN/(m/s)
bpto = 5 kN/(m/s)
Theoretical Max
Capture width (m)
Frequency (rad/s)
0
1
2
3
4
5
6
7
0.5
1
1.5
2

a)

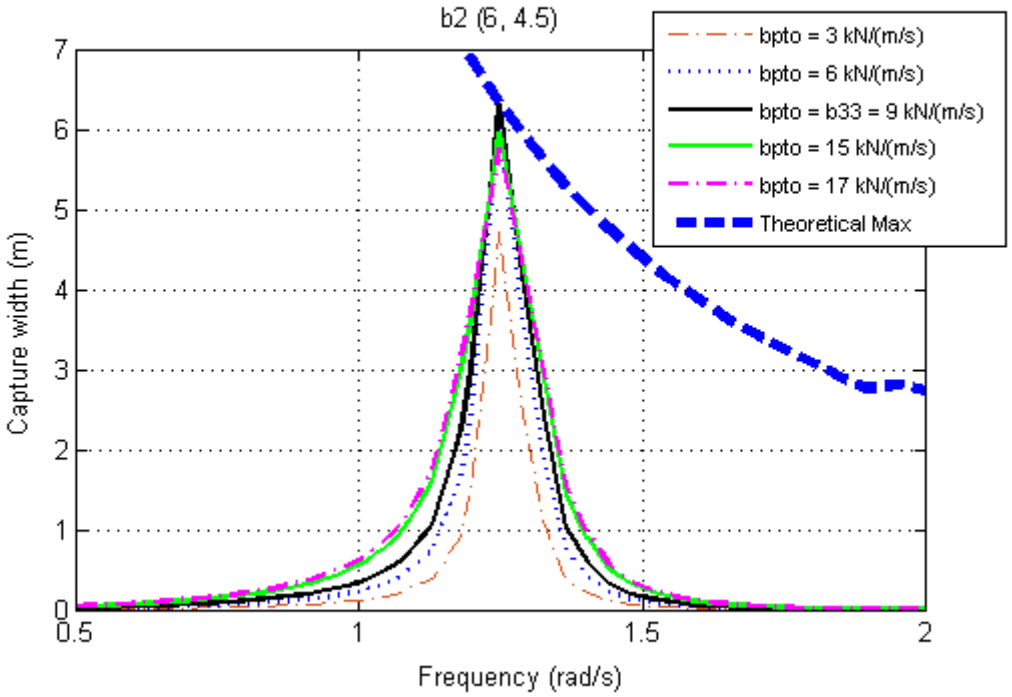
b2 (6, 4.5)
bpto = 3 kN/(m/s)
bpto = 6 kN/(m/s)
bpto = b33 = 9 kN/(m/s)
bpto = 15 kN/(m/s)
bpto = 17 kN/(m/s)
Theoretical Max
Capture width (m)
Frequency (rad/s)
0
1
2
3
4
5
6
7
0.5
1
1.5
2

b)

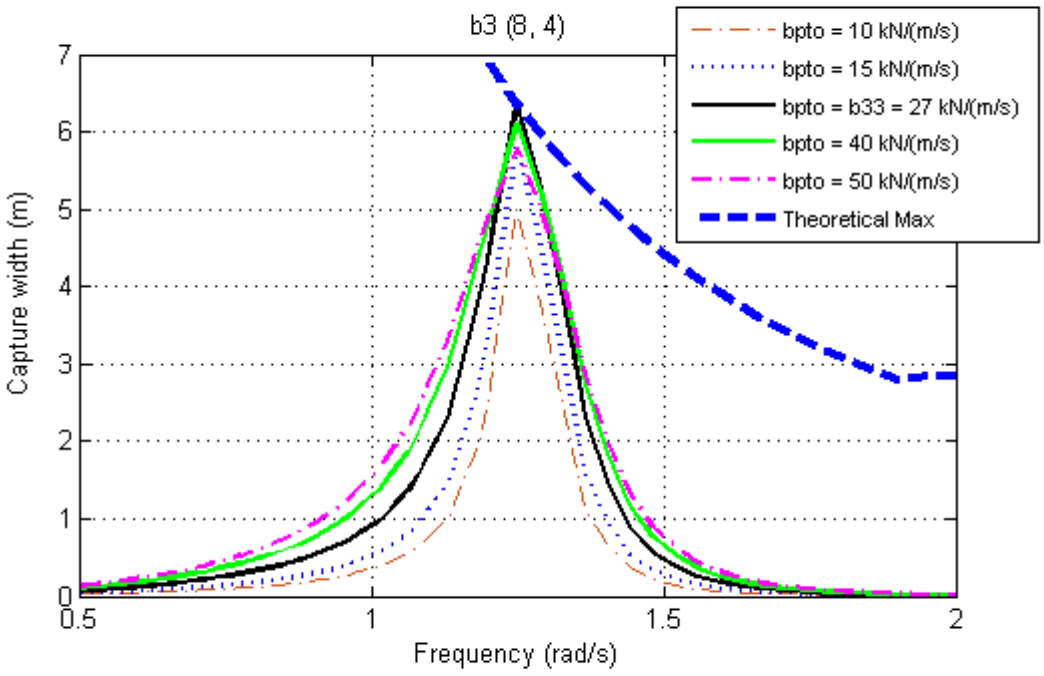

c)

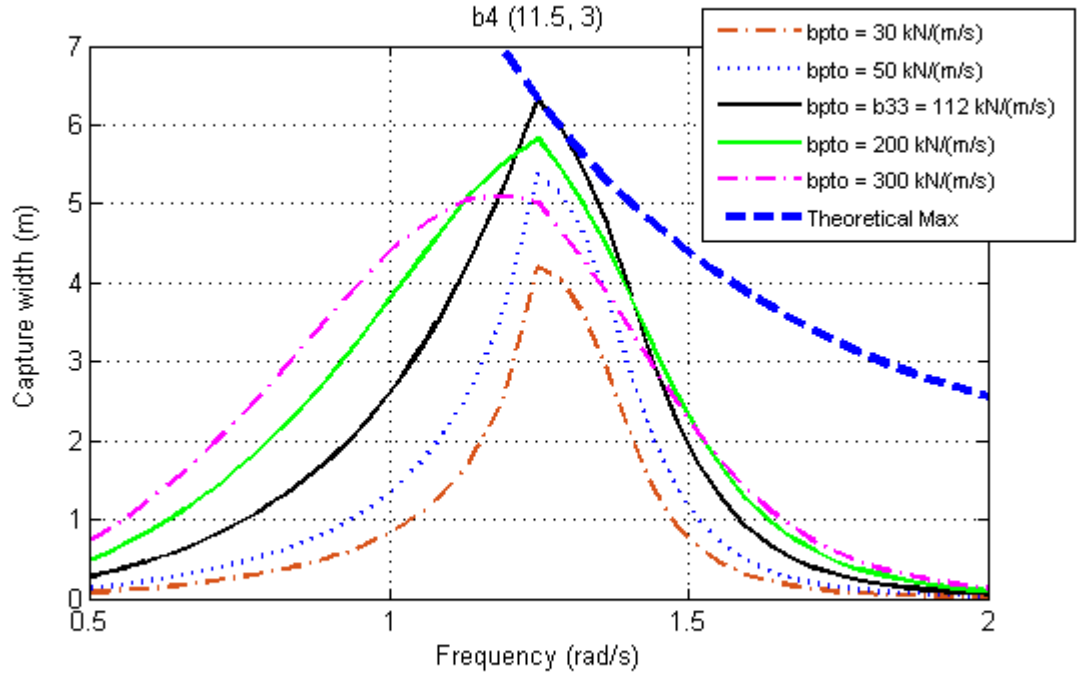

d)

Figure 5-7– Wave energy capture width Vs frequency with application of CPD method for; a) b1 (4, 5), b) b2 (6, 4.5), c) b3 (8, 4) and d) b4 (11.5, 3)

5.6.4 Full PTO control (reactive control)

Two conditions must be fulfilled to extract the maximum energy from a heaving point absorber. Reactive control continuously adapt the system to satisfy these two conditions. The first one is the "phase control", which requires that the oscillating velocity of the body must be in phase with the excitation force on the body. This happens naturally when the wave frequency equals the natural frequency of the body; otherwise, a force must act on the body in order to respect it. Mathematically, it occurs, for an arbitrary b_{PTO}, when the following equation is satisfied (see section 4.2.2):

$$\omega(m + a_{33} + a_{PTO}) - \frac{C_{33} + k_{PTO}}{\omega} = 0 \tag{5.19}$$

The second condition is called the "optimum amplitude" condition, and, in the case of no constrain for the heaving amplitude, it is fulfilled when the PTO damping is equal to the hydrodynamic damping coefficient at the incident wave frequency:

$$b_{PTO} = b_{33} \equiv b_{PTO,opt} \tag{5.20}$$

Applying these two conditions on the Eq.(5.14) results the maximum average power, which is the theoretical maximum absorbed power for a heaving point absorber, shown as follow:

$$\bar{P}_3 = \frac{1}{8}\frac{|f_3|^2}{b_{33}} \tag{5.21}$$

As it is mentioned in chapter 2, this control method was presented in the mid-1970 by Salter and Budal&Falnes [47,48]. To achieve this, the PTO must have an ability to adjust the coefficients of the PTO inertia, damping and spring terms, in such a manner that satisfies the optimum phase and amplitude conditions. In real, the PTO device requires to be an idealized device in both efficiently taking energy out from the oscillating body and feeding energy back to the oscillating device. Figure 5-8 shows the power absorption of the buoys applying the PTO control methods in frequency domain. The OPD control is applied by substituting the optimum damping (Eq.(5.15)) into the average power formula (Eq.(5.14)). The hydrodynamic damping at resonance frequency is considered for the CPD method. The average power results from the reactive control, which is the theoretical

maximum absorbed power, is calculated through the Eq.(5.21). As it is shown, three curves meet each other at the resonance frequency. The power absorption increase in the regions out of the resonance frequency applying the OPD method. It comes more evident for the frequency range smaller than the resonance frequency. More energy absorption occurs for the buoys with larger diameters. For instance, figure 5-8-d shows the power absorption for the buoy b4 (11.5, 3). It can seen that the value of the mechanical power for the $\omega = 0.74$ rad/s is 119 kW which is approximately equal to the maximum value at the resonance frequency. It is because of the frequency-dependency of the added mass, hydrodynamic damping and wave exciting force. For the frequencies smaller than resonance frequency, the hydrodynamic damping decreases and the wave excitation force increases, as it shown in figures 5-4-b and 5-5; and also we have the much increase of the optimized PTO damping, figure 5-8, which is dominated by $\frac{c_{33}}{\omega}$ (Eq.(5.15)).

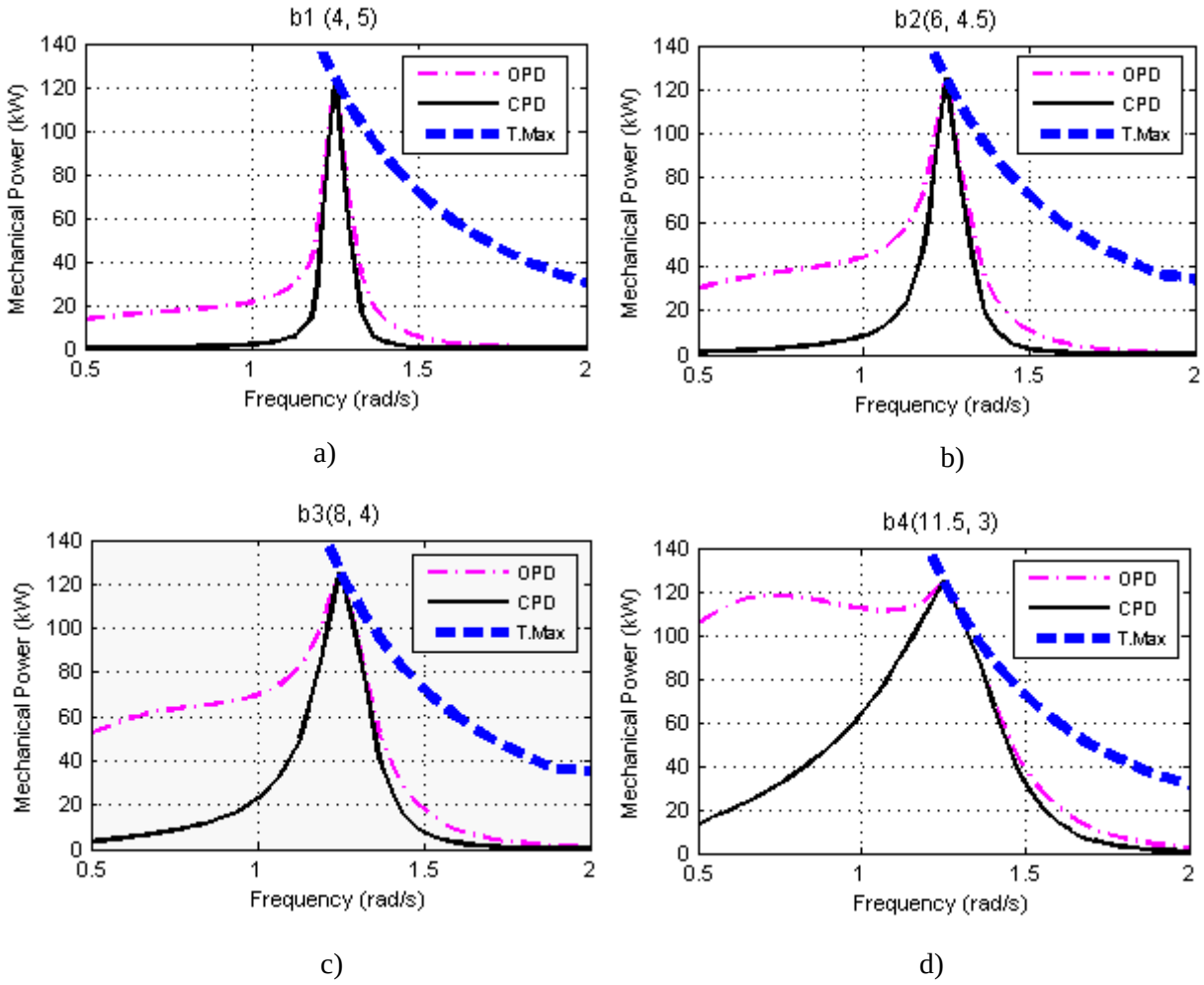

Figure 5-8– Mechanical power of the buoys applying OPD and CPD (considering bpto equal to the b33 of the resonance frequency) methods against the theoretical maximum power

5.7 Time-domain modeling of a heaving point absorber controlled by latching

5.7.1 FORTRAN code development

5.7.1.1 Introduction

A wave-to-wire model for a heaving point absorber is developed through a FORTRAN code. In this thesis, it is defined as the simulation of the WEC dynamics from the sea waves as input, to the electric power as output. The principal assumptions that are considered for the wave-to-wire model here are as follows:

- The hydrodynamic linear theory.
- The diameter of the cylinder is small relative to the wavelength ($KD < 0.5$), implying that the incident waves upon arriving at the structure do not undergo significant scattering or diffraction, therefore the effect of diffraction of waves from the surface of the cylinder can be neglected.
- The point absorber movement is restricted to heave motion.
- A pure damper b_{PTO} is considered as PTO system ($K_{PTO} = 0$).

The hydrodynamic parameters, such as added mass, hydrodynamic damping, wave exciting force are calculated based on linear potential theory by AQWA ANSYS code. Figure 5-9 illustrates the flowchart of the time domain solution of a heaving point absorber controlled by a constant-delay latching. The code calculates the wave spectrum and irregular wave forces based on the user definition of sea state, specified by a peak period,T_p, and a significant wave height, H_s. The latching condition is monitored in each time step by velocity checking. If latching condition is true ($\dot{X} = 0$) the latching force is applied for a pre-defined constant latching duration. For a given sea state, the code calculates the average produced power of the system using Eq.(5.9). Furthermore, it also calculates the annual energy production (AEP) using the joint probability distribution of the waves as the input.

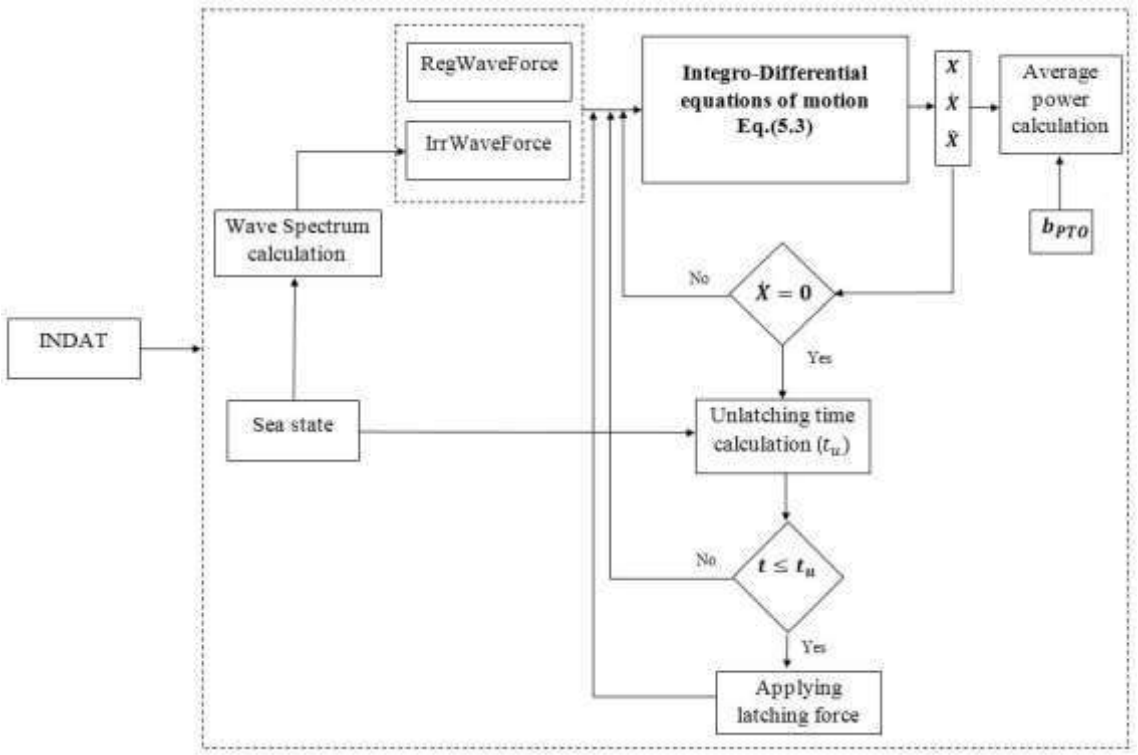

Figure 5-9- Time-domain simulation flowchart of a heaving point absorber controlled by a constant-delay latching control

5.7.1.2 Code structure

Figure 5-10 shows the structure of the code which consists of the inputs/outputs and the computational subroutines. This model is developed based on the code that was presented by Celis [121], for the time domain simulation of a heaving cylinder in regular waves. As it is described in the legend of the figure, the computational subroutines are illustrated with different colors. The light orange represents the subroutines that are part of the principle code written by Celis which are adapted for the wave-to-wire model of the system. The gray subroutine is the part of the principle code that remains unchanged and the green blocks are the subroutines that are added to simulate the behavior of the WEC in irregular sea with application of a constant-delay latching control.

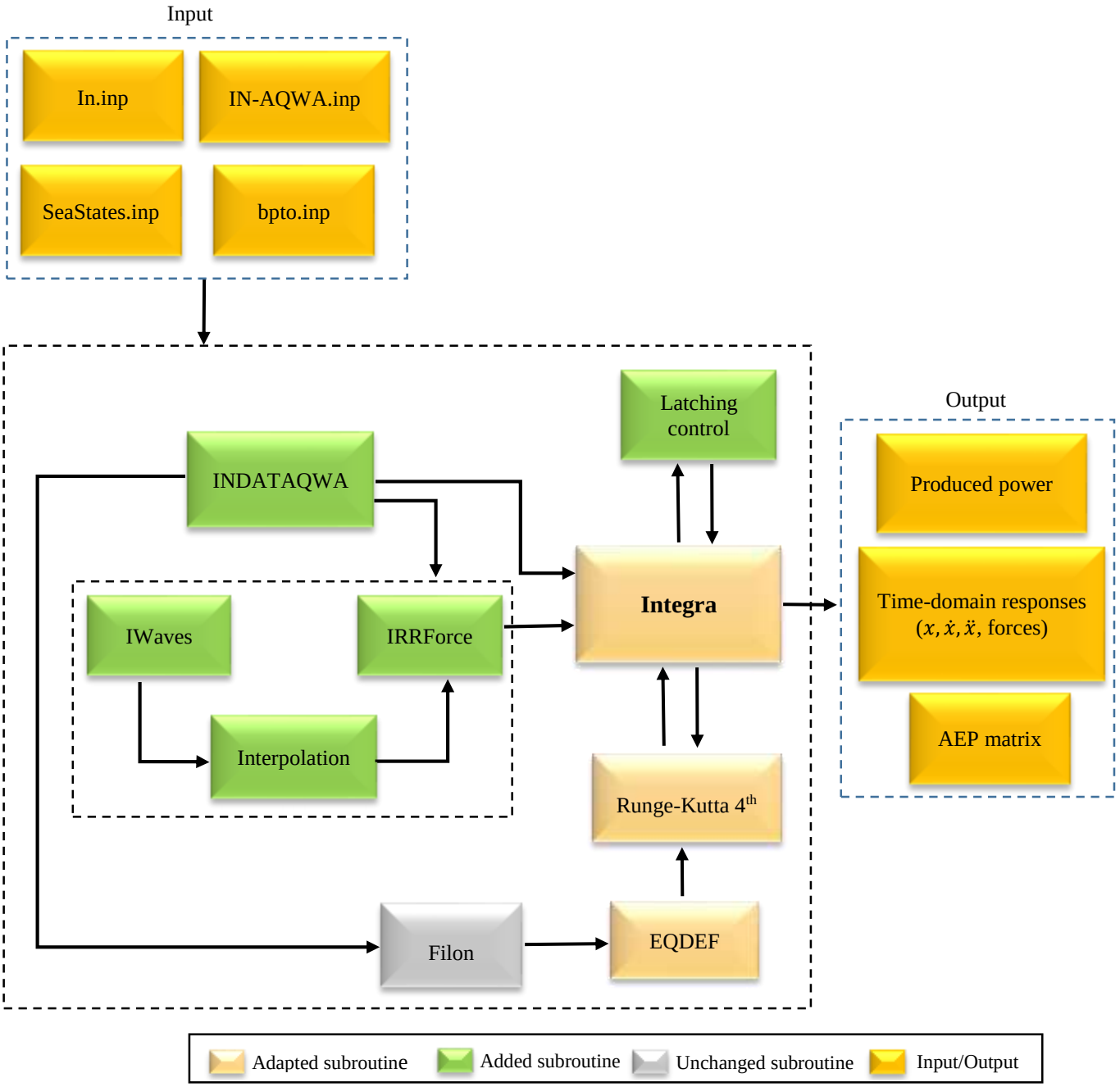

Figure 5-10– Wave-to-wire model structure

5.7.1.2.1 Input/Output

Input block consists of text files with the extension of $*.inp$ that provide a single sea state or/and a sea joint probability distribution (JPD) matrix ($SeaStates.inp$), a single or/and a range of PTO damping ($b_{PTO}.inp$) and the AQWA ANSYS output text file (IN-AQWA.inp). INDATAQWA extracts the required results such as hydrodynamic coefficients, phases, periods etc., from the IN-AQWA.inp. The initial and final time of

the simulation, time step, initial conditions, etc. can be defined in the In.inp file. Additionally, the user can run the simulation with or without application of latching control through In.inp file. *Output* block includes the instantaneous/mean power of the wave converter, displacement, velocity and acceleration of the floater, the hydrodynamic forces induced by the sea waves and mechanical forces due to the PTO and latching mechanism. The annual energy production (AEP) matrix is also calculated as an output. The code requires a sea JPD matrix to produce the AEP as output.

5.7.1.2.2 Dynamic equation solver

Integra can be considered as the main subroutine. It calls the other computational subroutines (e.g. latching control, Runge-Kutta 4th etc.) to simulate the hydro-mechanical system and produces the outputs. The latching and unlatching moments are identified through the latching control subroutine. For instance, the *Integra* calls the *latching control* subroutine in each time step to verify the latching condition ($\dot{x} = 0$). As soon as this condition comes true, the Integra locks the floater movement for a certain constant duration through the Runge-Kutta 4th and EQDEF subroutines. A latching force calculated via Eq.(5.8) is required to be applied on the buoy in order to latch the system. A direct convolution integration model is used for the analysis in time domain. In this model, the convolution terms in the equations of motion are not replaced by any approximations and are integrated directly at each time step. A Runge-Kutta 4th is used for the time integration. Kurniawan et al [122] compared four different time integration methods, the Euler's method, the improved Euler's (Heun's) method, Runge-Kutta 3th and Runge-Kutta 4th methods. The results showed that the Runge-Kutta 4th method has a relatively better performance comparing to the other methods. The hydro-mechanical integro-differential equation of motion described in section 5.4 (Eq.(5.3)) is constructed in EQDEF and updated in each time step. The EQDEF provides the Runge-Kutta 4th subroutine with the updated dynamic equation in each time step. The radiation impulse function $f_{r,33}$ (retardation function see Eq.(3.52)) is calculated through a numerical model called Filon method. The results for the buoys are shown in figure 5-11. As it can be seen, the maximum value of the impulse function for b1 (4, 5); $f_{r,33} = 1.52\ kN/m$ is quite smaller comparing to b2 (6, 4.5);$f_{r,33} = 7.13\ kN/m$, b3 (8, 4); $f_{r,33} = 21.7\ kN/m$ and b4 (11.5, 3); $f_{r,33} = 94.32\ kN/m$, due to the low hydrodynamic damping level (see

figure 5-4-b). The Runge-Kutta 4th and Filon methods are described in appendices I and II, respectively.

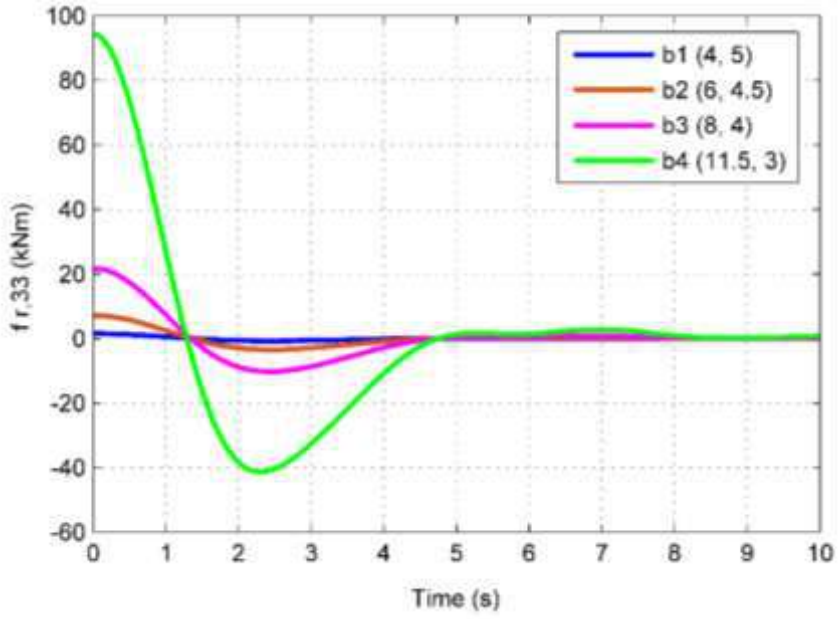

Figure 5-11 – Impulse response function of the buoys for heave motion

5.7.1.2.3 Sea characteristics

Real sea is mathematically represented by irregular waves which can be simulated as a superposition of regular waves. By considering a one directional wave propagation, a given sea state is adequately represented by a one dimensional energy sea spectrum. Since the buoys are axisymmetric and therefore quite insensitive to wave direction, a one-dimensional spectrum will be considered in the following analyses. *Iwave* subroutine calculates the spectrum of the sea local based on its modal period and significant wave height through the JONSWAP model. The characteristics of the local sea state, modal period $T_p = 9.7\ s$, significant wave height $Hs = 1.33\ m$ for the nearshore Rio de Janeiro, are considered for the simulation in this chapter (see figure 4-4). A range of frequency between $\omega_i = 0.016\ Hz$ ($T = 63\ s$) and $\omega_f = 0.334$ ($T = 3\ s$) with a frequency interval of $\Delta\omega = 0.002\ Hz$ and a peakedness factor of $\gamma = 3.3$ are considered for the calculation of the JONSWAP spectrum by Eq.(3.37). Figure 5-12 shows the resultant spectrum.

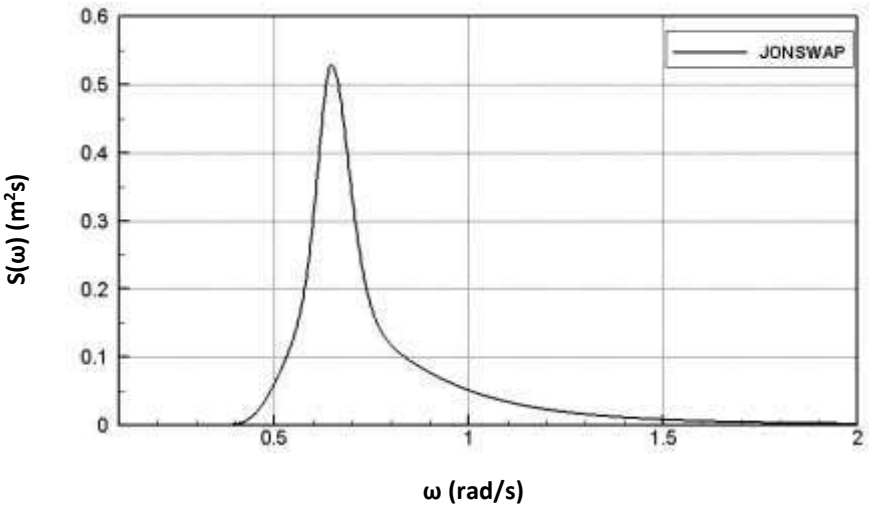

Figure 5-12- JONSWAP spectrum, $T_p = 9.7\ s,\ Hs = 1.33\ m$, typical for nearshore Rio de Janeiro - Brazil

IRRForce then calculates the irregular wave forces (linear first order wave forces) in each time step applying the Eq.(3.58). The spectrum is constructed using almost 1000 frequencies ($N \approx 1000$), while the number of frequencies in the frequency domain analyses performed by AQWA ANSYS is around 60. To calculate the irregular wave forces using Eq.(3.58), the spectrum values correspond to the frequencies of AQWA runs are required. *Interpolation* subroutine is employed to find the corresponding values of the spectrum.

5.7.2 Time-domain simulation results

Figures 5-13 to 20 shows the 100 seconds window of the time domain results of the buoys with and without application of latching control. The hydrodynamic coefficients are obtained through the frequency domain analyses using AQWA ANSYS. The constant-delay latching control presented by Sheng et al [77,78] (see section 5.3) is applied on the heaving point absorbers. Figures 5-13 to 16 illustrates the responses of the buoys result from a monochromatic wave of $T = 7\ s$ and $H = 2\ m$, with and without latching control. A constant PTO damping equal to the optimum value corresponding to the wave period of 7 s, as shown in figure 5-6, is considered for each system. The values are shown in table 5-1.

Table 5-1 – Optimum PTO damping values for a control-free system in a monochromatic wave of $T = 7$ s

	b1 (4, 5)	b2 (6, 4.5)	b3 (8, 4)	b4 (11.5, 3)
Optimum PTO damping at T=7 s for a control-free system (kN/(m/s))	65	150	250	550

The latching duration is calculated using Eq.(5.1). The buoy is halted for the latching duration of 1 s as it reaches the maximum heave excursion. As the result, as it shown in the third plot from top to bottom, the buoy velocity and the wave excitation force satisfy the optimum phase condition leading to a significant increase in power production. The forth plot from top to bottom shows the required latching force versus buoy displacement controlled by latching. It seen that the control system must provide about $150\ kN$, $300\ kN$, $550\ kN$ and $1000\ kN$ for the b1, b2, b3 and b4 respectively in order to latch them. This value increases and decreases during the latched situation that are mainly caused due to the increase and decrease of the excitation force. The PTO force plot illustrates an amplification for the controlled buoy resulting from the velocity increase. It is evident that the PTO system does not apply any forces on the device during the latched situation. The simulation results for the irregular sea of $T_p = 7\ s$ and $H_s = 2\ m$ are plotted in figure 5-21 to 24. The same latching method is applied with a constant latching duration of 1 s tuned to the energy period of the sea spectrum (it is assumed that $T_p = T_e$, see section 4.3.2). The damping values of table 5-1 are considered for the PTO system of the buoys in irregular wave simulations. Considering the second plot, from top to bottom, of each figure (figure 5-13 to 20), it can be inferred that, applying latching control, for the regular wave case the optimum phase condition is satisfied. For the simulations in irregular waves, the velocities of the controlled buoys are much in-phase with the excitation comparing to the control-free buoys, however this condition cannot be fully fulfilled. Significant increases in power production are obtained for both regular and irregular wave simulations. However, the values of the absorbed power for the buoys controlled by latching are not the optimum values. The optimum amplitude condition is needed to be satisfied in order to increase the power production of the buoys controlled by latching. To achieve this the PTO damping values should be determined to maximize the power production. The next section addresses the effect of latching control on the optimum values of the PTO damping.

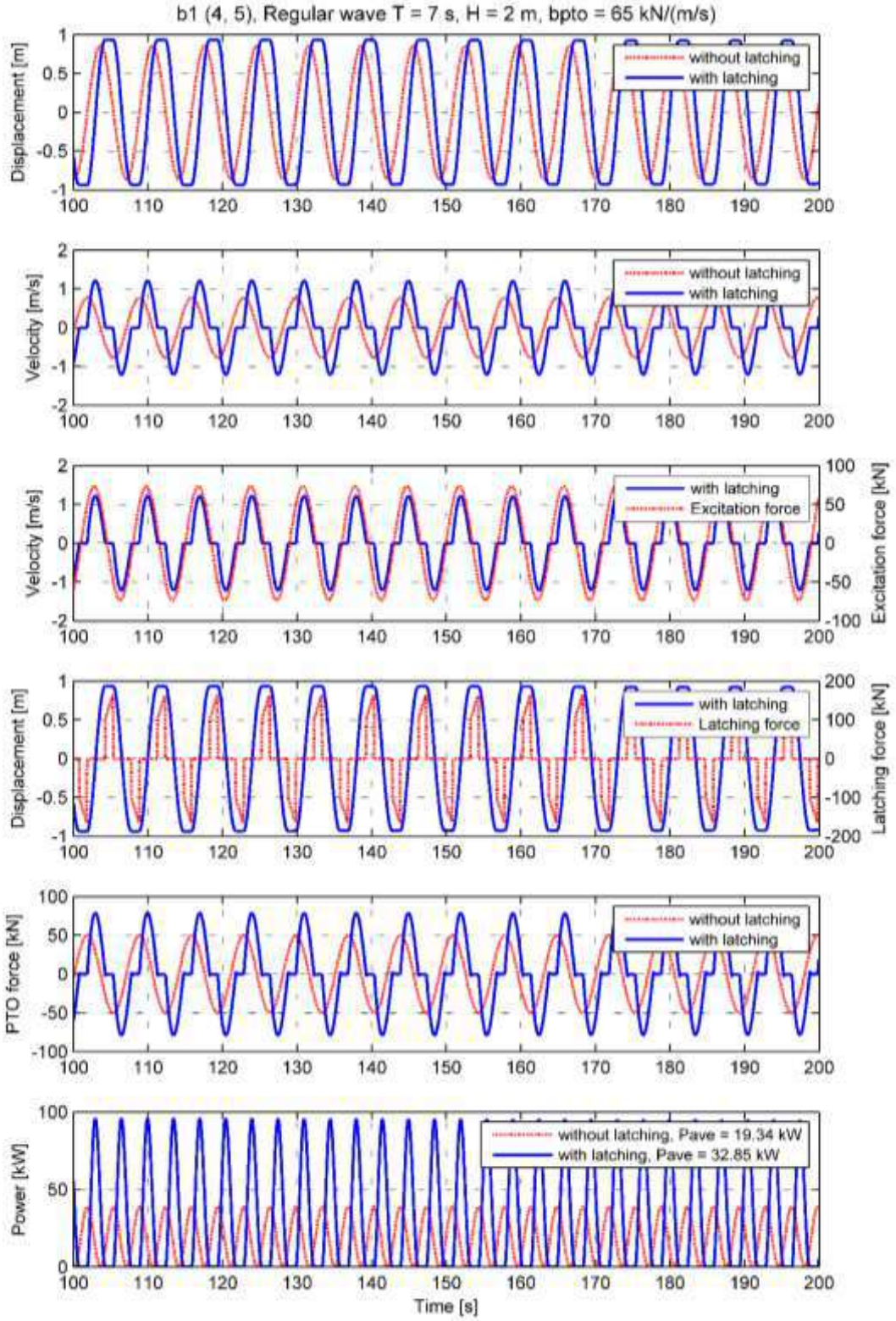

Figure 5-13– The time domain results of the buoy b1 (4, 5) in a regular wave of $T = 7\ s$ and $H = 2\ m$ with and without application of a constant-delay latching control, considering a constant PTO damping bpto = 65 kN/(m/s). From top to bottom: Displacement, velocity, excitation, latching force, PTO force and mechanical power

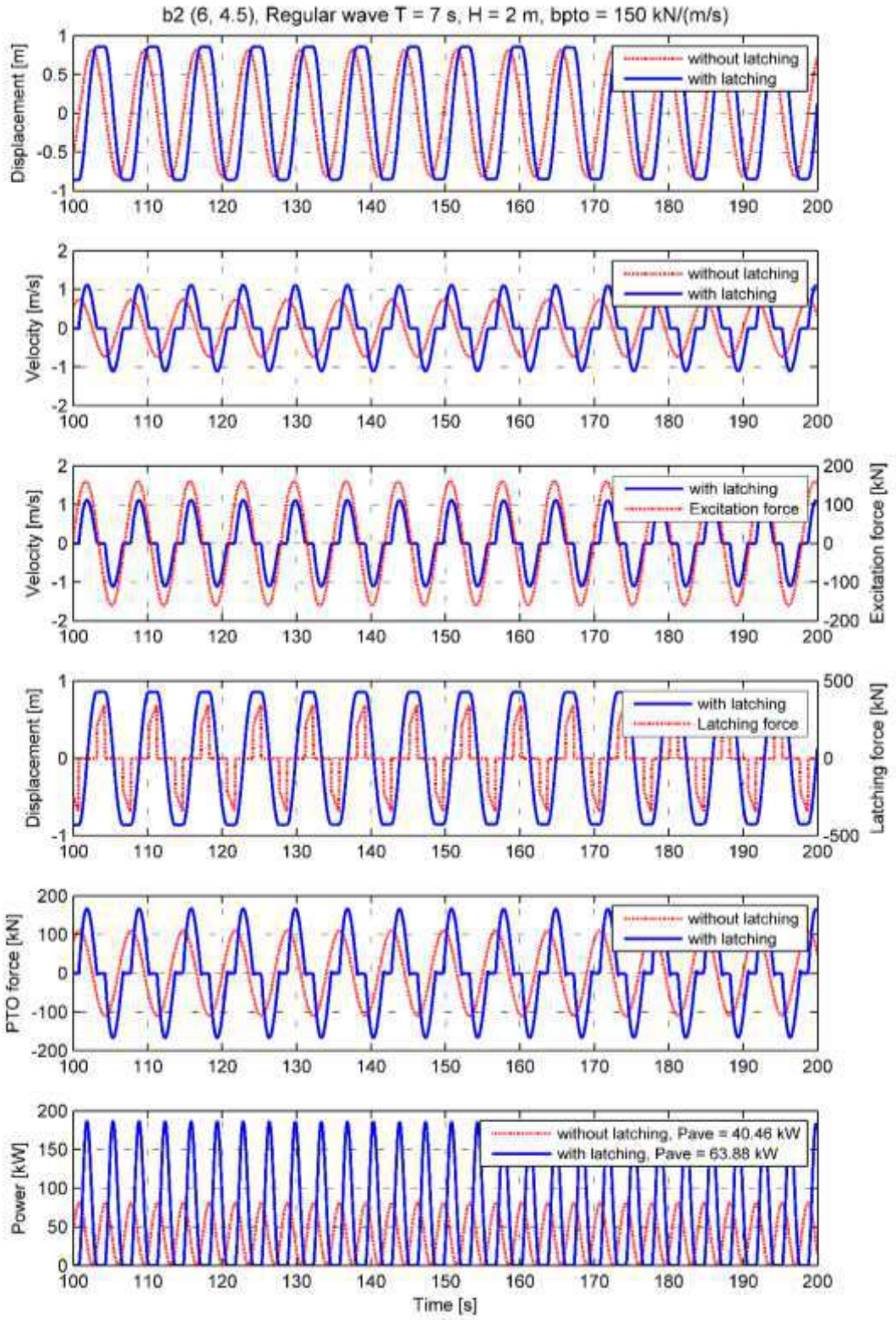

Figure 5-14- The time domain results of the buoy b2 (6, 4.5) in a regular wave of $T = 7\ s$ and $H = 2\ m$ with and without application of a constant-delay latching control, considering a constant PTO damping bpto = 150 kN/(m/s). From top to bottom: Displacement, velocity, excitation, latching force, PTO force and mechanical power

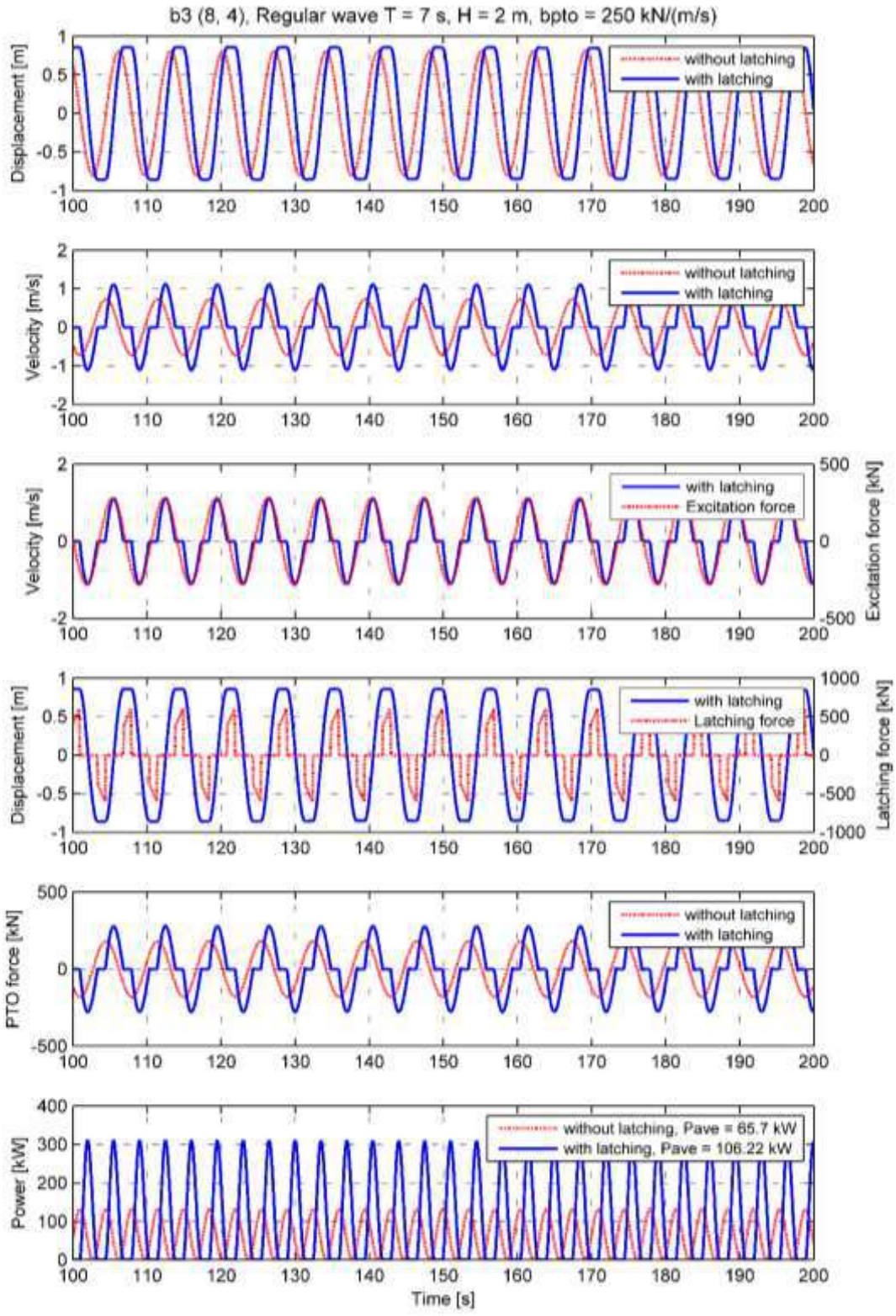

Figure 5-15 - The time domain results of the buoy b3 (8, 4) in a regular wave of $T = 7\ s$ and $H = 2\ m$ with and without application of a constant-delay latching control, considering a constant PTO damping bpto = 250 kN/(m/s). From top to bottom: Displacement, velocity, excitation, latching force, PTO force and mechanical power

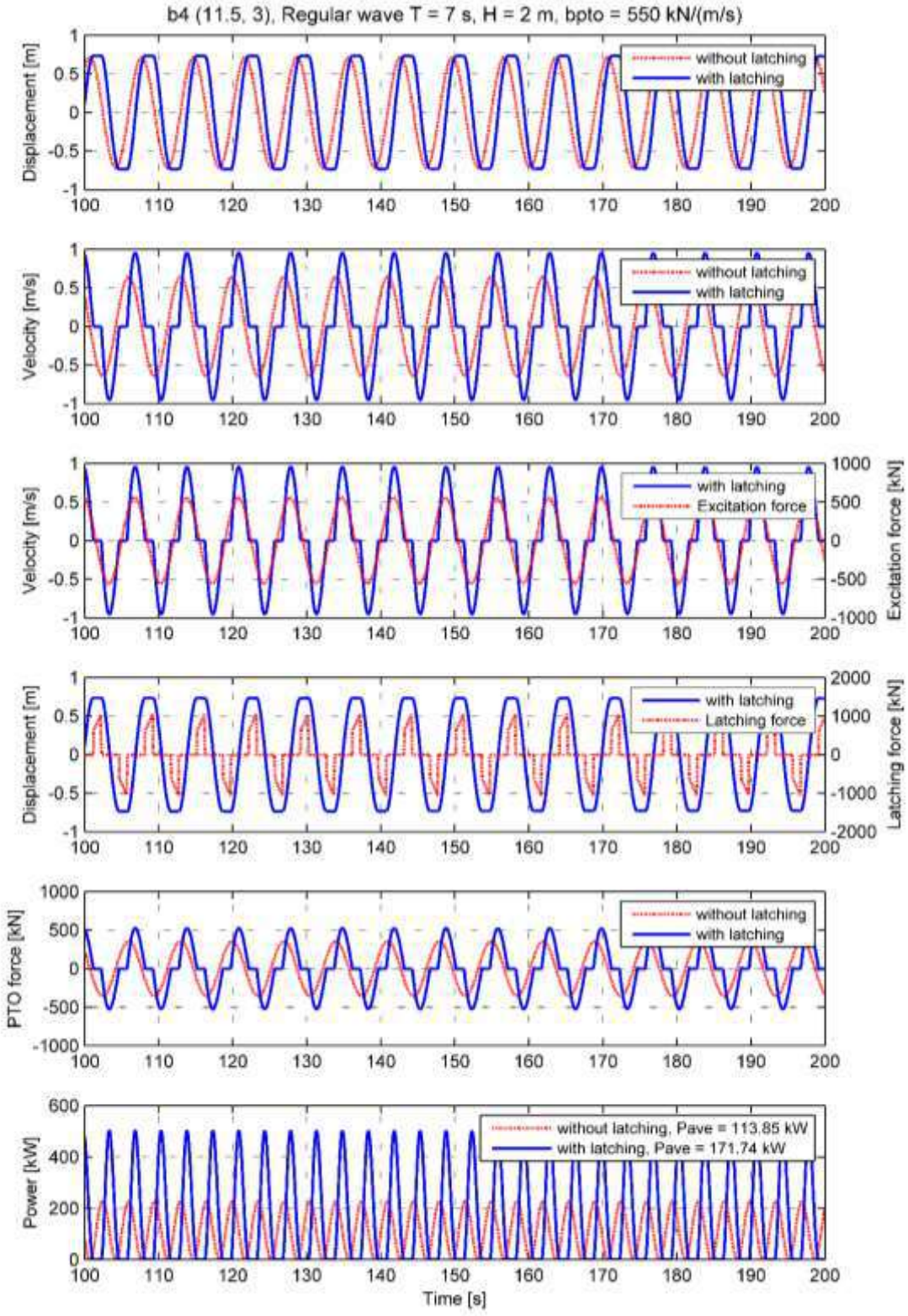

Figure 5-16- The time domain results of the buoy b4 (11.5, 3) in a regular wave of $T = 7\ s$ and $H = 2\ m$ with and without application of a constant-delay latching control, considering a constant PTO damping bpto = 550 kN/(m/s). From top to bottom: Displacement, velocity, excitation, latching force, PTO force and mechanical power

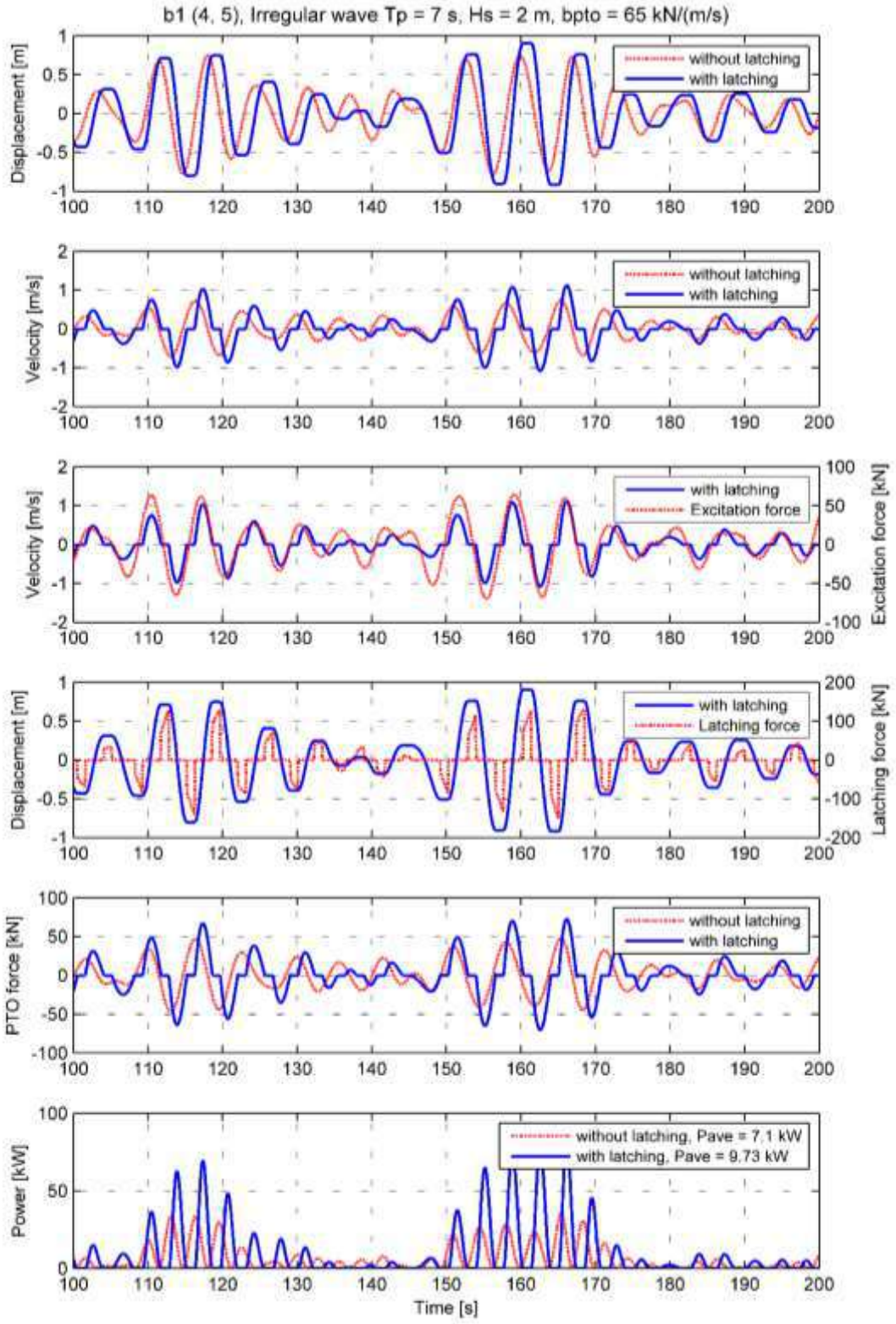

Figure 5-17- The time domain results of the buoy b4 (4, 5) in an irregular wave of $T_p = 7\ s$ and $H_s = 2\ m$ with and without application of a constant-delay latching control tuned to the spectrum energy period, considering a constant PTO damping bpto = 65 kN/(m/s). From top to bottom: Displacement, velocity, excitation, latching force, PTO force and mechanical power

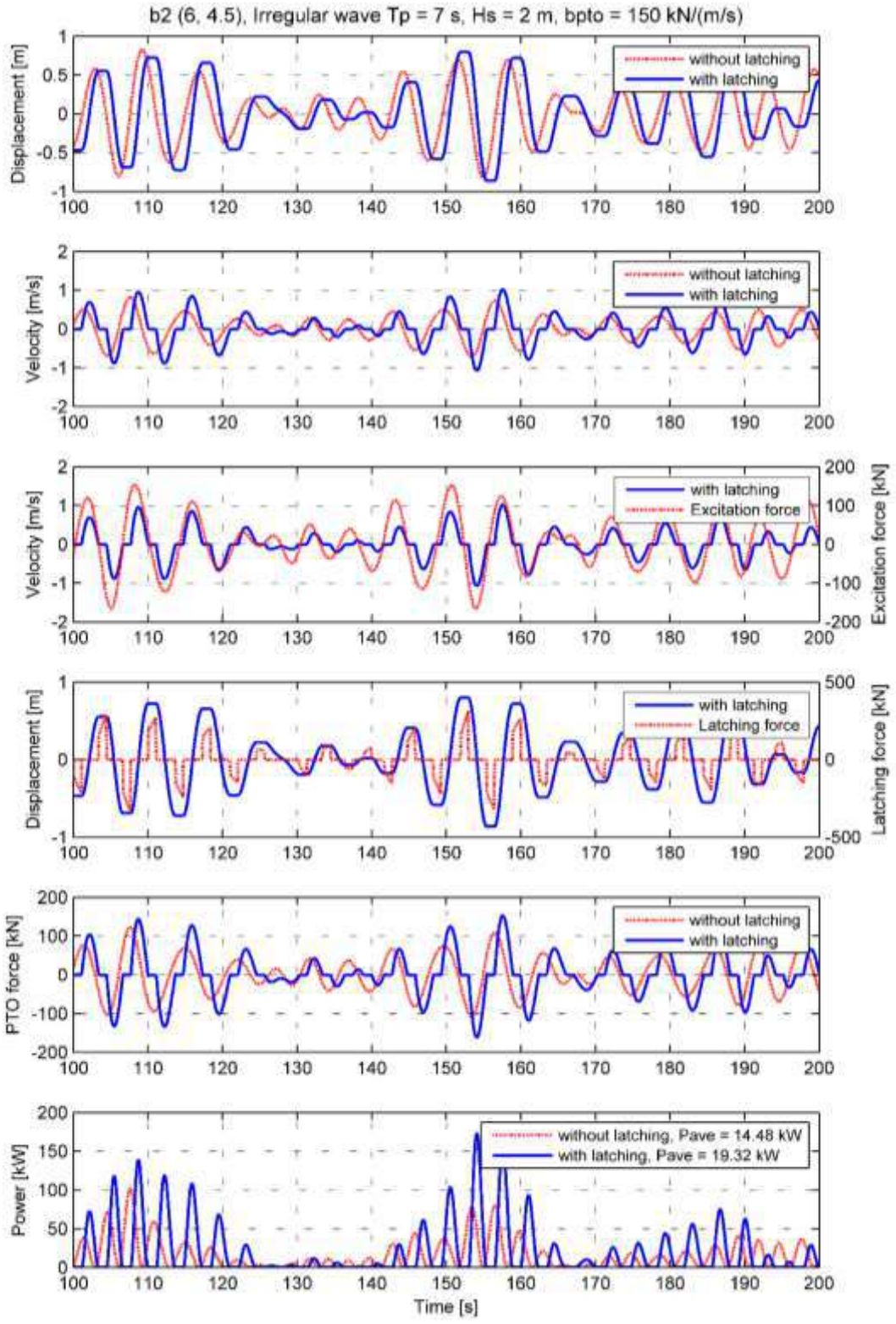

Figure 5-18- The time domain results of the buoy b4 (6, 4.5) in an irregular wave of $T_p = 7\ s$ and $H_s = 2\ m$ with and without application of a constant-delay latching control tuned to the spectrum energy period, considering a constant PTO damping bpto = 150 kN/(m/s). From top to bottom: Displacement, velocity, excitation, latching force, PTO force and mechanical power

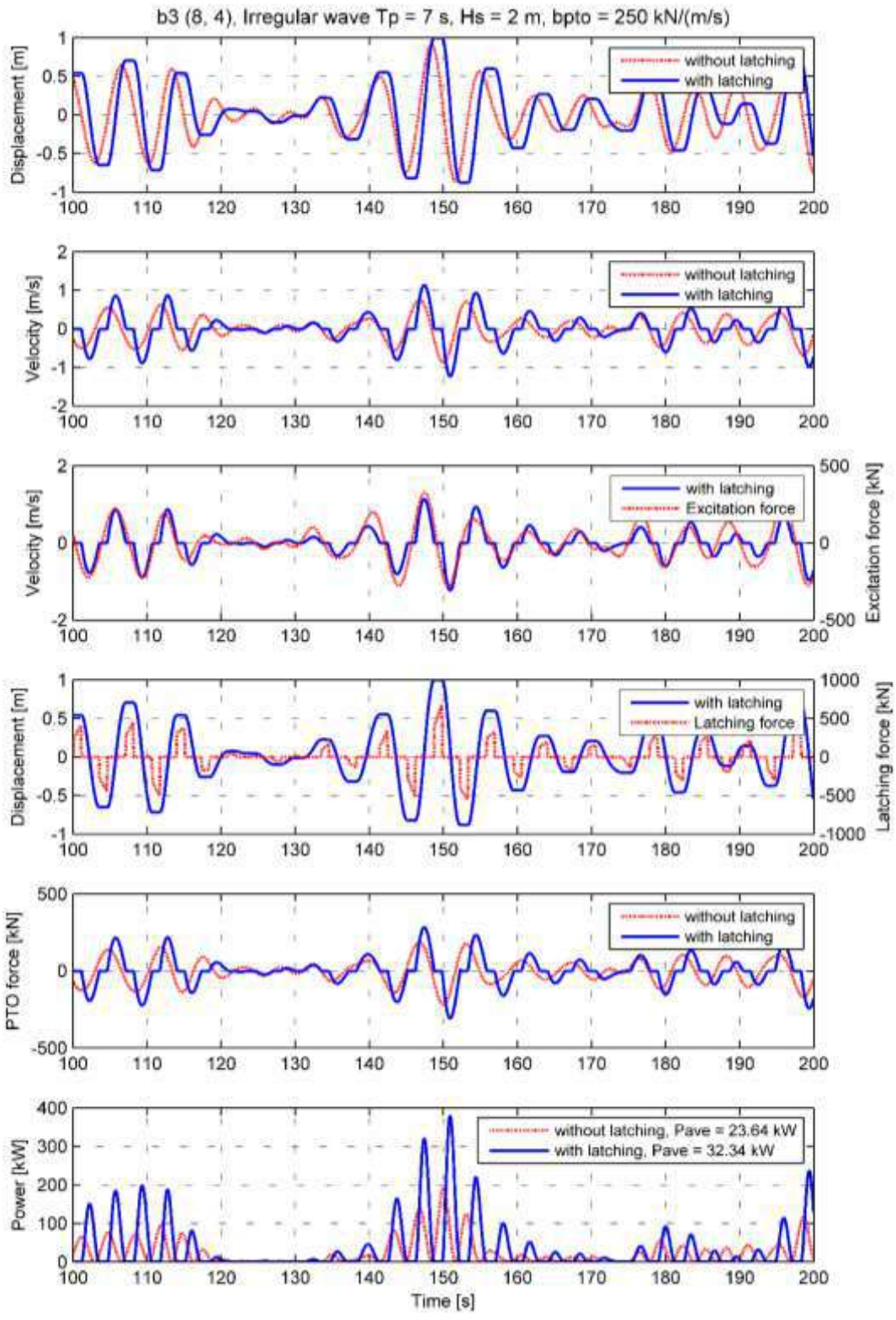

Figure 5-19- The time domain results of the buoy b4 (8, 4) in an irregular wave of $T_p = 7\ s$ and $H_s = 2\ m$ with and without application of a constant-delay latching control tuned to the spectrum energy period, considering a constant PTO damping bpto = 250 kN/(m/s). From top to bottom: Displacement, velocity, excitation, latching force, PTO force and mechanical power

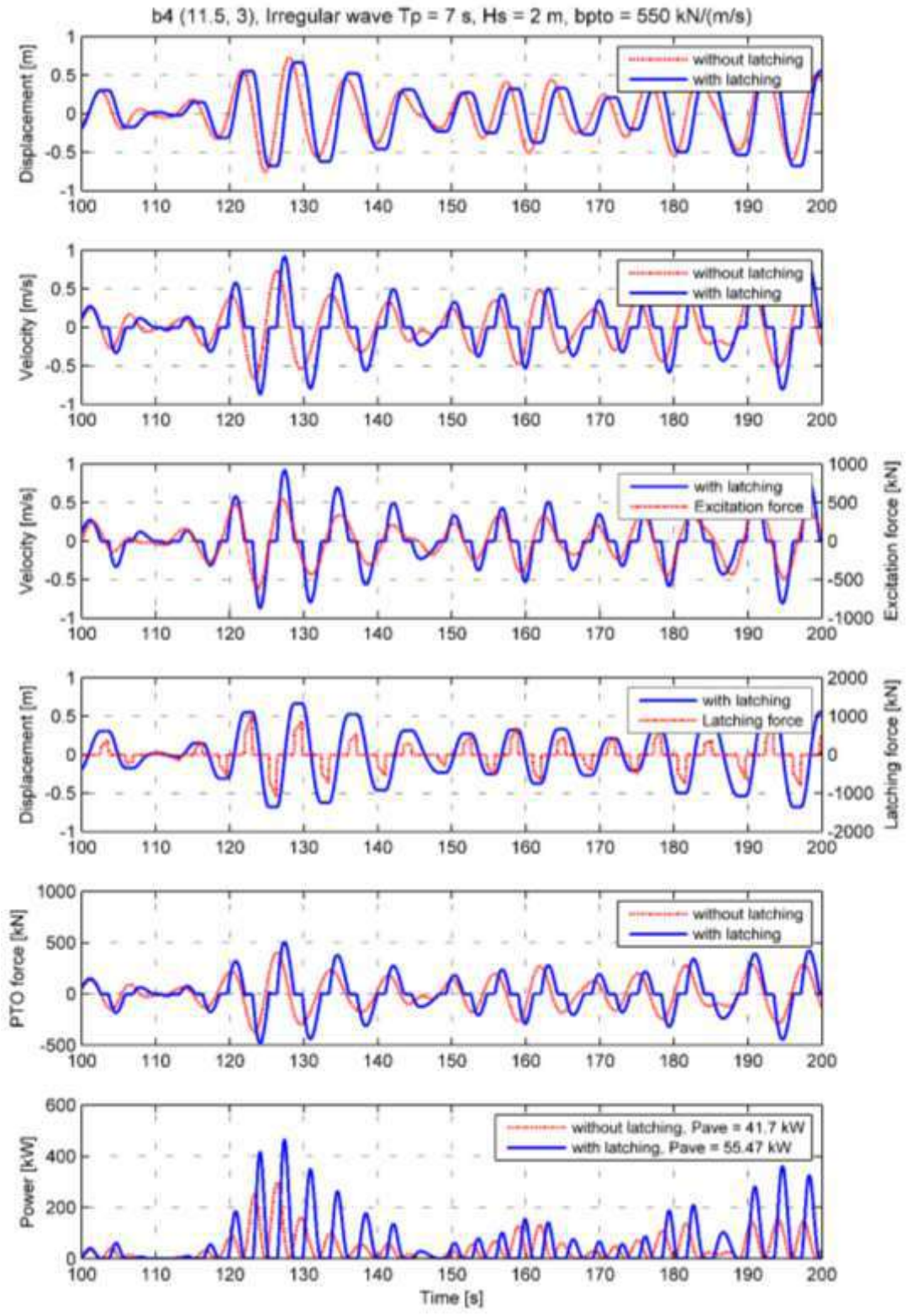

Figure 5-20- The time domain results of the buoy b4 (11.5, 3) in an irregular wave of $T_p = 7\ s$ and $H_s = 2\ m$ with and without application of a constant-delay latching control tuned to the spectrum energy period, considering a constant PTO damping bpto = 550 kN/(m/s). From top to bottom: Displacement, velocity, excitation, latching force, PTO force and mechanical power

5.8 Effect of a constant-delay latching control on the optimum PTO damping and power production

5.8.1 Regular waves

The function of latching control is to force the point absorber to oscillate in phase with the incident wave. As the result, the oscillation velocity is in phase with the wave excitation. This satisfies the optimum phase condition but does not guarantee the maximum power absorption. To achieve the maximum absorbed power the resistive force of the PTO system needs to be adjusted to its optimum value fulfilling the optimum amplitude condition. Figure 5-21 shows the power absorption by the buoys controlled by latching for more than 50 different PTO damping levels in regular waves of different periods. It can be seen that the maximum power absorption occurs for the PTO damping equal or close to the optimum damping value at the resonance frequency (see figure 5-6). These optimum values are around 2, 10, 28 and 110 kN/(m/s) for the b1, b2, b3 and b4 respectively (see figure 5-21).

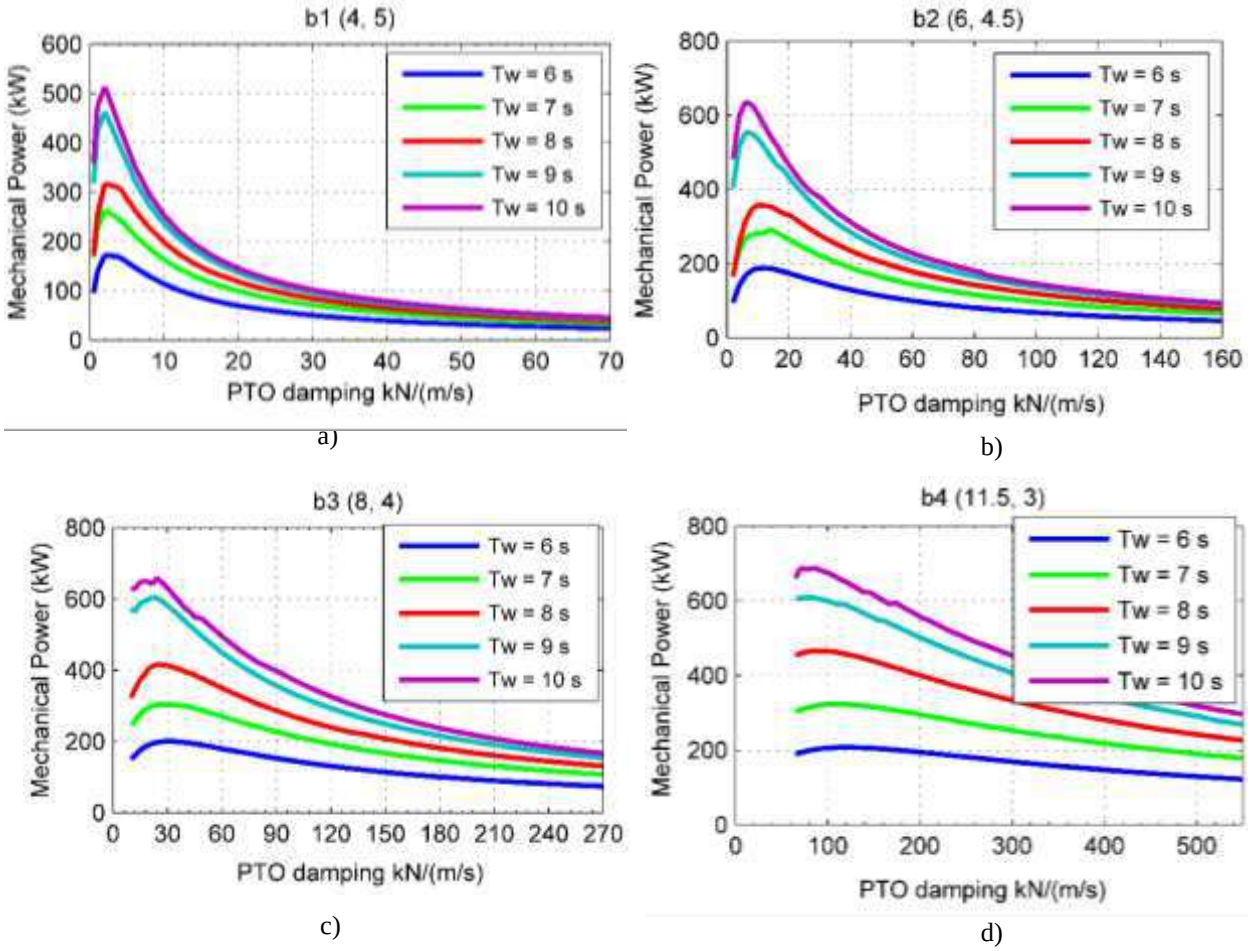

Figure 5-21– The mechanical power (kW) Vs different PTO damping level for the buoys controlled by a constant-delay latching in Regular waves of $H = 2\ m$

It can be seen that the optimum value of the PTO damping is independent of the wave period and the power absorption values converge for the high PTO damping levels. Figure 5-22-a and b show the maximum power and the corresponding PTO damping of the buoys controlled by a constant-delay latching control for different wave periods, with a constant wave height of $H = 2\ m$, respectively. The power production of the buoys controlled by the constant-delay latching are the same for the $T_w = 6\ s$ and they are diverging as the wave period becomes longer. It can be seen form figure 5-22-b that higher PTO damping level is required to obtain the maximum power for the larger buoys. This is due to the difference in the hydrodynamic damping level of the buoys (see figure 5-4-b). As it is illustrated, the optimum PTO damping for the longer waves ($Tw = 9$ and $10\ s$) has a lower level. It is because of the larger latching duartion which decreases the memory effect by keeping the buoy in a zero velocity situation for a longer time comparing to the shorter waves. This reduced memory effect results that the maximum power occurs at a lower damping level.

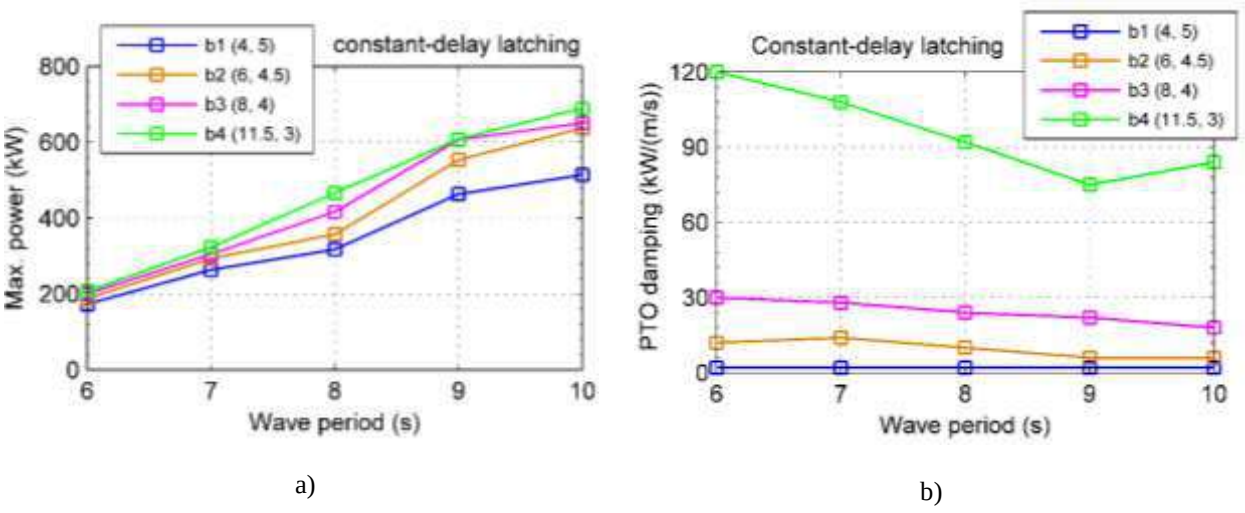

a) b)

Figure 5-22– a) the maximum power and b) the optimum PTO damping, for the buoys controlled by a constant-delay latching in regular waves with different buoys ($H = 2\ m$) for the b1, b2, b3 and b4.

Figure 5-23 to 26 illustrate the time domain responses of the buoys controlled by latching applying optimum PTO damping values in a regular wave of $T = 7\ s$ and $H = 2\ m$. As it can be seen, larger heave amplitude and velocity are achieved in camparison to the results plotted in figures-13 to 16. The reason is the optimum values of the PTO damping that provide the optimum apmplitude condition. However, the amplitudes are unrealistically large since it is assumed that there is no constraint on the motion. These

unrealistic values result a very large latching force (see the forth plot from top to bottom, figure-23 to 26). Mathematically, as it can be seen in Eq.(5.8), the velocity and displacement increase result in larger memory effect and dominantly larger hydrostatic force respectively. Consequently, a very large latching force is calculated to keep the buoy during the latching period. The fifth plot of figure-23 to 26, from top to bottom , shows the PTO forces. It can be seen that in the optimum energy absorption condition in regular waves (optimum phase and optimum amplitude), the PTO applied the same magnitude of force on the buoy with and without latching control. The larger amount of PTO force results from the larger PTO damping level, as it is showed in the figures-13 to 16 for the case of with latching control, decreases the displacement and velocity by braking the heave motion of the buoy. This leads to a lower power absorption which are evident in figure 5-21-a to d. Considering the constant-delay latching and an optimum PTO damping, as illustrated in figure-23 to 26, the mean power increases about 1263%, 624%, 364% and 183% for the buoys b1, b2, b3 and b4 respectively. It can be inferred that in regular waves, reducing the size of the buoy leaves it more sensetive to the latching control. However, it should be noted that applying constraints on the motion may reduces these percentages. The last plot of figure 5-23-a, shows the instantaneous power produced by the buoy b1 (4, 5). As it is illustrated, the maximum power levels are not the same for a part of the simulation time. It can be explained mathematically as the transient region which is caused by the general or homogenous part of the dynamic equation solution. After the transient dies away, the solution reaches to a steady-state condition which is dominated by its particular part.

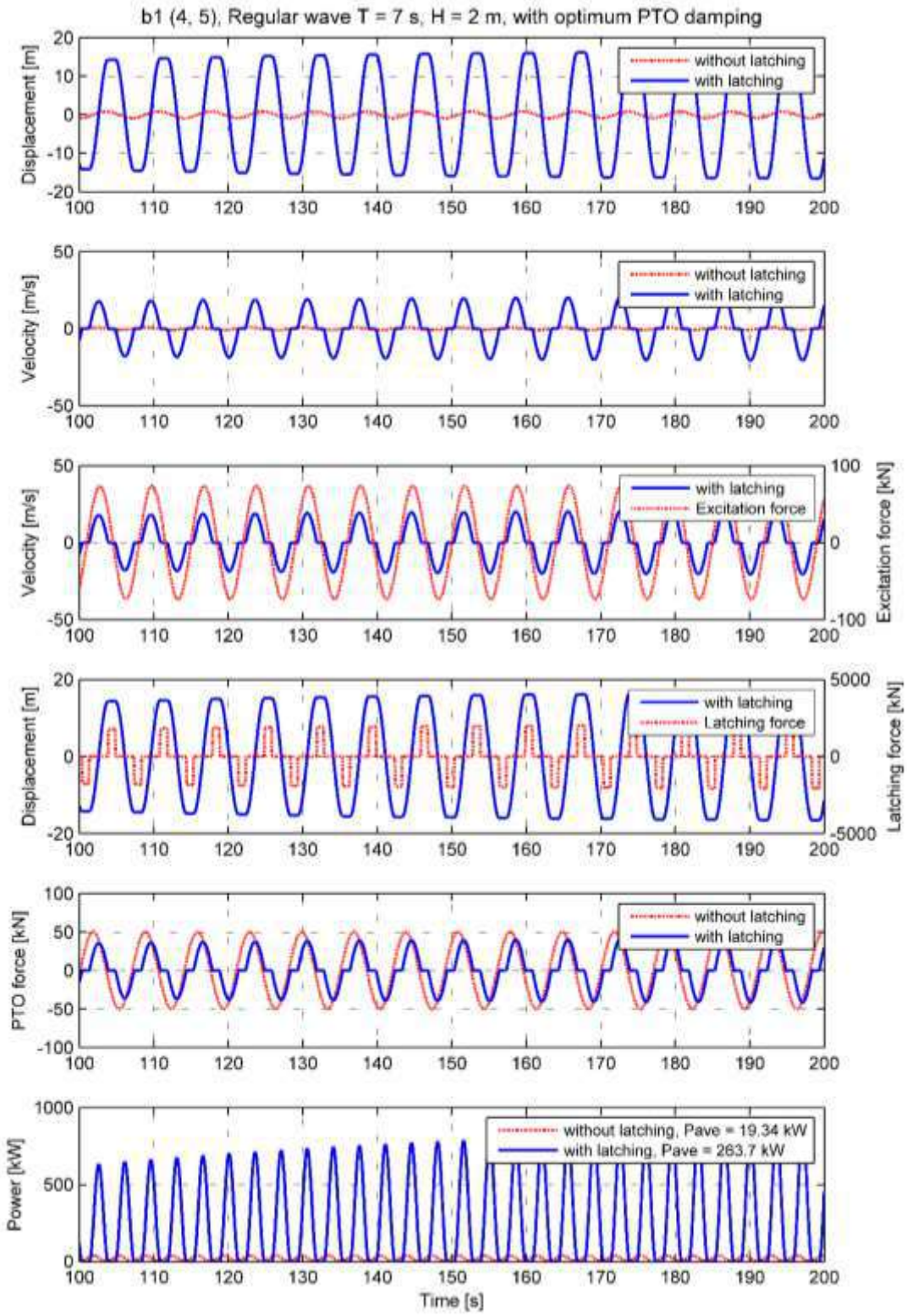

Figure 5-23- The time domain results of the buoy b1 (4, 5) in a regular wave of $T = 7\ s$ and $H = 2\ m$, with and without application of a constant-delay latching control, considering an optimum constant PTO damping; bpto = 65 kN/(m/s) for without latching and bpto = 2 kN/(m/s) for with latching. From top to bottom: Displacement, velocity, excitation, latching force, PTO force and mechanical power

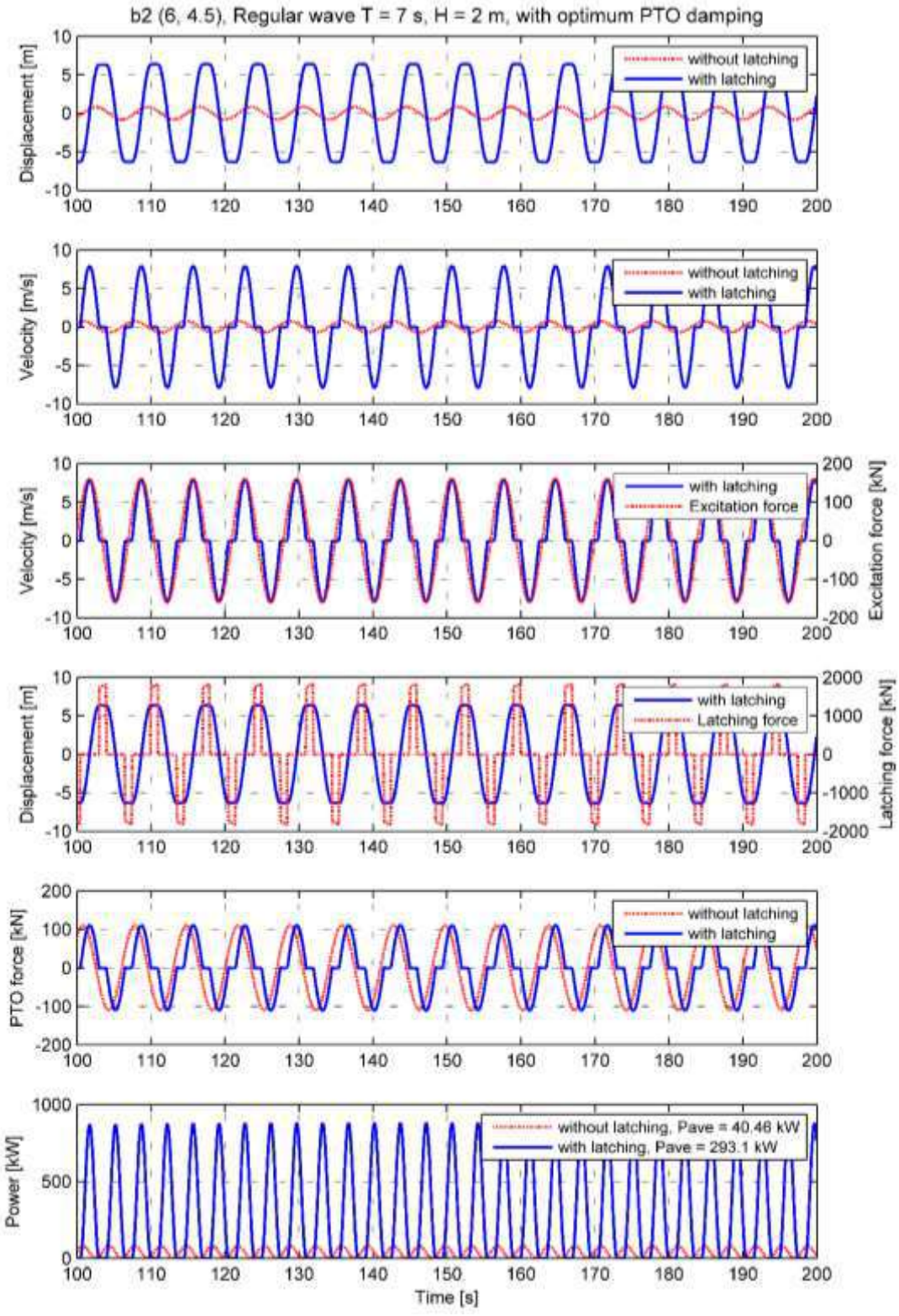

Figure 5-24- The time domain results of the buoy b2 (6, 4.5) in a regular wave of $T = 7\ s$ and $H = 2\ m$, with and without application of a constant-delay latching control, considering an optimum constant PTO damping; bpto = 150 kN/(m/s) for without latching and bpto = 14 kN/(m/s) for with latching. From top to bottom: Displacement, velocity, excitation, latching force, PTO force and mechanical power

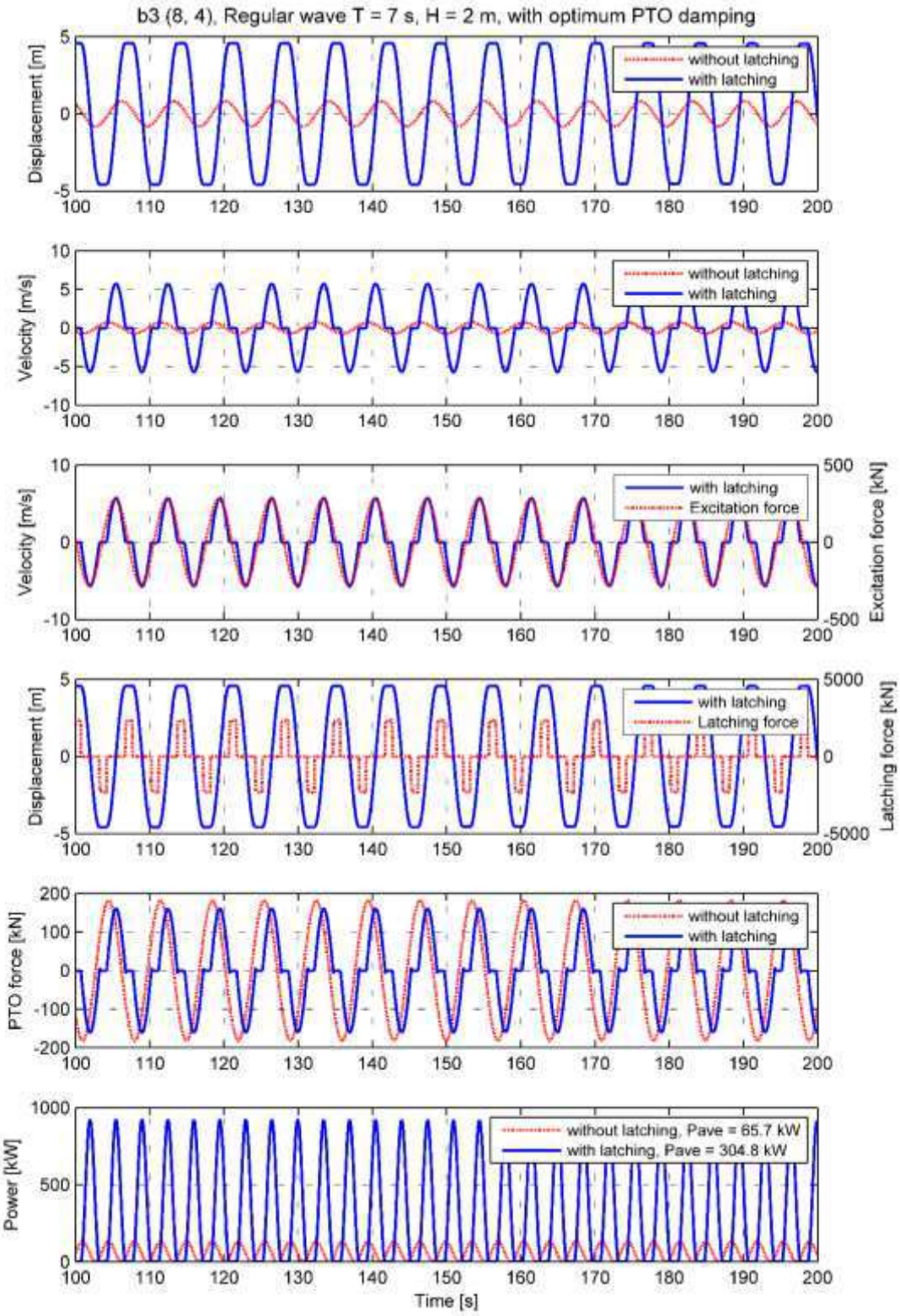

Figure 5-25- The time domain results of the buoy b3 (8, 4) in a regular wave of $T = 7\ s$ and $H = 2\ m$, with and without application of a constant-delay latching control, considering an optimum constant PTO damping; bpto = 250 kN/(m/s) for without latching and bpto = 28 kN/(m/s) for with latching. From top to bottom: Displacement, velocity, excitation, latching force, PTO force and mechanical power

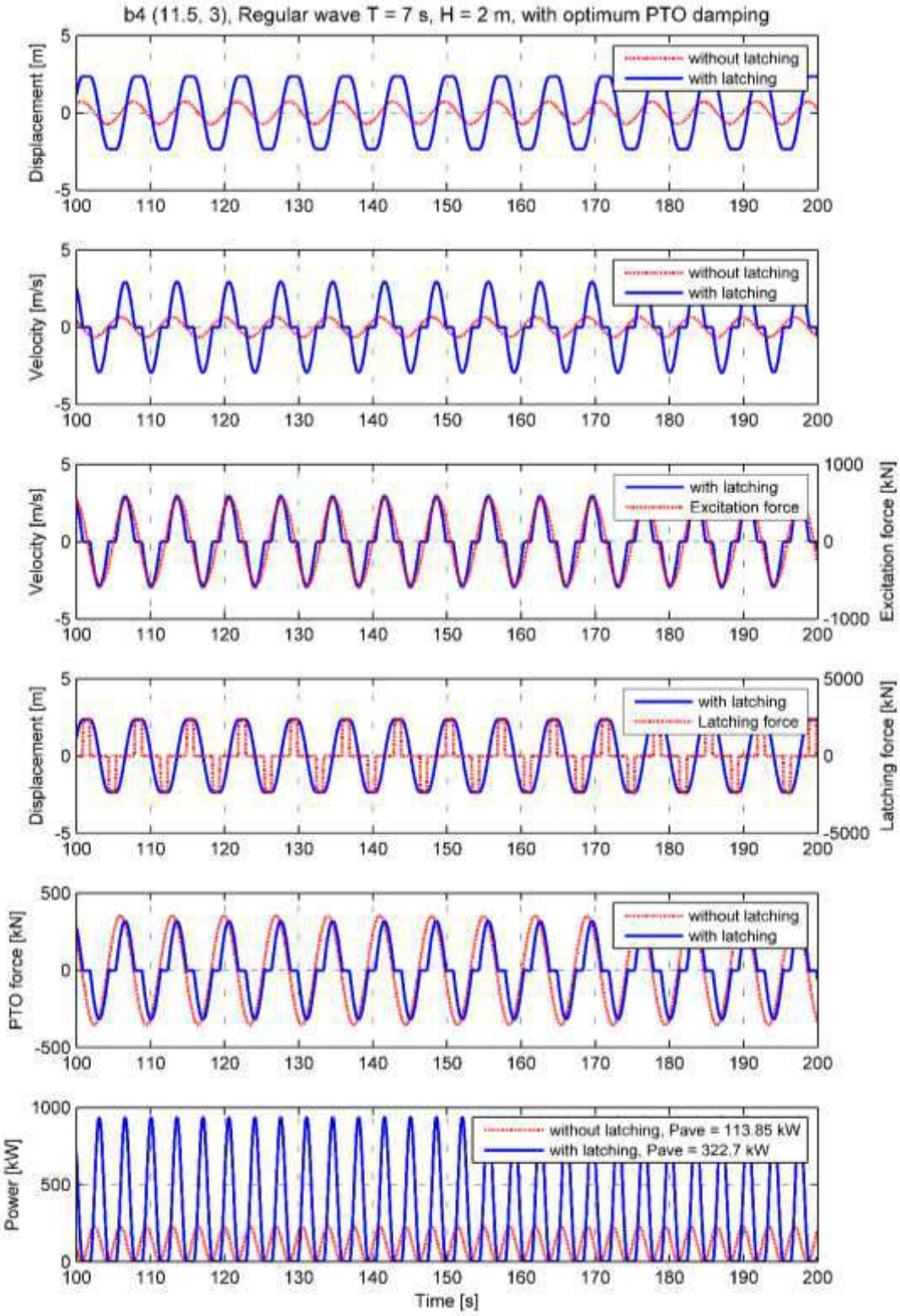

Figure 5-26- The time domain results of the buoy b4 (11.5, 3) in a regular wave of $T = 7\ s$ and $H = 2\ m$, with and without application of a constant-delay latching control, considering an optimum constant PTO damping; bpto = 550 kN/(m/s) for without latching and bpto = 108 kN/(m/s) for with latching. From top to bottom: Displacement, velocity, excitation, latching force, PTO force and mechanical power

5.8.2 Irregular waves

A constant-delay latching adjusted to the energy period of the sea wave spectrum is applied on the buoys. Considering the nearshore Rio de Janeiro as sea local, the predominant sea states with modal period of $T_p = 6 - 13\ s$ and an average constant significant height of $H_s = 1.33$ are considered for the analyses. Figure 5-27 shows the JONSWAP spectrum calculated using Eq.(3.37), for different modal period and a constant significant wave height of $H_s = 1.33\ m$.

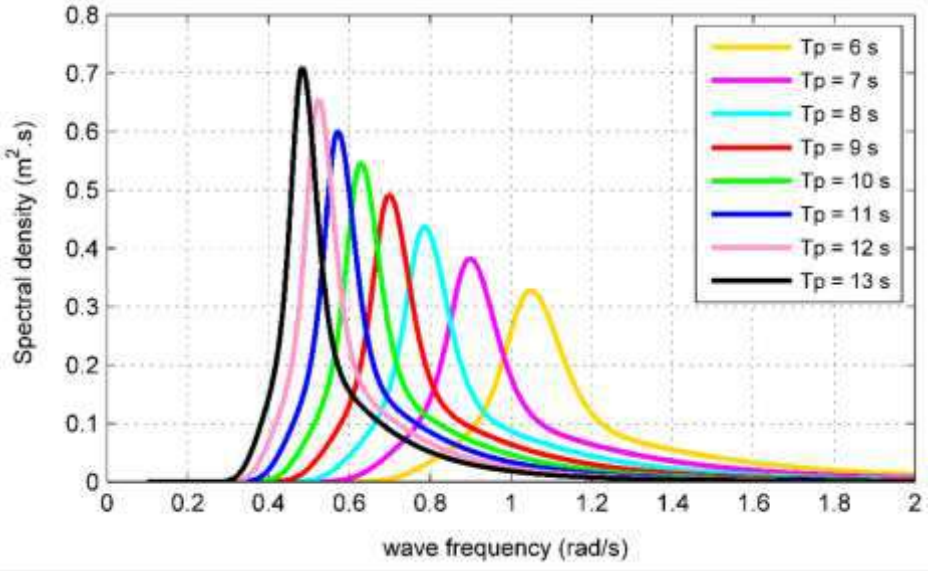

Figure 5-27– JONSWAP wave spectra for different modal period, T_p , with a significant wave height of $H_s = 1.33\ m$

Figure 5-28 and 29 show the effect of different PTO damping levels (40 to 60 different damping levels for each sea state) on the mean power production of the buoys with and without application of a constant-delay latching control respectively for different sea states. Additionally, each PTO damping is applied for each sea state considering 20 different series of wave random phase shifts, ε_n (see section 3.4.2). It means that there are 20 different mean power for each PTO in each sea state. The average of these values are calculated for each PTO damping. Consequently, an average line, which is illustrated for each sea state, is formed by connecting the average points corresponding to the PTO damping levels.

The effect of the wave random phase shift for either the control-free buoys or the buoys controlled by latching depends on the modal period of the sea state. As it can be seen in

figures 5-28 and 29, as the modal period of the sea state becomes longer the resulted mean power values start to spread out from their mean value. This dispersion is more evident for the PTO damping close to its optimum value in each sea state. More convergence of the produced power in different random phases can be observed for the smaller buoys in both controlled and control-free buoys. As it can be seen, the buoy $b1\ (4,5)$ has the less dispersion of mean power values comparing to the other buoys.

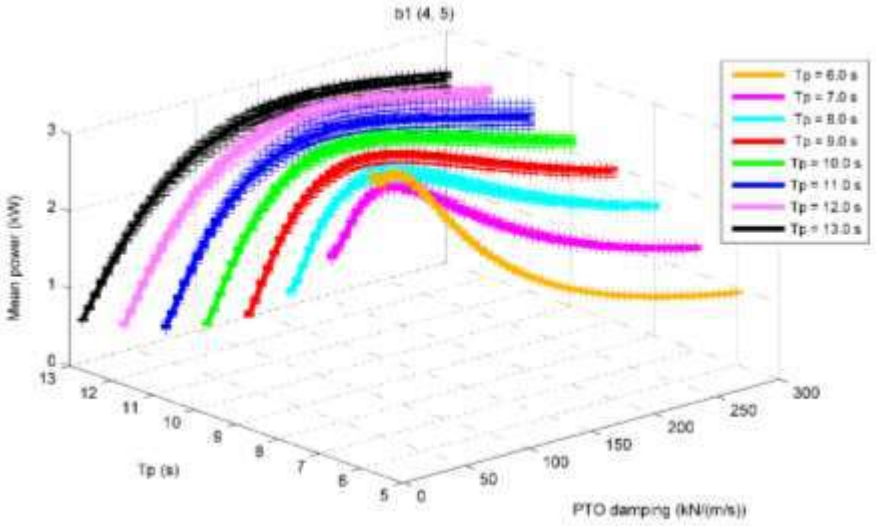

a)

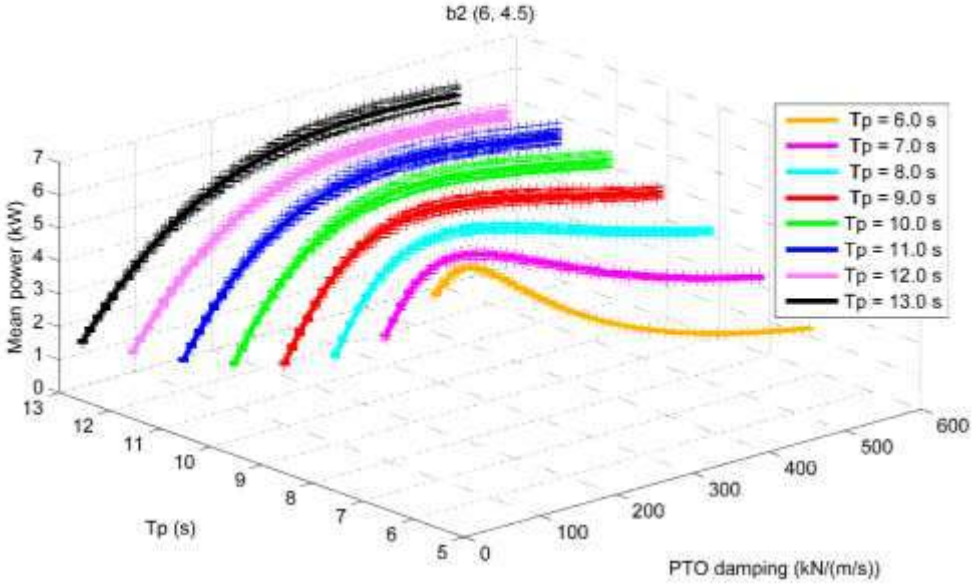

b)

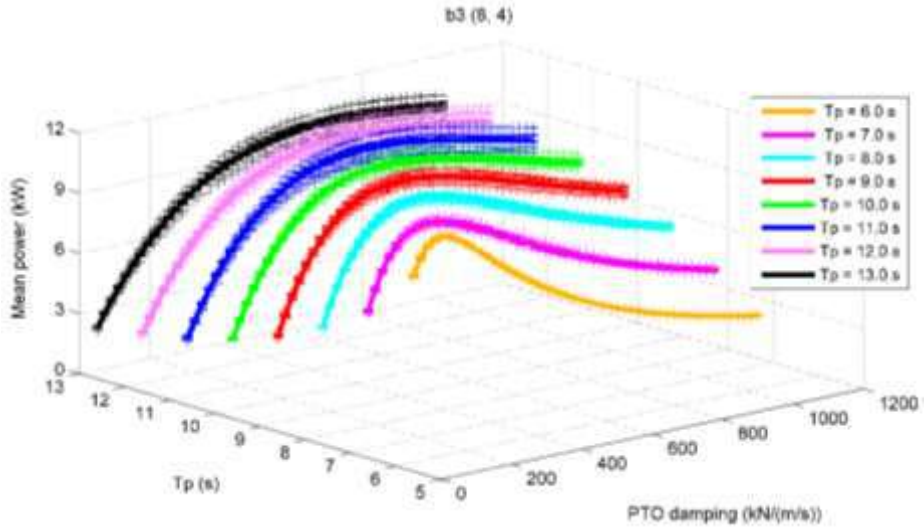

c)

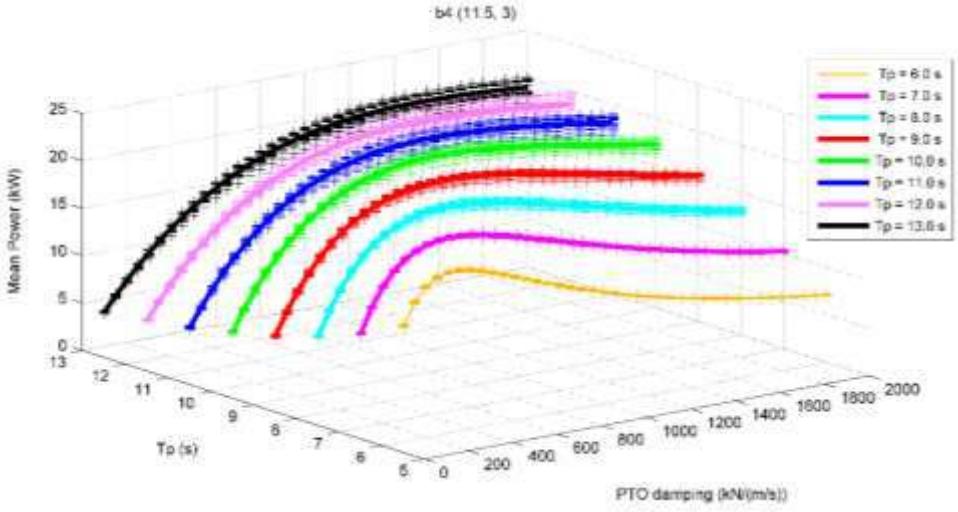

d)

Figure 5-28– The mean power (kW) of the control-free buoys for different sea states, $T_p = 6 - 13\ s$ and $H_s = 1.33\ m$, and different PTO damping (kN/(m/s)). The buoys performances are plotted for 20 different series of wave random phases in each sea state. The solid line in each sea state connects the average points of theses 20 mean power.

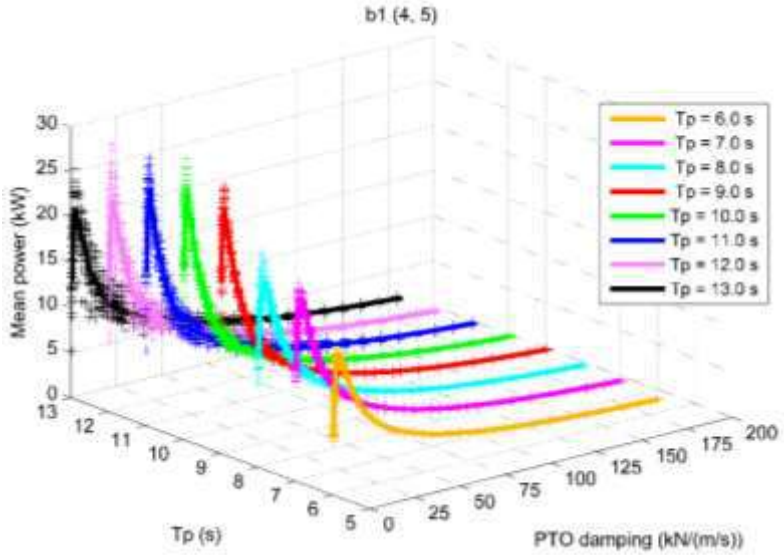
b1 (4, 5)
Mean power (kW)
Tp (s)
PTO damping (kN/(m/s))
Tp = 6.0 s
Tp = 7.0 s
Tp = 8.0 s
Tp = 9.0 s
Tp = 10.0 s
Tp = 11.0 s
Tp = 12.0 s
Tp = 13.0 s

a)

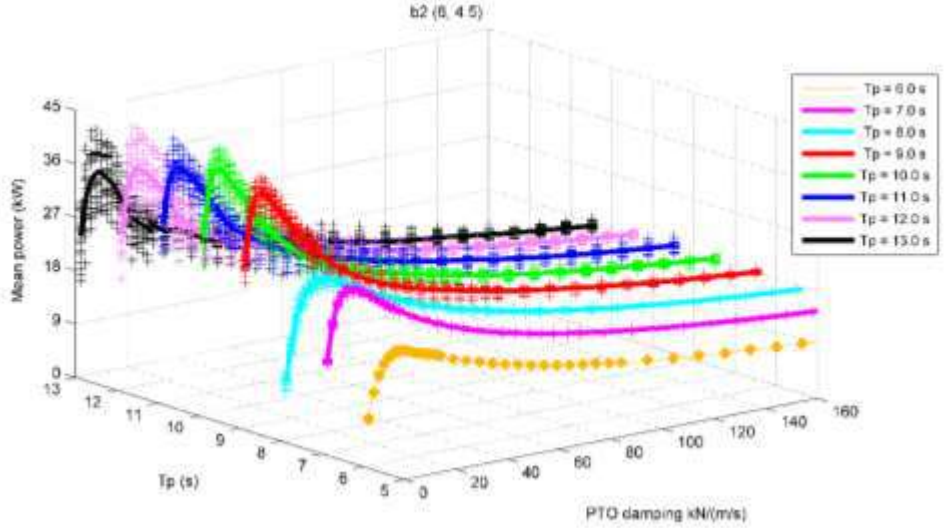
b2 (8, 4.5)
Mean power (kW)
Tp (s)
PTO damping kN/(m/s)
Tp = 6.0 s
Tp = 7.0 s
Tp = 8.0 s
Tp = 9.0 s
Tp = 10.0 s
Tp = 11.0 s
Tp = 12.0 s
Tp = 13.0 s

b)

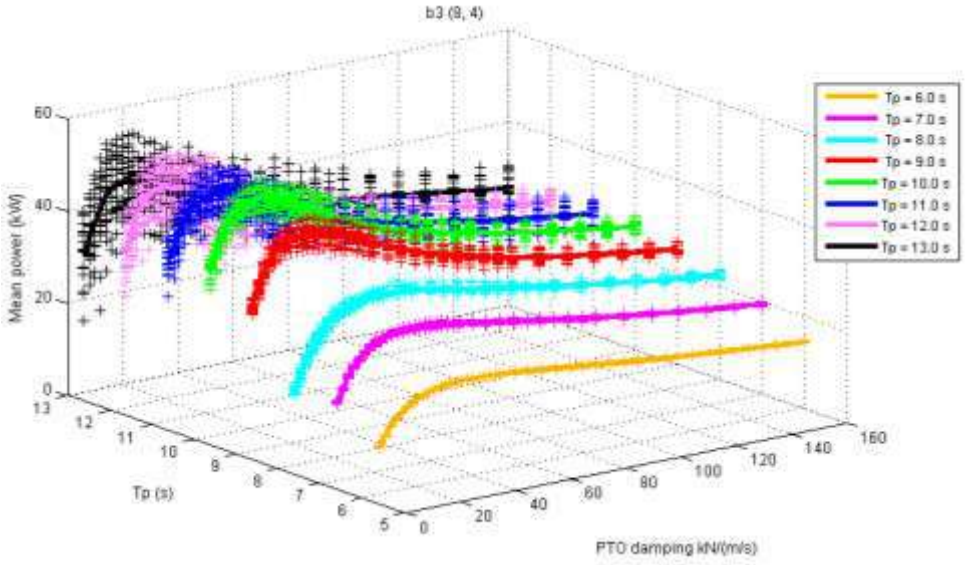

c)

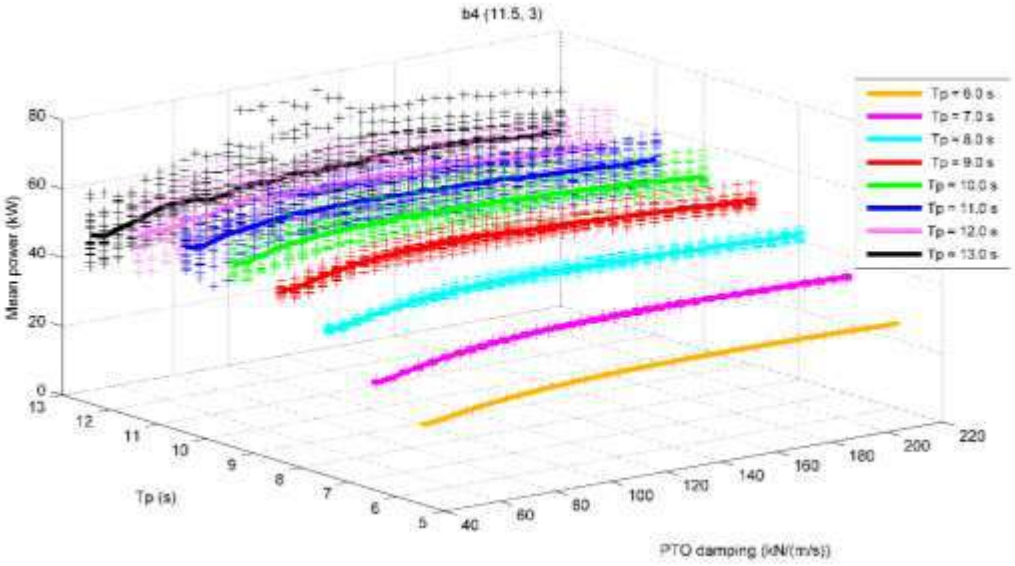

d)

Figure 5-29- The mean power (kW) of the buoys controlled by a constant-delay latching for different sea states, $T_p = 6 - 13\ s$ and $H_s = 1.33\ m$, and different PTO damping (kN/(m/s)). The buoys performances are plotted for 20 different series of wave random phases in each sea state. The solid line in each sea state connects the average points of theses 20 mean power.

Figures 30 and 31 show the average lines for the buoys with and without constant-delay latching control. By comparing the results shown in figure 30, it can be seen that in the case of the control-free buoys, the corresponding PTO damping which maximizes the power generation has a value close to the optimized PTO damping (see figure 5-6) at the period equal to the modal period of the sea state, T_p.

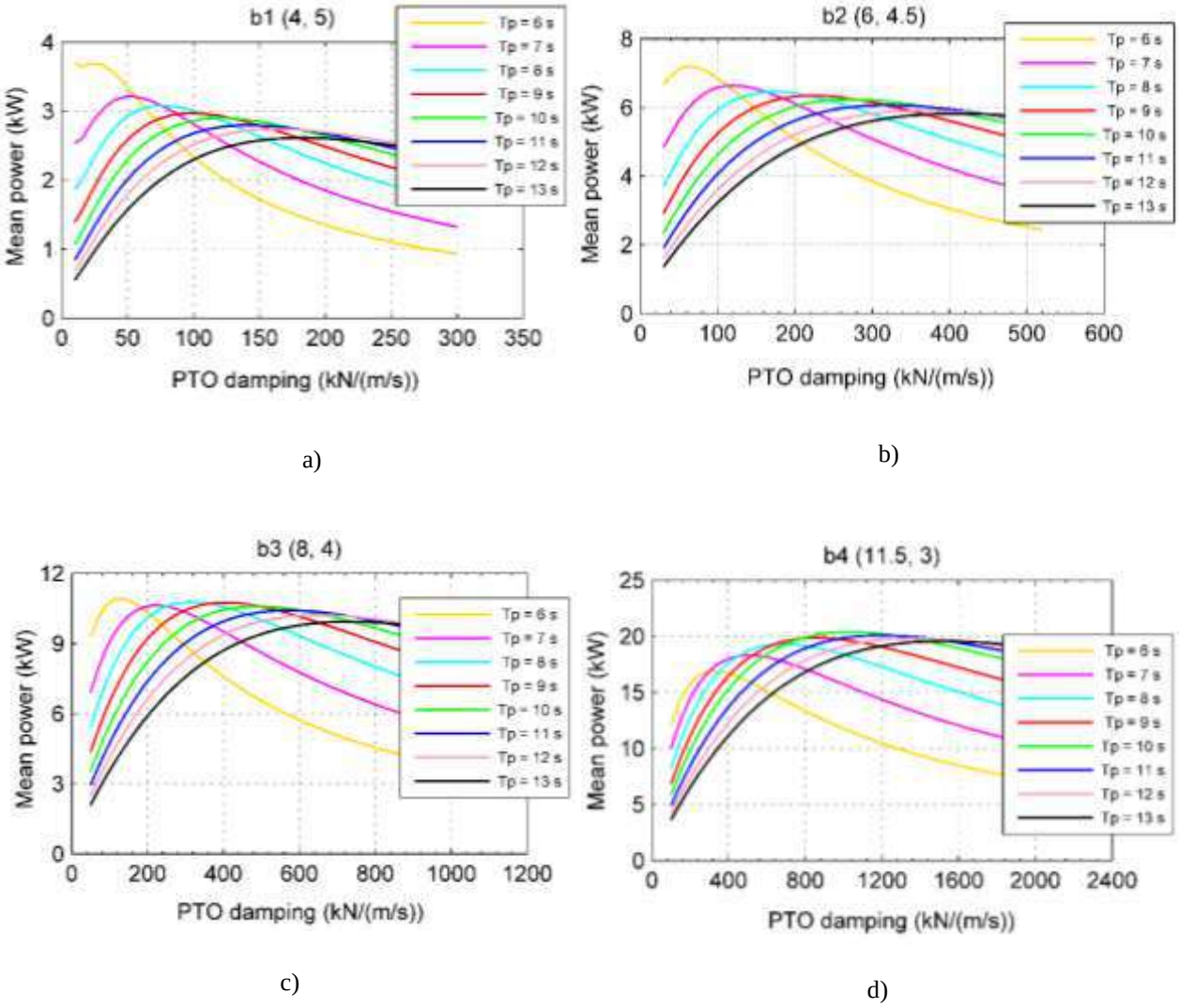

Figure 5-30 – The average of the mean power (kW) for 20 different series of wave random phases in each sea state versus the PTO damping (kN/(m/s)). The results are shown for the control-free buoys.

For the control-free case, the mean power increases with the size of the buoy. However, it requires that PTO system provide a high level of resistance that increase the costs. For instance, considering the buoys $b1(4,5)$ and $b4$ $(11.5,3)$ in the sea state of the $T_p = 6\ s$, a PTO damping increase of about 13 times (from 25 kN/(m/s) for b1 to 325 kN/(m/s) for b4) is required to

generate only 4 times (from 3.7 kW for b1 to 16.89 kW for b4) more power. The values of the optimum PTO damping and the maximum mean power corresponding to each sea states for the buoys with and without constant-delay latching control are shown in Table 5-2. As it can be seen in figure 5-30 and table 5-2, except the largest buoy b4 (11.5, 3) , the maximum mean power of the buoys decreases as the modal period becomes longer and the largest value occurs in the sea state of $T_p = 6\,s$. It is shown that the optimum PTO damping for the control-free buoys in irregular waves is dependent on the modal period of the sea states and its value increases with the wave period. In the case of using a large buoy, it may bring serious practical challenges regarding the providing the PTO system with such a high resistance.

For the buoys controlled by a constant-delay latching, figure 5-31, the mean power of the buoys significantly increases comparing to the control-free condition. However, the results show the decrease of the maximum mean power for the $T_p \geq 10\,s$. This phenomenon occurs for all the buoys when the latching duration is equal or greater than half of the buoys natural period or in the other words, a total latching duration of $5\,s$ is applied in each oscillation cycle of the buoy (see section 5.3). For instance, the mean power decreases when $T_p = 11\,s$ and the corresponding latching duration is equal to 3 which is greater than half of the natural period ($T_n = 5\,s$). A parameter that can help us to address the performance of the WEC is the capture width which is the ratio of the mean power produced by the system to the wave power in width unit (see Eq.(4.65)) for each sea state. In each sea state, the capture width show the ability of each buoy in absorbing energy in comparison to the available sea energy. Figure 5-32 illustrates the capture width of the buoys for different sea states of the same significant wave height, $H_s = 1.33\,m$, with and without the application of a constant-delay latching control. As it is illustrated, in the case of control-free buoys, figure 5-32-a, the capture width decreases as the modal period becomes longer. The reason is that as the modal period becomes larger, the frequencies in which the buoy oscillate moves away from the resonance region and the buoy tends to follow the waves due to the large wavelength in comparison to the buoy diameter. This results in smaller heave amplitudes and consequently only a small fraction of the sea energy can be absorbed by the buoy.

As it is shown in figure 5-32-b, there is a peak for capture width curve of the buoys controlled by constant-delay latching in $T_p = 9\,s$. The largest buoy b4 (11.5, 3) has the highest capture width values in each sea state and these values decrease as the buoy size

becomes smaller. Also, a decline in the capture width value corresponding to the $T_p = 8$ is observed for the buoys b1 (4, 5), b2 (6, 4.5) and b3 (11.5, 3). It can be inferred from the capture width illustration that the performance of the constant delay-latching control decreases as the latching duration becomes equal or greater than the half of the buoys natural period, and for the different buoys with the same natural period, it is independent of the buoy size. However, in comparison to the control - free condition, it does not imply that the effectiveness of the latching control decreases for this range of period.

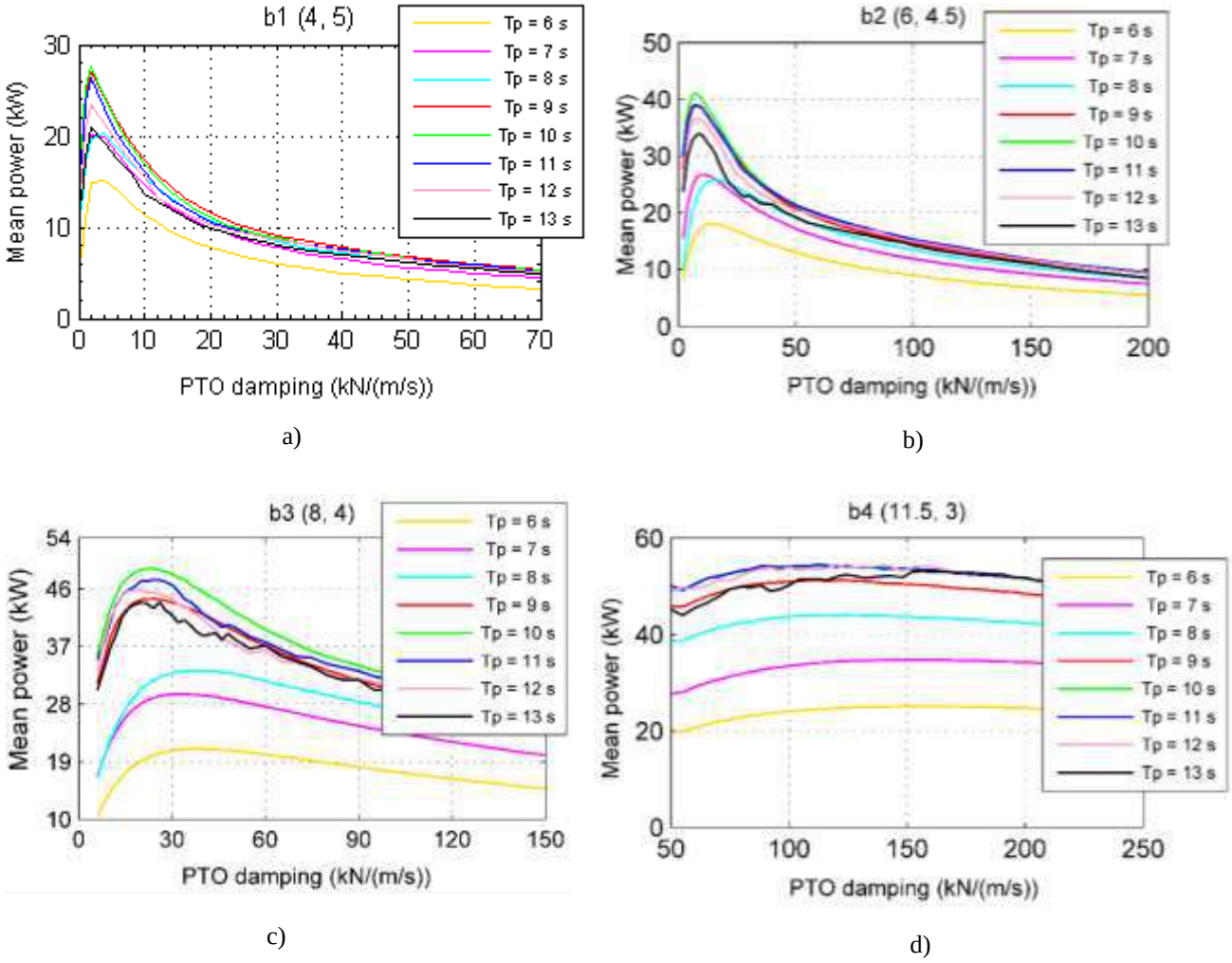

Figure 5-31 - The average of the mean power (kW) for 20 different series of wave random phases in each sea state versus the PTO damping (kN/(m/s)). The results are shown for the buoys controlled by a constant-delay latching.

It is shown in figure 5-33 through two bar graphs that are depicted based on the table 5-2 data. The colors represent the buoys and the bars values, vertical axes, illustrate the increase of mean power, figure 5-33-a, and the corresponding decrease in optimum PTO damping level, figure 5-33-b, in percent. The horizontal axis represents the sea states that

are numbered form 1 to 8 corresponding to the sea state of $T_p = 6$ to $13\ s$ with a significant wave height of $H_s = 1.33\ m$.

Table 5-2- The average of the mean power (kW) and the optimum PTO damping values for 20 different series of wave random phases in each sea state. The results are shown for the control-free and the constant-delay latching controlled buoys.

Buoys	Sea states, $H_s = 1.33\ m$	**Control-free**		**Constant-delay latching**	
		Optimum b_{PTO} (kN/(m/s))	Max. mean power (kW)	Optimum b_{PTO} (kN/(m/s))	Max. mean power (kW)
b1 (4, 5)	$T_p = 6\ s$	25	3.7	4	15.2
	$T_p = 7\ s$	50	3.2	2	20.16
	$T_p = 8\ s$	75	3.1	4	20.36
	$T_p = 9\ s$	100	3.0	2	27.03
	$T_p = 10\ s$	125	2.9	2	27.51
	$T_p = 11\ s$	140	2.8	2	26.32
	$T_p = 12\ s$	165	2.7	2	23.36
	$T_p = 13\ s$	185	2.6	2	21.02
b2 (6, 4.5)	$T_p = 6\ s$	60	7.19	14	18.04
	$T_p = 7\ s$	120	6.64	10	26.73
	$T_p = 8\ s$	170	6.45	16	25.92
	$T_p = 9\ s$	230	6.34	8	39.0
	$T_p = 10\ s$	280	6.23	8	40.97
	$T_p = 11\ s$	340	6.01	8	38.92
	$T_p = 12\ s$	380	5.89	8	36.7
	$T_p = 13\ s$	430	5.81	8	33.86
b3 (8, 4)	$T_p = 6\ s$	130	10.93	36	21.01
	$T_p = 7\ s$	230	10.63	34	29.63
	$T_p = 8\ s$	330	10.78	39	33.28
	$T_p = 9\ s$	430	10.75	24	44.49
	$T_p = 10\ s$	510	10.59	24	49.22
	$T_p = 11\ s$	590	10.42	24	47.44
	$T_p = 12\ s$	670	10.22	20	45.95
	$T_p = 13\ s$	730	9.34	20	43.87
b4 (11.5, 3)	$T_p = 6\ s$	325	16.89	156	25.05
	$T_p = 7\ s$	500	18.31	156	34.72
	$T_p = 8\ s$	700	19.31	126	43.95
	$T_p = 9\ s$	850	19.86	124	51.23
	$T_p = 10\ s$	1025	20.38	116	54.18
	$T_p = 11\ s$	1200	20.08	112	54.49
	$T_p = 12\ s$	1350	19.8	108	54.0
	$T_p = 13\ s$	1525	19.56	156	53.12

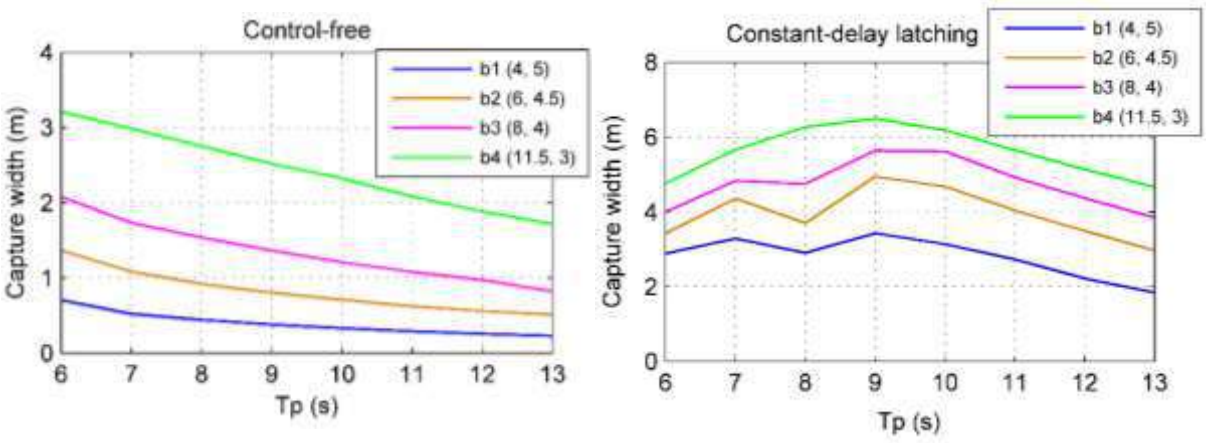

a) b)

Figure 5-32 - Capture width (in meter) for the control-free and constant-delay latching controlled buoys in different sea state with a significant height of $H_s = 1.33\ m$. The results are based on the average of the mean power (kW) for 20 different series of wave random phases in each sea state.

In figure 5-33-a, the increase of the maximum mean power becomes larger up to $T_p = 10\ s$ (sea state $= 5$), and it decreases for the larger modal periods. Comparing to the control-free buoys, the mean power growth in the range of the predominant sea states of the local sea shows that, not only the constant-delay latching does not lose its effect for the modal periods of T_p greater than $10\ s$, but also presents a better performance comparing to the shorter ones. The largest mean power growth belongs to the smallest buoy, b1 (4, 5), which is approximately more than 500 percent for the $T_p \geq 7\ s$ and 300 percent for the $T_p = 6\ s$, and it decreases with the buoy size increase. The reason may be the lower hydrodynamic damping level of the smaller buoys at the resonance frequency that causes larger heave amplitudes. The results indicate that the largest increase in maximum mean power occurs in sea states of $T_p = 10$ and $11\ s$. However, it should be noted that the mean power growth of the b3 (8, 4) and b4 (11.5, 3) converge to a constant value for the $T_p \geq 10\ s$.

As figure 5-33-b shows, the decrease of the required optimum PTO damping to extract the maximum energy is approximately more than 80 percent for all four buoys for the sea states of $T_p \geq 8\ s$ (sea state ≥ 3). It can be seen that there are a small differences between the values for different buoys in the seas states greater than three. Thus, it can be inferred that the diminution of the optimum PTO damping is independent of the buoy size, at least

for the range of $T_p \geq 8\ s$. The results show that the buoy b1 (4, 5) shows the largest reduction in optimum PTO damping in all sea states comparing to the other buoys.

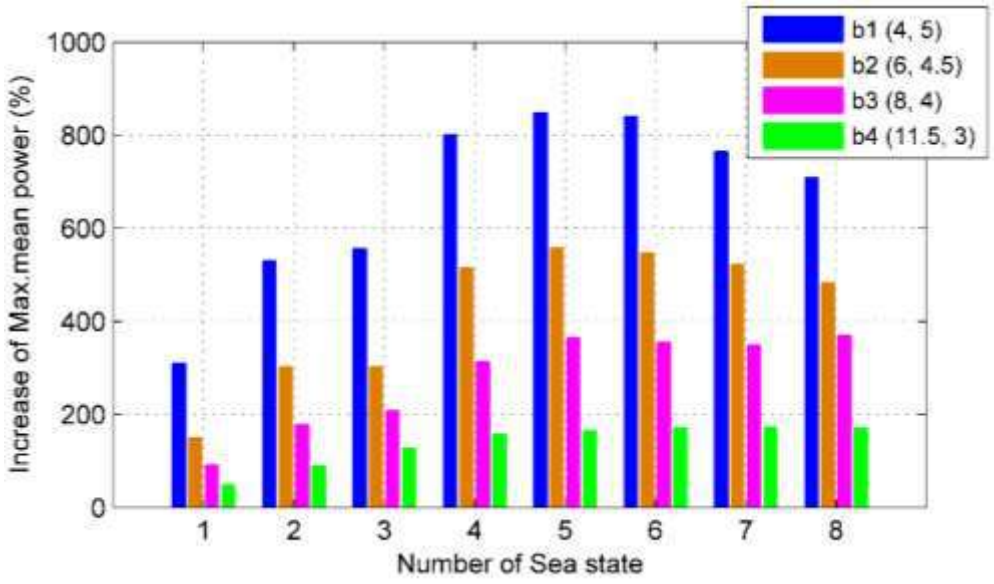

a)

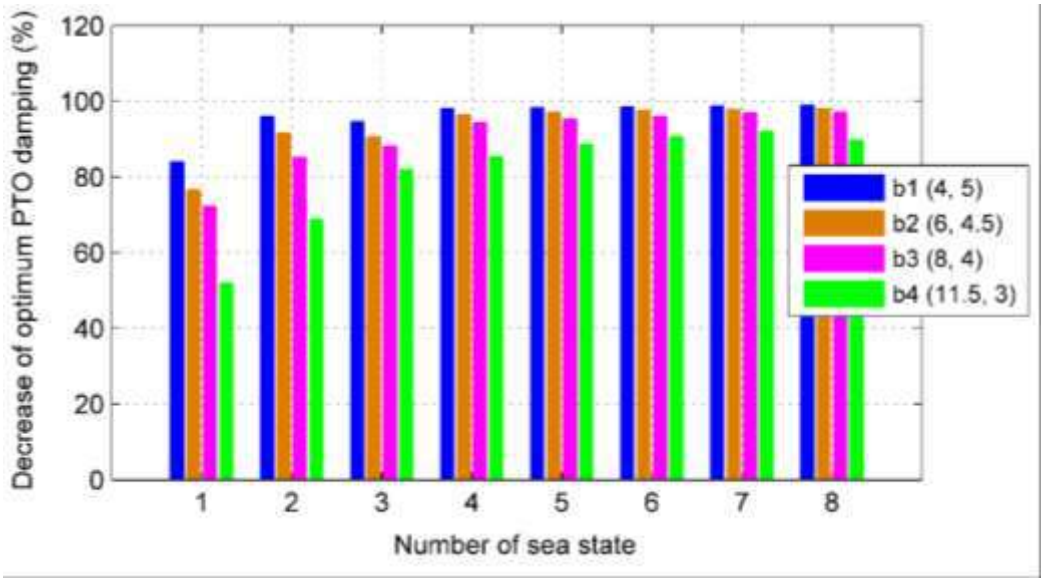

b)

Figure 5-33 – The bar graphs of the; a) increase of the mean power (in percent), and b) decrease of the optimum PTO damping value (in percent) for the buoys controlled by a constant-delay latching in comparison to the control-free ones. The horizontal axes represent the number of sea state from 1 to 8 corresponding to the $T_p = 6\ s$ to13 s. The results are based on the average of the mean power (kW) for 20 different series of wave random phases in each sea state.

As illustrated in figure 5-31, applying a constant-delay latching control, the optimized PTO damping values corresponding to the frequencies close to the resonance (see figure 5-6), maximize the mean power for each buoy and they are independent of the wave period. It means that by adjusting the PTO damping to a constant level, with a good approximation, the maximum power can be produced for different sea states. In practice, it facilitates the PTO control and reduces the costs.

This behavior can be explained better by plotting the heave spectrum of the controlled buoys, figure 5-34. A 600 s window of the time domain heave response of the buoys in an irregular wave of $T_p = 10\ s$ and $H_s = 1.33\ m$ is considered. Five different PTO damping including the optimum one, which maximizes the mean power, are applied for the power generation. The heave spectrum is calculated applying Fast Fourier Transform (FFT) technique. The constant-delay latching control forces the buoys to resonate at $T_p = 10\ s$ by locking them for a constant latching duration, calculated by Eq.(5.1), at each heave motion extermum during their oscillation. It is illustrated by figure 5-34 that with application of a constant-delay latching control the extermum of the heave displacement of the system occurred at $f \cong 0.1\ Hz$ ($T_p = 10\ s$) and the resultant responses in time domain are dominated by the heave motions of frequencies between $0.08\ Hz$ and $0.12\ Hz$. The controlled buoy oscillates at the frequency of $0.1\ Hz$ with a hydrodynamic damping corresponding to its natural frequency (the resonance frequency of its control-free condition, $f \cong 0.2\ Hz$), because of this an optimized PTO damping value close to the control-free buoy resonance frequency maximizes the mean produced power. In figure 5-34, the blue curve represents the heave oscillation of the buoy without PTO system that is evidently, the largest heave amplitude in comparison to the buoys coupled with a PTO. The PTO resistance apply a force on the oscillating buoy in vertical direction to produce electricity, which result in heave amplitude reduction. As it discussed previously, due to the higher hydrodynamic damping level, these forces are greater for the larger buoys. In the case of applying the optimum PTO damping value, the maximum mean power is obtained and it is called that the system is “optimally-damped”. Reducing the PTO damping leaves the buoy with larger heave amplitude while decreasing the mean power. Thus, the applied damping is lower than the optimum value and the system is “under-damped”. In the other hand, increasing the PTO damping results in diminution in heave amplitude and consequently mean power. It this case, the PTO decreases the buoy

motion more than the optimum limit and the system is “over-damped”. These three conditions are illustrated in figure 5-34.

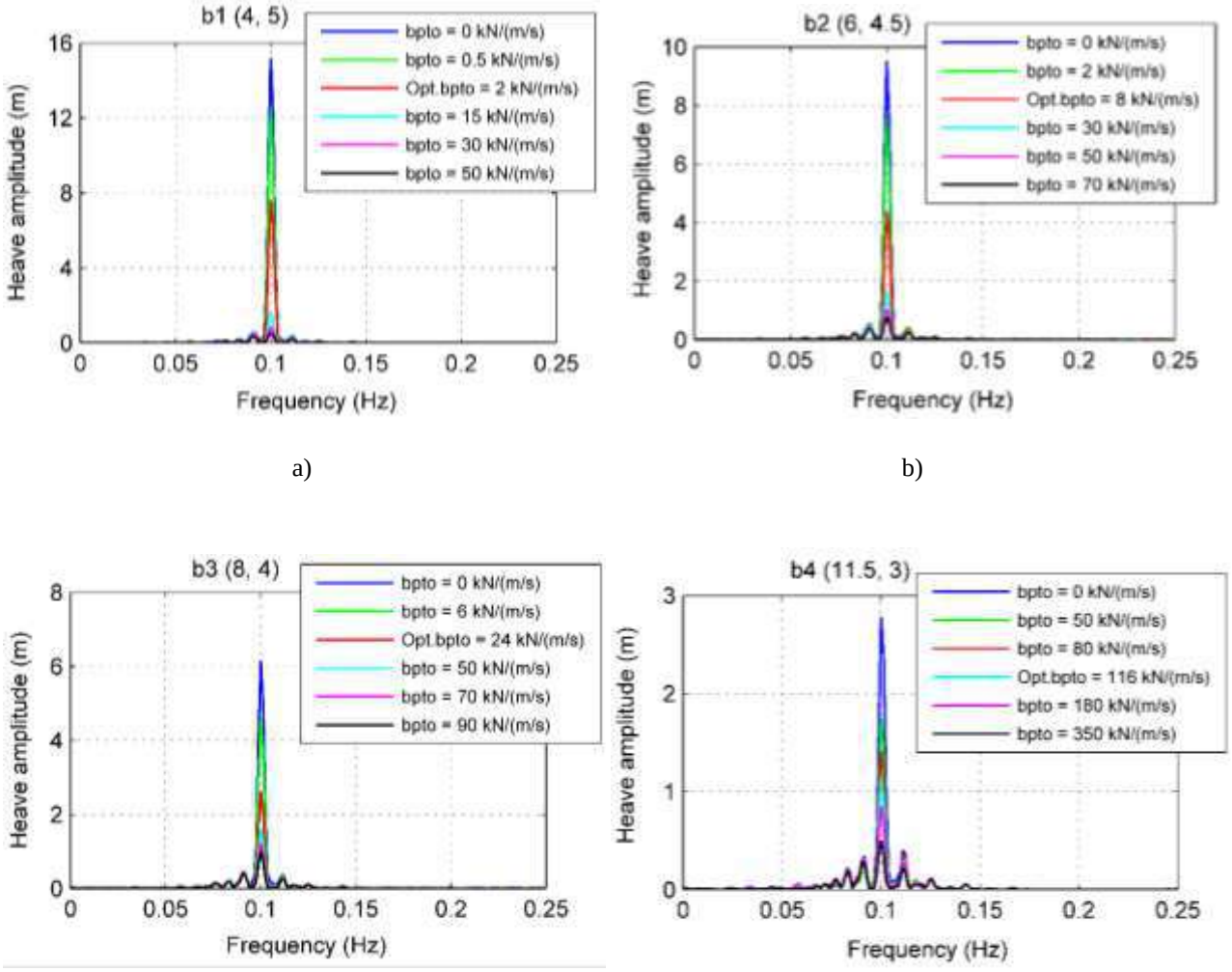

Figure 5-34 – Heave spectrum of the buoys controlled by a constant-delay latching in an irregular wave of $T_p = 10\ s$ and $H_s = 1.33\ m$

Figure 5-35 to 38 show the time domain responses of the optimally-damped buoys with and without the application of the constant-delay latching control. Larger amplification in displacement, velocity and mean power can be observed in the buoy b1 (4, 5) in comparison to the other buoys. However, the buoy b4 (11.5, 3) produces the largest amount of power. In prctice, an important issue that must be considered is the latching force (the forth plot form top to bottom). This is the required force that a latching control system must provide to halt the buoy motion. It can be calculated using Eq.(5.8). As it is

expressed, latching force magnitude is dominated by the hydrostatic force , thus it icreases with the buoy size. In the case of using large buoys, this may bring some serious challenges related to the latching mechanical system.

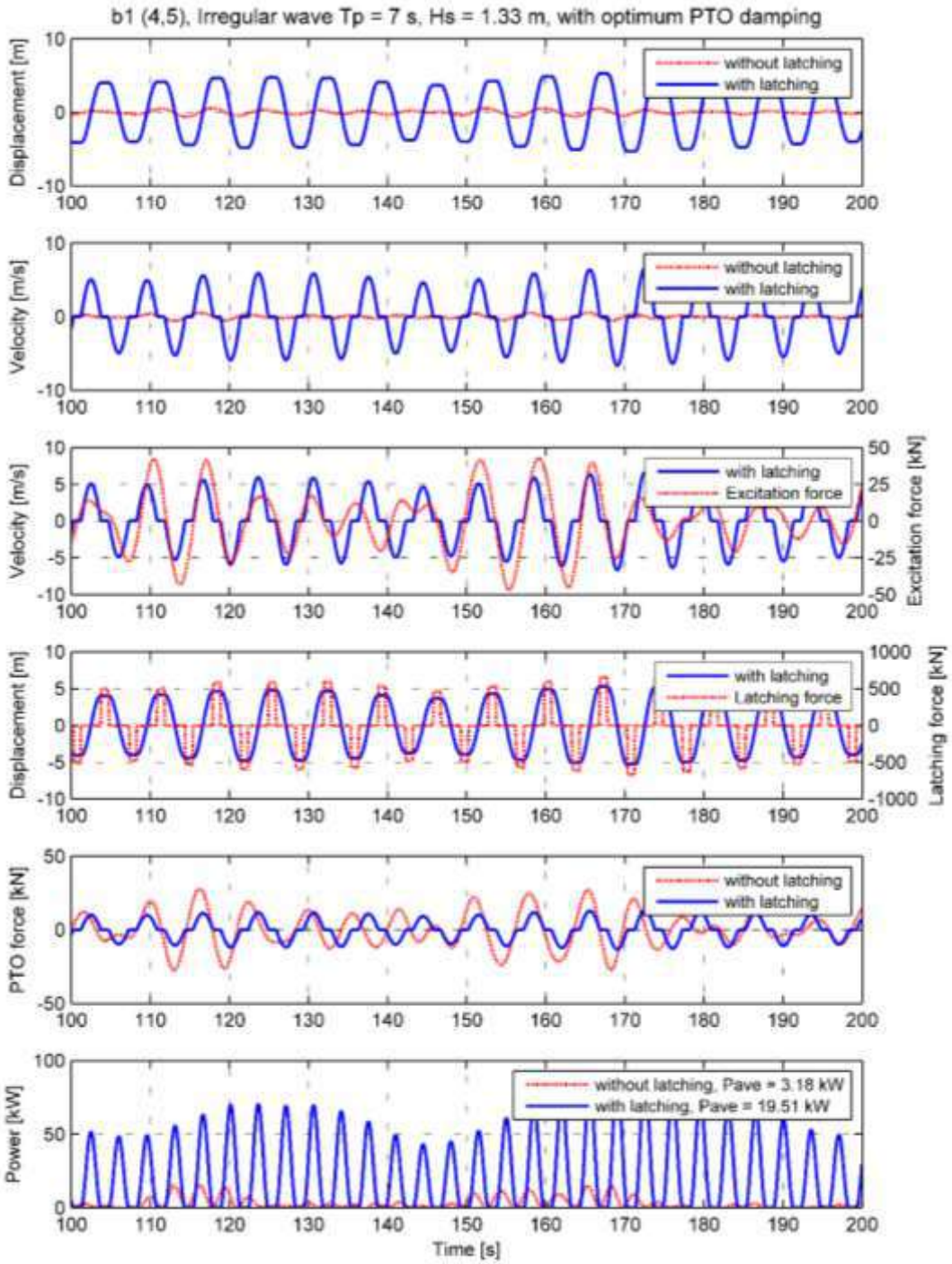

Figure 5-35 - The time domain results of the buoy b1 (4, 5) in an irregular wave of $T_p = 7\ s$ and $H_s = 1.33\ m$, with and without application of a constant-delay latching control, considering an optimum constant PTO damping; bpto = 50 kN/(m/s) for without latching and bpto = 2 kN/(m/s) for with latching. From top to bottom: Displacement, velocity, excitation, latching force, PTO force and mechanical power.

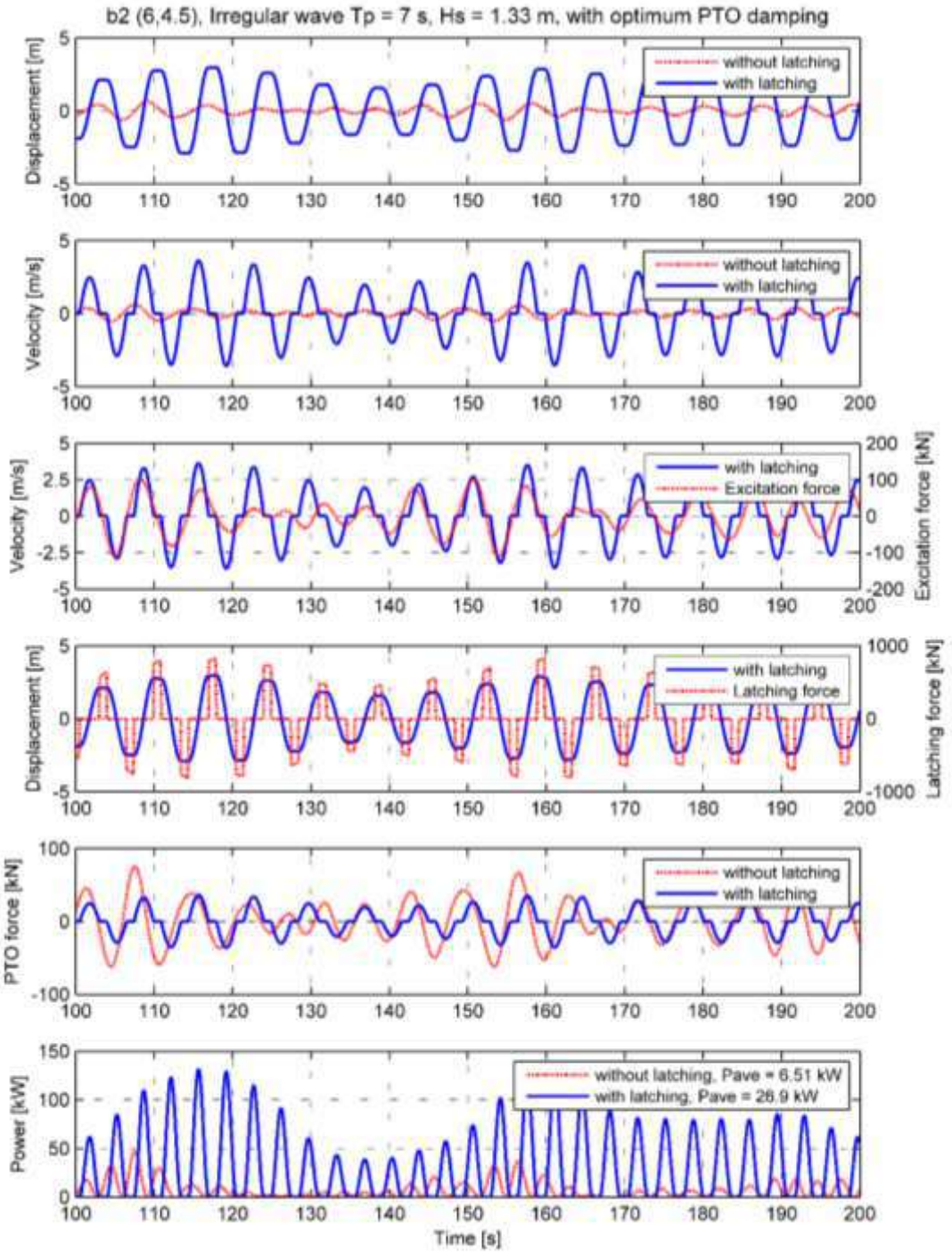

Figure 5-36 - The time domain results of the buoy b2 (6, 4.5) in an irregular wave of $T_p = 7\ s$ and $H_s = 1.33\ m$, with and without application of a constant-delay latching control, considering an optimum constant PTO damping; bpto = 120 kN/(m/s) for without latching and bpto = 10 kN/(m/s) for with latching. From top to bottom: Displacement, velocity, excitation, latching force, PTO force and mechanical power.

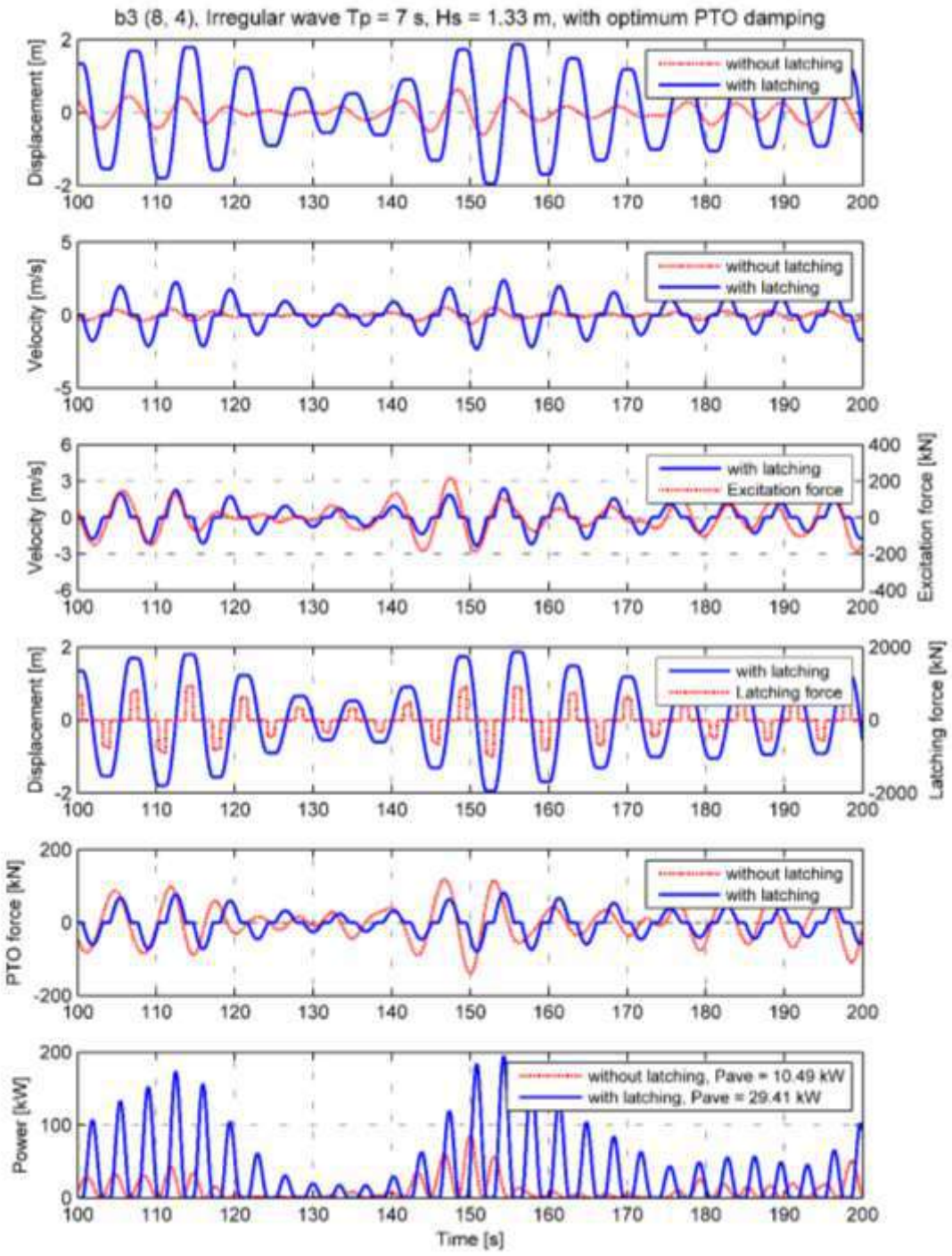

Figure 5-37 - The time domain results of the buoy b3 (8, 4) in an irregular wave of $T_p = 7\ s$ and $H_s = 1.33\ m$, with and without application of a constant-delay latching control, considering an optimum constant PTO damping; bpto = 230 kN/(m/s) for without latching and bpto = 34 kN/(m/s) for with latching. From top to bottom: Displacement, velocity, excitation, latching force, PTO force and mechanical power.

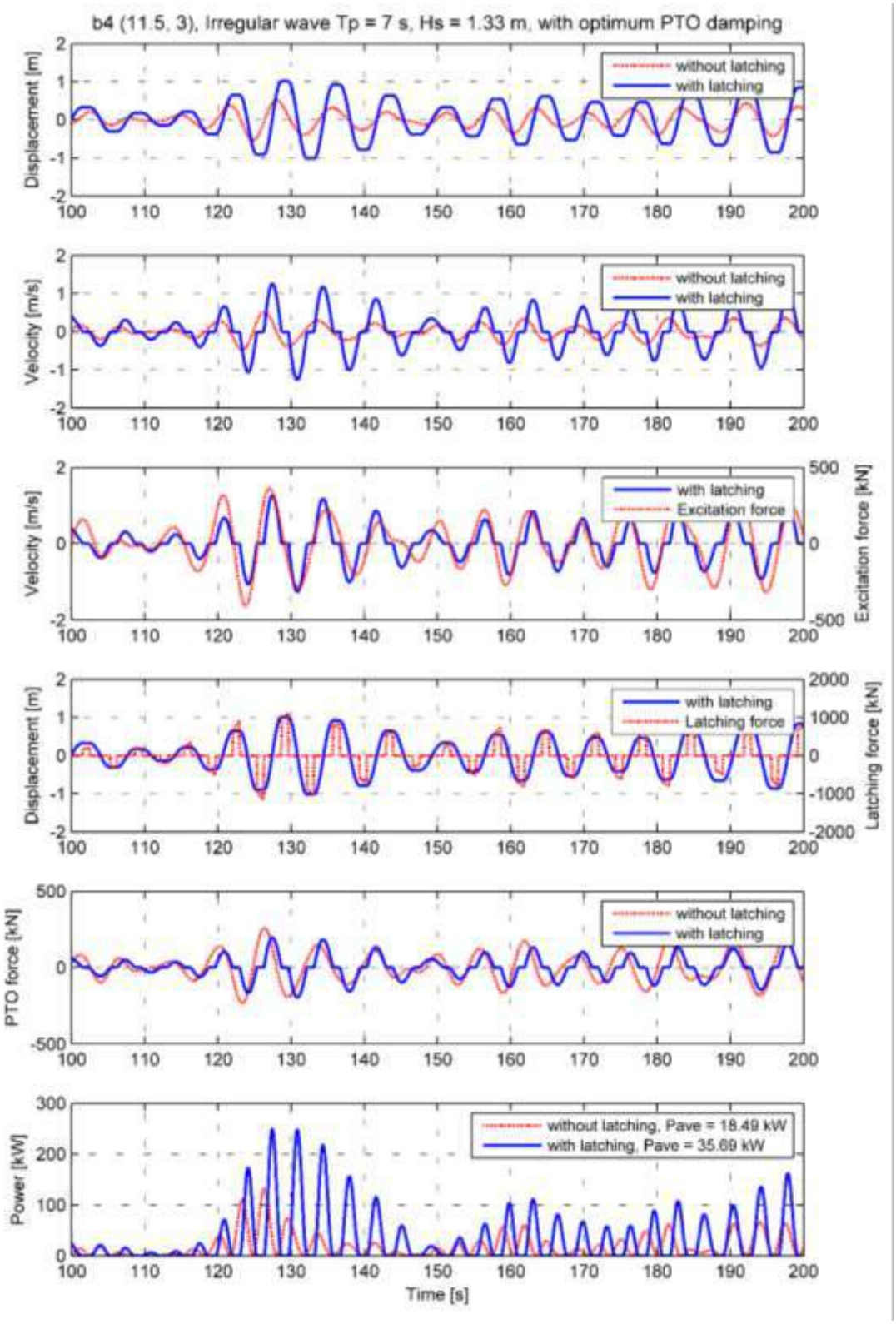

Figure 5-38 - The time domain results of the buoy b4 (11.5, 3) in an irregular wave of $T_p = 7\ s$ and $H_s = 1.33\ m$, with and without application of a constant-delay latching control, considering an optimum constant PTO damping; bpto = 500 kN/(m/s) for without latching and bpto = 156 kN/(m/s) for with latching. From top to bottom: Displacement, velocity, excitation, latching force, PTO force and mechanical power.

Comparing the PTO force of the optimally-damped buoys with and without application of a constant-delay latching control shows the reduction in the maximum PTO force for the controlled buoys. It means that with application of the constant-dely latching control, the buoy produces more mean power requiring lower PTO force level. The maximum PTO focre diminution is about 60%, 48%, 40% and 12% for the buoys b1 (4, 5), b2 (6, 4.5), b3 (8, 4) and b4 (11.5, 3) respectively. The results show that the buoy b1 (4, 5) has the largest decrease.

5.9 Effect of latching control on the PA optimum dimensions

Chapter 4 presents a preliminary optimization study through a series of frequency domain analyses and application of a statistical method called design of experiment (DOE). The optimization process is applied for a range of control-free buoys with different diameters and drafts considering the sea characteristics of the nearshore Rio de Janeiro, Brazil. As the result, a buoy with diameter of 13.5 m and draft of 3 m is determined as the optimum buoy. The large dimensions of the buoy is because of the range of the prevailing wave period of the local sea that is beyond 7 s. In practice, utilizing such a big buoy brings some challenges, e.g. large structural load, large support structure (in the case of bottom-mounted support), very large loads in extreme sea conditions, etc. that leads to a significant increase in capital cost. The challenge is to use a smaller buoy that has the same (or approximately the same) performance as the larger one. To achieve this a constant-delay latching control is selected to be applied on the point absorber. As it is explained and discussed in the previous section, applying this control system changes the characteristics of the oscillation of the buoys e.g. natural period, displacement, velocity etc. that result in a different behavior of the oscillator in the sea. This implies the necessity of addressing the effect of the constant-delay latching control on the optimum dimensions of the buoy.

The behavior of the buoys with and without the application of a constant-delay latching control in the range of the predominant wave period of the local sea applying different PTO damping level is addressed in section 5.8. To obtain the more realistic results, each PTO damping is applied for each sea state considering 20 different series of wave random phase. According to these results, figures 5-39 and 40 show the resultant maximum mean power and the corresponding optimum PTO damping for each sea state. It should be noted

that this maximum value is selected based on the average of the mean power values for each PTO damping level. As it showed in the previous section, applying this type of latching control significantly amplifies the power production. As figures 5-39 shows, the maximum power level is almost constant for different sea states and the buoys are not sensitive to the sea state modal period. However, the required optimum PTO damping to provide that maximum level of power production increases with the wave period. In the other hand, as figure 5-40 illustrates, except the largest buoy, a constant level of PTO damping can maximizes the power absorption in the range of the predominant sea states. considering the controlled buoys, the higher level of mean power is obtained by increasing the buoy size. However, it should be kept in mind that to choose the optimum buoy for extracting wave energy, the point absorbers should not be designed to absorb the maximum possible energy from the incident ocean waves. It is because, only a small fraction of the available energy at sea can be absorbed by point absorbers and maximizing the absorbed power in relation to the available energy at sea results in systems with large dimensions leading to a prohibitively high cost [27,100]. Instead, the challenge is to design the WECs to maximize the absorbed energy relative to the cost.

In the other hand, the PTO system has a limited power capacity that is adjusted according to the WEC maximum produced power. It can be seen form figure 5-40-b that the larger buoys require higher level of PTO damping to provide the maximum mean power. Moreover, it seen that in the case of the largest buoy, the PTO damping should be tuned according to the sea state modal period, while for instance, the optimum PTO damping of buoy b1 (4, 5) is independent of wave period and constant in the range of predominant sea states. The higher design requirements such as large buoy dimension, high PTO damping levels leads to a larger capital cost of the WEC. Therefore, an economic WEC should operate close to its installed power capacity a rather large fraction of its lifetime [120]. Considering figure 5-40-a, let us assume that we design the b4 based on its design limits that are achieved at its maximum mean power at sea state of $T_p = 10\ s$. Then, it can be seen that its maximum mean power has been changed from 47 kW at $T_p = 10\ s$ to 25 kW at $T_p = 6\ s$ and it almost continues constant for the sea states with energy periods more than 10 s. It implies that b4 does not use its maximum capacity (which requires the design limits) during a significant part of its lifetime that here is approximately 58%.

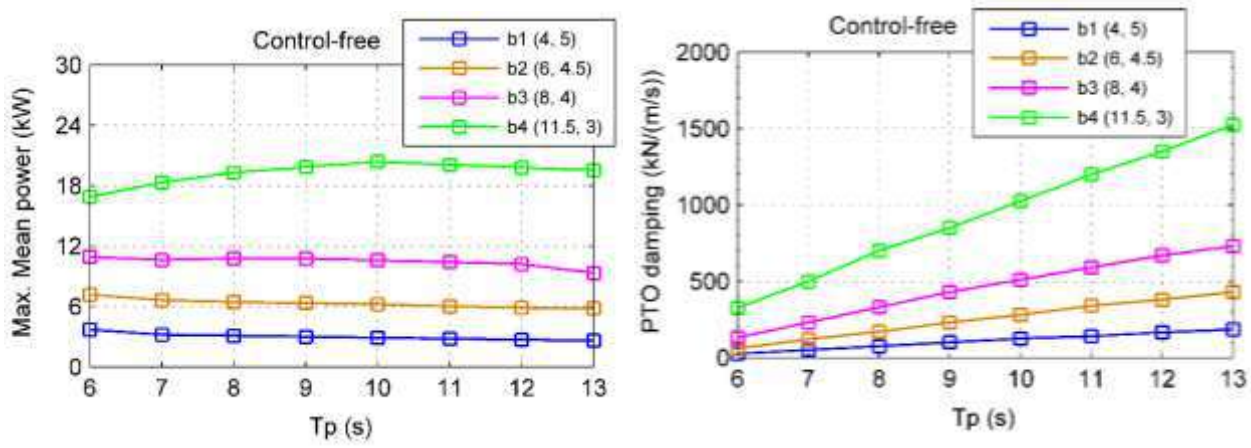

a) b)

Figure 5-39 - The a) maximum mean power (kW) and b) optimum PTO damping of the control-free buoys for different sea states with significant wave height of $H_s = 1.33\ m$.

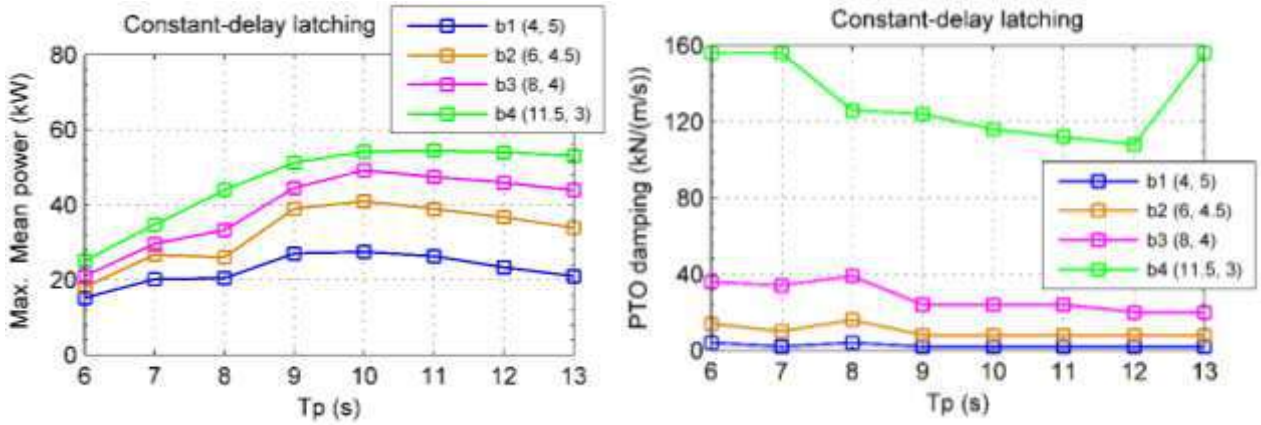

a) b)

Figure 5-40 –The a) maximum mean power (kW) and b) optimum PTO damping of the buoys controlled by a constant-delay latching for different sea states with significant wave height of $H_s = 1.33\ m$.

This is the percentage of the occurrence of the sea states with energy periods less than 10 s, in accordance to the data illustrated in the joint probability distribution of the local sea waves, figure 4-4. This percentage is smaller for the buoys b3 and b2 and b1. For instance, in the case of buoy b1 (4, 5), the mean power changes slightly with sea state and a

diminution of 37% can be observed when comparing its maximum ($T_p = 10\ s$) and minimum ($T_p = 6\ s$) values. This value is about 55% for the buoy b4 (11.5, 3).

A useful parameter that can help us to evaluate the performance of a pint absorber is the ratio of the instantaneous power to the mean power. Figure 5-41-a shows this dimensionless parameter for the buoys b1 (4, 5) and b4 (11.5, 3). The results show the performance of the buoys during a time window of 600 seconds in an irregular wave of $T_p = 10\ s$ and $H_s = 1.33\ m$. As it is illustrated, the ratio is more excessive for the buoy b4 (11.5, 3). The maximum values of the ratio of buoy b4 are approximately two times larger than the maximum values of buoy b1. Additionally, the deviation of the maximum instantaneous power values from the mean level is less chaotic for the buoy b1. It implies that the power production is smoother and hence, conversion-efficiency requirement of the PTO system is less strict. Figure 5-41-b shows the maximum mean power produced by the buoys b1(4, 5) and b4 (11.5, 3) in the range of predominant sea states. The buoy performance is calculated for the twenty different wave random phases for each sea states (see figure 5-31). It can be inferred from the results that changing the wave random phase, which occur constantly in a real sea, has significant effect on the larger buoy comparing to the small one. The maximum mean power levels of the larger buoy are more dispersed and it affect the power generation smoothness. It can be seen that the mean power dispersion is larger for the T_p longer than 9 s which is the range of the energetic waves of the sea local. Thus, it can be inferred that, for the buoys with the same natural period and controlled by a constant-delay latching in irregular waves, the mean power increases with the size, but it imposes some limits i.e. high level of required PTO damping, large time of unused capacity during the system lifetime, less smooth power generation and etc.

A parameter that can affect the estimation of the WEC cost is the power-to-volume ratio. Figure 5-42 show this ratio for the buoys with and without the constant-delay latching control. The maximum mean power values are taken from the table 5-2 and the buoys volume is calculated assuming 2 m of air gap (the height of the buoy above the water level at its static equilibrium). It can be observed that in the case of control-free buoys, figure 5-42-a, the largest buoy b4 (11.5, 3) shows a better performance for the modal period greater than 7 seconds. It implies a relatively higher power absorption of the buoy b4 in longer wave periods. Nevertheless, the power-to-volume ratio values of the smaller buoys are close to the corresponding value of the buoy b4 with a coincidence at $T_p = 7\ s$. As it is illustrated in figure 5-42-b, the results are different for the buoys controlled by a

constant-delay latching. Evidently, significant improvement is observed for the buoys in comparison to the control-free condition. The smallest buoy b1 has the highest values of the power-to-volume ratio for the entire range of the predominant sea states. It means that, buoy b1 absorbs more energy per one cubic meter of its volume. The results support the idea of "small is beautiful" , which was presented by Falnes for the control-free buoys [120].

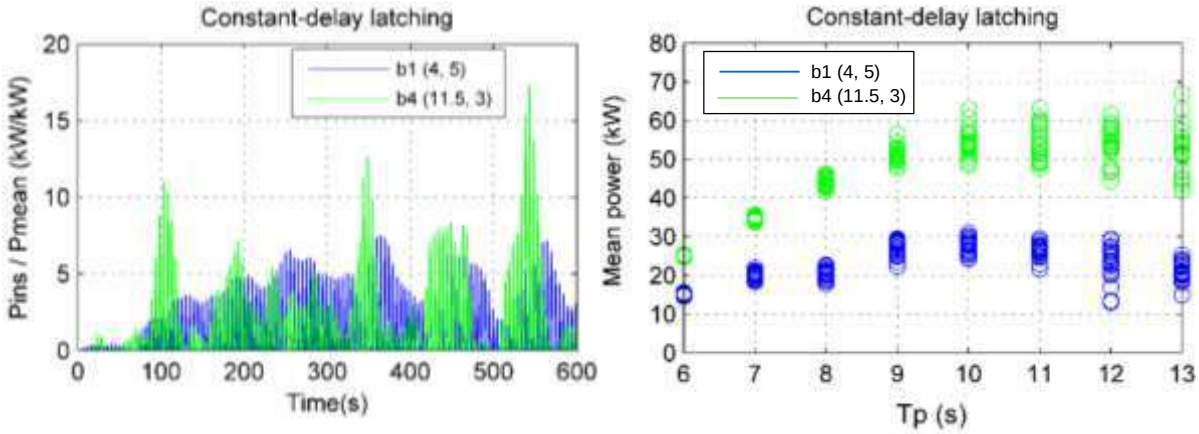

a) b)

Figure 5-41 – a) The ratio of the instantaneous power to the mean power versus time in second applying an optimum PTO damping in an irregular wave of $T_p = 10\ s$ and $H_s = 1.33\ m$; b) The mean power versus sea state modal period in second for 20 different wave random phases. An optimum PTO damping and a significant wave height equal to 1.33 m are applied for the sea states.

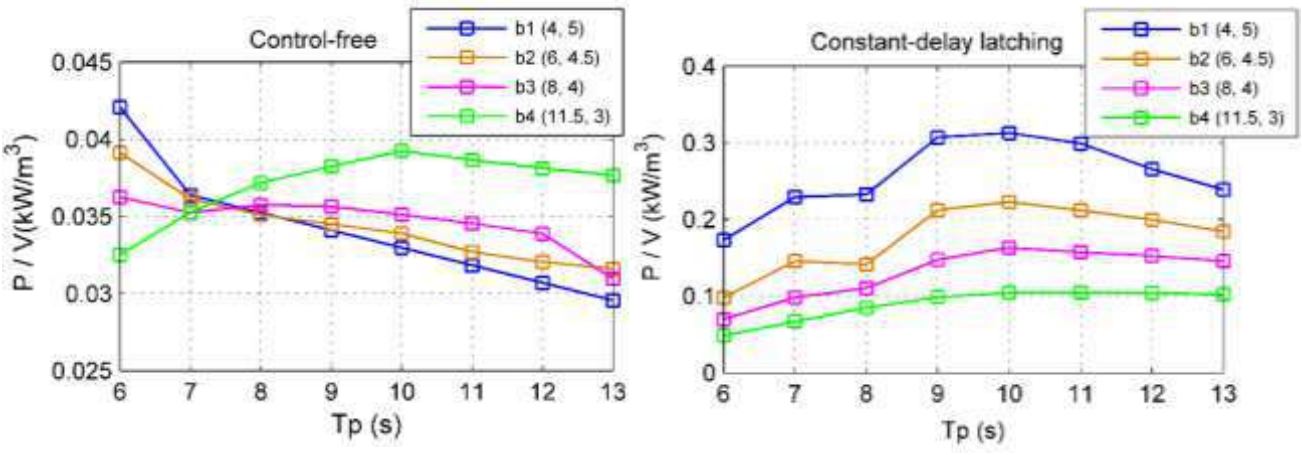

a) b)

Figure 5-42 – The power-to-volume ratio of the buoys with and without application of a constant-delay latching control in a range of sea states with a significant wave height of $H_s = 1.33\ m$.

Accordingly, it can be said that, for instance, for a sea site such as nearshore Rio de Janeiro with a cylindrical point absorber controlled by a latching system, a 5 MW wave farm should consist of 167 units of b1 (4, 5) with capacity of 30 kW rather than 84 units of b4 (11.5, 3) with capacity of 60 kW.

5.10 Annual energy production (AEP)

The annual energy production (AEP) is calculated by multiplying the mechanical power matrix (MPM) $\bar{P}_m(H_s, T_p)$, applying Eq.(5.9), with the matrix of the number of occurrence of the waves $p(H_S, T_P)$, figure 5-43, which describes the wave distribution of the site's sea states, using the following equation [123]:

$$AEP = (8766)\gamma_1\gamma_2\gamma_3 \left\{\sum_{i=1}^{n} P_m(H_{S_i}, T_{P_i}).p(H_{S_i}, T_{P_i})\right\} / total\ wave\ occurance \quad [kWh] \quad (5.22)$$

γ_1 is the conversion efficiency coefficient, which take into account the losses between the generated mechanical power and the electrical power output and, γ_2 is the transmission efficiency which is the ratio of the power received over a transmission path to the power transmitted. γ_3 is the operational availability coefficient that is considered to be equal to 0.95 (based on the considerations in [123]) and, 8766 is the number of hours in a Julian year.

		Tp (s)												
		4	5	6	7	8	9	10	11	12	13	14	15	16
Hs (m)	0.25	0.6	2	8.4	84	79.8	35	19	18	5.8	1.2	3	2	1.6
	0.75	7.6	23.8	101	602.2	866.6	456	376	280.8	169.4	84	32.8	12.2	3.4
	1.25	0.8	12.8	50.8	199.2	483.6	480.8	492	404.4	279	137	51.8	15	10.2
	1.75	0	0.4	19.4	70.2	154.8	201.8	287	350	215.2	141.2	42.6	9.8	4
	2.25	0	0	0.6	14	63.6	97.4	147	174	162	82.8	22.8	9.8	11.2
	2.75	0	0	0	1.4	17.8	29.6	50	69	97.8	72.8	25.6	6.8	8.4
	3.25	0	0	0	0	0.4	10	11	20	39.6	31	26	7	1.8
	3.75	0	0	0	0	0	0	5	4.4	10.6	15.4	4.4	1.2	0.2
	4.25	0	0	0	0	0	0	0	0.2	4.8	3.8	0.6	0	0.6
	4.75	0	0	0	0	0	0	0	0	0	1.2	0.6	0.8	0

Figure 5-43– Matrix representation of the number of occurrence of the sea waves for the nearshore region of Rio de Janeiro

Considering an ideal PTO system and neglecting the transmission losses, the coefficients γ_1 , and γ_2 are equal to 1. The electrical power can be obtained by following expression:

$$P_e = P_m \times \gamma_1 \tag{5.23}$$

Where P_m is the mechanical power. The annual average electrical power can be calculated by summing the product of the electrical power matrix (EPM) and the matrix of the number of occurrence of the waves divided by the total number of the wave occurrence. The rated or maximum power (capacity) of a WEC depends on the capacity factor (C_f) and annual average electrical power, expressed as follow:

$$P_{rated} = \frac{P_{ae}}{C_f} \tag{5.24}$$

The capacity factor is a dimensionless parameter that can be defined for a given WEC as the ratio between the actual electrical energy generation over a given period of time and the theoretical maximum possible electrical energy output over the same period of time [124]. Assuming a capacity factor of 30%, the device rated power can be determined by iteratively changing its value until the capacity factor equaled the considered percentage [123]. Figure 5-44 illustrate the flowchart of the MATLAB code that is developed to calculate the rated power.

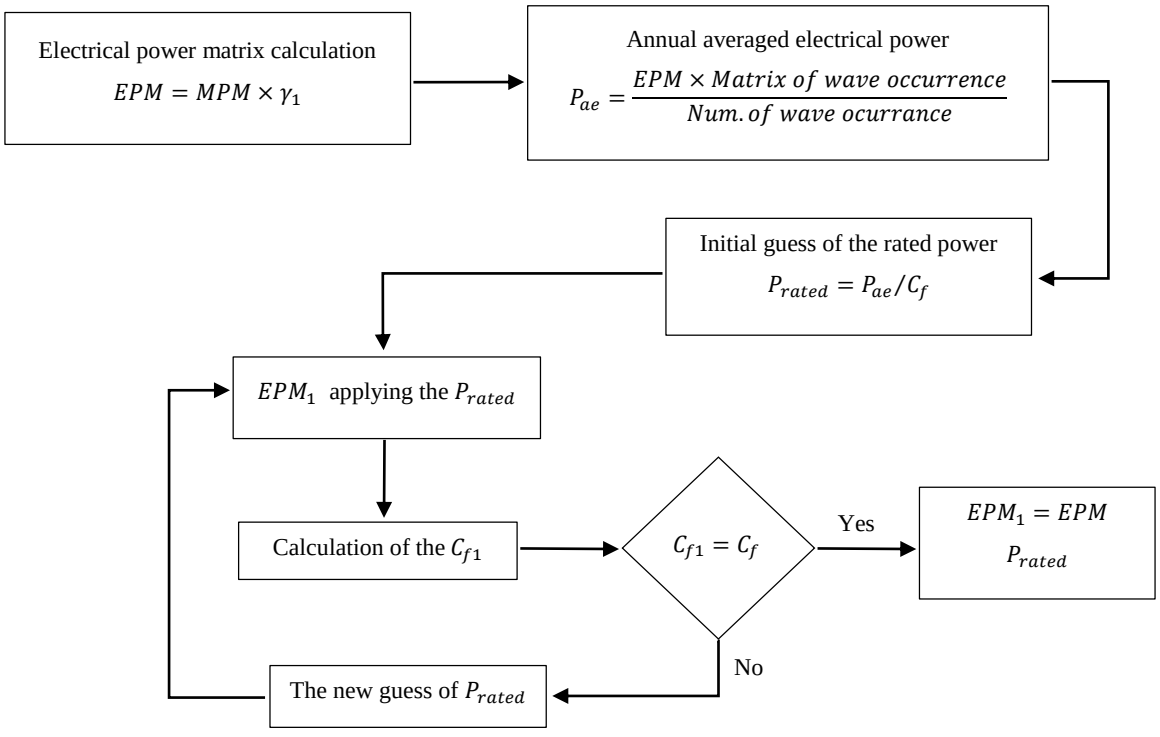

Figure 5-44 – The rated power calculation process

The annual mechanical power matrix (AMPM), which is determined by multiplying the mechanical power matrix with the joint probability distribution, and the electrical power matrix (EPM) of the buoys are illustrated in figures 5-45 to 60. Two different strategies are considered for the constant-delay latching control. In the first one, the latching duration is tuned to the peak period (modal period) of the local sea and this constant value is applied for the other sea states. In the second approach, the latching duration is changed according to the sea state modal period, thus it is tuned to each sea state. Additionally, the control-free matrices are calculated applying the simple control of the PTO damping level. Consequently, the approaches for the AEP calculation can be divided into following four cases:

- *Case 1*: Control-free buoys with application of a constant PTO damping. This is the optimum PTO damping value at the sea local peak period (modal period), $T_p = 9.7\ s \approx 10\ s$.
- *Case 2:* Control-free buoys with application of a tuned PTO damping. The optimum value of the PTO damping are considered for each sea states.
- *Case 3:* Constant latching duration with a constant PTO damping. A constant-delay latching control tuned to the peak period of the sea local, $T_p = 9.7\ s$ is applied. This case is called "constant latching duration", because the same latching duration is applied for all 130 sea states. The optimum PTO damping value is corresponded to the sea local peak period (modal period), $T_p = 9.7\ s \approx 10\ s$.
- *Case 4:* Tuned latching duration with a constant PTO damping. A constant-delay latching control tuned to each sea state is applied. The optimum PTO damping value is corresponded to the sea local peak period (modal period), $T_p = 9.7\ s \approx 10\ s$.

		AMPM - b1 (4, 5) – control-free, constant optimum bpto = 125 kN/(m/s)												
		Tp (s)												
		4	5	6	7	8	9	10	11	12	13	14	15	16
Hs (m)	0.25	0.01	0.08	0.59	7.38	7.8	3.52	1.88	1.74	0.53	0.11	0.25	0.16	0.12
	0.75	0.96	9.01	63.41	476.37	762.67	412.2	335.33	244	140.27	66.31	24.6	8.61	2.28
	1.25	0.28	13.46	88.59	437.71	1182.23	1207.26	1218.86	976.12	641.72	300.39	107.9	29.42	18.98
	1.75	0	0.82	66.31	302.34	741.72	993.15	1393.56	1655.84	970.15	606.82	173.93	37.67	14.59
	2.25	0	0	3.39	99.67	503.75	792.39	1179.91	1360.78	1207.26	588.22	153.88	62.27	67.53
	2.75	0	0	0	14.89	210.61	359.73	599.52	806.1	1088.74	772.58	258.1	64.54	75.66
	3.25	0	0	0	0	6.61	169.74	184.22	326.34	615.72	459.49	366.12	92.8	22.64
	3.75	0	0	0	0	0	0	111.48	95.58	219.43	303.9	82.49	21.18	3.35
	4.25	0	0	0	0	0	0	0	5.58	127.63	96.32	14.45	0	12.91
	4.75	0	0	0	0	0	0	0	0	0	37.99	18.05	22.65	0
												AEP (kWh)		27999.53
												Rated.P (kW)		11

(a)

		EPM - b1 (4, 5) – control-free, constant optimum bpto = 125 kN/(m/s)												
		Tp (s)												
		4	5	6	7	8	9	10	11	12	13	14	15	16
Hs (m)	0.25	0.01	0.04	0.07	0.09	0.10	0.10	0.10	0.10	0.09	0.09	0.08	0.08	0.07
	0.75	0.13	0.38	0.63	0.79	0.88	0.90	0.89	0.87	0.83	0.79	0.75	0.71	0.67
	1.25	0.35	1.05	1.74	2.20	2.44	2.51	2.48	2.41	2.30	2.19	2.08	1.96	1.86
	1.75	0.00	2.06	3.42	4.31	4.79	4.92	4.86	4.73	4.51	4.30	4.08	3.84	3.65
	2.25	0.00	0.00	5.65	7.12	7.92	8.14	8.03	7.82	7.45	7.10	6.75	6.35	6.03
	2.75	0.00	0.00	0.00	10.64	11.00	11.00	11.00	11.00	11.00	10.61	10.08	9.49	9.01
	3.25	0.00	0.00	0.00	0.00	11.00	11.00	11.00	11.00	11.00	11.00	11.00	11.00	11.00
	3.75	0.00	0.00	0.00	0.00	0.00	0.00	11.00	11.00	11.00	11.00	11.00	11.00	11.00
	4.25	0.00	0.00	0.00	0.00	0.00	0.00	0.00	11.00	11.00	11.00	11.00	0.00	11.00
	4.75	0.00	0.00	0.00	0.00	0.00	0.00	0.00	0.00	0.00	11.00	11.00	11.00	0.00

(b)

Figure 5-45 – The a) annual mechanical power matrix and b) electrical power matrix for the control-free buoy b1 (4, 5) applying a constant PTO damping (case 1)

		AMPM - b2 (6, 4.5) – control-free , constant optimum bpto = 280 kN/(m/s)												
		Tp (s)												
		4	5	6	7	8	9	10	11	12	13	14	15	16
Hs (m)	0.25	0.02	0.17	1.19	15.3	16.34	7.48	4.05	3.7	1.13	0.22	0.53	0.33	0.25
	0.75	1.93	18.14	129.29	987.45	1596.67	877.43	720.63	520.07	296.51	139.78	51.89	18.17	4.8
	1.25	0.56	27.1	180.63	907.33	2475.03	2569.86	2619.31	2080.52	1356.52	633.24	227.63	62.05	40.01
	1.75	0	1.66	135.21	626.71	1552.82	2114.08	2994.75	3529.27	2050.79	1279.2	366.92	79.46	30.76
	2.25	0	0	6.91	206.61	1054.62	1686.74	2535.62	2900.38	2552.01	1240.01	324.62	131.34	142.36
	2.75	0	0	0	30.86	440.92	765.74	1288.36	1718.13	2301.48	1628.64	544.49	136.14	159.49
	3.25	0	0	0	0	13.84	361.32	395.88	695.56	1301.56	968.63	772.36	195.74	47.73
	3.75	0	0	0	0	0	0	239.57	203.73	463.84	640.64	174.02	44.67	7.06
	4.25	0	0	0	0	0	0	0	11.89	269.79	203.04	30.48	0	27.21
	4.75	0	0	0	0	0	0	0	0	0	80.09	38.07	47.79	0
												AEP (kWh)		59340.1
												Rated.P (kW)		22

(a)

		EPM - b2 (6, 4.5) - control-free, constant optimum bpto = 280 kN/(m/s)												
		Tp (s)												
		4	5	6	7	8	9	10	11	12	13	14	15	16
Hs (m)	0.25	0.03	0.08	0.14	0.18	0.20	0.21	0.21	0.21	0.19	0.18	0.18	0.17	0.16
	0.75	0.25	0.76	1.28	1.64	1.84	1.92	1.91	1.85	1.75	1.66	1.58	1.49	1.41
	1.25	0.71	2.12	3.56	4.55	5.12	5.34	5.32	5.14	4.86	4.62	4.39	4.14	3.92
	1.75	0.00	4.15	6.97	8.93	10.03	10.48	10.45	10.08	9.53	9.06	8.61	8.11	7.69
	2.25	0.00	0.00	11.52	14.76	16.58	17.32	17.25	16.67	15.75	14.98	14.24	13.40	12.71
	2.75	0.00	0.00	0.00	22.00	22.00	22.00	22.00	22.00	22.00	22.00	21.27	20.02	18.99
	3.25	0.00	0.00	0.00	0.00	22.00	22.00	22.00	22.00	22.00	22.00	22.00	22.00	22.00
	3.75	0.00	0.00	0.00	0.00	0.00	0.00	22.00	22.00	22.00	22.00	22.00	22.00	22.00
	4.25	0.00	0.00	0.00	0.00	0.00	0.00	0.00	22.00	22.00	22.00	22.00	0.00	22.00
	4.75	0.00	0.00	0.00	0.00	0.00	0.00	0.00	0.00	0.00	22.00	22.00	22.00	0.00

(b)

Figure 5-46 - The a) annual mechanical power matrix and b) electrical power matrix for the control-free buoy b2 (6, 4.5) applying a constant PTO damping (case 1)

		AMPM - b3 (8, 4) – control-free, constant optimum bpto = 510 kN/(m/s)												
		Tp (s)												
		4	5	6	7	8	9	10	11	12	13	14	15	16
Hs (m)	0.25	0.03	0.27	1.9	24.93	27.11	12.46	6.74	6.25	1.94	0.38	0.9	0.56	0.42
	0.75	3.13	28.55	205.13	1608.3	2650.11	1460.82	1200.86	877.64	510.06	240.46	88.25	30.72	8.13
	1.25	0.92	42.65	286.6	1477.8	4107.99	4278.52	4364.83	3510.99	2333.49	1089.41	387.15	104.91	67.72
	1.75	0	2.61	214.52	1020.75	2577.33	3519.7	4990.46	5955.83	3527.77	2200.7	624.04	134.35	52.05
	2.25	0	0	10.97	336.51	1750.43	2808.23	4225.37	4894.54	4389.98	2133.27	552.12	222.08	240.92
	2.75	0	0	0	50.27	731.83	1274.87	2146.93	2899.43	3959.01	2801.86	926.05	230.19	269.92
	3.25	0	0	0	0	22.97	601.56	659.69	1173.8	2238.95	1666.4	1313.62	330.97	80.79
	3.75	0	0	0	0	0	0	399.22	343.81	797.9	1102.13	295.97	75.54	11.95
	4.25	0	0	0	0	0	0	0	20.07	464.09	349.31	51.84	0	46.05
	4.75	0	0	0	0	0	0	0	0	0	137.79	64.75	80.8	0
												AEP (kWh)		99926.58
							(a)					Rated.P (kW)		37

		EPM - b3 (8, 4) - control-free, constant optimum bpto = 510 kN/(m/s)												
		Tp (s)												
		4	5	6	7	8	9	10	11	12	13	14	15	16
Hs (m)	0.25	0.05	0.13	0.23	0.30	0.34	0.36	0.35	0.35	0.33	0.32	0.30	0.28	0.27
	0.75	0.41	1.20	2.03	2.67	3.06	3.20	3.19	3.13	3.01	2.86	2.69	2.52	2.39
	1.25	1.15	3.33	5.64	7.42	8.49	8.90	8.87	8.68	8.36	7.95	7.47	6.99	6.64
	1.75	0.00	6.53	11.06	14.54	16.65	17.44	17.41	17.02	16.39	15.59	14.65	13.71	13.01
	2.25	0.00	0.00	18.28	24.04	27.52	28.83	28.74	28.13	27.10	25.76	24.22	22.66	21.51
	2.75	0.00	0.00	0.00	35.91	37.00	37.00	37.00	37.00	37.00	37.00	36.17	33.85	32.13
	3.25	0.00	0.00	0.00	0.00	37.00	37.00	37.00	37.00	37.00	37.00	37.00	37.00	37.00
	3.75	0.00	0.00	0.00	0.00	0.00	0.00	37.00	37.00	37.00	37.00	37.00	37.00	37.00
	4.25	0.00	0.00	0.00	0.00	0.00	0.00	0.00	37.00	37.00	37.00	37.00	0.00	37.00
	4.75	0.00	0.00	0.00	0.00	0.00	0.00	0.00	0.00	0.00	37.00	37.00	37.00	0.00

(b)

Figure 5-47 - The a) annual mechanical power matrix and b) electrical power matrix for the control-free buoy b3 (8, 4) applying a constant PTO damping (case 1)

		AMPM - b4 (11.5, 3) - control-free, constant optimum, bpto = 1025 kN/(m/s)												
		Tp (s)												
		4	5	6	7	8	9	10	11	12	13	14	15	16
Hs (m)	0.25	0.06	0.5	3.47	46.36	50.78	23.36	12.76	11.82	3.69	0.74	1.76	1.1	0.82
	0.75	6.52	53.16	375.37	2990.92	4962.76	2738.59	2273.48	1659.62	970.12	467.23	173.65	60.3	15.77
	1.25	1.91	79.41	524.44	2748.22	7692.87	8020.92	8263.55	6639.26	4438.26	2116.77	761.78	205.94	131.41
	1.75	0	4.86	392.54	1898.26	4826.47	6598.38	9447.99	11262.44	6709.75	4276.06	1227.91	263.71	101
	2.25	0	0	20.07	625.8	3277.96	5264.58	7999.52	9255.56	8349.65	4145.03	1086.38	435.94	467.5
	2.75	0	0	0	93.48	1370.46	2389.99	4064.59	5482.8	7529.95	5444.14	1822.16	451.86	523.77
	3.25	0	0	0	0	43.01	1127.73	1248.94	2219.65	4258.43	3237.88	2584.77	649.67	156.76
	3.75	0	0	0	0	0	0	755.81	650.13	1517.6	2141.49	582.37	148.28	23.19
	4.25	0	0	0	0	0	0	0	37.96	882.69	678.73	102	0	89.36
	4.75	0	0	0	0	0	0	0	0	0	267.73	127.41	158.6	0
												AEP (kWh)		189601.6
							(a)					Rated.P (kW)		70

		EPM - b4 (11.5, 3) - control-free, constant optimum bpto = 1025 kN/(m/s)												
		Tp (s)												
		4	5	6	7	8	9	10	11	12	13	14	15	16
Hs (m)	0.25	0.10	0.25	0.41	0.55	0.64	0.67	0.66	0.66	0.64	0.62	0.59	0.55	0.52
	0.75	0.86	2.23	3.72	4.97	5.73	6.01	6.04	5.91	5.73	5.56	5.29	4.94	4.64
	1.25	2.38	6.20	10.32	13.80	15.91	16.68	16.79	16.42	15.91	15.45	14.71	13.73	12.88
	1.75	0.00	12.16	20.23	27.04	31.18	32.70	32.97	32.18	31.18	30.28	28.82	26.91	25.25
	2.25	0.00	0.00	33.45	44.70	51.54	54.05	54.42	53.19	51.54	50.06	47.65	44.48	41.74
	2.75	0.00	0.00	0.00	66.77	70.00	70.00	70.00	70.00	70.00	70.00	70.00	66.45	62.35
	3.25	0.00	0.00	0.00	0.00	70.00	70.00	70.00	70.00	70.00	70.00	70.00	70.00	70.00
	3.75	0.00	0.00	0.00	0.00	0.00	0.00	70.00	70.00	70.00	70.00	70.00	70.00	70.00
	4.25	0.00	0.00	0.00	0.00	0.00	0.00	0.00	70.00	70.00	70.00	70.00	0.00	70.00
	4.75	0.00	0.00	0.00	0.00	0.00	0.00	0.00	0.00	0.00	70.00	70.00	70.00	0.00

(b)

Figure 5-48 - The a) annual mechanical power matrix and b) electrical power matrix for the control-free buoy b4 (11.5, 3) applying a constant PTO damping (case 1)

		AMPM - b1 (4, 5) - control-free, tuned optimum bpto												
		Tp (s)												
		4	5	6	7	8	9	10	11	12	13	14	15	16
Hs (m)	0.25	0.03	0.82	1.08	9.42	8.5	3.59	1.88	1.75	0.54	0.11	0.27	0.17	0.13
	0.75	3.69	87.78		607.75	830.68	421.04	335.33	245.06	143.06	69.2	26.23	9.41	2.55
	1.25	1.08	131.14	163.93	558.43	1287.65	1233.16	1218.84	980.36	654.5	313.48	115.06	32.14	21.27
	1.75	0	8.03	122.7	385.72	807.86	1014.45	1393.54	1663.02	989.47	633.26	185.46	41.16	16.35
	2.25	0	0	6.27	127.16	548.67	809.39	1179.9	1366.68	1231.31	613.86	164.09	68.03	75.66
	2.75	0	0	0	19	229.39	367.44	599.51	809.59	1110.43	806.25	275.22	70.52	84.76
	3.25	0	0	0	0	7.2	173.38	184.21	327.75	627.98	479.51	390.4	101.39	25.37
	3.75	0	0	0	0	0	0	111.48	96	223.8	317.14	87.96	23.14	3.75
	4.25	0	0	0	0	0	0	0	5.6	130.17	100.52	15.41	0	14.46
	4.75	0	0	0	0	0	0	0	0	0	39.65	19.24	24.75	0
												AEP (kWh)		29480.26
												Rated.P (kW)		11

(a)

		EPM - b1 (4, 5) - control-free, tuned optimum bpto												
		Tp (s)												
		4	5	6	7	8	9	10	11	12	13	14	15	16
Hs (m)	0.25	0.05	0.41	0.13	0.11	0.11	0.10	0.10	0.10	0.09	0.09	0.09	0.09	0.08
	0.75	0.49	3.69	1.16	1.01	0.96	0.92	0.89	0.87	0.84	0.82	0.80	0.77	0.75
	1.25	1.35	10.25	3.23	2.80	2.66	2.56	2.48	2.42	2.35	2.29	2.22	2.14	2.08
	1.75	0.00	11.00	6.32	5.49	5.22	5.03	4.86	4.75	4.60	4.48	4.35	4.20	4.09
	2.25	0.00	0.00	10.46	9.08	8.63	8.31	8.03	7.85	7.60	7.41	7.20	6.94	6.75
	2.75	0.00	0.00	0.00	11.00	11.00	11.00	11.00	11.00	11.00	11.00	10.75	10.37	10.09
	3.25	0.00	0.00	0.00	0.00	11.00	11.00	11.00	11.00	11.00	11.00	11.00	11.00	11.00
	3.75	0.00	0.00	0.00	0.00	0.00	0.00	11.00	11.00	11.00	11.00	11.00	11.00	11.00
	4.25	0.00	0.00	0.00	0.00	0.00	0.00	0.00	11.00	11.00	11.00	11.00	0.00	11.00
	4.75	0.00	0.00	0.00	0.00	0.00	0.00	0.00	0.00	0.00	11.00	11.00	11.00	0.00

(b)

Figure 5-49 - The a) annual mechanical power matrix and b) electrical power matrix for the control-free buoy b1 (4, 5) applying a tuned optimum PTO damping (case 2)

		b2 (6, 4.5) - control-free, tuned optimum bpto												
		Tp (s)												
		4	5	6	7	8	9	10	11	12	13	14	15	16
Hs (m)	0.25	0.04	0.96	2.12	19.3	17.73	7.62	4.05	3.72	1.15	0.23	0.57	0.36	0.28
	0.75	4.53	103.31	229.48	1244.97	1732.48	893.99	720.62	521.69	302.92	146.31	55.74	20.03	5.44
	1.25	1.32	154.33	320.61	1143.95	2685.55	2618.35	2619.26	2087.02	1385.87	662.85	244.52	68.4	45.3
	1.75	0	9.45	239.98	790.15	1684.9	2153.97	2994.69	3540.29	2095.15	1339.01	394.13	87.59	34.82
	2.25	0	0	12.27	260.49	1144.32	1718.57	2535.57	2909.44	2607.22	1297.98	348.71	144.79	161.16
	2.75	0	0	0	38.91	478.42	780.19	1288.34	1723.49	2351.27	1704.79	584.88	150.08	180.56
	3.25	0	0	0	0	15.02	368.14	395.87	697.74	1329.72	1013.92	829.66	215.78	54.04
	3.75	0	0	0	0	0	0	239.57	204.37	473.88	670.59	186.93	49.25	7.99
	4.25	0	0	0	0	0	0	0	11.93	275.62	212.54	32.74	0	30.8
	4.75	0	0	0	0	0	0	0	0	0	83.84	40.9	52.68	0
												AEP (kWh)		62166.22
												Rated.P (kW)		23

(a)

		EPM - b2 (6, 4.5) - control-free, tuned optimum bpto												
		Tp (s)												
		4	5	6	7	8	9	10	11	12	13	14	15	16
Hs (m)	0.25	0.07	0.48	0.25	0.23	0.22	0.22	0.21	0.21	0.20	0.19	0.19	0.18	0.18
	0.75	0.60	4.34	2.27	2.07	2.00	1.96	1.91	1.86	1.79	1.74	1.70	1.64	1.60
	1.25	1.66	12.06	6.31	5.74	5.55	5.45	5.32	5.16	4.97	4.84	4.72	4.56	4.44
	1.75	0.00	23.00	12.37	11.26	10.88	10.67	10.45	10.12	9.74	9.48	9.25	8.94	8.70
	2.25	0.00	0.00	20.45	18.61	17.99	17.64	17.25	16.72	16.09	15.68	15.29	14.77	14.39
	2.75	0.00	0.00	0.00	23.00	23.00	23.00	23.00	23.00	23.00	23.00	22.85	22.07	21.49
	3.25	0.00	0.00	0.00	0.00	23.00	23.00	23.00	23.00	23.00	23.00	23.00	23.00	23.00
	3.75	0.00	0.00	0.00	0.00	0.00	0.00	23.00	23.00	23.00	23.00	23.00	23.00	23.00
	4.25	0.00	0.00	0.00	0.00	0.00	0.00	0.00	23.00	23.00	23.00	23.00	0.00	23.00
	4.75	0.00	0.00	0.00	0.00	0.00	0.00	0.00	0.00	0.00	23.00	23.00	23.00	0.00

(b)

Figure 5-50 - The a) annual mechanical power matrix and b) electrical power matrix for the control-free buoy b2 (6, 4.5) applying a tuned optimum PTO damping (case 2)

		AMPM - b3 (8, 4) - control-free, tuned optimum bpto												
		Tp (s)												
		4	5	6	7	8	9	10	11	12	13	14	15	16
Hs (m)	0.25	0.05	1	3.2	31.06	29.41	12.71	6.74	6.27	1.98	0.4	0.96	0.62	0.48
	0.75	5.42	107.37	345.93	2004.24	2874.85	1489.94	1200.82	880.85	520.41	251.3	94.64	33.83	9.2
	1.25	1.58	160.41	483.31	1841.6	4456.36	4363.8	4364.68	3523.83	2380.88	1138.5	415.15	115.54	76.67
	1.75	0	9.82	361.76	1272.04	2795.9	3589.86	4990.28	5977.62	3599.41	2299.88	669.18	147.96	58.93
	2.25	0	0	18.5	419.35	1898.88	2864.21	4225.22	4912.45	4479.13	2229.41	592.05	244.58	272.76
	2.75	0	0	0	62.64	793.89	1300.28	2146.85	2910.04	4039.41	2928.13	993.03	253.52	305.59
	3.25	0	0	0	0	24.92	613.55	659.67	1178.1	2284.42	1741.49	1408.63	364.5	91.46
	3.75	0	0	0	0	0	0	399.21	345.06	814.11	1151.8	317.37	83.19	13.53
	4.25	0	0	0	0	0	0	0	20.15	473.51	365.05	55.59	0	52.13
	4.75	0	0	0	0	0	0	0	0	0	144	69.44	88.98	0
												AEP (kWh)		104306.4
												Rated.P (kW)		39

(a)

		EPM - b3 (8, 4) - control-free, tuned optimum bpto												
		Tp (s)												
		4	5	6	7	8	9	10	11	12	13	14	15	16
Hs (m)	0.25	0.08	0.50	0.38	0.37	0.37	0.36	0.35	0.35	0.34	0.33	0.32	0.31	0.30
	0.75	0.71	4.51	3.43	3.33	3.32	3.27	3.19	3.14	3.07	2.99	2.89	2.77	2.71
	1.25	1.98	12.53	9.51	9.24	9.21	9.08	8.87	8.71	8.53	8.31	8.01	7.70	7.52
	1.75	0.00	24.56	18.65	18.12	18.06	17.79	17.41	17.08	16.73	16.29	15.71	15.10	14.73
	2.25	0.00	0.00	30.83	29.95	29.86	29.41	28.74	28.23	27.65	26.93	25.97	24.96	24.35
	2.75	0.00	0.00	0.00	39.00	39.00	39.00	39.00	39.00	39.00	39.00	38.79	37.28	36.38
	3.25	0.00	0.00	0.00	0.00	39.00	39.00	39.00	39.00	39.00	39.00	39.00	39.00	39.00
	3.75	0.00	0.00	0.00	0.00	0.00	0.00	39.00	39.00	39.00	39.00	39.00	39.00	39.00
	4.25	0.00	0.00	0.00	0.00	0.00	0.00	0.00	39.00	39.00	39.00	39.00	0.00	39.00
	4.75	0.00	0.00	0.00	0.00	0.00	0.00	0.00	0.00	0.00	39.00	39.00	39.00	0.00

(b)

Figure 5-51 - The a) annual mechanical power matrix and b) electrical power matrix for the control-free buoy b3 (8, 4) applying a tuned optimum PTO damping (case 2)

		b4 (11.5, 3) - control-free, tuned optimum bpto												
		Tp (s)												
		4	5	6	7	8	9	10	11	12	13	14	15	16
Hs (m)	0.25	0.09	1.08	5.04	54.63	53.93	23.66	12.76	11.91	3.79	0.78	1.92	1.23	0.95
	0.75	10.03	116.09	545.64	3524.54	5271.29	2774.52	2273.31	1672.21	997.56	493.93	189.1	67.65	18.24
	1.25	2.93	173.42	762.33	3238.53	8171.13	8126.15	8262.91	6689.64	4563.81	2237.71	829.55	231.06	152.02
	1.75	0	10.62	570.61	2236.93	5126.52	6684.94	9447.27	11347.91	6899.56	4520.36	1337.15	295.88	116.85
	2.25	0	0	29.17	737.45	3481.75	5333.65	7998.9	9325.8	8585.84	4381.85	1183.02	489.1	540.83
	2.75	0	0	0	110.16	1455.66	2421.35	4064.28	5524.41	7742.96	5755.18	1984.26	506.97	605.93
	3.25	0	0	0	0	45.69	1142.53	1248.84	2236.5	4378.9	3422.87	2814.71	728.91	181.35
	3.75	0	0	0	0	0	0	755.75	655.07	1560.53	2263.84	634.17	166.36	26.83
	4.25	0	0	0	0	0	0	0	38.25	907.66	717.5	111.08	0	103.37
	4.75	0	0	0	0	0	0	0	0	0	283.03	138.75	177.95	0
												AEP (kWh)		197049.9
												Rated.P (kW)		74

(a)

		b4 (11.5, 3) - control-free, tuned optimum bpto												
		Tp (s)												
		4	5	6	7	8	9	10	11	12	13	14	15	16
Hs (m)	0.25	0.15	0.54	0.60	0.65	0.68	0.68	0.66	0.66	0.65	0.65	0.64	0.62	0.60
	0.75	1.32	4.88	5.40	5.85	6.08	6.08	6.04	5.96	5.89	5.88	5.77	5.55	5.37
	1.25	3.67	13.55	15.01	16.26	16.90	16.90	16.79	16.54	16.36	16.33	16.01	15.40	14.90
	1.75	0.00	26.56	29.41	31.87	33.12	33.13	32.96	32.42	32.06	32.01	31.39	30.19	29.21
	2.25	0.00	0.00	48.62	52.67	54.74	54.76	54.41	53.60	53.00	52.92	51.89	49.91	48.29
	2.75	0.00	0.00	0.00	74.00	74.00	74.00	74.00	74.00	74.00	74.00	74.00	74.00	72.13
	3.25	0.00	0.00	0.00	0.00	74.00	74.00	74.00	74.00	74.00	74.00	74.00	74.00	74.00
	3.75	0.00	0.00	0.00	0.00	0.00	0.00	74.00	74.00	74.00	74.00	74.00	74.00	74.00
	4.25	0.00	0.00	0.00	0.00	0.00	0.00	0.00	74.00	74.00	74.00	74.00	0.00	74.00
	4.75	0.00	0.00	0.00	0.00	0.00	0.00	0.00	0.00	0.00	74.00	74.00	74.00	0.00

(b)

Figure 5-52 - The a) annual mechanical power matrix and b) electrical power matrix for the control-free buoy b4 (11.5, 3) applying a tuned optimum PTO damping (case 2)

		AMPM - b1 (4, 5) – constant latching duration, constant bpto = 2 kN/(m/s)												
		Tp (s)												
		4	5	6	7	8	9	10	11	12	13	14	15	16
Hs (m)	0.25	0	0	0.02	1.16	4.1	12.21	18.79	11.16	1.85	0.32	0.68	0.36	0.24
	0.75	0.04	0.17	2.13	74.68	401.02	1432.22	3345.79	1567.41	485.33	200.66	66.91	19.78	4.55
	1.25	0.01	0.25	2.98	68.62	621.63	4194.75	12161.11	6270.38	2220.36	909.06	293.54	67.57	37.95
	1.75	0	0.02	2.23	47.39	390.01	3450.79	13904.2	10636.69	3356.74	1836.38	473.16	86.52	29.17
	2.25	0	0	0.11	15.62	264.88	2753.25	11772.55	8741.31	4177.14	1780.11	418.62	143.03	135.02
	2.75	0	0	0	2.33	110.74	1249.91	5981.68	5178.18	3767.06	2338.02	702.14	148.25	151.27
	3.25	0	0	0	0	3.48	589.78	1838.01	2096.33	2130.4	1390.53	996	213.15	45.27
	3.75	0	0	0	0	0	0	1112.3	614.01	759.22	919.68	224.41	48.65	6.7
	4.25	0	0	0	0	0	0	0	35.85	441.59	291.48	39.31	0	25.81
	4.75	0	0	0	0	0	0	0	0	0	114.98	49.1	52.04	0
												AEP (kWh)		126111.5
												Rated.P (kW)		42

(a)

		EPM - b1 (4, 5) - constant latching duration, constant bpto = 2 kN/(m/s)												
		Tp (s)												
		4	5	6	7	8	9	10	11	12	13	14	15	16
Hs (m)	0.25	0.00	0.00	0.00	0.01	0.05	0.35	0.97	0.62	0.32	0.27	0.23	0.18	0.15
	0.75	0.00	0.01	0.02	0.12	0.46	3.14	8.89	5.58	2.86	2.39	2.04	1.62	1.34
	1.25	0.01	0.02	0.06	0.34	1.29	8.72	24.71	15.51	7.96	6.64	5.67	4.50	3.72
	1.75	0.00	0.04	0.11	0.68	2.52	17.10	42.00	30.39	15.60	13.01	11.11	8.83	7.29
	2.25	0.00	0.00	0.19	1.12	4.16	28.27	42.00	42.00	25.78	21.50	18.36	14.59	12.06
	2.75	0.00	0.00	0.00	1.67	6.22	42.00	42.00	42.00	38.52	32.12	27.43	21.80	18.01
	3.25	0.00	0.00	0.00	0.00	8.69	42.00	42.00	42.00	42.00	42.00	38.31	30.45	25.15
	3.75	0.00	0.00	0.00	0.00	0.00	0.00	42.00	42.00	42.00	42.00	42.00	40.54	33.49
	4.25	0.00	0.00	0.00	0.00	0.00	0.00	0.00	42.00	42.00	42.00	42.00	0.00	42.00
	4.75	0.00	0.00	0.00	0.00	0.00	0.00	0.00	0.00	0.00	42.00	42.00	42.00	0.00

(b)

Figure 5-53 - The a) annual mechanical power matrix and b) electrical power matrix for the controlled buoy b1 (4, 5) applying a constant latching duration and PTO damping (case 3)

		AMPM - b2 (6, 4.5) - constant latching duration, constant bpto = 8 kN/(m/s)												
		Tp (s)												
		4	5	6	7	8	9	10	11	12	13	14	15	16
Hs (m)	0.25	0	0.01	0.07	2.7	7.46	16.89	28.51	14.54	2.29	0.4	0.7	0.36	0.17
	0.75	0.11	0.54	7.16	174.1	728.75	1979.9	5076.91	2040.73	601.16	254.33	68.65	19.78	3.22
	1.25	0.03	0.81	10	159.97	1129.64	5798.84	18453.3	8163.88	2750.28	1152.22	301.16	67.55	26.81
	1.75	0	0.05	7.48	110.5	708.73	4770.39	21098.27	13848.72	4157.87	2327.59	485.44	86.49	20.61
	2.25	0	0	0.38	36.43	481.35	3806.1	17863.69	11380.98	5174.07	2256.27	429.48	142.98	95.4
	2.75	0	0	0	5.44	201.24	1727.88	9076.62	6741.86	4666.12	2963.41	720.37	148.2	106.88
	3.25	0	0	0	0	6.32	815.31	2789	2729.37	2638.85	1762.48	1021.85	213.08	31.99
	3.75	0	0	0	0	0	0	1687.8	799.43	940.42	1165.68	230.23	48.63	4.73
	4.25	0	0	0	0	0	0	0	46.67	546.98	369.45	40.33	0	18.23
	4.75	0	0	0	0	0	0	0	0	0	145.73	50.37	52.02	0
												AEP (kWh)		173922.1
												Rated.P (kW)		55

(a)

		EPM - b2 (6, 4.5) - constant latching duration, constant bpto = 8 kN/(m/s)												
		Tp (s)												
		4	5	6	7	8	9	10	11	12	13	14	15	16
Hs (m)	0.25	0.00	0.00	0.01	0.03	0.09	0.48	1.47	0.81	0.39	0.34	0.23	0.18	0.11
	0.75	0.01	0.02	0.07	0.29	0.84	4.34	13.49	7.27	3.55	3.03	2.09	1.62	0.95
	1.25	0.04	0.06	0.20	0.80	2.34	12.06	37.49	20.19	9.86	8.41	5.81	4.50	2.63
	1.75	0.00	0.12	0.39	1.57	4.58	23.64	55.00	39.57	19.32	16.48	11.40	8.83	5.15
	2.25	0.00	0.00	0.64	2.60	7.57	39.08	55.00	55.00	31.94	27.25	18.84	14.59	8.52
	2.75	0.00	0.00	0.00	3.89	11.31	55.00	55.00	55.00	47.71	40.71	28.14	21.79	12.72
	3.25	0.00	0.00	0.00	0.00	15.79	55.00	55.00	55.00	55.00	55.00	39.30	30.44	17.77
	3.75	0.00	0.00	0.00	0.00	0.00	0.00	55.00	55.00	55.00	55.00	52.33	40.53	23.66
	4.25	0.00	0.00	0.00	0.00	0.00	0.00	0.00	55.00	55.00	55.00	55.00	0.00	30.39
	4.75	0.00	0.00	0.00	0.00	0.00	0.00	0.00	0.00	0.00	55.00	55.00	55.00	0.00

(b)

Figure 5-54 - The a) annual mechanical power matrix and b) electrical power matrix for the controlled buoy b2 (6, 4.5) applying a constant latching duration and PTO damping (case 3)

		AMPM - b3 (8, 4) - constant latching duration, constant bpto = 24 kN/(m/s)												
		Tp (s)												
		4	5	6	7	8	9	10	11	12	13	14	15	16
Hs (m)	0.25	0	0.01	0.15	4.21	14.95	21.48	29.45	16.29	2.55	0.31	0.73	0.47	0.32
	0.75	0.31	1.15	16.54	271.4	1460.78	2519.27	5245.66	2286.78	670.49	195.21	72.31	25.7	6.15
	1.25	0.09	2.05	35.54	249.38	2264.39	7378.56	19066.68	9148.21	3067.45	884.37	317.2	87.77	51.23
	1.75	0	0.13	26.6	172.25	1420.66	6069.94	21799.58	15518.48	4637.37	1786.51	511.29	112.39	39.37
	2.25	0	0	1.36	56.79	964.86	4842.96	18457.48	12753.2	5770.77	1731.77	452.36	185.79	182.24
	2.75	0	0	0	8.48	403.39	2198.59	9378.33	7554.74	5204.25	2274.53	758.73	192.58	204.18
	3.25	0	0	0	0	12.66	1037.42	2881.7	3058.45	2943.17	1352.77	1076.28	276.89	61.11
	3.75	0	0	0	0	0	0	1743.9	895.82	1048.87	894.7	242.49	63.2	9.04
	4.25	0	0	0	0	0	0	0	52.3	610.06	283.57	42.47	0	34.83
	4.75	0	0	0	0	0	0	0	0	0	111.86	53.05	67.6	0
												AEP (kWh)		190183.4
												Rated.P (kW)		63

(a)

		EPM - b3 (8, 4) - constant latching duration, constant bpto = 24 kN/(m/s)												
		Tp (s)												
		4	5	6	7	8	9	10	11	12	13	14	15	16
Hs (m)	0.25	0.00	0.01	0.02	0.05	0.19	0.61	1.52	0.90	0.44	0.26	0.24	0.23	0.20
	0.75	0.04	0.05	0.16	0.45	1.69	5.52	13.94	8.14	3.96	2.32	2.20	2.11	1.81
	1.25	0.11	0.16	0.70	1.25	4.68	15.35	38.74	22.62	10.99	6.46	6.12	5.85	5.02
	1.75	0.00	0.31	1.37	2.45	9.18	30.08	63.00	44.34	21.55	12.65	12.00	11.47	9.84
	2.25	0.00	0.00	2.27	4.06	15.17	49.72	63.00	63.00	35.62	20.92	19.84	18.96	16.27
	2.75	0.00	0.00	0.00	6.06	22.66	63.00	63.00	63.00	53.21	31.24	29.64	28.32	24.31
	3.25	0.00	0.00	0.00	0.00	31.65	63.00	63.00	63.00	63.00	43.64	41.40	39.56	33.95
	3.75	0.00	0.00	0.00	0.00	0.00	0.00	63.00	63.00	63.00	58.10	55.11	52.66	45.20
	4.25	0.00	0.00	0.00	0.00	0.00	0.00	0.00	63.00	63.00	63.00	63.00	0.00	58.06
	4.75	0.00	0.00	0.00	0.00	0.00	0.00	0.00	0.00	0.00	63.00	63.00	63.00	0.00

(b)

Figure 5-55 - The a) annual mechanical power matrix and b) electrical power matrix for the controlled buoy b3 (8, 4) applying a constant latching duration and PTO damping (case 3)

		AMPM - b4 (11.5, 3) - constant latching duration, constant bpto = 116 kN/(m/s)												
		Tp (s)												
		4	5	6	7	8	9	10	11	12	13	14	15	16
Hs (m)	0.25	0.01	0.05	0.59	13.51	29.04	30.84	34.45	28.13	6.2	0.99	2.17	1.21	0.78
	0.75	1.4	5.35	64.17	871.93	2838.26	3615.71	6135.57	3948.87	1629.57	622.09	213.93	66.65	14.97
	1.25	0.41	7.99	89.66	801.17	4399.64	10589.87	22301.28	15797.35	7455.26	2818.35	938.48	227.62	124.74
	1.75	0	0.49	67.11	553.39	2760.31	8711.71	25497.8	26797.69	11270.85	5693.32	1512.73	291.48	95.88
	2.25	0	0	3.43	182.44	1874.7	6950.72	21588.73	22022.54	14025.5	5518.87	1338.37	481.83	443.78
	2.75	0	0	0	27.25	783.78	3155.46	10969.33	13045.71	12648.6	7248.56	2244.82	499.43	497.2
	3.25	0	0	0	0	24.6	1488.92	3370.58	5281.41	7153.2	4311.05	3184.31	718.07	148.81
	3.75	0	0	0	0	0	0	2039.75	1546.92	2549.22	2851.27	717.45	163.89	22.01
	4.25	0	0	0	0	0	0	0	90.32	1482.71	903.68	125.66	0	84.82
	4.75	0	0	0	0	0	0	0	0	0	356.47	156.97	175.3	0
												AEP (kWh)		317203.5
												Rated.P (kW)		113

(a)

		b4 (11.5, 3) - constant latching duration, constant bpto = 116 kN/(m/s)												
		Tp (s)												
		4	5	6	7	8	9	10	11	12	13	14	15	16
Hs (m)	0.25	0.02	0.02	0.07	0.16	0.36	0.88	1.78	1.56	1.07	0.82	0.72	0.61	0.49
	0.75	0.18	0.22	0.64	1.45	3.28	7.93	16.30	14.06	9.62	7.41	6.52	5.46	4.40
	1.25	0.51	0.62	1.76	4.02	9.10	22.03	45.31	39.06	26.72	20.57	18.12	15.17	12.23
	1.75	0.00	1.22	3.46	7.88	17.83	43.17	88.97	76.56	52.37	40.32	35.51	29.74	23.97
	2.25	0.00	0.00	5.72	13.03	29.48	71.36	113.00	113.00	86.58	66.65	58.70	49.17	39.62
	2.75	0.00	0.00	0.00	19.47	44.03	106.60	113.00	113.00	113.00	99.57	87.69	73.45	59.19
	3.25	0.00	0.00	0.00	0.00	61.50	113.00	113.00	113.00	113.00	113.00	113.00	102.58	82.67
	3.75	0.00	0.00	0.00	0.00	0.00	0.00	113.00	113.00	113.00	113.00	113.00	113.00	110.06
	4.25	0.00	0.00	0.00	0.00	0.00	0.00	0.00	113.00	113.00	113.00	113.00	0.00	113.00
	4.75	0.00	0.00	0.00	0.00	0.00	0.00	0.00	0.00	0.00	113.00	113.00	113.00	0.00

(b)

Figure 5-56 - The a) annual mechanical power matrix and b) electrical power matrix for the controlled buoy b4 (11.5, 3) applying a constant latching duration and PTO damping (case 3)

		AMPM - b1 (4, 5) - tuned latching duration, tuned bpto												
		Tp (s)												
		4	5	6	7	8	9	10	11	12	13	14	15	16
Hs (m)	0.25	0.01	0.27	4.49	57.86	52.28	35.23	18.9	19.08	4.23	1.08	1.78	1.52	1.09
	0.75	1.19	28.99	485.67	3733.12	5109.26	4131.32	3366.27	2678.46	1112.14	680.13	175.08	83.66	20.8
	1.25	0.35	43.32	678.55	3430.19	7919.97	12100	12235.55	10715.13	5087.99	3081.3	768.07	285.71	173.31
	1.75	0	2.65	507.9	2369.31	4968.94	9954.01	13989.32	18176.5	7692.02	6224.49	1238.04	365.86	133.21
	2.25	0	0	25.97	781.09	3374.73	7941.91	11844.61	14937.59	9571.99	6033.77	1095.34	604.8	616.59
	2.75	0	0	0	116.68	1410.92	3605.44	6018.3	8848.72	8632.3	7924.83	1837.19	626.89	690.81
	3.25	0	0	0	0	44.28	1701.25	1849.26	3582.31	4881.85	4713.26	2606.09	901.33	206.75
	3.75	0	0	0	0	0	0	1119.11	1049.26	1739.77	3117.28	587.17	205.71	30.58
	4.25	0	0	0	0	0	0	0	61.26	1011.91	987.99	102.84	0	117.85
	4.75	0	0	0	0	0	0	0	0	0	389.73	128.47	220.04	0
												AEP (kWh)		258573.8
												Rated.P (kW)		97

(a)

		EPM - b1 (4, 5) - tuned latching duration, tuned bpto												
		Tp (s)												
		4	5	6	7	8	9	10	11	12	13	14	15	16
Hs (m)	0.25	0.02	0.14	0.53	0.69	0.66	1.01	0.97	1.06	0.73	0.90	0.59	0.76	0.68
	0.75	0.16	1.22	4.81	6.20	5.90	9.06	8.94	9.54	6.57	8.10	5.34	6.86	6.12
	1.25	0.44	3.38	13.36	17.22	16.38	25.17	24.86	26.50	18.24	22.49	14.83	19.05	16.99
	1.75	0.00	6.63	26.18	33.75	32.10	49.33	48.81	51.93	35.74	44.08	29.06	37.33	33.30
	2.25	0.00	0.00	43.28	55.79	53.06	81.54	80.58	85.85	59.09	72.87	48.04	61.71	55.05
	2.75	0.00	0.00	0.00	83.34	79.27	97.00	97.00	97.00	88.26	97.00	71.77	92.19	82.24
	3.25	0.00	0.00	0.00	0.00	97.00	97.00	97.00	97.00	97.00	97.00	97.00	97.00	97.00
	3.75	0.00	0.00	0.00	0.00	0.00	0.00	97.00	97.00	97.00	97.00	97.00	97.00	97.00
	4.25	0.00	0.00	0.00	0.00	0.00	0.00	0.00	97.00	97.00	97.00	97.00	0.00	97.00
	4.75	0.00	0.00	0.00	0.00	0.00	0.00	0.00	0.00	0.00	97.00	97.00	97.00	0.00

(b)

Figure 5-57 - The a) annual mechanical power matrix and b) electrical power matrix for the controlled buoy b1 (4, 5) applying tuned latching duration and PTO damping (case 4)

		AMPM - b2 (6, 4.5) - tuned latching duration, tuned bpto												
		Tp (s)												
		4	5	6	7	8	9	10	11	12	13	14	15	16
Hs (m)	0.25	0.02	0.63	5.56	79.13	70.14	50.22	26.62	26.14	7.98	1.26	2.92	1.82	1.53
	0.75	2.83	67.22	601.47	5105.72	6855.71	5889.11	4740.9	3670.54	2096.7	793.55	287.53	100.05	29.26
	1.25	0.83	100.42	840.33	4691.41	10627.17	17248.32	17232.01	14683.92	9592.35	3595.1	1261.36	341.71	243.85
	1.75	0	6.15	628.99	3240.46	6667.43	14189.25	19701.93	24908.92	14501.7	7262.43	2033.18	437.58	187.43
	2.25	0	0	32.16	1068.28	4528.28	11321.04	16681.42	20470.34	18045.99	7039.9	1798.83	723.34	867.54
	2.75	0	0	0	159.58	1893.2	5139.48	8475.91	12126.22	16274.4	9246.29	3017.13	749.77	971.97
	3.25	0	0	0	0	59.42	2425.1	2604.41	4909.16	9203.7	5499.2	4279.86	1077.99	290.9
	3.75	0	0	0	0	0	0	1576.1	1437.89	3279.96	3637.09	964.28	246.03	43.03
	4.25	0	0	0	0	0	0	0	83.95	1907.74	1152.74	168.9	0	165.82
	4.75	0	0	0	0	0	0	0	0	0	454.72	210.97	263.17	0
												AEP (kWh)		372213.5
												Rated.P (kW)		139

(a)

		EPM - b2 (6, 4.5) - tuned latching duration, tuned bpto												
		Tp (s)												
		4	5	6	7	8	9	10	11	12	13	14	15	16
Hs (m)	0.25	0.04	0.31	0.66	0.94	0.88	1.43	1.37	1.45	1.38	1.05	0.97	0.91	0.96
	0.75	0.37	2.82	5.96	8.48	7.91	12.91	12.60	13.07	12.38	9.45	8.77	8.20	8.61
	1.25	1.03	7.85	16.54	23.55	21.98	35.87	35.01	36.31	34.38	26.24	24.35	22.78	23.91
	1.75	0.00	15.38	32.42	46.16	43.07	70.31	68.74	71.17	67.39	51.43	47.73	44.65	46.86
	2.25	0.00	0.00	53.60	76.31	71.20	116.23	113.48	117.65	111.40	85.02	78.90	73.81	77.46
	2.75	0.00	0.00	0.00	113.99	106.36	139.00	139.00	139.00	139.00	127.01	117.86	110.26	115.71
	3.25	0.00	0.00	0.00	0.00	139.00	139.00	139.00	139.00	139.00	139.00	139.00	139.00	139.00
	3.75	0.00	0.00	0.00	0.00	0.00	0.00	139.00	139.00	139.00	139.00	139.00	139.00	139.00
	4.25	0.00	0.00	0.00	0.00	0.00	0.00	0.00	139.00	139.00	139.00	139.00	0.00	139.00
	4.75	0.00	0.00	0.00	0.00	0.00	0.00	0.00	0.00	0.00	139.00	139.00	139.00	0.00

(b)

Figure 5-58 - The a) annual mechanical power matrix and b) electrical power matrix for the controlled buoy b2 (6, 4.5) applying tuned latching duration and PTO damping (case 4)

		AMPM - b3 (8, 4) - tuned latching duration, tuned bpto												
		Tp (s)												
		4	5	6	7	8	9	10	11	12	13	14	15	16
Hs (m)	0.25	0.04	0.89	6.29	87.77	93.77	53.46	29.86	29.47	8.59	1.68	3.62	1.96	1.64
	0.75	4.46	95.28	680.49	5662.73	9164.4	6268.67	5318.63	4137.74	2259.07	1058.49	356.12	107.69	31.29
	1.25	1.31	142.34	950.74	5203.22	14205.91	18360	19331.91	16552.94	10335.19	4795.39	1562.23	367.79	260.76
	1.75	0	8.72	711.63	3593.98	8912.71	15103.77	22102.82	28079.42	15624.73	9687.1	2518.15	470.96	200.43
	2.25	0	0	36.38	1184.83	6053.2	12050.7	18714.24	23075.88	19443.49	9390.28	2227.9	778.53	927.7
	2.75	0	0	0	176.99	2530.74	5470.73	9508.79	13669.68	17534.7	12333.32	3736.81	806.97	1039.37
	3.25	0	0	0	0	79.43	2581.4	2921.79	5534.02	9916.45	7335.19	5300.73	1160.25	311.08
	3.75	0	0	0	0	0	0	1768.16	1620.91	3533.97	4851.39	1194.29	264.81	46.02
	4.25	0	0	0	0	0	0	0	94.64	2055.48	1537.6	209.18	0	177.32
	4.75	0	0	0	0	0	0	0	0	0	606.53	261.3	283.25	0
												AEP (kWh)		426976.2
												Rated.P (kW)		159

(a)

		EPM - b3 (8, 4) - tuned latching duration, tuned bpto												
		Tp (s)												
		4	5	6	7	8	9	10	11	12	13	14	15	16
Hs (m)	0.25	0.07	0.44	0.75	1.04	1.18	1.53	1.54	1.64	1.48	1.40	1.21	0.98	1.02
	0.75	0.59	4.00	6.74	9.40	10.58	13.75	14.13	14.74	13.34	12.60	10.86	8.83	9.20
	1.25	1.63	11.12	18.72	26.12	29.38	38.19	39.28	40.93	37.04	35.00	30.16	24.52	25.57
	1.75	0.00	21.80	36.68	51.20	57.58	74.85	77.12	80.23	72.61	68.61	59.11	48.06	50.11
	2.25	0.00	0.00	60.64	84.63	95.18	123.72	127.31	132.62	120.02	113.41	97.71	79.44	82.83
	2.75	0.00	0.00	0.00	126.42	142.18	159.00	159.00	159.00	159.00	159.00	145.97	118.67	123.73
	3.25	0.00	0.00	0.00	0.00	159.00	159.00	159.00	159.00	159.00	159.00	159.00	159.00	159.00
	3.75	0.00	0.00	0.00	0.00	0.00	0.00	159.00	159.00	159.00	159.00	159.00	159.00	159.00
	4.25	0.00	0.00	0.00	0.00	0.00	0.00	0.00	159.00	159.00	159.00	159.00	0.00	159.00
	4.75	0.00	0.00	0.00	0.00	0.00	0.00	0.00	0.00	0.00	159.00	159.00	159.00	0.00

(b)

Figure 5-59 - The a) annual mechanical power matrix and b) electrical power matrix for the controlled buoy b3 (8, 4) applying tuned latching duration and PTO damping (case 4)

		AMPM - b4 (11.5, 3) - tuned latching duration, tuned bpto												
		Tp (s)												
		4	5	6	7	8	9	10	11	12	13	14	15	16
Hs (m)	0.25	0.08	1.13	7.56	105.34	123.58	58.67	34.53	29.33	9.92	1.55	5.42	2.44	2.84
	0.75	8.73	120.94	817.84	6796.83	12078.49	6880	6149.49	4117.89	2607.09	978.84	533.19	134.17	54.36
	1.25	2.55	180.68	1142.64	6245.29	18723.09	20150.5	22351.88	16473.53	11927.34	4434.56	2339.05	458.22	453.03
	1.75	0	11.07	855.27	4313.76	11746.77	16576.72	25555.65	27944.7	18031.75	8958.2	3770.29	586.77	348.21
	2.25	0	0	43.73	1422.12	7977.99	13225.9	21637.71	22965.17	22438.79	8683.71	3335.72	969.96	1611.72
	2.75	0	0	0	212.44	3335.47	6004.24	10994.22	13604.1	20235.95	11405.3	5594.93	1005.4	1805.72
	3.25	0	0	0	0	104.69	2833.14	3378.22	5507.47	11444.09	6783.26	7936.51	1445.53	540.44
	3.75	0	0	0	0	0	0	2044.38	1613.13	4078.38	4486.35	1788.15	329.92	79.95
	4.25	0	0	0	0	0	0	0	94.18	2372.13	1421.91	313.2	0	308.06
	4.75	0	0	0	0	0	0	0	0	0	560.89	391.23	352.89	0
												AEP (kWh)		479363.7
												Rated.P (kW)		179

(a)

		EPM - b4 (11.5, 3) - tuned latching duration, tuned bpto												
		Tp (s)												
		4	5	6	7	8	9	10	11	12	13	14	15	16
Hs (m)	0.25	0.13	0.56	0.90	1.25	1.55	1.68	1.78	1.63	1.71	1.29	1.81	1.22	1.78
	0.75	1.15	5.08	8.10	11.29	13.94	15.09	16.34	14.66	15.39	11.65	16.26	11.00	15.99
	1.25	3.19	14.12	22.49	31.35	38.72	41.91	45.41	40.74	42.75	32.37	45.16	30.55	44.41
	1.75	0.00	27.67	44.09	61.45	75.88	82.14	89.17	79.84	83.79	63.44	88.50	59.87	87.05
	2.25	0.00	0.00	72.88	101.58	125.44	135.79	147.20	131.98	138.51	104.88	146.30	98.98	143.90
	2.75	0.00	0.00	0.00	151.74	179.00	179.00	179.00	179.00	179.00	156.67	179.00	147.85	179.00
	3.25	0.00	0.00	0.00	0.00	179.00	179.00	179.00	179.00	179.00	179.00	179.00	179.00	179.00
	3.75	0.00	0.00	0.00	0.00	0.00	0.00	179.00	179.00	179.00	179.00	179.00	179.00	179.00
	4.25	0.00	0.00	0.00	0.00	0.00	0.00	0.00	179.00	179.00	179.00	179.00	0.00	179.00
	4.75	0.00	0.00	0.00	0.00	0.00	0.00	0.00	0.00	0.00	179.00	179.00	179.00	0.00

(b)

Figure 5-60 - The a) annual mechanical power matrix and b) electrical power matrix for the controlled buoy b4 (11.5, 3) applying tuned latching duration and PTO damping (case 4)

Considering the annual mechanical power matrix for the control-free buoys, figures 5-45 to 52, it can be seen that the major power absorption is achieved in the range of $7 < T_p < 13\ s$, which is the region with the largest number of wave occurrence during a year (the red regions). In the case of applying a constant latching duration tuned to the $T_p = 10\ s$, figures 5-53 to 56, the annual power absorption is concentrated in this sea state. It is because that the buoy is forced to oscillate in resonance with that certain frequency. However, a large annual power absorption growth can be observed in comparison to the control-free cases. The case, in which the latching duration is tuned to each sea state (case 4), can be considered as the best condition for the buoys power absorption. The largest amount of annual power absorption in the range of the most energetic waves of the local sea is achieved in comparison to the other three cases.

The AEP analyses results are shown in table 5-3. Additionally, a bar graph is used in figure 5-61 to illustrate the effect of the constant-delay latching control and the optimized PTO damping on the annual energy production and the rated power of the buoys. It is evident that the AEP and rated power increases with the buoy size. A significant improvement can be observed for the cases with a constant-delay latching control (cases 3 and 4) in comparison to the control-free ones (cases 1 and 2). Comparison of the bar graphs of cases 1 and 2 shows that the values of the AEP and rated power are slightly increase with application of tuned PTO damping. It can be explained using the figure 5-30. Choosing a constant PTO damping that maximizes the absorbed power in sea state with modal period of $T_p = 10\ s$ leads to a power absorption close to the optimum value in the sea states of $T_p > 7\ s$, which are the predominant waves of the local sea. For instance, in the case of buoy b4 (11.5, 3), applying a constant PTO damping equal to $1025\ kN/(m/s)$ results in power absorption of 18.9, 19.5, 19,4, 18.6 and 18 kW in $T_p = 8, 9, 11, 12$ and $13\ s$ respectively, which are approximately equal to the maximum values for each sea state (see table 5-2). A notable increase can be observed in case 4 in comparison to the case 3. It implies the importance of applying a constant-delay latching control tuned to each sea state. The AEP values increase about the 105%, 113%, 124% and 51% for the buoys b1, b2, b3 and b4 respectively. Additionally, the values of the rated power increase about the 130%, 152% and 152% and 58% for the buoys b1, b2, b3 and b4 respectively. The largest buoy b4 (11.5, 3) shows the lowest growth while produces the largest amount of power.

Table 5-3 – The results of the AEP analyses of the buoys

	b1 (4, 5)		**b2 (6, 4.5)**		**b3 (8, 4)**		**b4 (11.5, 3)**	
	$AEP\ (MWh)$	$P_{rated}\ (kW)$	$AEP\ (MWh)$	$P_{rated}\ (kW)$	$AEP\ (MWh)$	$P_{rated}\ (kW)$	$AEP\ (MWh)$	$P_{rated}\ (kW)$
Case 1	28	11	59	22	100	37	190	70
Case 2	29.5	11	62	23	104	39	197	74
Case 3	126	42	174	55	190	63	317	113
Case 4	259	97	372	139	427	159	479.5	179

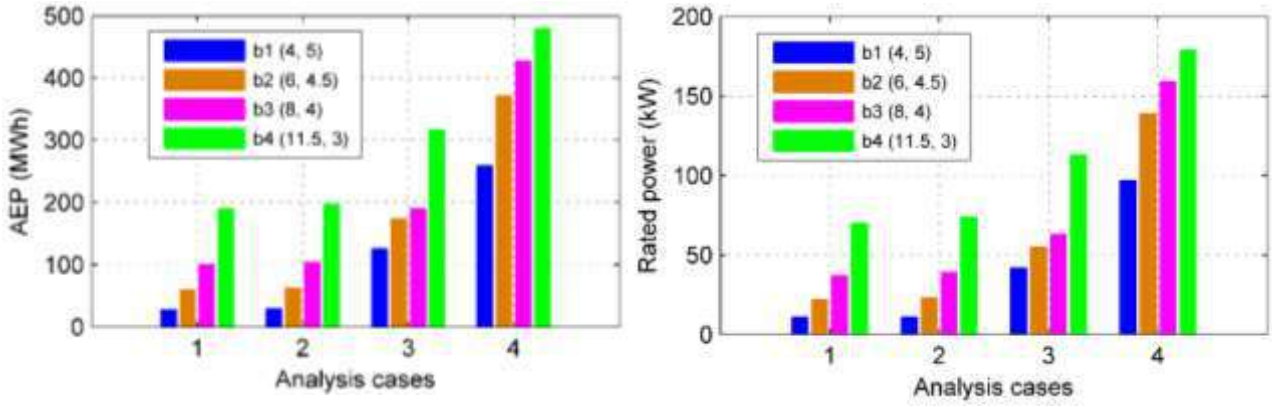

a) b)

Figure 5-61 – The bar graphs of the; a) annual energy production (AEP) and b) rated power of the buoys for four analysis cases. Case 1: control-free, constant b_{PTO}, case 2: control-free, tuned b_{PTO}, case 3: Constant latching, constant b_{PTO} and case 4: tuned latching, tuned b_{PTO}.

5.11 Conclusion

This chapter addresses the application of a constant-delay latching control presented by Sheng et al [77,78] in four heaving point absorber WECs (cylindrical buoys) with the same natural period and different size. The analyses are performed considering the nearshore Rio de Janeiro as the local sea. The buoys are selected based on the optimization study in frequency domain presented in chapter 4. The objective is to evaluate the effect of applying a constant-delay latching control on the power production and PTO system as well as the optimum dimensions of the point absorber WECs. A wave-to-wire model is developed through a FORTRAN code to analyze the performance of the unconstrained buoys through the linear hydrodynamic theory.

An ideal (100% conversion efficiency) power take-off (PTO) system that works as a pure damper (stiffness is equal to zero) is considered for the energy conversion. A practical PTO control strategy called “constant PTO damping” (CPD) is applied to maximize the energy absorption by tuning the PTO damping to the energy period of the sea spectrum. The analyses are performed for twenty different wave random phases for each sea states and the average value of the mean power is considered as the mean power generated by the buoy. As the result, more deviation from the average value is observed for the sea states with larger modal periods. The effect of different wave random phase is more significant for the controlled buoys. It may be a challenge for the instantaneous control of the PTO in a real sea. In the control-free case, the maximum mean power values in each sea state are slightly different for each buoy, while the corresponding optimum PTO damping values increase with sea state modal period. In contrast, for the buoys controlled by a constant-delay latching, the optimum PTO damping values are independent of the wave period and approximately the same for all sea states.

Application of the constant-delay latching control significantly increases the power generation and it is very sensitive to the buoy dimensions. It is observed that the smallest buoy has a better performance and shows the largest percentage of power growth comparing to the other buoys. The capture width curves of the buoys show that the largest buoy can absorb more energy, nevertheless, it is seen that using a large size buoy brings some practical challenges. For instance, the necessity of providing a high level of PTO damping to maximize the power and large time of unused capacity during the system lifetime. To compare the power production smoothness, the ratio of the instantaneous power to the mean power of each buoys are calculated. It can be seen that this ratio is less expressive for the smallest buoy leading to a smoother power production. It facilitates the conversion-efficiency control of the WEC. Finally, the power-to-volume ratio that affect the estimation of the WEC cost is analyzed. This ratio shows the performance of the heaving point absorber relative to its volume. It is observed that, for the buoys with the same natural period and controlled by a constant-delay latching control, this ratio decreases with the buoy size increase. In other words, the smallest buoy produces more energy in one cubic meter of its volume comparing to the larger ones.

The annual energy production of the buoys are calculated and compared for the four cases. Comparison of the AEP and rated power values for the control-free buoys with a constant optimum PTO damping, corresponding to the energy period of the local sea spectrum, and tuned PTO damping (cases 1 and 2) shows small differences. The effect of latching

duration are addressed in cases 3 and 4. It is observed that applying a latching duration tuned to each sea state (case 4) results in more than 50% of increase in AEP and rated power values comparing to the condition of applying a constant latching duration tuned to the energy period of the sea (case 3).

Chapter 6

6. Case study: A point absorber controlled by an adapted constant-delay latching control for the nearshore Rio de Janeiro, Brazil

6.1 Introduction

There exist more than hundred different wave energy converter (WEC) patents developed by different universities, companies etc. However, Falcão [5] classified the WEC technology into three main categories: *a) oscillating water column (OWC), b) oscillating bodies* and *c) overtopping* systems. An OWC utilizes the oscillation of a water column inside the converter to pressurize a trapped air into an air turbine to generate power. Its support can be a fixed structure installed on the coast (onshore) or a breakwater i.e. Pico, LIMPET [25,35], or floating base for deeper water i.e.. Mighty Whale, Ocean Energy, Spar buoy [32–34]. The oscillating bodies can be surface or submerse oscillators. They can be categorized based on the local of their installation as *onshore*, *nearshore* and *offshore*. The first generation of the Brazilian WEC, called "COPPE hyperbaric wave converter" [20] is an example of the onshore system which was installed on the coast. The Uppsala University WEC [31] is a surface oscillator nearshore type system that was installed in a relatively shallow water nearshore west coast of Sweden. The CETO[1] and Oyster [37] are submerged oscillator installed in nearshore. The former system takes advantage of the pressure difference resulting from the waves below the water surface in vertical direction and the later one, which is mounted in the seabed, oscillates forth and back due to the wave surge. The overtopping device is relatively large and can be a fixed or floating structure. It simply collects the water waves in its reservoir at a height more than the ocean surface level. Then the resultant potential energy due to the higher level of collected water can be transformed into electricity through a low-head hydro turbine.

This chapter addresses the performance of the wave energy converter proposed by the COPPE/UFRJ that is the second generation of the Brazilian WEC to be installed near to the Rio de Janeiro coastline. It can be categorized as a nearshore surface point absorber. The PTO system is a combination of a gearbox and a rotational generator system that is used in the wind turbine industry. This chapter addresses the performance of the WEC with and without the application of a constant-delay latching control. Additionally, an adapted constant-delay latching control based on the specific characteristics of the device is proposed to improve the power generation. The AEP calculation of the device is performed and the results are compared to the control-free model.

[1] http://carnegiewave.com/

6.2 The COPPE nearshore point absorber; WEC description

6.2.1 Oscillating buoy and support structure

The system is a surface point absorber WEC type that consists of an oscillating buoy and a bottom-mounted support structure. The oscillating part is a semisubmersible conical cylinder allowed to move only in heave direction, figure 6.1. The support structure consists of four columns of very small diameters relative to the wavelengths (no diffraction), which are mounted on the seabed through a concrete base, and a top deck. The buoy moves in the vertical direction (heave) using eight roller bearings. Four of them are placed on its top and the others on the end of the cylindrical section.

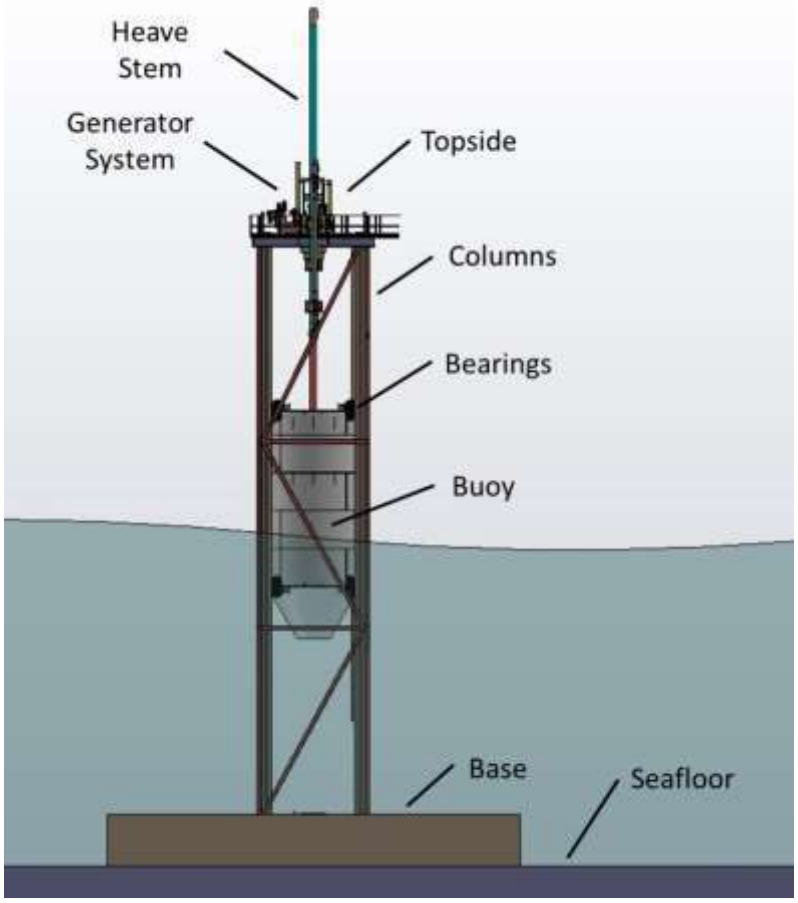

Figure 6-1 – COPPE nearshore point absorber WEC

6.2.2 Power take-off system

The PTO system consists of a gearbox and a rotational generator located on the topside deck, figure 6-2. The vertical movement of the buoy is transmitted via a central rod (heave stem) to the gearbox. Then, the pulley converts the vertical movement into rotation to drive the electrical generator. A backstop system guarantees the constant rotation direction, thus, the buoy can drive the electrical generator either in upward or downward direction. The electric generator has a solid cylindrical flywheel coupled to its axle that amplify the rotational inertia. The PTO system also includes a speed multiplier to provide the sufficient rotational velocity. As it is illustrated in figure 6-2, the pulley converts the vertical motion of the buoy to a rotational motion on the flywheel axle.

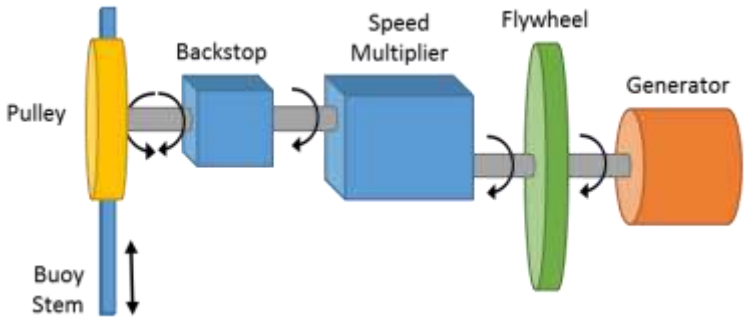

Figure 6-2 – The power take-off (PTO) system of the COPPE nearshore point absorber WEC

6.2.3 Local sea characteristics

The sea site that is considered for the WEC installation locates near to a small island called “Ilha Rasa” with a local water depth of about 20 m and a distance of 14 km form the Copacabana beach of Rio de Janeiro. Figure 6-3 shows the google map illustration of the “Ilha Rasa” location. The yellow point represent the approximate location of the WEC. The wave characteristic of the region is explained earlier in the chapter 4, section 4.3.2. Figures 6-4 and 5 show the joint probability distribution (JPD) and a combined scatter and energy diagram of the local sea respectively.

Figure 6-3 – The approximate location of the COPPE nearshore point absorber WEC (source: google maps)

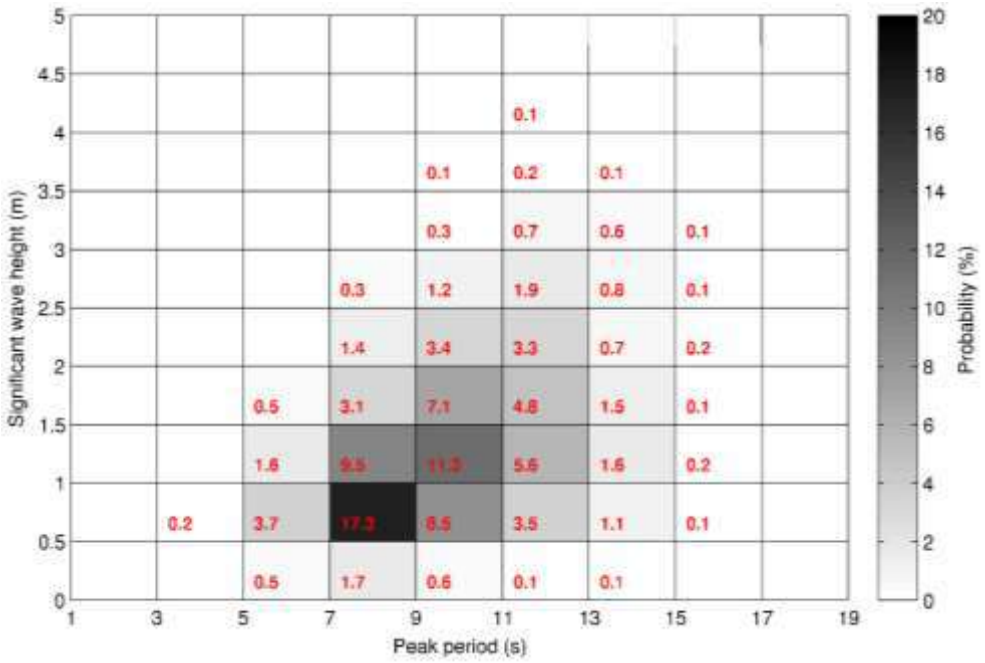

Figure 6-4 - Joint Probability Distribution (%) for the nearshore region of Rio de Janeiro

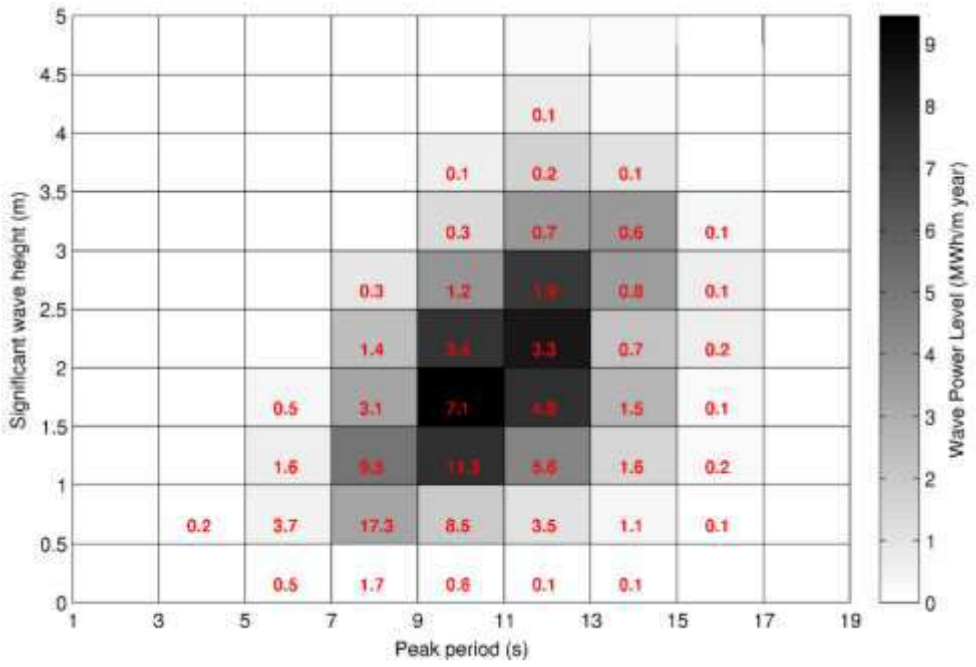

Figure 6-5 - Combined scatter and energy diagram: the colors denote the annual wave power level (MWh/m year), and the numbers indicate the probability occurrence per year (%) in terms of significant wave height and peak period.

6.3 Frequency domain analyses

The frequency domain analyses of the WEC is performed using AQWA ANSYS. The effect of viscosity is neglected and it is assumed that there is no friction between the buoy roller bearings and the support columns. Figure 6-6 illustrates the generic model of the WEC, where an oscillating cylinder with a conical bottom is connected to a fixed reference through a PTO system. The conical bottom of the cylinder is considered to reduce the slamming effect. The meshed model is created, as illustrated in figure 6-7, and the required inputs such as water depth, center of gravity, radii of gyration, wave heading angles, range of wave frequencies etc. are provided.

As the result, figure 6-8 shows the added mass, hydrodynamic damping and the excitation response of the buoy. Since the buoy diameter is small relative to the wavelengths, it is assumed that there is no diffraction effect. The value of the added mass when frequency tends to the infinite ($\omega \to \infty$) is equal to 11 ton. The maximum value of the hydrodynamic damping is equal to 6.5 $kN/(m/s)$ that occurs at $\omega = 1.26\, rad/s$ ($\approx 5\, s$). Figure 6-9-a shows that the maximum heave RAO value is equal to 4.7 corresponding to the $\omega = 1.57\, rad/s$ ($T = 4\, s$), which is the natural frequency of the buoy.

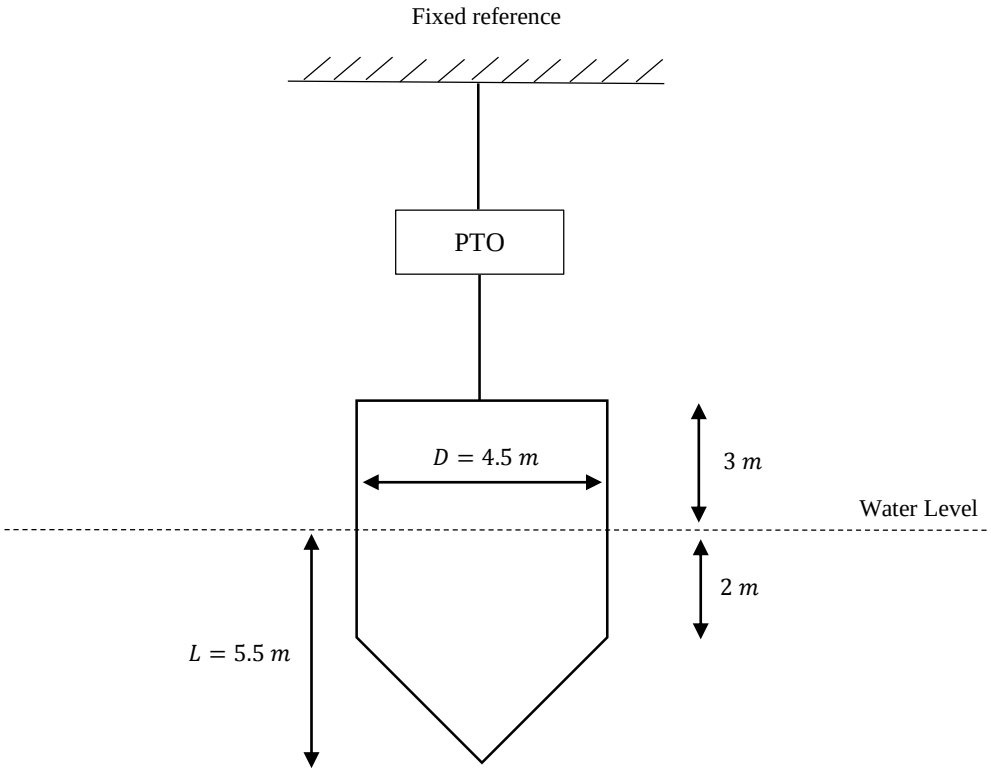

Figure 6-6 – The generic model of the COPPE nearshore point absorber WEC connected to a fixed reference through a PTO system

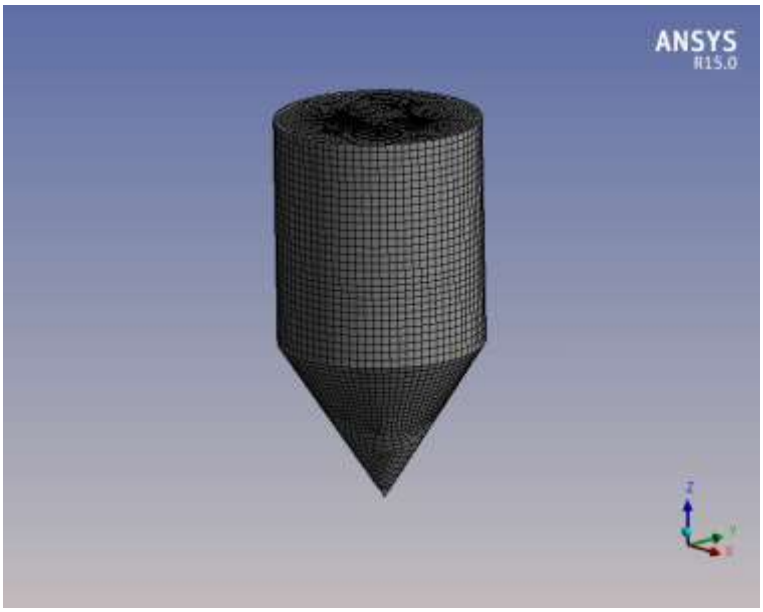

Figure 6-7 – The 3D meshed geometry of the COPPE nearshore point absorber buoy

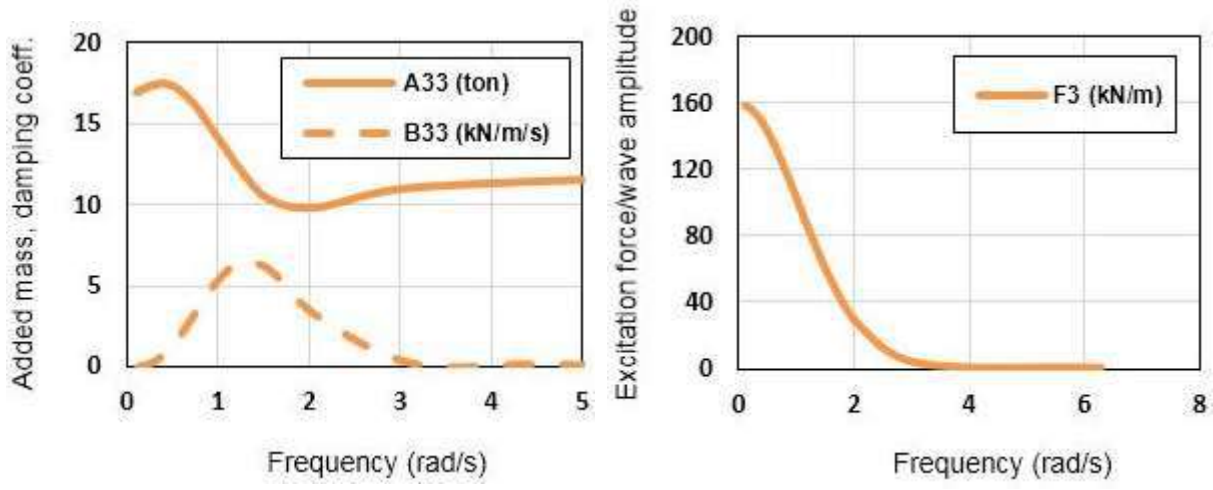

a) b)

Figure 6-8 – a) added mass and hydrodynamic damping, and b) excitation response (no diffraction) of the oscillating buoy of the COPPE nearshore point absorber

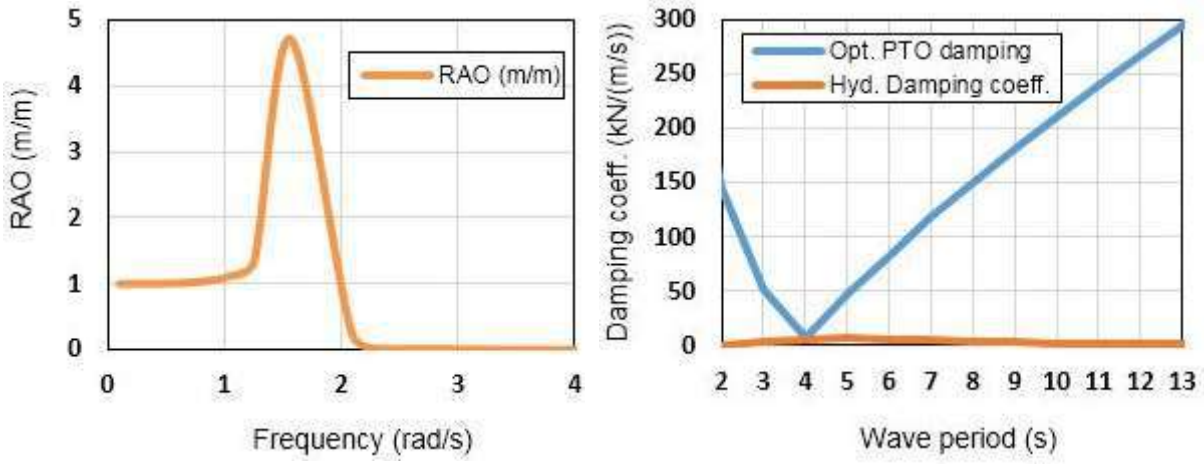

a) b)

Figure 6-9 – The a) buoy RAO in heave direction and b) the optimum PTO damping and the hydrodynamic damping in a range of wave period

Figure 6-9-b shows the optimum PTO damping values that maximize the energy absorption in each wave period. These values are frequency dependent and calculated using Eq.(5.15). As the first approach, the power production of the buoy is calculated for different incident waves considering a pure damper as the PTO system. The power generation of the buoy is calculated considering a constant PTO damping equal to the

hydrodynamic damping at the resonance frequency (CPD) and then, the calculations are performed considering the application of the optimum PTO damping for each wave period (OPD) (see section 5.6). The results are compared to the theoretical maximum power and plotted in figure 6-10.

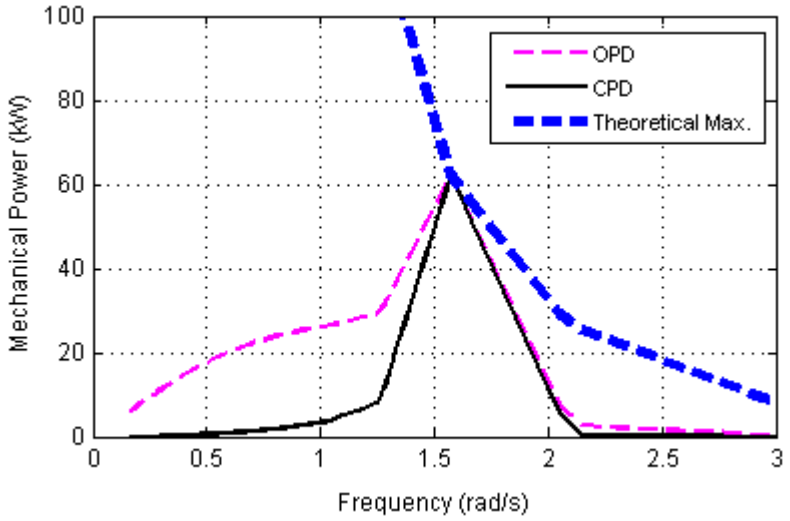

Figure 6-10 – Mechanical power of the COPPE nearshore point absorber considering a pure damper as the PTO system and applying OPD and CPD methods comparing to the theoretical maximum power.

As it can be seen, applying optimum PTO damping method (OPD) improves the power production for the wave periods larger than the natural period. Three curves meet each other at the resonance frequency where the maximum power is achieved.

6.4 Wave-to-wire model of the COPPE nearshore WEC

The FORTRAN code that is presented in chapter 5 is adapted to model the COPPE nearshore point absorber. The principal assumptions are as follow: the hydrodynamic linear theory consideration (see section 3.6), neglecting the effect of the diffraction, the restriction of the buoy motion in only heave direction and no constrained oscillation. Two major adaption must be applied on the code in order to model the COPPE nearshore WEC.

- The first one is related to the buoy geometry. As it can be seen in figure 6-6, the water plane area of the oscillating buoy is not constant along the buoy height and it changes when the buoy experiences the displacements more than two meters (the height of the submerged cylindrical part). This affect the magnitude of the hydrostatic force, which has a significant contribution comparing to the other

forces (see Eq.(5.3)). Therefore, in this model the instantaneous hydrostatic force is calculated directly using below equation:

$$F_{hs} = W - F_b \tag{6.1}$$

where W and F_b are the buoy weight and the buoyance force respectively.

- The electro-mechanical PTO device is the second major change that must be applied on the code. As it is illustrated in figure 6-2, the PTO system of the COPPE nearshore WEC consists of a gearbox (mechanical part) and a rotational generator (electrical part). This machinery should be coupled to the hydrodynamic of the WEC in order to address the performance of the device.

6.4.1 The electro-mechanical PTO model

To provide an equilibrium between the available wave energy and the PTO system, a minimum generator speed must be obtained to start the power generation. During this initial stage, there is no electrical load and only mechanical parts including the flywheel inertia, backstop and speed multiplier are applying forces on the body. This causes that the buoy gain speed in small waves. In the other hand, the unlimited increase in speed would overheat the generator. Therefore, a nominal maximum speed is considered to maintain a constant level of power output, which is $48\ kW$ for this generator. The power output of the generator can be expressed as:

$$P\ (W) = T(N.m) \times w\left(\frac{rd}{s}\right) \tag{6.2}$$

Figure 6-11 illustrates the power and torque against the flywheel speed provided by the generator manufacturer. As it can be seen the power generation increases with the speed up to the nominal maximum speed and then the generator torque starts to reduce to keep the power output in a constant level.

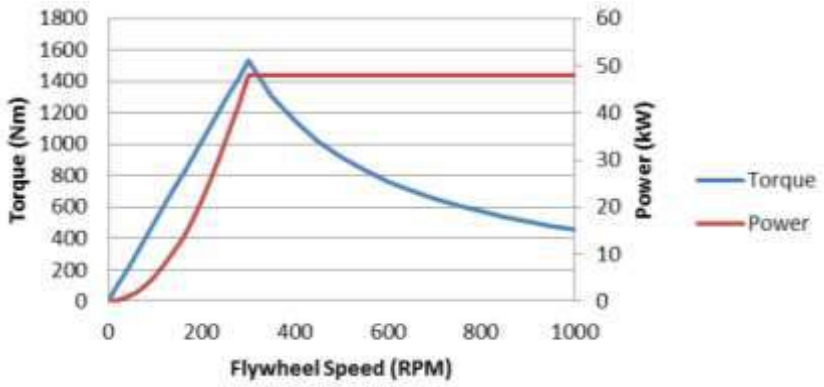

Figure 6-11 – The power (kW) and torque (Nm) of the electrical generator versus flywheel speed (RPM)

The flywheel and generator torques can be expressed as:

$$T_g(N.m) = \frac{P(w)}{w\left(\frac{rd}{s}\right)} \tag{6.3}$$

$$T_{fw}\,(N.m) = \propto I_{fw} \tag{6.4}$$

where, $\propto$ is the angular acceleration and it is calculated by dividing the actual angular velocity by the time increment. I_{fw} is the flywheel inertia, which is calculated as follow:

$$I_{fw} = \frac{1}{2} m \times r^2 \tag{6.5}$$

where m and r are the mass and the radius of the flywheel. As it is shown in figure 6-11, up to $RPM = 300$, the generator torque increases with the speed linearly, with a constant positive tangent. In the other part, where the flywheel speed is more than 300 rpm, a quadratic equation describes the relation between the generator torque and the flywheel speed. The following equations express this relation:

$$T_g = 48.7 w_f \tag{6.6}$$

$$T_g = 0.1754\, {w_f}^2 - 36.3\, w_f + 2362.6 \tag{6.7}$$

Substituting the angular velocity in rad/s gives the generator torque in Nm. The w_f is the angular velocity of the flywheel which can be calculated as follow:

$$w_f\left(\frac{rad}{s}\right) = \frac{2\pi}{60} S_f(RPM) \tag{6.8}$$

where S_f is the flywheel speed. The resultant angular velocity of the flywheel provided by the buoy motion can be calculated as:

$$w_f = C_x \frac{V_b}{R_p} \tag{6.9}$$

where the C_x is the coefficient of the speed multiplier, V_b is the buoy velocity and R_p is the radius of the pulley. Based on the energy balance equation, the initial energy at the flywheel (E_{fw1}) plus the flywheel energy obtained from the buoy acceleration (E_b) are equal to the final energy at the flywheel (E_{fw2}) plus the energy delivered to the generator (E_g). It can be expressed as follow:

$$E_{fw1} + E_b = E_{fw2} + E_g \tag{6.10}$$

$$E_{fw1} = \frac{1}{2} I_{fw} w_1^2 \tag{6.11}$$

$$E_b = \frac{1}{2} I_{fw} dw^2 \tag{6.12}$$

$$E_g = T_g w_2 dt \tag{6.13}$$

where, dw is angular velocity increment of the flywheel and dt is the analysis time interval, as follow:

$$dw = w_2 - w_1 \tag{6.14}$$

$$dt = t_2 - t_1 \tag{6.15}$$

Using equations (6.10) and (6.11), the final flywheel angular velocity can be calculated as follow:

$$w_2 = \sqrt{\frac{E_{fw1} - E_g + E_b}{1/2\, I_{fw}}} \tag{6.16}$$

In the situation that there is no additional energy from the buoy or its energy is not sufficient to drive the PTO system, the w_2 can be calculated assuming $E_b = 0$, as follow:

$$w_2 = \sqrt{\frac{E_{fw1} - E_g}{1/2\, I_{fw}}} \tag{6.17}$$

6.4.2 The coupled Hydro-electro-mechanical system

The effect of the PTO device on the oscillating body can be simulated as an external electro-mechanical force (F_{PTO}). The result is a coupled Hydro-electro-mechanical system. In each time step, the generator and flywheel inertia torques are calculated using the position and the velocity of the oscillating body. The summation of the torques is then converted to an axial force and exerted on the buoy. Figure 6-12 illustrates the coupled system analyses process. A FORTRAN subroutine presented in the general report of the project [107] is used to model the PTO. However, some modifications are applied on that subroutine to be compatible with the FORTRAN code that is presented in chapter 5.

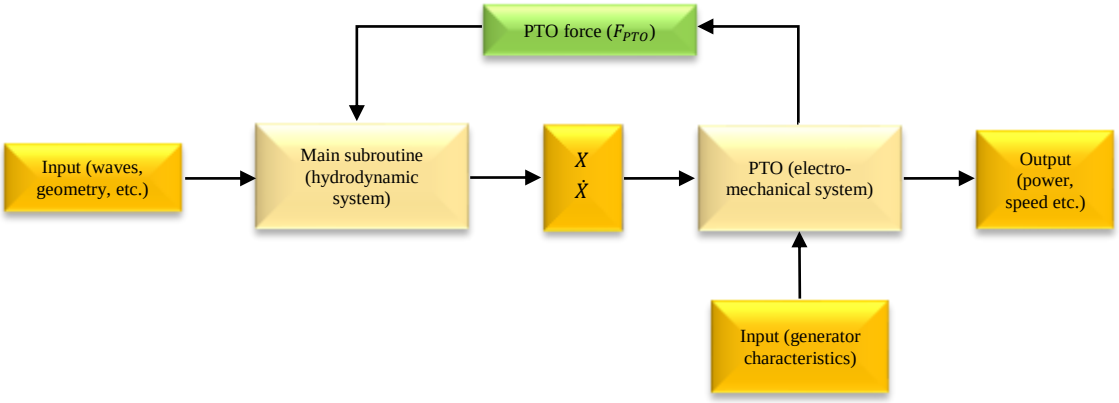

Figure 6-12 - The coupled Hydro-electro-mechanical simulation flowchart of the COPPE nearshore point absorber

Taking into account of the PTO restrictions in power generation, two operational modes can be considered:

1. The buoy velocity is high enough to drive the PTO.
2. The buoy velocity is too slow to drive the PTO.

In the case of first operation mode, the buoy motion is coupled to the PTO system and the PTO force is the summation of the generator and flywheel forces (electro-mechanical force), while in the second mode, the buoy and the PTO system are coupled if the generator rotation is greater than the minimum necessary. It should be noted that, independent of the mode of the operation, the generator only produces electricity when its rotation is inside the range of the minimum necessary and the nominal maximum, which is called the "PTO operational range". Therefore, there is only one situation of uncoupling, it is when the buoy velocity is too slow to drive the PTO and the generator rotation is out of the PTO operational range. It occurs when the buoy is reaching to its heave extremum where its velocity decreases and tends to zero. In this case, the generator consumes the delivered energy until its speed drops below the minimum necessary. In this situation, if there is not any wave excitation the generator motion dies away through a friction force due to the PTO mechanical parts.

The uncoupling condition is considered to prevent the high rotations that hurt the electro-mechanical system.

The PTO force applied on the buoy can be calculated for four different conditions as follow:

1. Operational mode 1 and $w_{min} < w_f < w_{max}$, the PTO force is the summation of the flywheel and generator forces (electro-mechanical force):

$$F_{PTO} = ((T_f + T_g)/R_p)C_x \tag{6.18}$$

2. Operational mode 1 and $w_f < w_{min}$ or $w_f > w_{max}$, the generator and the flywheel are uncoupled and the PTO force is equal to the flywheel force (mechanical force):

$$F_{PTO} = (T_v/R_p)C_x \tag{6.19}$$

3. Operational mode 2 and $w_{min} < w_f < w_{max}$, the buoy cannot add any velocity to the PTO system. In this situation, the generator produces electrical power consuming the flywheel energy. This imposes a small negative torque on the flywheel. Then, the resultant force can be calculated as follow:

$$F_{PTO} = ((T_f + T_g)/R_p)C_x \quad (6.20)$$

4. operational mode 2 and $w_f < w_{min}$ or $w_f > w_{max}$, the PTO and the buoy are uncoupled and there is no PTO force applying on the system:

$$F_{PTO} = 0 \quad (6.21)$$

Figure 6-13 illustrates the calculation process of PTO force and electrical power.

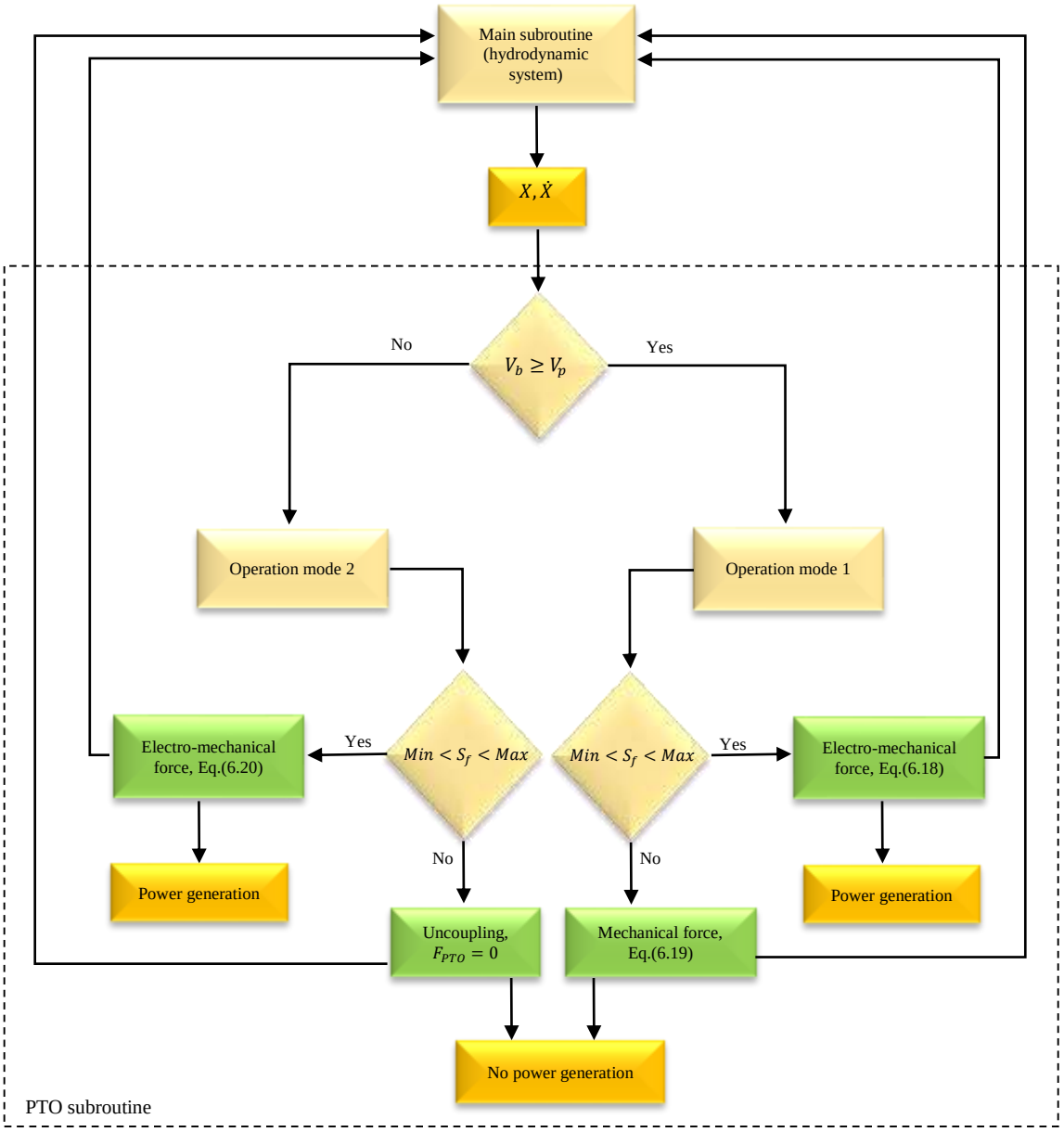

Figure 6-13 – The PTO force and electrical power calculation flowchart

In each time-step, the velocity of the buoy is compared to the flywheel velocity to identify the mode of operation of the PTO system. After calculation of the values of the w_f, T_g, T_v and energies of the buoy, flywheel and generator, and based on the value of the flywheel speed, the PTO force and electrical power are determined. The main subroutine use the PTO force to solve the Cummins' equation and calculate the buoy response for the next time-step.

6.5 The performance analyses of the COPPE nearshore point absorber WEC; application of a constant-delay latching control

6.5.1 Introduction

In the previous chapter the power generation of the wave energy converters are mainly dependent on the hydrodynamic behavior of the system. It is because of using a pure damper as PTO system which is linearly related to the buoy velocity. Additionally, in those cases, the PTO system can generates electricity without any limit, which leads to unrealistic and overestimated results. In practice, there are different variables that constraint the performance of a PTO system. In the case of the COPPE nearshore WEC, these constraints, which are explained in section 6.4.2, limit the performance of the system to a specific range (RPM_{min}, RPM_{max}) and impose coupling and uncoupling between the PTO and the buoy during its oscillation. In this case, based on the available specification of the system provided by the manufacturer, an operational range between 50 and 400 rpm is considered for the generator speed. Additionally, the effect of friction and losses are included that makes the power generation dies away if there is no wave excitation. This section addresses the performance of the COPPE nearshore WEC with and without applying a constant-delay latching control.

6.5.2 The control-free COPPE WEC in regular waves

As the first approach, the control-free WEC is analyzed in regular waves with wave height of $2\,m$ considering no practical limit for the PTO system. It means that the minimum necessary rotation is equal to zero, $RPM_{min} = 0$ and the maximum allowed rotation is considered unlimited by assigning a large value, $RPM_{max} = 6000$. Three values are considered for the speed multiplier coefficient $C_x = 5, 10$ and 20. The results are plotted in figure 6-14. The results show the better performance of the PTO with the $C_x = 20$,

specially for the wave periods larger than 6 seconds. Figure 6-14-b illustrates the maximum and minimum values of the generator rotation for different C_x. Except the case of $C_x = 5$ in the wave period of 4 s, the maximum values are under the upper bound of the generator speed. As it can be seen, as the wave period becomes larger, the generator speed and consequently the power generation decrease. It is because that the longer waves (the wave with longer wavelengths) lose their effect on the buoy due to its small diameter and the buoy "follow" the waves upward and downward (see section 4.3.3.2). The WEC with larger C_x can compensate this drop by amplifying the delivered velocity of the buoy to the PTO system (see Eq.(6.9)).

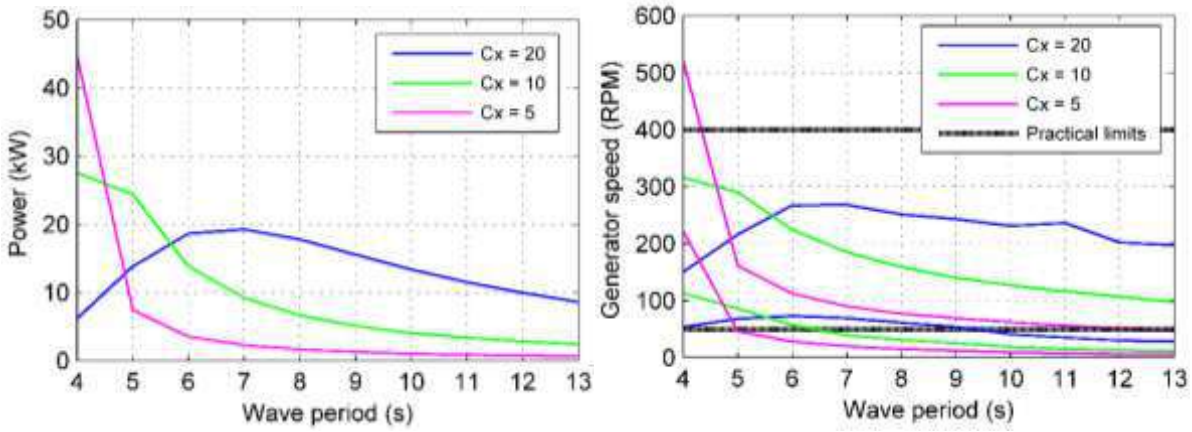

a) b)

Figure 6-14 – a) The power production (kW) of the control-free COPPE nearshore WEC with an unconstrained PTO system; b) The corresponding maximum and minimum generator speed (rpm)

The generator cannot generate electricity when its speed is under the practical lower bound. Therefore, to decrease the situation of no power generation it is important to keep the minimum values of generator speed above the lower bound. It can be seen in figure 6-14-b that the WEC with $C_x = 5$ and 10 cannot provide the minimum necessary rotation for the wave periods greater than 5 and 6 s respectively. This occurs for the WEC with the largest C_x only after wave period of 9 s. At the wave period of $T_w = 4\ s$, when the buoy is in resonance with the incoming wave, the WEC with the smallest C_x generates the largest amount of energy. The reason can be explained by a step-by-step analysis of the behavior of the PTO system. The results plotted in Figure 6-15 can help us to understand this issue. It shows the buoy velocity in heave and PTO force of the WEC

device for $C_x = 5, 10$ and 20. The PTO force zero crossing represents the second operational mode and it occurs when the velocity is zero or close to zero. They are the moments that the buoy is reaching to its heave motion extremum, so the buoy velocity is not sufficient to drive the flywheel ($V_b < V_p$) and the flywheel rotation is smaller than the minimum necessary to generate electrical power, $RPM_f < RPM_{min}$. In the results illustrated in figure 6-15, due to the assumption of an unconstrained PTO, the zero crossing does not occur and the PTO force has values close to zero in this situation.

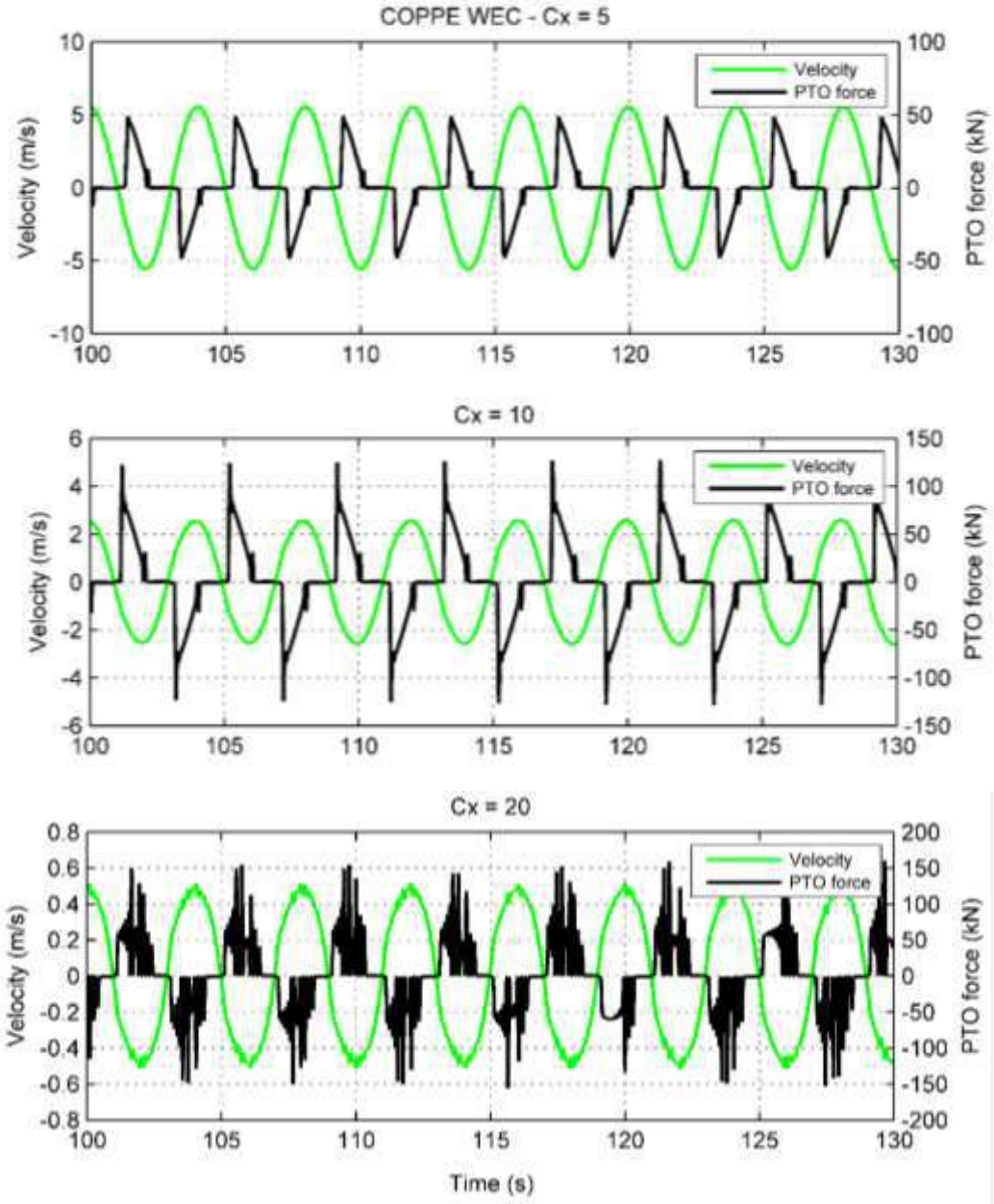

Figure 6-15 – The buoy velocity (m/s) and the PTO force (kN) of the COPPE nearshore WEC in a regular wave of $T_w = 4\ s$ and $H = 2\ m$ for three different speed multiplier coefficients, $C_x = 5, 10$ and 20.

It can be seen that, as the C_x becomes larger, the PTO forces values maintain close to the zero for a shorter time duration. It is because that the flywheel speed is significantly amplified by the larger C_x and it helps the generator to keep its rotation more than the minimum required during the low velocities of the buoy. Considering the plot corresponding to the $C_x = 10$, it can be observed that there are two moments of sudden increase in PTO force. The first one occurs right after the coupling the buoy and PTO system and the second one happens right after the buoy maximum velocity. Mathematically, it can be explained as the effect of the suddenly amplification of the flywheel rotation. When the buoy passes its heave extermum, the buoy velocity cannot overcome the flywheel speed and there is no driving force (buoy at its heave extremum). However, the flywheel is rotating with a speed that gained form the speed multiplier. After velocity zero crossing, the buoy needs some time steps to reach the sufficient velocity to drive the flywheel. In this moment, the flywheel rotation is significantly amplified and consequently a relatively large PTO force is applied on the buoy (see Eq.(6.18)). Then the velocity of the buoy and the flywheel reach to an equilibrium and the delivered velocity of the buoy to the PTO is constantly larger than the flywheel rotational velocity until the buoy velocity extremum. The flywheel speed is continuously increasing form the coupling moment up to the buoy maximum velocity. Right after the extremum, the reduced velocity is not sufficient ($V_b < V_p$) to drive the flywheel resulting in a diminution in PTO force (see Eq.(6.20)) and the flywheel speed. This results that the buoy velocity in the next time step overcomes the flywheel speed and a sudden increase occur in the PTO force (Eq.(6.18)). This instability continues for some time steps until an equilibrium. As it can be seen in the case of $C_x = 20$, these instabilities are continues during the buoy oscillation between two heave extermums. It can be inferred that more instabilities occurred for the larger speed multiplier coefficient values C_x .

At the resonant condition, as it is shown in figures 6-15 and 16, applying the smaller C_x increases the generator speed and consequently more amount of power generation can be obtained. The buoy velocity has its maximum value in the resonant condition. In the case of PTO with $C_x = 20$, the delivered velocity from the buoy to the PTO is highly amplified. Consequently, a large rotation is induced to the flywheel. On the sequence, the buoy velocity cannot overcome the flywheel amplified velocity and, as explained above, the instabilities are appeared. This prevent the continuous increase of the generator rotation. As it can be seen in figure 6-16, the largest generator speed is about 500 rpm

corresponding to the $C_x = 5$. In the other hand, higher flywheel speed results in larger PTO force that decrease the buoy velocity. It can be observed that the buoy velocity is about 5 meter per second for the PTO with $C_x = 5$, which is larger than 1.5 and 0.4 meter per second for the $C_x = 10$ and 20 respectively.

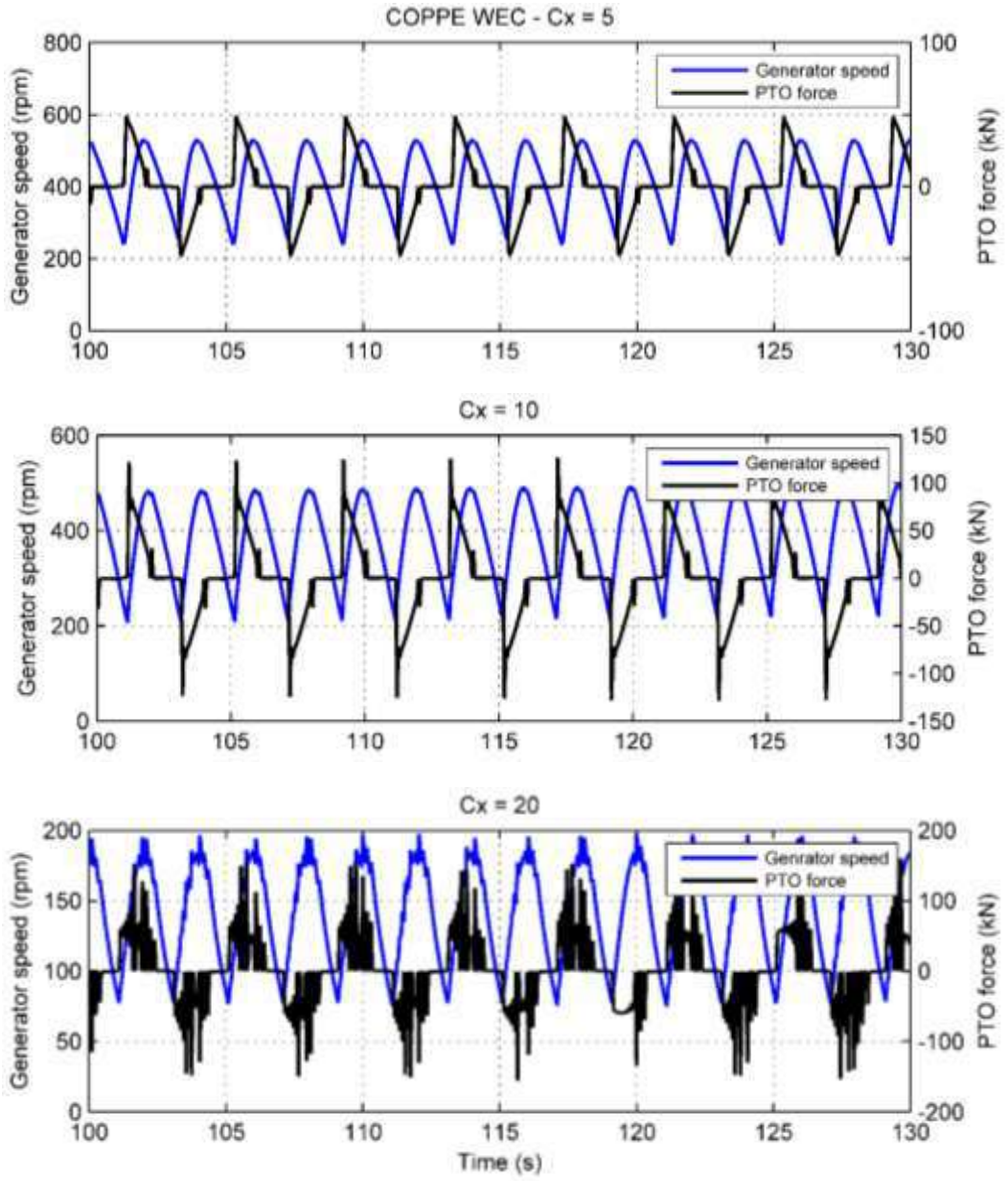

Figure 6-16 - The generator speed (rpm) and the PTO force (kN) of the COPPE nearshore WEC in a regular wave of $T_w = 4\ s$ and $H = 2\ m$ for three different speed multiplier coefficients, $C_x = 5, 10$ and 20.

Figure 6-17 illustrates the PTO with different C_x in a regular wave of $T_w = 10\ s$ and $H = 2\ m$. The results show that the largest speed multiplier coefficient increases the generator speed significantly and makes PTO has a better performance comparing to the others. Actually, the slow velocity of the buoy in the wave period larger than the resonant region can be compensated by a sufficiently large speed multiplier coefficient.

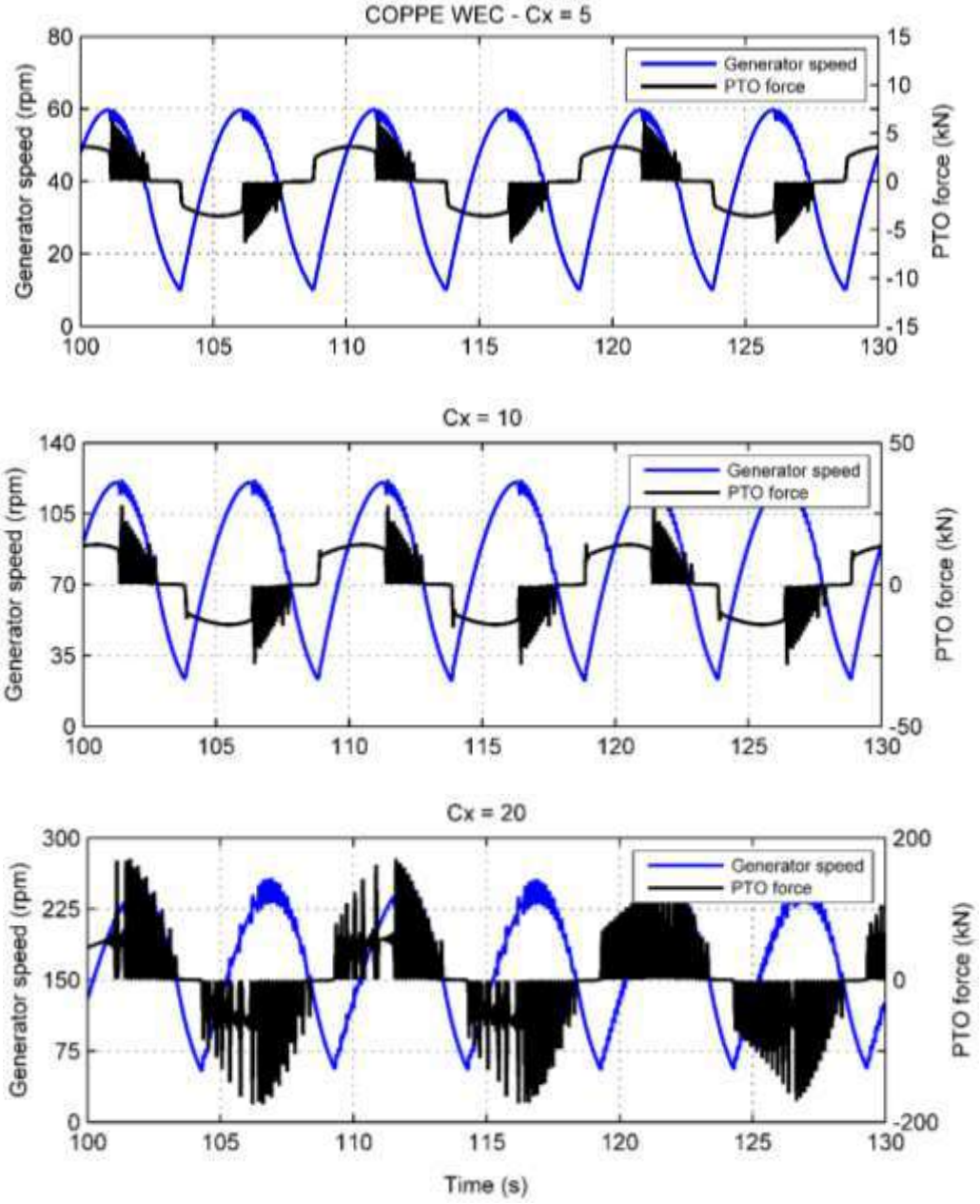

Figure 6-17 - The generator speed (rpm) and the PTO force (kN) of the COPPE nearshore WEC in a regular wave of $T_w = 10\ s$ and $H = 2\ m$ for three different speed multiplier coefficients, $C_x = 5, 10$ and 20.

It can be inferred that for the case study PTO system in an unconstrained condition, applying the largest C_x results in a better performance in the wave periods larger than the buoy natural period while the highest power generation corresponds to the PTO system with $C_x = 5$ which occurs in the wave period equal to the buoy natural period (figure 6-14). The maximum wave power that can be absorbed by a heaving axisymmetric body presented by Budal and Falnes [45] can be calculated as:

$$P_{max} = JL_{max} \tag{6.22}$$

where J is the energy flux per unit wave crest width and the L_{max} is the maximum absorption width which is defined as $L_{max} = \lambda/2\pi$. For linear deep-water waves, $\lambda = gT^2/2\pi$ and $J = \rho g^2 T H^2/32\pi$ (see section 3.4). An upper limit also proposed by the Budal and Falnes [55] called "Budal's upper bound" which presents the power P_u that can be absorbed by a given submerged body volume V. It is calculated as follow:

$$\frac{P_u}{V} < \frac{\rho g \pi H}{4T} \tag{6.23}$$

These two power values can be considered as the theoretical maximum wave absorption by a semi-submerged heaving body with an optimum heaving amplitude [46]. These two curves are shown in figure 6-18. Additionally, the figure illustrates the performance of the control-free COPPE nearshore WEC considering an unconstrained PTO system and three different speed multiplier coefficient C_x, in a range of regular wave periods. The power generation of the WEC device considering a pure damper as the PTO system with application of the CPD and OPD strategies are also plotted (the PTO control strategies are explained in section 5.6). The intersection point of the theoretical maximum curves can be defined as:

$$T_c = (32\pi^4 V/g^2 H)^{1/4} \tag{6.24}$$

$$P_c = \frac{(\rho g^{3/2}/8)}{(V^3 H^5/2)^{1/4}} \tag{6.25}$$

In figure 6-18, the vertical axis represents the power generation of the devices, considering a wave height of 2 meters, which is normalized using P_c. Evidently, the maximum power generation occurs in the wave period equal to the buoy natural period.

The models with a pure damper as PTO, reach to this maximum value applying a PTO damping equal to their hydrodynamic damping corresponding to that period. For the wave periods more than 6 seconds, which is the range of the local sea predominant wave, the model with OPD control strategy shows the best performance following by the $C_x = 20$ model. The same power generation level can be observed for the model with $C_x = 5$ and the model with CPD strategy. It can be seen that, except the resonant condition, the maximum power level does not exceed the 20 percent of the theoretical maximum power.

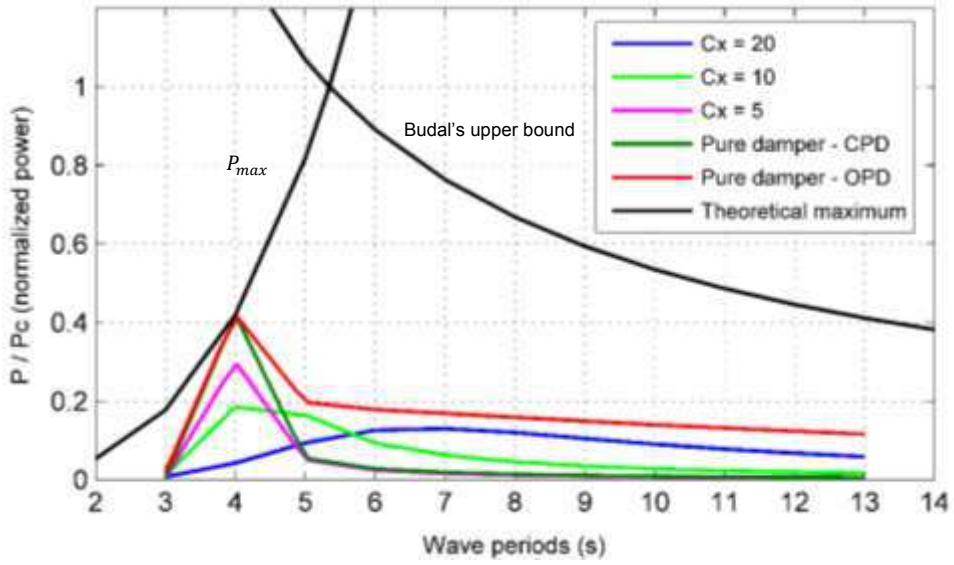

Figure 6-18 – The power generation of the COPPE nearshore buoy in a range of regular waves with a wave height of 2 meter. The case study PTO system considering no constraint is applied for three different speed multiplier coefficients, $C_x = 5, 10$ and 20. The power generation of the buoy is analyzed considering a pure damper as PTO system applying CPD and OPD control strategies.

6.5.3 Application of a constant-delay latching control

6.5.3.1 Regular wave analyses

This section addresses the application of a latching control strategy proposed by Sheng et al [77], on the COPPE nearshore WEC. Based on this method, which is explained in detail in chapter 5, the latching duration is calculated as the half of the subtraction of the incoming wave period and the buoy natural period ($(T_w - T_N)/2$) (see section 5.3). As the result, the velocity phase of the buoy is equal to the wave excitation phase leading to a resonant condition. This amplifies the buoy motion and improves the power generation

of the WEC. Figure 6-19 illustrates the results of the application of the constant-delay latching (in this chapter it is called "CDL") control on the COPPE nearshore WEC in a range of regular waves with $H = 2\ m$. Three different speed multiplier coefficients $C_x = 5, 10$ and 20 are considered for the PTO system. Additionally, the power curve of the COPPE WEC buoy applying the CDL and a pure damper as the PTO system is plotted and the results are compared to the control-free (CF) systems.

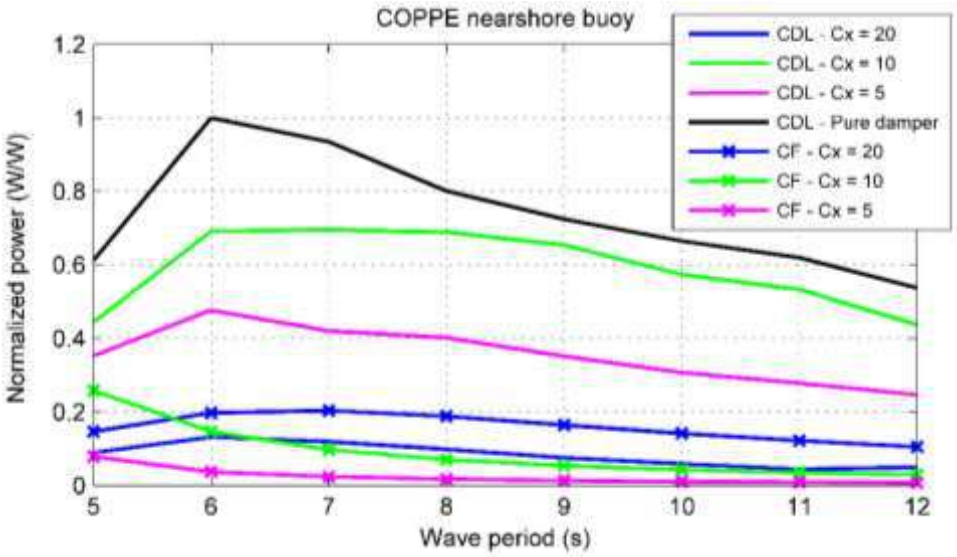

Figure 6-19 – The power generation of the COPPE nearshore WEC buoy considering; 1) CDL control and case study PTO system (CDL – $Cx = 5, 10$ and 20), 2) CDL control and pure damper PTO system (CDL – pure damper), and 3) control-free system and case study PTO system (CF – $Cx = 5, 10$ and 20). The results are shown for a range of regular waves of $H = 2\ m$. The power values are normalized using the maximum power value.

It can be seen that the controlled buoy with a pure damper PTO has a better performance comparing to the other systems. Comparing the controlled buoys and the control-free ones shows that, except the case of CDL-$C_x = 20$, applying the CDL control improves the power generation. It can be explained using the results shown in figure 6-20. This figure illustrates the results of the application of the CDL control on the COPPE WEC in a regular wave of $T_w = 9\ s$ and $H = 2\ m$. Considering the velocity and wave excitation results, it is shown that, the optimum phase condition is not fully fulfilled. It can be observed that in the cases of the PTO system with $C_x = 10$ and 20, the buoy velocity phase is somehow closer to the optimum condition. The mean power generated by the WECs are about 7, 62 and 33 kW for the $C_x = 20, 10$ and 5 respectively. In analogy with

the systems with a pure damper as the PTO, it can be explained that the buoys with the PTO of $C_x = 20$ and 5 are overdamped and underdamped respectively. In the other words, the optimum amplitude condition is not satisfied for these cases. For the system of $C_x = 20$, large amount of the PTO force decreases the heave amplitude, while the PTO with $C_x = 5$ cannot absorb the maximum energy due to the application of a resistance smaller than the optimum value.

Considering the results plotted in figure 6-19, it can be inferred that the speed multiplier coefficient equal to 10 can be considered as the optimum value providing the optimum phase and amplitude. It should be noted that the displacements in the figure 6-20- b and c, decreases in the case of considering the effect of viscosity.

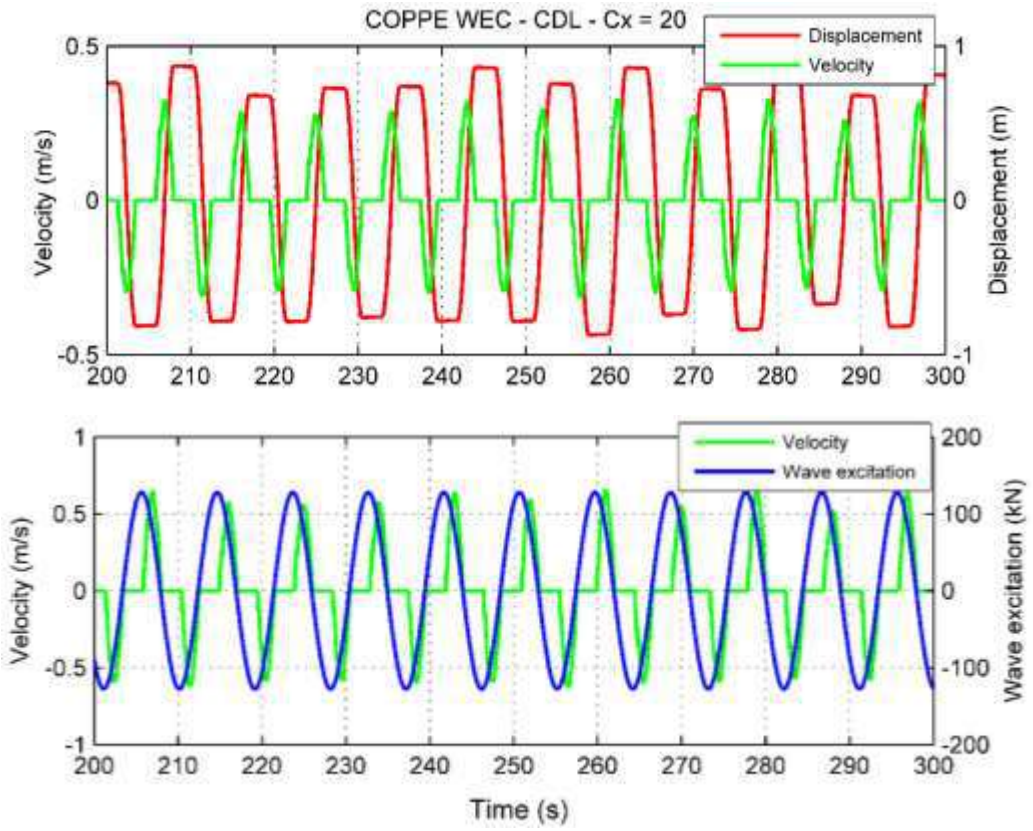

a)

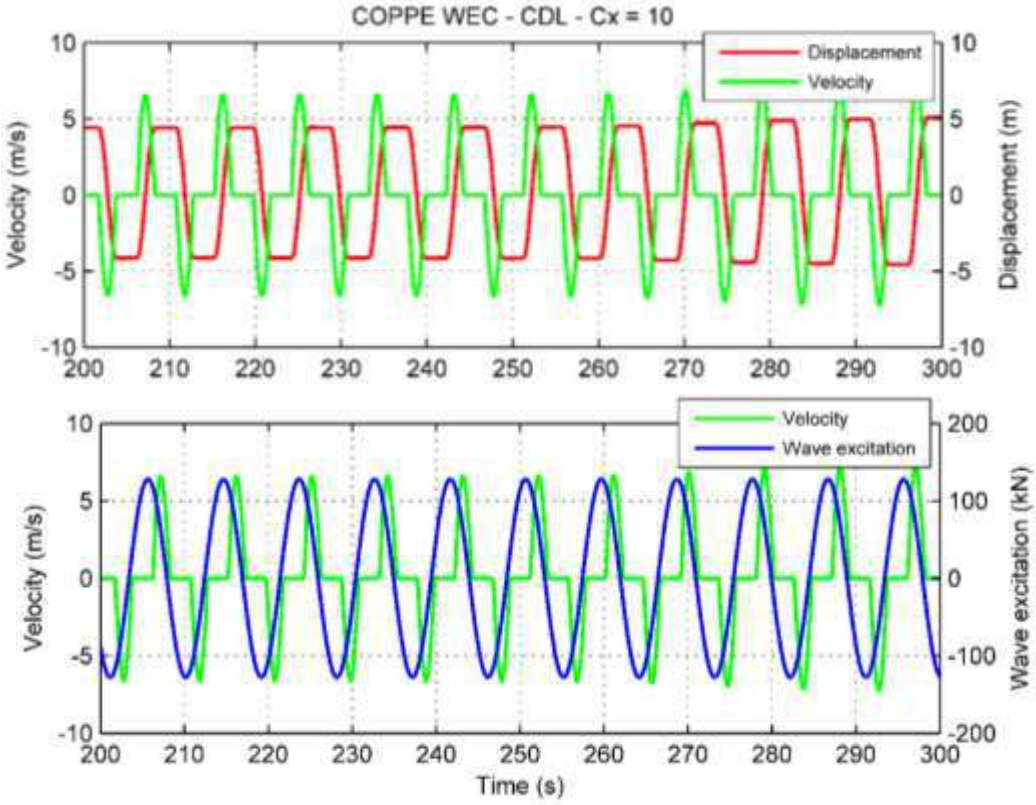

b)

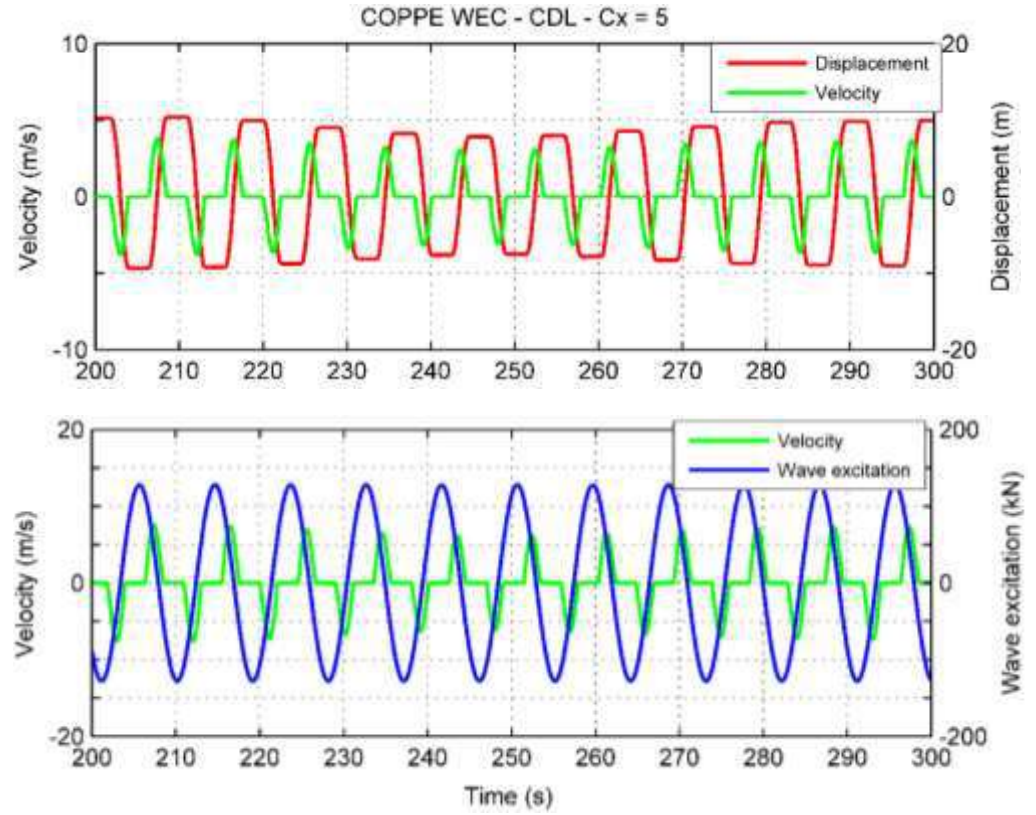

c)

Figure 6-20 - The results of the application of the CDL control on the COPPE nearshore WEC considering three values of the speed multiplier coefficient $C_x =$ a) 20, b) 10 and c) 5. The buoy oscillation is tuned to a regular wave of $T_w = 9$ s and $H = 2$ m.

6.5.3.2 Irregular wave analyses

This section addresses the performance of the COPPE nearshore WEC in the irregular waves. The wave spectrums are calculated for each sea state using the JONSWAP model (see section 3.5). The practical limit of the generator speed is considered in the simulation in order to have more realistic result of the device performance. The operational range of the generator that is provided by the manufacturer is 50 to $400\ rpm$. It means that, for the generator speed values out of this range, the generator-flywheel system is uncoupled and the PTO does not produce electrical power (see section 6.4.2). The analyses are performed for the control-free and CDL control conditions. Figure 6-21 shows the generated power and the corresponding average generator speed in a range of sea states of $T_p = 5$ to 13 and $H_s = 1.33\ m$. Four WEC models are considered for the simulations as follow:

- Unconstrained control-free (UCF) model. No practical generator speed limit, no CDL control.
- Constrained control-free (CCF) model. Practical generator speed limit, no CDL control.
- Unconstrained constant-delay latching (UCDL) model. No practical generator speed limit, CDL control.
- Constrained constant-delay latching (CCDL) model. Practical generator speed limit, CDL control.

As it is illustrated in figure 6-21, applying the CDL control improves the power generation of the device in irregular waves. In the case of Control-free WECs, the system of $C_x = 20$ has a better performance and preduces more power comparing to the others. The reason can be explained refering to the figure 5-32 in chapter five. It is shown in that figure that in the case of a control-free buoy in irregular waves, high PTO damping levels are required to generate the maximum power. As it explained in section 6.5.2.2, the speed multiplier coefficient of $C_x = 20$ provides a higher damping level comparing to the $C_x = 10$ and 5, therefore, more power can be obtained in irregular waves specifically in the sea states of T_p more than 7 seconds, which is the range of the predominant waves in the local sea. The displacement and the PTO force of the CCF-COPPE WEC are plotted in figure 6-22, for different C_x in the sea state of $T_p = 8\ s$ and $H_s = 1.33\ m$. It can be observed that by increasing the C_x the PTO force increases and this results in the diminution of the displacement. In other words, in this situation the relative optimum amplitude occurs in

the case of $C_x = 20$. It should be noted that, in this case, the $C_x = 20$ provides the optimum power generation in comparison to the $C_x = 10$ and 5 which are the speed multiplier coefficients provided by the PTO system manufacturer, hence, theoretically, there may be other values of C_x that results in a higher level of power production.

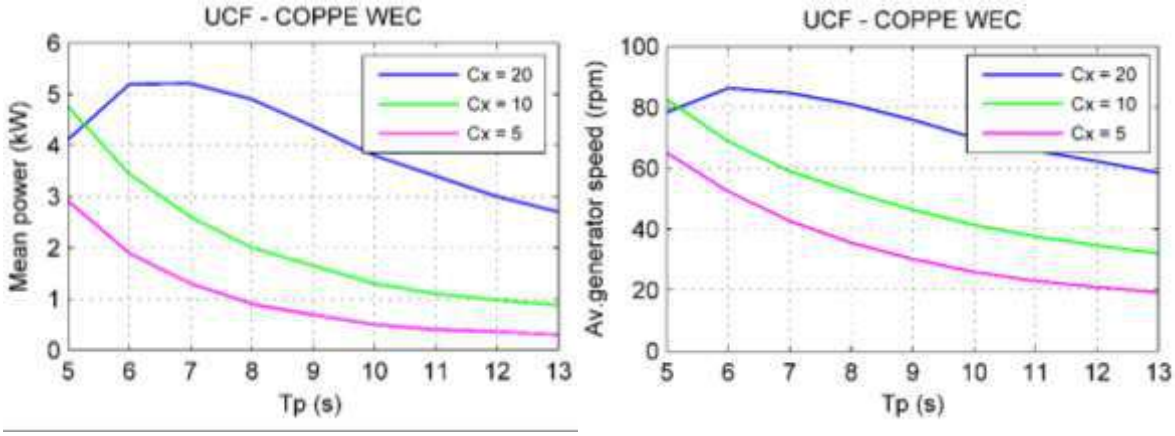

a)

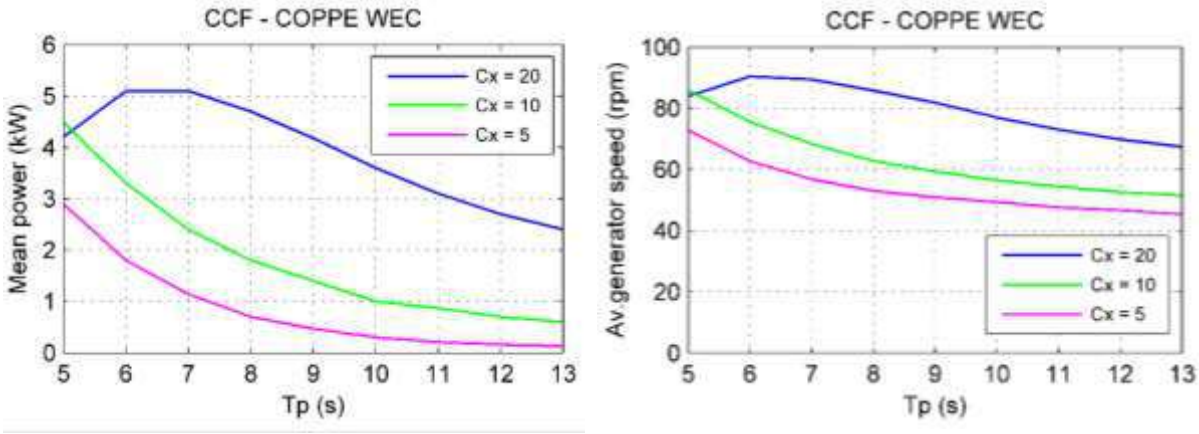

b)

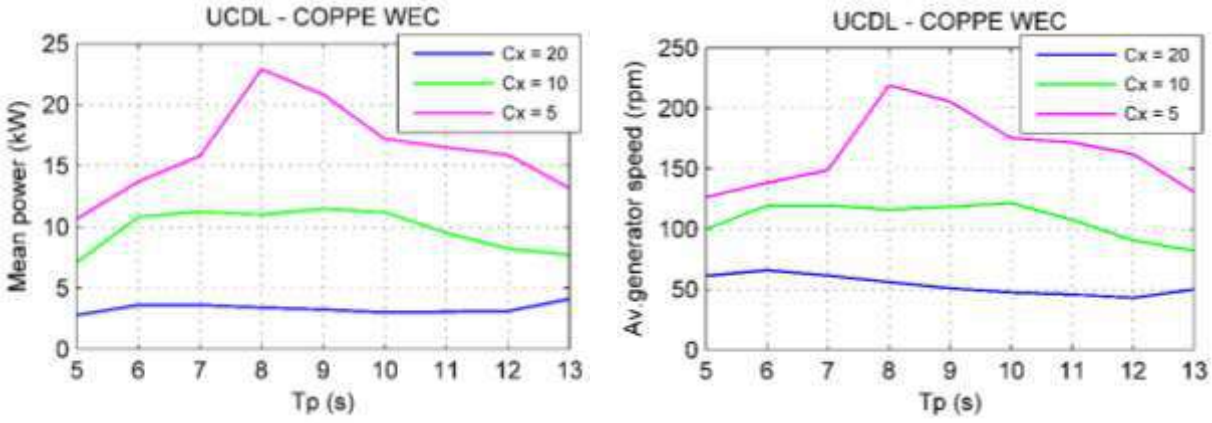

c)

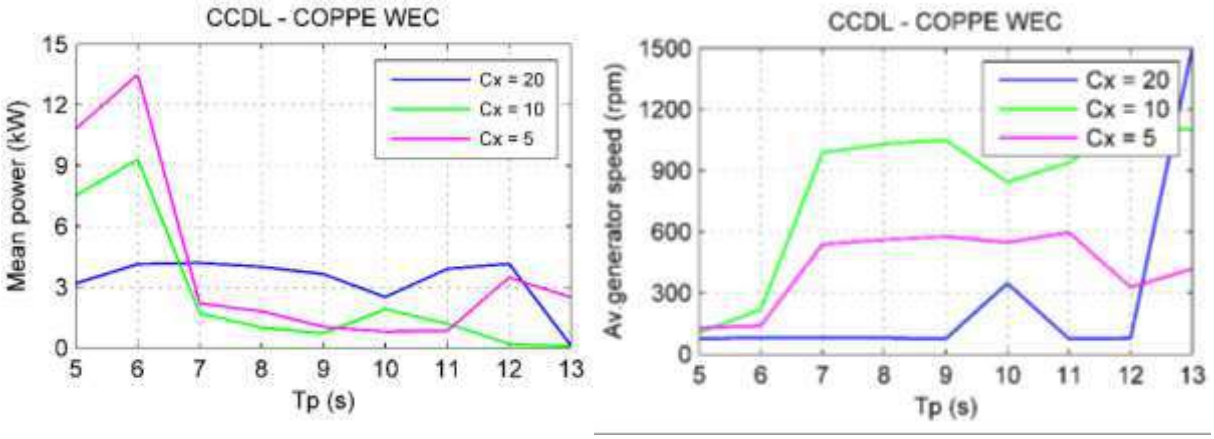

d)

Figure 6-21 – The mean power and the average generator speed of the COPPE WEC in arrange of sea state of $H_s = 1.33\ m$ applying four conditions as follow; UCF: unconstrained control-free, CCF: constrained control-free, UCDL: unconstrained constant-delay latching, CCDL: constrained constant-delay latching.

Figure 6-23 .shows the results of the simulation of the unconstrained and constrained control-free COPPE nearshore WEC in a time window of 50 seconds in an irregular wave of $T_p = 8\ s$ and $H_s = 1.33\ m$. As it is expected, in the unconstrained case, there is no moment of PTO-WEC uncoupling ($F_{PTO} = 0$). It is because of that the generator can prodeuce power even when its speed is smaller than the lower bound value ($50\ rpm$). As the result, when the buoy velocity tends to zero (the buoy is reaching to its heave extermum), the PTO is working in its second operational mode and is still coupled with the WEC. In this situation, the buoy cannot drive the flywheel while the flywheel-generator system applies forces on the WEC. Consequently, as the time passes, the generator speed decreases until the next moment that the buoy velocity becomes greater than the flywheel velocity. The constrained control-free WEC has a different behavior in the same situation. Figure 6-23-b shows that, as the buoy velocity is reaching to zero, the generator speed is below the PTO lower bound and the WEC-PTO uncoupling occurs. Besides that, the PTO does not generate electricity and generator speed gradually decreases due to the losses (the losses coefficients is considered equal to 1%) until the next PTO-WEC coupling moment. Because of this, the lower values of the generator speed in CCF model are kept close to $50\ rpm$ and this results in a higher average value comparing to the UCF WEC. It can be seen in figure 6-21-c and d that applying the CDL control increases the power production while maintain the average generator speed in the operational range, except for the $C_x = 20$ in the T_p more that 11 seconds.

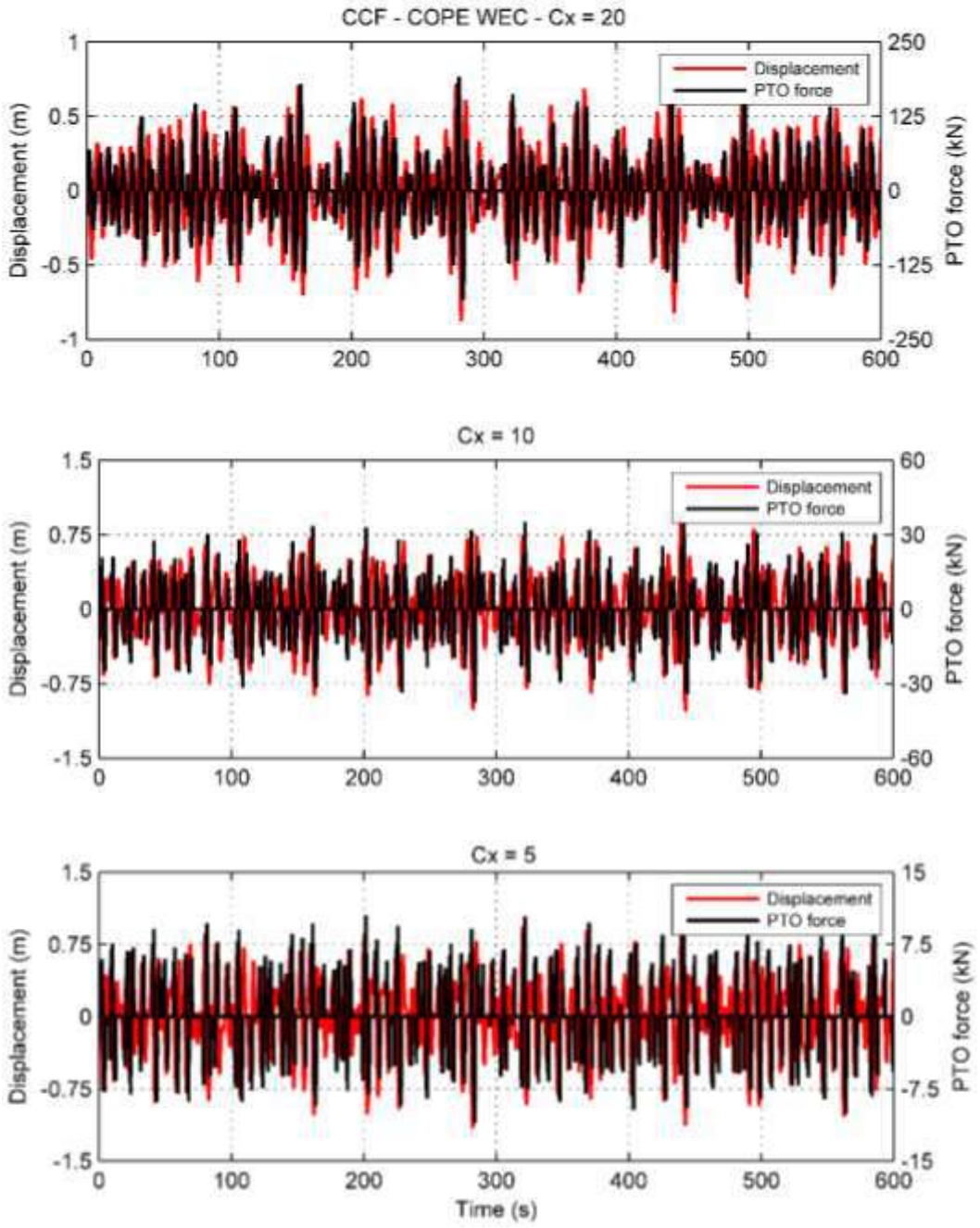

Figure 6-22 – The displacement and PTO force of the CCF COPPE WEC in 600 seconds time window for three different speed multiplier coefficients of $C_x = 20, 10$ and 5 in the sea state of $T_p = 8\ s$ and $H_s = 1.33\ m$

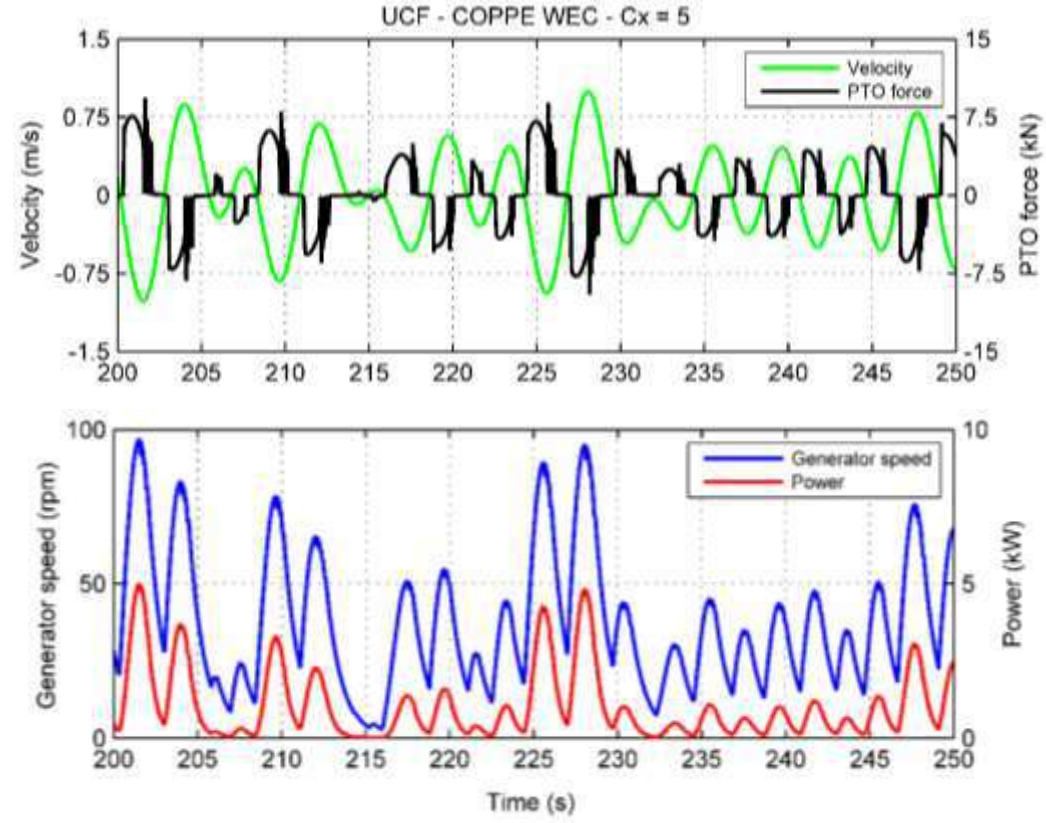

a)

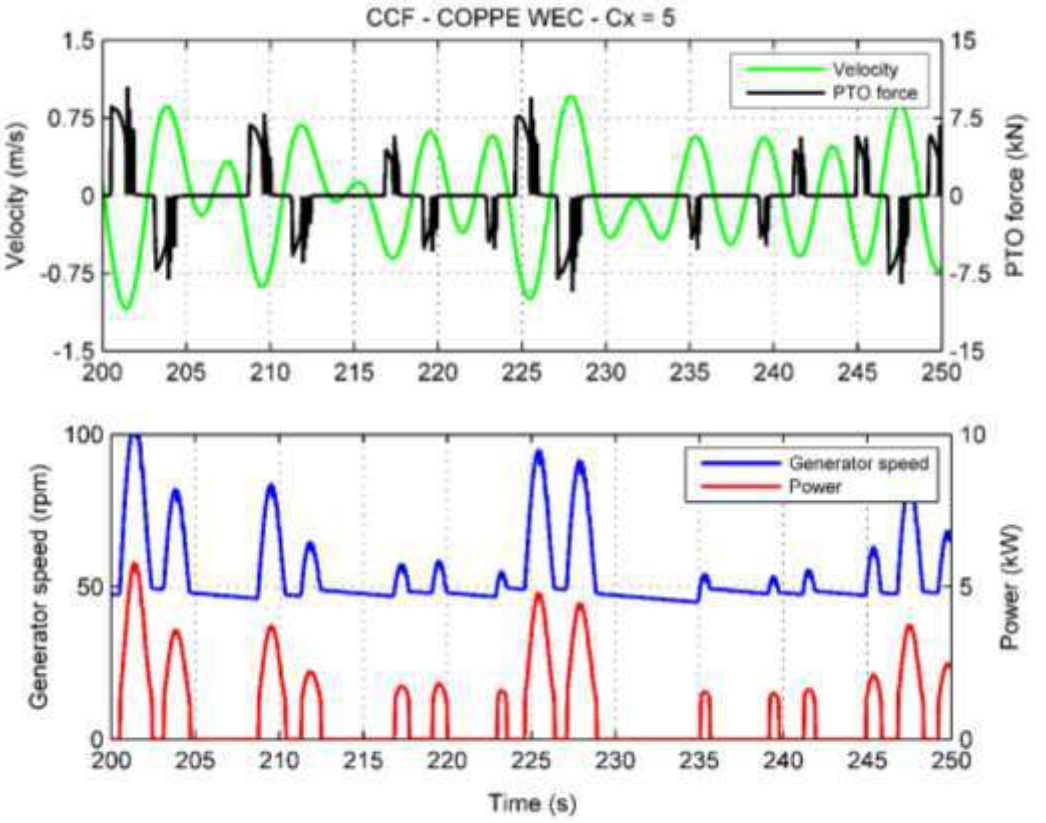

b)

Figure 6-23 – The time domain simulation results of the; a) UCF and b) CCF COPPE WEC in a sea state of $T_p = 8$ s and $H_s = 1.33$ m.

In the UCDL case, the smaller C_x results in a higher mean power level or, in other words, the optimum amplitude occurs applying the smallest speed multiplier coefficient, $C_x = 5$. In the CCDL model the mean power decreases with the sea state peak period. As it is shown, it is because of the excessive amplification of the generator speed. It can be explains that the generator does not apply forces on the oscillating buoy when its speed reahces to 400 rpm (upper bound of the PTO limit). In this situation, if the buoy velocity overcomes the flywheel speed, the WEC-PTO system is coupled and the PTO force applying on the buoy is only the mechanical force of the flywheel. This implies that, the flywheel energy is not consumed by the generator and the delivered energy from the buoy to the PTO increases the flywheel speed in each time step. Moreover, as it is illustrated in figure 6-24-a, since the flywheel speed is too high, the buoy only can drive the PTO during a few time intervals when its velocity is maximum. It can be observed that the generator speed starts to decrease gradually during 90 seconds of the simulation. It is because that the buoy velocity cannot reach the amplified speed of the generator, thus there is no additional energy delivered from the buoy to the PTO. In the other hand, in the UCDL model, figure 6-24-b, the generator always consumes the flywheel energy and applies force on the system. This does not let the exaggerated amplification of the generator speed. This also is the reason of lower buoy velocity comparing to the CCDL model.

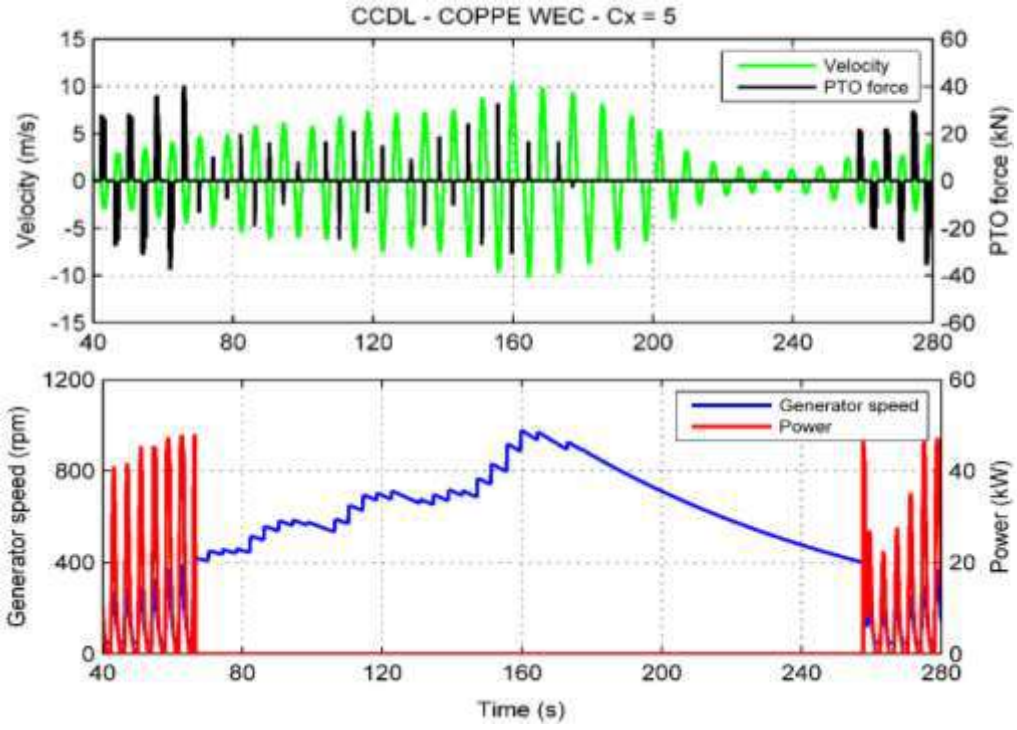

a)

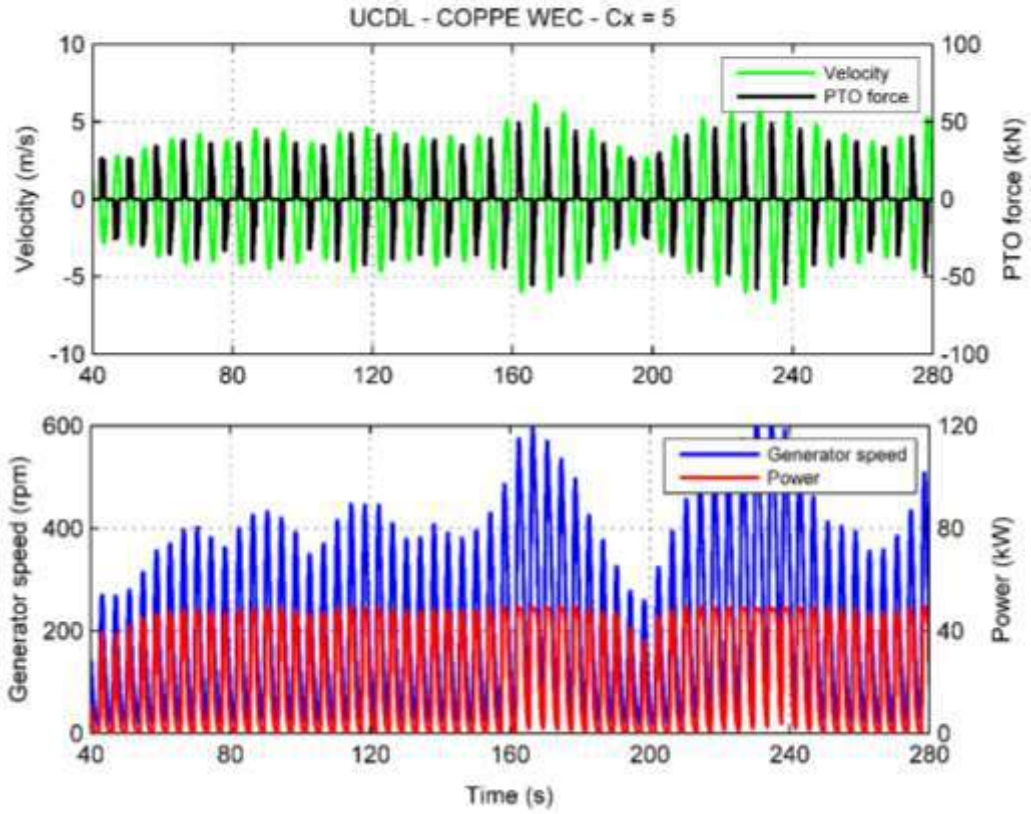

b)

Figure 6-24 - The time domain simulation results of the; a) UCDL and b) CCDL COPPE WEC in a sea state of $T_p = 8\ s$ and $H_s = 1.33\ m$.

As it is shown in figure 6-21-c and d, the CDL WEC with the PTO of $C_x = 20$ is not sensetive to the application of the PTO limits. As it is explained in section 5.8.2, for the WECs controlled by a constant-delay latching in an irregular sea, the optimum power generation is obtained by tuning the PTO damping to the hydrodynamic damping of the buoy at its resonance frequency. The speed multiplier coefficient of $C_x = 20$ applies a high damping force on the buoy that overdamped the buoy motion and consequently cannot satisfy the optimum amplitude requirement. Therefore, the generator speed does not exceed the upper bound of the PTO limit ($400\ rpm$) and the small differences of the average generator speed, between the constrained and unconstrained cases, are because of the slight variations of the lower bound values.

6.5.3.3 Latching force in irregular waves

An important issue that affect the implementation of a CDL control in a real sea is the required force that must be provided to latch the buoy. The latching force can be calculated using the following equation (see section 5.4).

$$F_{latching} = -F_{e,3}(t) + \int_{-\infty}^{t} f_{r,33}(t-\tau)\dot{X}_3(\tau)d\tau - F_{hs} - F_{PTO} \quad (6.26)$$

Where the first term is the wave excitation force, the second one is the memory effect and the third on is the hydrostatic force, all in heave direction. The last term is the PTO force acting in the opposite direction of the buoy velocity. When the buoy reaches to its heave extremum (moment of zero velocity), the PTO force is zero (CCDL model) or close to zero (UCDL model), so the applied latching force includes the wave excitation, memory effect and the hydrostatic force. In a real sea, the latching force is not constant and varies by changing the waves and buoy position. Therefore, the latching mechanism should be designed to be able to provide the maximum latching force experienced by the buoy. Figure 6-25 illustrates the maximum required latching force that is calculated for the UCDL and CCDL models in the range of predominant sea states of the local sea (nearshore Rio de Janeiro). It can be observed that, in the case of $C_x = 20$ the PTO limit does not impose significant changes in the maximum latching force values. As explained in the previous section, it is due to the high damping force of the PTO system that makes the WEC to be less sensitive to the application of such limits. In contrast, applying the PTO constraints increases the maximum latching force for the models of $C_x = 5$ and 10. It can be explained using the Figure 6-26 that illustrates the displacement in heave (X3), wave excitation in heave (Fe,3), hydrostatic (Fhs), memory effect (Fmemory) and PTO forces (Fpto) of the COPPE WEC of $C_x = 10$, applying the UCDL and CCDL in an irregular wave of $T_p = 8\,s$ and $H_s = 1.33\,m$. As it can be seen, the total force is dominated by the contribution of the hydrostatic force. Due to the larger displacements, this force is higher for CCDL model and it implies that a higher force should be compensated in the moment of zero velocity to latch the buoy.

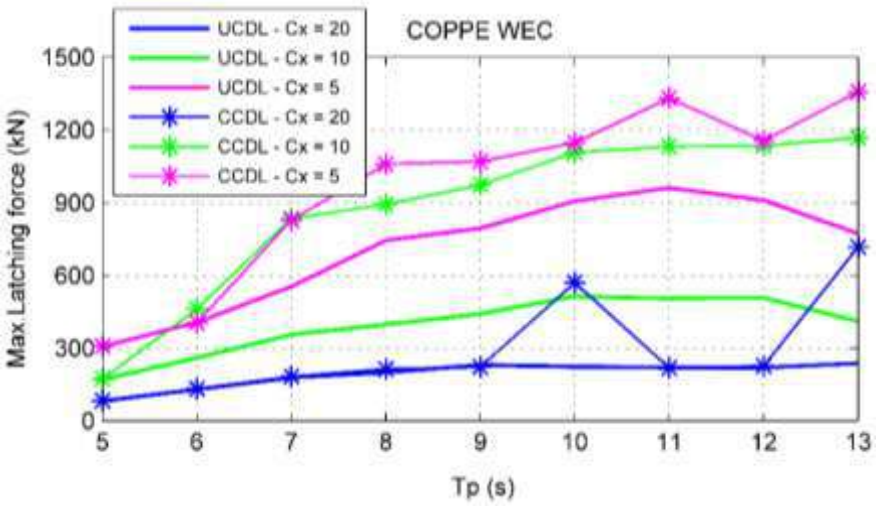

Figure 6-25 – The maximum latching force experienced by the controlled COPPE nearshore WEC during 600 seconds of the simulation for each sea state. The results are shown for the UCDL and CCDL models considering a significant wave height of $H_s = 1.33$ m

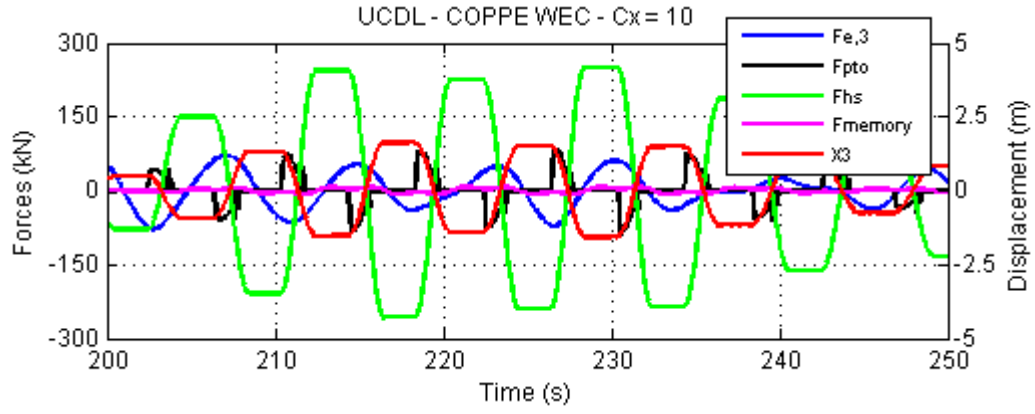

a)

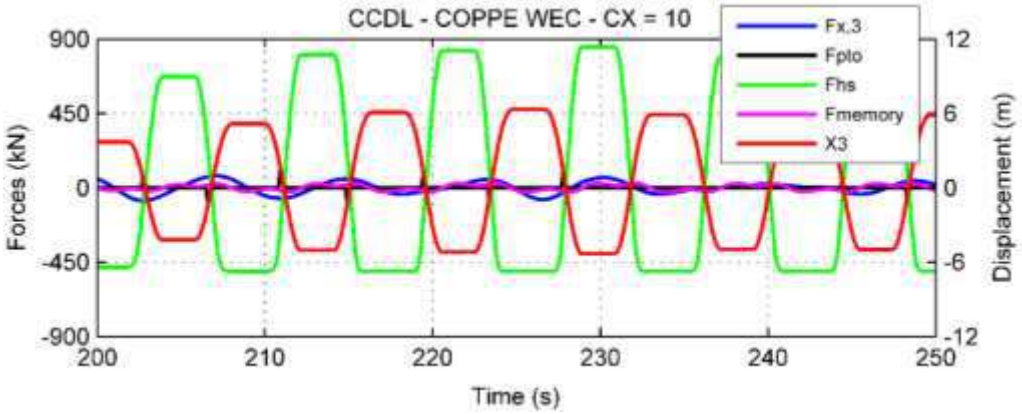

b)

Figure 6-26 – The results of the time domain simulation of the CCDL and UCDL COPPE nearshore WEC in an irregular wave of $T_p = 8\ s$ and $H_s = 1.33\ m$.

It should be noted that, the unconstrained PTO system is an ideal condition that cannot be satisfied in practice. Therefore, considering the real condition (CCDL model), a mechanism must be designed to provide a high level of latching force. As it is illustrated in figure 6-25, the COPPE WEC that utilizes the PTO system of $C_x = 5$ or 10 to maximize the power generation, requires a latching system that is able to provide a maximum force of $1200\ kN$. It should be considered that this is the maximum force that may occur in only one instant during a 600 seconds of the simulation and it often corresponds to the exaggerated displacement of the buoy. Nevertheless, considering the effect of viscosity may slightly reduce the latching force level.

6.5.4 Application of an adapted constant-delay latching

Section 5.3 addresses the performance of the COPPE WEC considering the ideal and real conditions. In the ideal condition, the PTO system generates electricity freely while in the real condition the PTO operates only in a specific range of the generator speed that is provided by the manufacturer. For the control-free WECs, the PTO limit does not affect the power production significantly. In the case of the controlled WEC, applying the PTO constraint reduces the power production despite the high level of generator speed. It implies that the application of the CDL control on the COPPE WEC in a real condition not only does not improve the performance of the system but also may lead to the PTO failure by causing too high generator speed. Therefore, a modified constant-delay latching control must be adapted for improving the performance of the device. As it is illustrated in figure 6-21-b, low rotations and consequently low power generation are obtained, due to the low level of the buoy oscillation velocity. This implies the necessity of using a control system. In the other hand, figure 6-21-d shows that applying the CDL control considering a constrained PTO exceedingly increases the generator speed that are out of the operational range of the generator. As the result, the power generation is zero for a large fraction of time during the WEC performance (see figure 6-24-b). It can be inferred that, the constant-delay latching control should be adapted to eliminate or at least minimize the unnecessary amplification of the generator speed. To achieve this goal, a threshold generator speed in which the latching does not apply on the system should be determined for the PTO. It means that the latching mechanism keeps the buoy at its heave extremum only if the generator speed is less than the threshold value at that moment. As the result, for the rotations larger than the threshold, the velocity of the buoy is not

amplified due to the no latching control situation and this prevents the excessive growth of the generator speed. To determine the optimum threshold, a series of time domain simulations are performed and the results are shown in the figure 6-27. The proposed adapted constrained constant-delay latching (ACCDL) control is applied on the COPPE nearshore WEC and the responses are calculated in the range of the predominant sea states of the local sea (nearshore Rio de Janeiro) with a significant wave height of $H_s = 1.33\ m$. A range of 50 to 300 rpm is considered for the generator speed threshold. In each sea state, the simulations are performed considering the twenty different series of the wave random phase for each threshold value. The different series of random phase are considered to address its effect in the applied phase control (constant-delay latching). The plotted results show that the effect of random phase of the wave is more evident for the sea states of peak period (modal period) larger than 6 seconds. Additionally, it can be seen by comparing the results of the COPPE WEC with different C_x that the dispersion of the generated power value from its average line in each sea state is larger for the smallest C_x. It is observed that after a certain value, increasing the generator speed threshold does not affect the power generation and this appears as a maximum for the cases of $C_x = 5$ and 10 , and a minimum for the $C_x = 20$ in the average curve of each sea state. Figure 6-27 shows that in the cases of $C_x = 5$ and 10 , the maximum power generation occurs in the sea states with a peak period smaller than 8 seconds, while for the WEC with $C_x = 20$ the maximum power generation can be obtained in the T_p larger than 8 seconds.

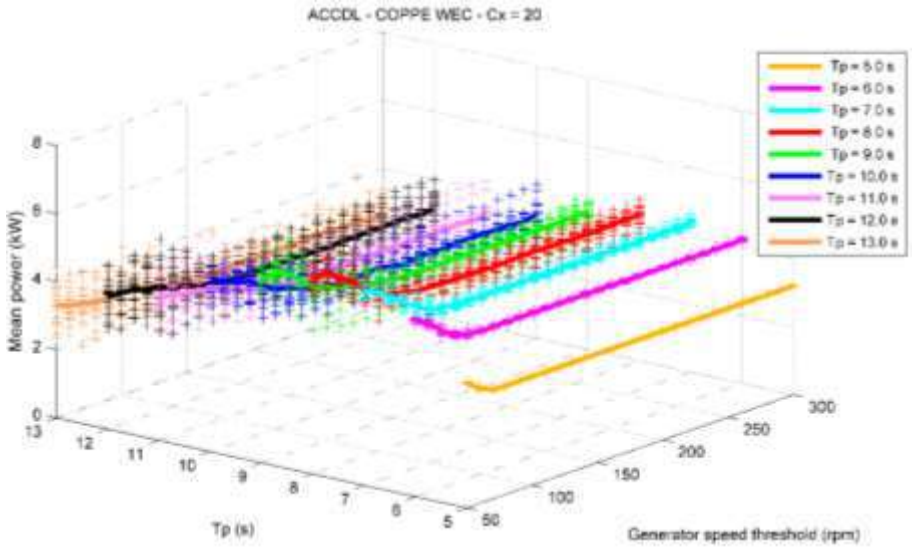

a)

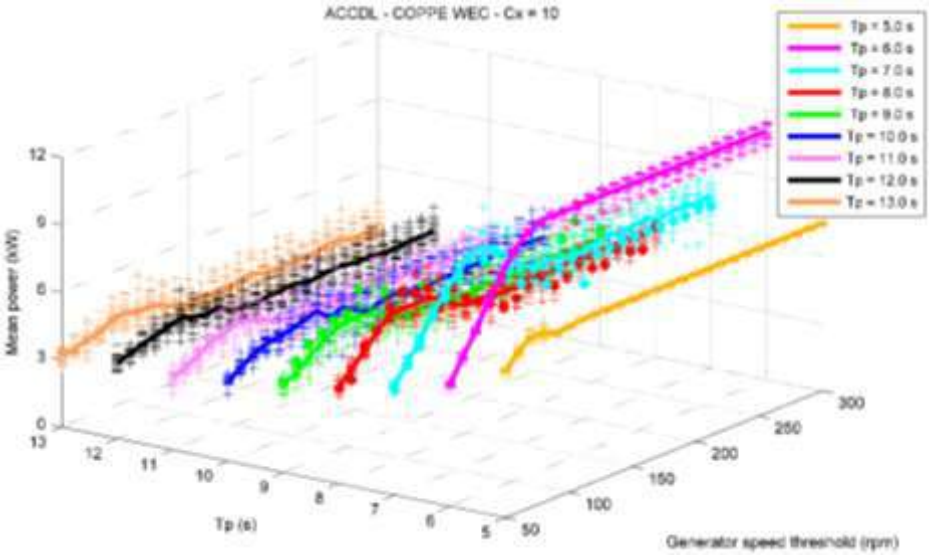

b)

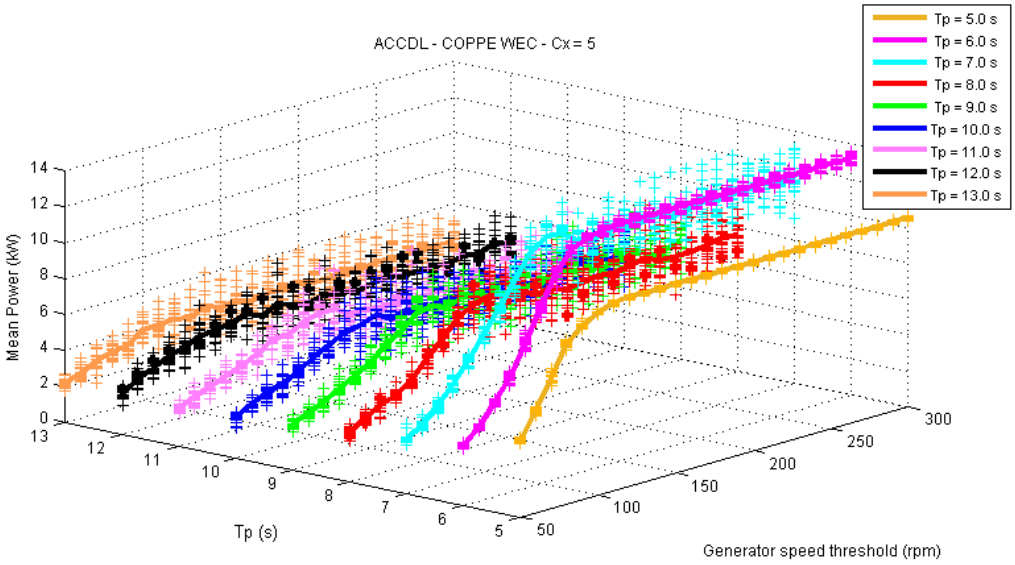

c)

Figure 6-27 - The mean power (kW) of the COPPE nearshore WEC considering an adapted constrained constant-delay latching model for different sea states, $T_p = 5 - 13\ s$ and $H_s = 1.33\ m$, and three different speed multiplier coefficients of $C_x = 5, 10$ and 20. The buoys performances are plotted for 20 different series of wave random phases in each sea state. The solid line connects the average values of theses 20 mean power in the corresponding sea state.

Figure 6-28 shows the average lines of the generated power. The higher level of power is obtained in the sea states with a peak period smaller than 7 seconds. It can be seen that the optimum value of the generator speed threshold are about 50, 120 and 140 rpm for the $C_x = 20, 10$ and 5 and the maximum power generation can be obtained applying a generator speed multiplier coefficient of $C_x = 5$. Note that to optimize the performance of the COPPE nearshore WEC, the objective should be the maximization of the produced power by the device in the range of the energetic waves of the local sea, which is between 9 and 13 seconds (see figure 6-5). It can be seen that the generated power of the three systems in the mentioned range of sea state does not vary significantly leading to a more stable power output. It can be considered as an advantage of the application of the ACCDL control strategy.

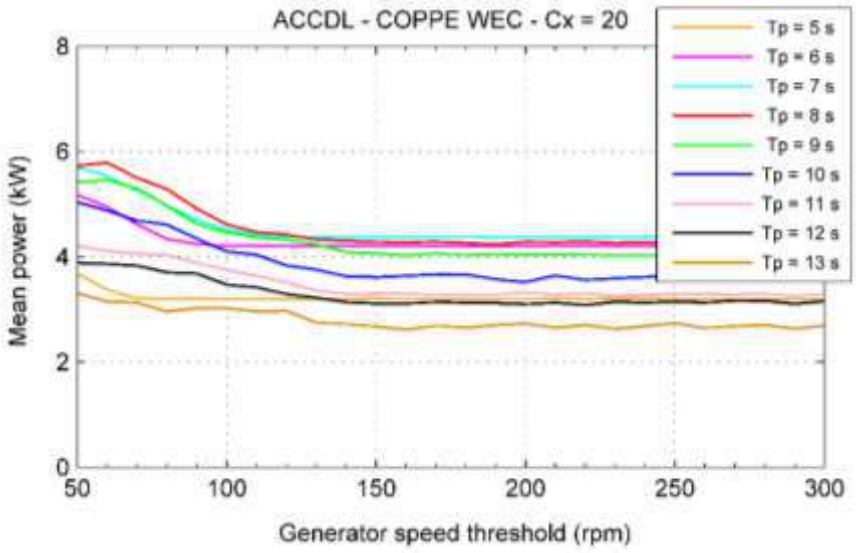

a)

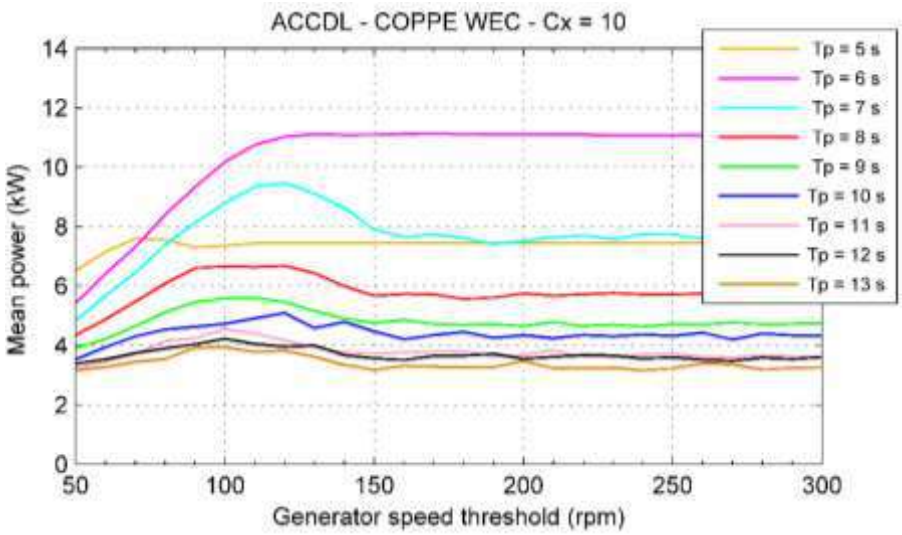

b)

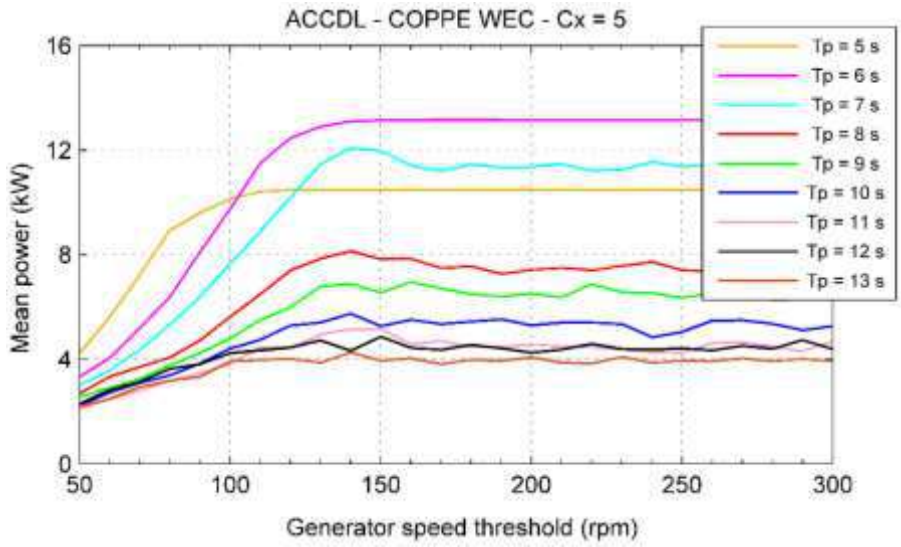

c)

Figure 6-28 – The average of the mean power (kW) for 20 different series of wave random phases in each sea state versus the generator speed threshold (rpm). The results are shown for the adapted constrained constant-delay latching model of the COPPE nearshore WEC considering a significant wave height of $H_s = 1.33\ m$.

Figure 6-29 illustrates the average generator speed of the ACCDL COPPE WEC for different sea states. In the case of $C_x = 20$, in each sea state, the average generator speed slightly changes by increasing the threshold value. In the other two devices, the average generator speed increases up to a certain value and continues as a constant value for the larger thresholds. For instance, as it is shown in figure 6-29-b, the average generator speed range corresponding to the optimum threshold (110 rpm) is about 100 to 125 rpm. Increasing the threshold to a rotation equal to 150 rpm results a larger range of average generator speed of 100 to 215 rpm, however, it leads to a slight reduction in power generation. This is because that there are more moments of "No operational PTO" in which, the generator speed is larger than the upper bound of the PTO limit (400 rpm) and the power generation is zero. To better understand the behavior of the device, the ACCDL COPPE WEC model of $C_x = 10$ for two values of the generator speed threshold (GST) is simulated considering an irregular wave of $T_p = 7\ s$ and $H_s = 1.33\ m$, figure 6-30. It can be observed that, there are five times of the "No operational PTO" moments in the case of $GST = 150\ rpm$. This situation occurs only two times in the case of applying the optimum generator speed threshold, $GST = 110\ rpm$. Moreover, the duration of the

moment of zero power generation is smaller for the optimum model leading to a higher and smoother power generation.

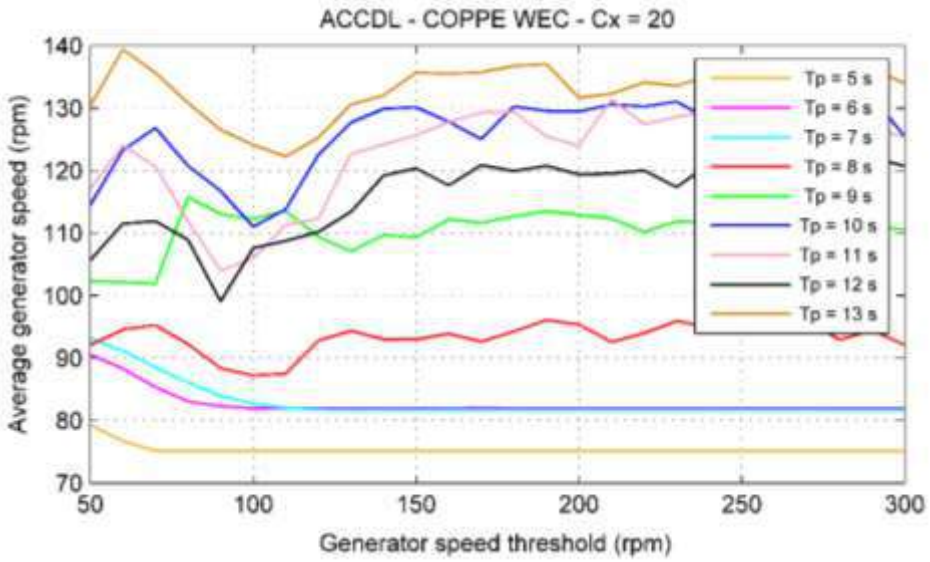

a)

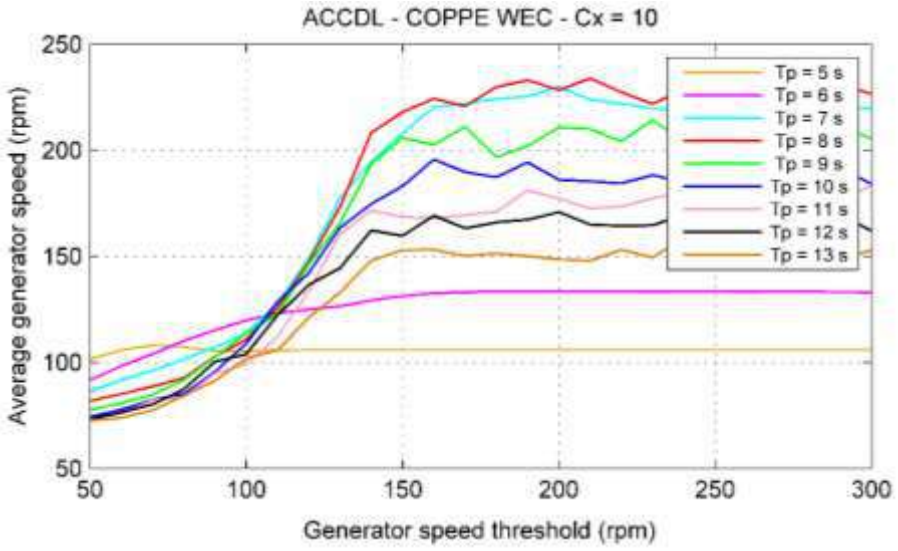

b)

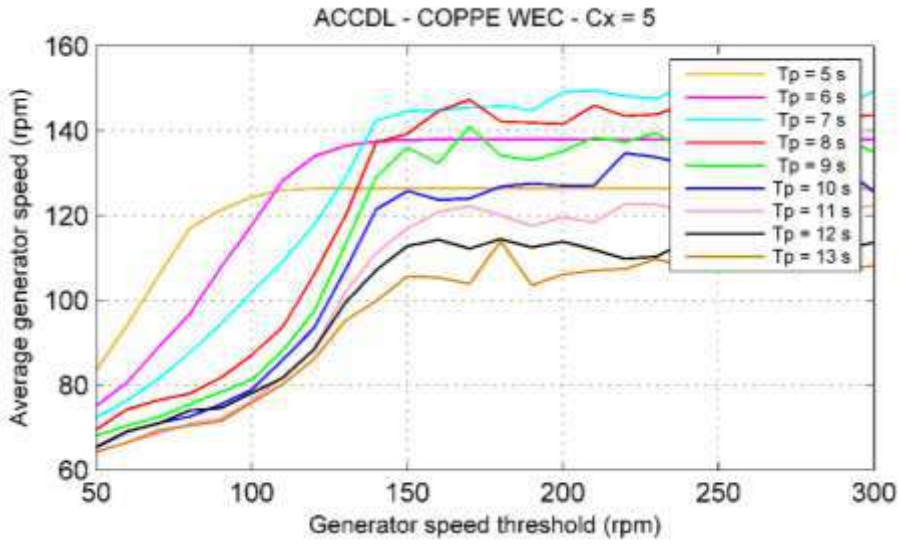

c)

Figure 6-29 - The average generator speed (rpm) for 20 different series of wave random phases in each sea state versus the generator speed threshold (rpm). The results are shown for the adapted constrained constant-delay latching model of the COPPE nearshore WEC considering a significant wave height of $H_s = 1.33\ m$.

.

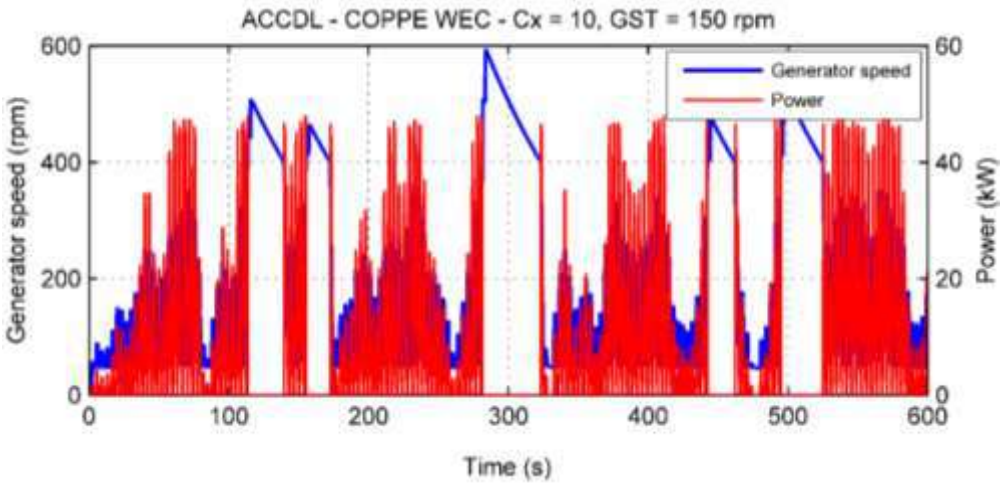

a)

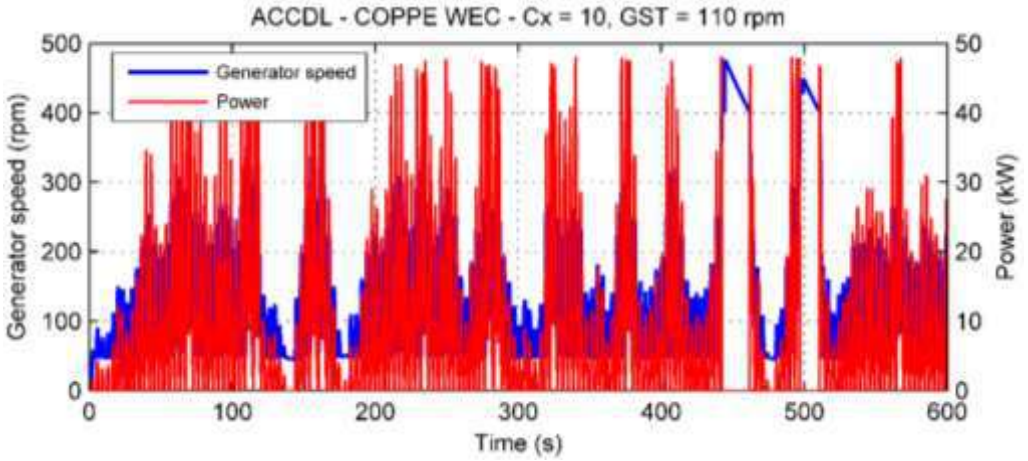

b)

Figure 6-30 - The instantaneous generator speed (rpm) and power generation (kW) of the adapted constrained constant-delay latching COPPE nearshore WEC model of $C_x = 10$ for a generator speed threshold equal to; a) 150 rpm, and b) 110 rpm. The simulations are performed in an irregular wave of $T_p = 7$ s and $H_s = 1.33$ m.

The maximum latching force of the buoy in each sea state for different values of the generator speed threshold is plotted in figure 6-31. This maximum force is the mean value of the forces calculated for the twenty different wave random phase in each sea state. The results show that as the generator speed threshold becomes larger the latching force increases and it continues until the force value reaches to a maximum and after that, it tends to a constant level.

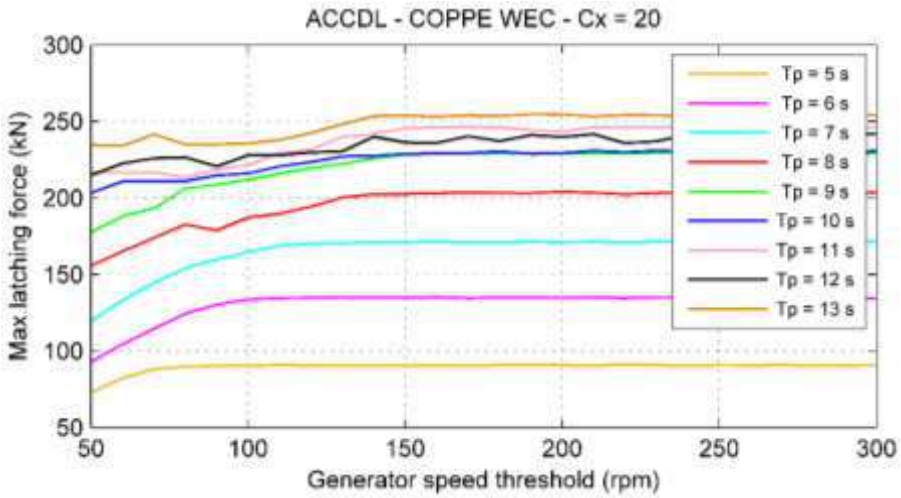

a)

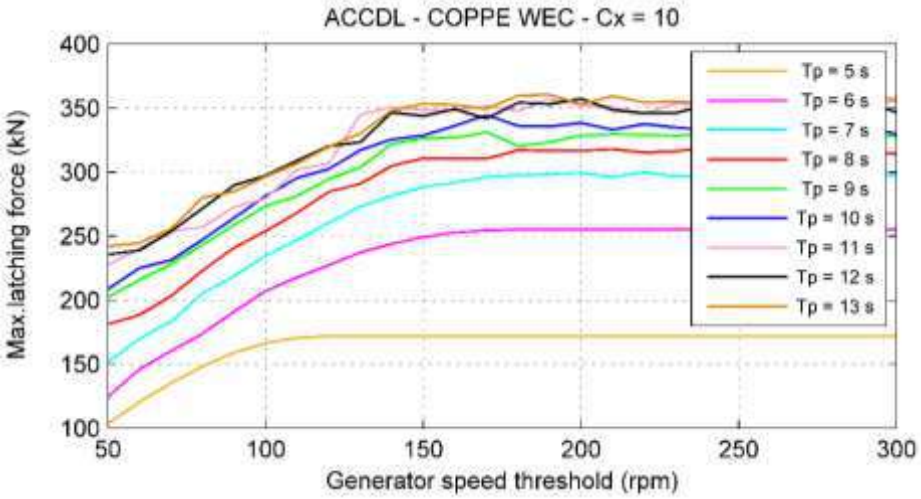

b)

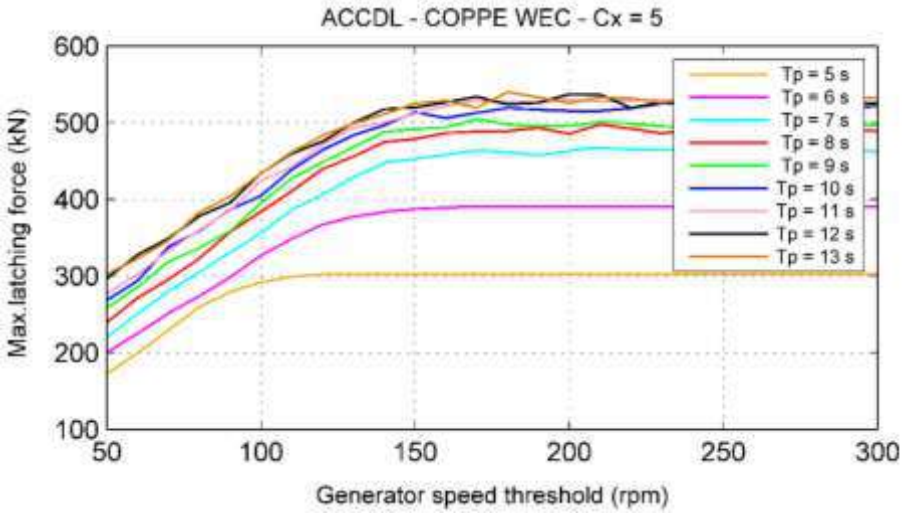

c)

Figure 6-31 - The average generator speed (rpm) for 20 different series of wave random phases in each sea state versus the generator speed threshold (rpm). The results are shown for the adapted constrained constant-delay latching model of the COPPE nearshore WEC considering a significant wave height of $H_s = 1.33\ m$.

As it can be seen, the latching force is sensitive to the sea state peak period and higher forces are required to halt the buoy in the sea states with larger peak period. In the other hand, comparing the WECs with different C_x shows that the latching force decreases with the increase of the speed multiplier coefficient. The higher C_x makes the PTO system to apply more forces on the buoy and consequently decreases the buoy heave displacement.

This leads to a lower hydrostatic force that is the predominant term in the equation of the latching force (see section 6.5.3.3).

The results of the CCDL and the optimum adapted CCDL in a range of the sea states with a significant wave height of $H_s = 1.33\,m$ are plotted in figure 6-32-a to c. It is shown that applying an optimum ACCDL control increases the power generation and it decreases with the increase of the seas state peak period. Considering the plots a and b, it can be observed that the application of the CCDL control results in an excessive amplification of the generator speed that not only does not improve the power production, but also may lead to the PTO system failure. Applying the ACCDL control prevents the exaggerated increase of the generator speed and leads to a higher power generation level by decreasing the "No operational PTO" moments during the buoy oscillation. It can be seen that the PTO system of $C_x = 20$ has the lowest level of the generators speed and the same level of speed values are obtained for both CCDL and ACCDL cases. It is due to the high PTO forces applied on the buoy that diminish the buoy motion in heave direction. In other words, in this situation the large electro-mechanical damping of the PTO system overdamps the buoy motion and leaves it insensitive to the control system. The PTO force values versus the buoy displacement in heave for the CCDL and optimum ACCDL models are shown in figure 6-33-a to c. The simulations are performed in an irregular wave of $T_p = 8\,s$ and $H_s = 1.33\,m$.

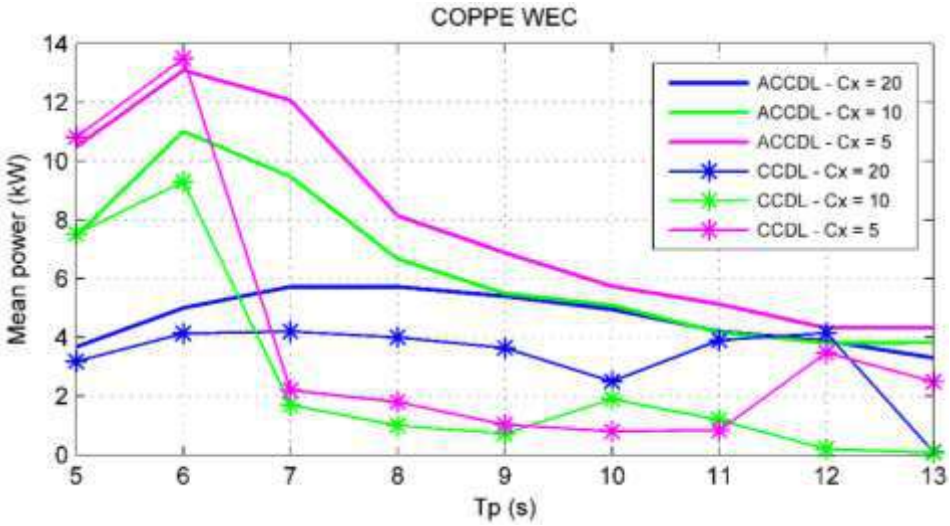

a)

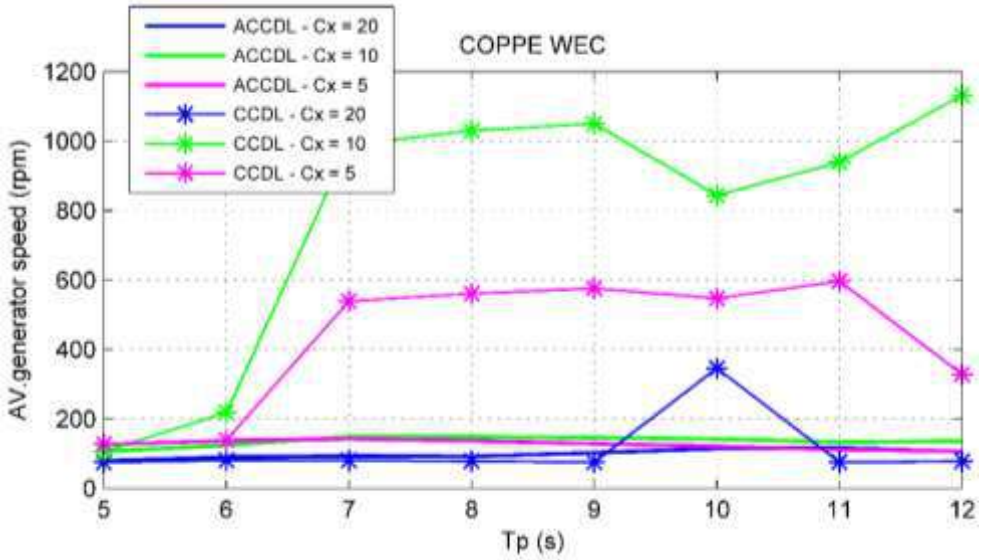

b)

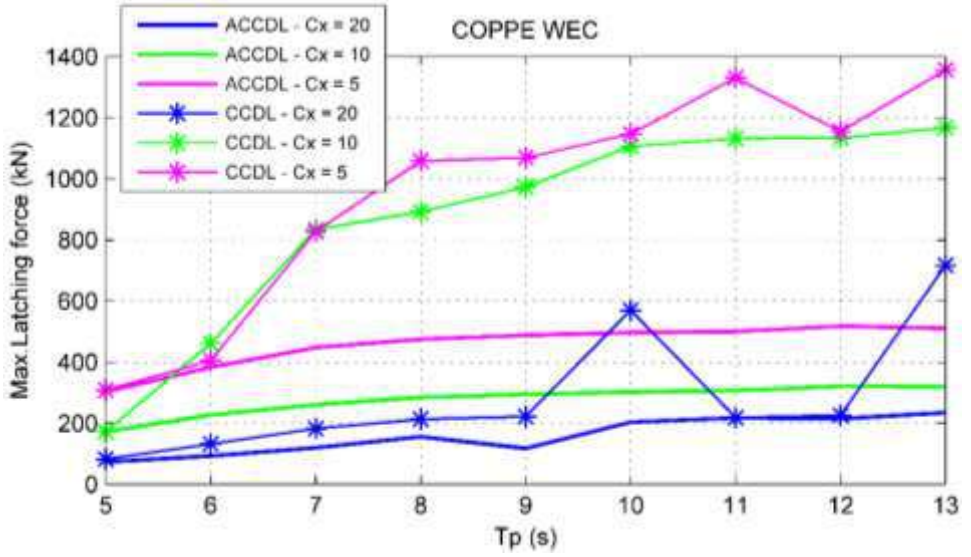

c)

Figure 6-32 – The a) mean power, b) average generator speed and c) maximum latching force of the COPPE nearshore WEC applying the CCDL and optimum ACCDL control strategy. The simulations are performed for three different speed multiplier coefficients, C_x, in a range of sea states with a significant wave height of $H_s = 1.33\ m$. The ACCDL results represent the average of the value corresponding to the twenty different wave random phase in each sea state.

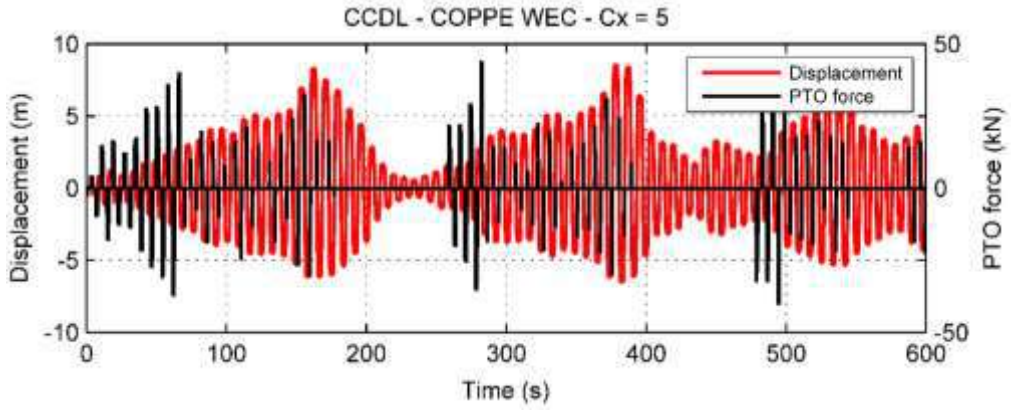
CCDL - COPPE WEC - Cx = 5
Displacement
PTO force
Displacement (m)
PTO force (kN)
Time (s)

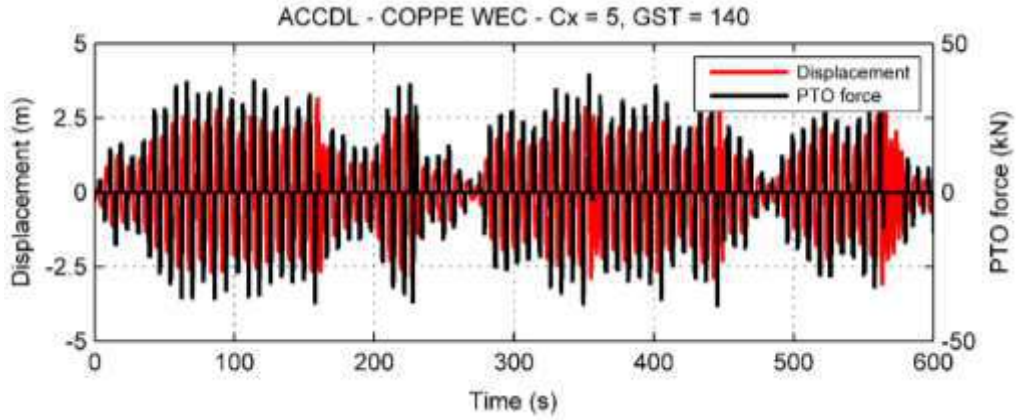
ACCDL - COPPE WEC - Cx = 5, GST = 140
Displacement
PTO force
Displacement (m)
PTO force (kN)
Time (s)

a)

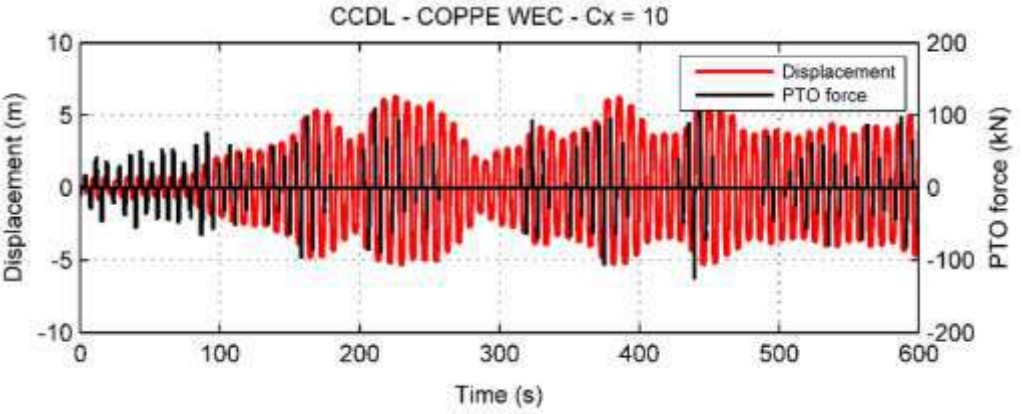
CCDL - COPPE WEC - Cx = 10
Displacement
PTO force
Displacement (m)
PTO force (kN)
Time (s)

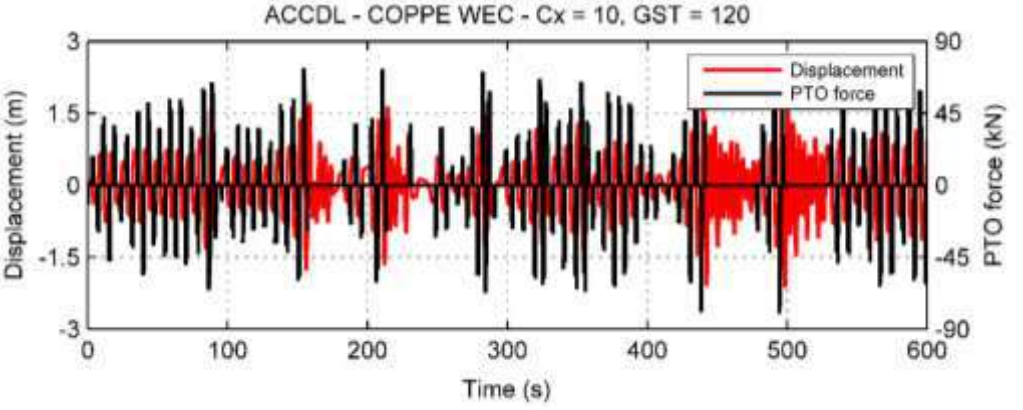
ACCDL - COPPE WEC - Cx = 10, GST = 120
Displacement
PTO force
Displacement (m)
PTO force (kN)
Time (s)

b)

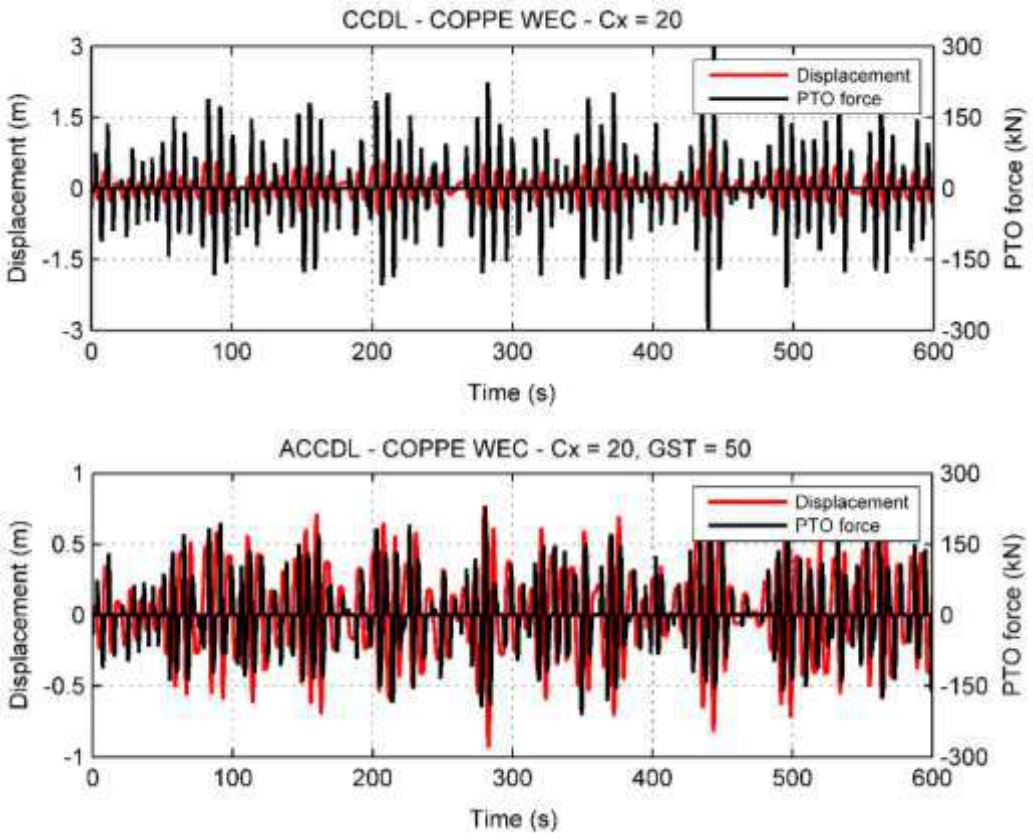

c)

Figure 6-33 – The displacement in heave and the PTO force of the COPPE nearshore WEC applying the CCDL and the optimum ACCDL for three different speed multiplier coefficients C_x . The simulations are performed for an irregular wave of $T_p = 8\ s$ and $H_s = 1.33\ m$.

As it is shown in figure 6-33, applying the ACCDL control strategy decreases the buoy displacement. Therefore, comparing to the CCDL model, higher power production is achieved by smaller motion amplitudes. It implies that the optimum amplitude of the oscillation can be obtained through the application of an optimum ACCDL strategy and it helps the COPPE WEC to efficiently absorb the wave energy and converts it into electricity.

Figure 6-28-c shows the maximum latching force for each model. In the case of $C_x = 5$ and 10, the latching force resulting from the application of the CCDL control are higher comparing to the ACCDL models. However, in the case of $C_x = 20$, the resulting latching force of two models (CCDL and ACCDL) does not change significantly except for the sea states of $T_p = 10$ and 13 s. Numerically, it can be explained that the optimum phase condition (the phase of the buoy velocity is equal to the incoming wave excitation phase) is fully satisfied, in certain moments during the simulation, between the buoy oscillation

and a wave with a large excitation force. This results in a large displacement and consequently large hydrostatic and latching force. However, it should be kept in mind that the latching force value changes for different wave random phases and these changes are more significant for the sea states with larger peak period. In addition, it can be observed that, in the case of applying an ACCDL control, the latching mechanism must provide higher forces in a model that produces higher level of electrical power. Therefore, in practice, the capacity of the latching mechanism can impose some limits on the WEC and consequently affect the power generation.

6.5.5 Annual energy production (AEP)

A detailed explanation of the AEP calculation is presented in chapter five, section 5.10. It is applied in this section to calculate the mechanical and electrical power matrices and the rated power of the COPPE nearshore WEC. The simulations are performed for the CCF, CCDL and ACCDL models considering three values of speed multiplier coefficients of $C_x = 5, 10$ and 20. Additionally, the annual power production of the COPPE WEC buoy applying a pure damper as the PTO system is calculated and the results are compared to the other models. It helps us to address the effect of the PTO system in the annual power production. An efficiency coefficient of 0.8, provided by the manufacturer, is considered for the PTO device. The operational availability and the transmission efficiency coefficients are equal to 0.95 and 1, respectively. A capacity factor of 30% is applied to calculate the AEP, noting that a detailed study are required to calculate the exact value of the capacity factor. Figure 6-34 describes the wave distribution of the local sea (nearshore Rio de Janeiro) which is based on a numerical method that is explained in chapter four, section 4.3.2. Figure 6-35 to 6-37 show the Annual energy production matrices for the COPPE nearshore WEC applying the CCF, CCDL and the optimum ACDL models for three speed multiplier coefficients of $C_x = 5, 10$ and 20. Figure 6-38 illustrates the annual power calculation of the COPPE WEC buoy applying pure damper PTO. It is assumed that the latching duration is tuned to each sea state using the Eq.(5.1).

		Tp (s)												
		4	5	6	7	8	9	10	11	12	13	14	15	16
Hs (m)	0.25	0.6	2	8.4	84	79.8	35	19	18	5.8	1.2	3	2	1.6
	0.75	7.6	23.8	101	602.2	866.6	456	376	280.8	169.4	84	32.8	12.2	3.4
	1.25	0.8	12.8	50.8	199.2	483.6	480.8	492	404.4	279	137	51.8	15	10.2
	1.75	0	0.4	19.4	70.2	154.8	201.8	287	350	215.2	141.2	42.6	9.8	4
	2.25	0	0	0.6	14	63.6	97.4	147	174	162	82.8	22.8	9.8	11.2
	2.75	0	0	0	1.4	17.8	29.6	50	69	97.8	72.8	25.6	6.8	8.4
	3.25	0	0	0	0	0.4	10	11	20	39.6	31	26	7	1.8
	3.75	0	0	0	0	0	0	5	4.4	10.6	15.4	4.4	1.2	0.2
	4.25	0	0	0	0	0	0	0	0.2	4.8	3.8	0.6	0	0.6
	4.75	0	0	0	0	0	0	0	0	0	1.2	0.6	0.8	0

Figure 6-34 – Matrix representation of the number of occurrence of the sea waves for the nearshore region of Rio de Janeiro

		AMPM - CCF - COPPE WEC - Cx = 5												
		Tp (s)												
		4	5	6	7	8	9	10	11	12	13	14	15	16
Hs (m)	0.25	0.02	0.00	0.00	0.00	0.00	0.00	0.00	0.00	0.00	0.00	0.00	0.00	0.00
	0.75	17.75	18.19	42.18	124.60	76.23	15.24	4.28	2.60	2.28	1.67	0.84	0.39	0.13
	1.25	5.30	31.39	77.56	191.01	291.08	181.79	116.81	64.98	33.60	14.13	5.09	1.57	1.23
	1.75	0.00	1.97	61.04	144.59	214.04	192.59	191.78	175.01	84.74	46.61	12.66	2.77	1.14
	2.25	0.00	0.00	3.16	49.17	153.26	167.16	184.52	169.76	129.45	56.58	13.92	5.66	6.53
	2.75	0.00	0.00	0.00	7.43	65.65	79.00	99.70	109.03	128.54	82.82	23.32	4.56	4.54
	3.25	0.00	0.00	0.00	0.00	2.09	38.06	31.61	46.00	76.33	43.87	28.87	6.29	1.13
	3.75	0.00	0.00	0.00	0.00	0.00	0.00	19.41	13.72	24.97	28.00	6.43	1.26	0.17
	4.25	0.00	0.00	0.00	0.00	0.00	0.00	0.00	0.77	14.05	8.73	1.03	0.00	0.65
	4.75	0.00	0.00	0.00	0.00	0.00	0.00	0.00	0.00	0.00	3.22	1.28	1.35	0.00
												AEP (kWh)		3343.56

		EPM - CCF - COPPE WEC - Cx = 5												
		Tp (s)												
		4	5	6	7	8	9	10	11	12	13	14	15	16
Hs (m)	0.25	0.03	0.00	0.00	0.00	0.00	0.00	0.00	0.00	0.00	0.00	0.00	0.00	0.00
	0.75	1.48	0.76	0.42	0.21	0.09	0.03	0.01	0.01	0.01	0.02	0.03	0.03	0.04
	1.25	1.48	1.48	1.48	0.96	0.60	0.38	0.24	0.16	0.12	0.10	0.10	0.10	0.12
	1.75	0.00	1.48	1.48	1.48	1.38	0.95	0.67	0.50	0.39	0.33	0.30	0.28	0.28
	2.25	0.00	0.00	1.48	1.48	1.48	1.48	1.26	0.98	0.80	0.68	0.61	0.58	0.58
	2.75	0.00	0.00	0.00	1.48	1.48	1.48	1.48	1.48	1.31	1.14	0.91	0.67	0.54
	3.25	0.00	0.00	0.00	0.00	1.48	1.48	1.48	1.48	1.48	1.42	1.11	0.90	0.63
	3.75	0.00	0.00	0.00	0.00	0.00	0.00	1.48	1.48	1.48	1.48	1.46	1.05	0.84
	4.25	0.00	0.00	0.00	0.00	0.00	0.00	0.00	1.48	1.48	1.48	1.48	0.00	1.08
	4.75	0.00	0.00	0.00	0.00	0.00	0.00	0.00	0.00	0.00	1.48	1.48	1.48	0.00
												Rated power (kW)		1.48

a)

		AMPM - CCF - COPPE WEC - Cx = 10												
		Tp (s)												
		4	5	6	7	8	9	10	11	12	13	14	15	16
Hs (m)	0.25	0.16	0.17	0.25	0.24	0.00	0.00	0.00	0.00	0.01	0.00	0.01	0.01	0.01
	0.75	14.22	30.86	93.03	388.63	390.54	145.34	83.75	44.32	20.05	7.94	2.67	0.92	0.27
	1.25	3.75	50.02	145.31	417.92	756.79	581.22	459.10	301.41	166.26	68.47	22.38	5.79	3.68
	1.75	0.00	3.20	112.70	305.22	513.11	525.00	588.63	595.41	306.58	173.65	45.43	8.66	2.84
	2.25	0.00	0.00	5.80	102.56	359.41	436.78	525.03	518.12	409.93	168.74	38.56	12.52	11.74
	2.75	0.00	0.00	0.00	12.28	151.15	201.79	274.32	309.13	355.05	210.91	61.14	13.27	13.75
	3.25	0.00	0.00	0.00	0.00	3.44	91.47	84.13	123.33	193.59	124.85	85.89	19.14	4.15
	3.75	0.00	0.00	0.00	0.00	0.00	0.00	45.93	34.00	66.21	80.00	18.98	4.33	0.61
	4.25	0.00	0.00	0.00	0.00	0.00	0.00	0.00	1.72	35.41	23.45	3.27	0.00	2.20
	4.75	0.00	0.00	0.00	0.00	0.00	0.00	0.00	0.00	0.00	8.19	3.73	4.11	0.00
												AEP (kWh)		9618.49

		EPM - CCF - COPPE WEC - Cx = 10												
		Tp (s)												
		4	5	6	7	8	9	10	11	12	13	14	15	16
Hs (m)	0.25	0.26	0.08	0.03	0.00	0.00	0.00	0.00	0.00	0.00	0.00	0.00	0.00	0.01
	0.75	1.87	1.30	0.92	0.65	0.45	0.32	0.22	0.16	0.12	0.09	0.08	0.08	0.08
	1.25	4.60	3.91	2.86	2.10	1.56	1.21	0.93	0.75	0.60	0.50	0.43	0.39	0.36
	1.75	0.00	4.60	4.60	4.35	3.31	2.60	2.05	1.70	1.42	1.23	1.07	0.88	0.71
	2.25	0.00	0.00	4.60	4.60	4.60	4.48	3.57	2.98	2.53	2.04	1.69	1.28	1.05
	2.75	0.00	0.00	0.00	4.60	4.60	4.60	4.60	4.48	3.63	2.90	2.39	1.95	1.64
	3.25	0.00	0.00	0.00	0.00	4.60	4.60	4.60	4.60	4.60	4.03	3.30	2.73	2.30
	3.75	0.00	0.00	0.00	0.00	0.00	0.00	4.60	4.60	4.60	4.60	4.31	3.61	3.03
	4.25	0.00	0.00	0.00	0.00	0.00	0.00	0.00	4.60	4.60	4.60	4.60	0.00	3.66
	4.75	0.00	0.00	0.00	0.00	0.00	0.00	0.00	0.00	0.00	4.60	4.60	4.60	0.00
												Rated power (kW)		4.6

b)

		AMPM - CCF - COPPE WEC - Cx = 20												
		Tp (s)												
		4	5	6	7	8	9	10	11	12	13	14	15	16
Hs (m)	0.25	0.12	0.28	0.90	6.15	3.53	0.80	0.17	0.05	0.01	0.00	0.00	0.00	0.00
	0.75	6.75	33.62	160.50	929.08	1216.55	542.15	370.09	232.54	110.95	44.17	14.34	4.47	0.95
	1.25	1.61	47.91	232.46	921.07	2099.53	1837.24	1621.03	1147.45	682.28	293.79	99.36	25.46	15.44
	1.75	0.00	2.89	174.97	650.19	1276.58	1558.44	1919.21	2063.07	1093.45	635.35	172.28	35.43	13.12
	2.25	0.00	0.00	0.00	0.00	0.00	0.00	709.50	1296.94	1178.13	581.42	156.24	60.67	62.85
	2.75	0.00	0.00	0.00	0.00	0.00	0.00	0.00	243.86	447.02	537.94	195.50	54.34	63.17
	3.25	0.00	0.00	0.00	0.00	0.00	0.00	0.00	0.00	48.28	113.64	142.29	43.79	12.56
	3.75	0.00	0.00	0.00	0.00	0.00	0.00	0.00	0.00	0.00	8.88	11.39	4.88	1.22
	4.25	0.00	0.00	0.00	0.00	0.00	0.00	0.00	0.00	0.00	0.00	0.14	0.00	1.50
	4.75	0.00	0.00	0.00	0.00	0.00	0.00	0.00	0.00	0.00	0.00	0.00	0.20	0.00
												AEP (kWh)		21515.32

		EPM - CCF - COPPE WEC - Cx = 20												
		Tp (s)												
		4	5	6	7	8	9	10	11	12	13	14	15	16
Hs (m)	0.25	0.19	0.14	0.11	0.07	0.04	0.02	0.01	0.00	0.00	0.00	0.00	0.00	0.00
	0.75	0.89	1.41	1.59	1.54	1.40	1.19	0.98	0.83	0.65	0.53	0.44	0.37	0.28
	1.25	2.01	3.74	4.58	4.62	4.34	3.82	3.29	2.84	2.45	2.14	1.92	1.70	1.51
	1.75	0.00	7.23	9.02	9.26	8.25	7.72	6.70	5.89	5.08	4.50	4.04	3.62	3.28
	2.25	0.00	0.00	0.00	0.00	0.00	0.00	4.83	7.45	7.27	7.02	6.85	6.19	5.61
	2.75	0.00	0.00	0.00	0.00	0.00	0.00	0.00	3.53	4.57	7.39	7.64	7.99	7.52
	3.25	0.00	0.00	0.00	0.00	0.00	0.00	0.00	0.00	1.22	3.67	5.47	6.26	6.98
	3.75	0.00	0.00	0.00	0.00	0.00	0.00	0.00	0.00	0.00	0.58	2.59	4.07	6.10
	4.25	0.00	0.00	0.00	0.00	0.00	0.00	0.00	0.00	0.00	0.00	0.23	0.00	2.49
	4.75	0.00	0.00	0.00	0.00	0.00	0.00	0.00	0.00	0.00	0.00	0.00	0.25	0.00
												Rated power (kW)		10.76

c)

Figure 6-35 – The annual mechanical power and electrical power matrices of the COPPE nearshore WEC - CCF model for three speed multiplier coefficients of $C_x = a)\ 5, b)\ 10$ and $c)\ 20$.

		AMPM - CCDL - COPPE WEC - Cx = 5												
		Tp (s)												
		4	5	6	7	8	9	10	11	12	13	14	15	16
Hs (m)	0.25	0.02	0.81	0.74	13.96	15.80	8.55	7.73	5.90	2.38	0.60	1.37	1.40	0.66
	0.75	18.22	87.27	396.23	2668.21	3739.86	1790.99	1628.75	960.77	762.28	409.47	105.92	32.95	7.87
	1.25	5.44	125.40	597.88	0.00	513.86	0.00	353.81	156.70	815.12	516.88	91.55	42.25	11.03
	1.75	0.00	7.45	0.00	0.00	0.00	96.04	285.68	50.22	251.56	55.50	35.66	0.45	2.86
	2.25	0.00	0.00	0.00	0.00	0.00	0.00	72.56	0.00	0.00	137.87	0.00	0.00	0.46
	2.75	0.00	0.00	0.00	0.00	0.00	0.00	0.00	0.00	0.00	0.00	0.00	0.00	10.26
	3.25	0.00	0.00	0.00	0.00	0.00	0.00	0.00	2.52	0.00	0.00	0.00	0.00	0.00
	3.75	0.00	0.00	0.00	0.00	0.00	0.00	0.00	0.00	0.00	0.00	0.00	0.00	0.05
	4.25	0.00	0.00	0.00	0.00	0.00	0.00	0.00	0.00	0.00	0.00	0.00	0.00	0.00
	4.75	0.00	0.00	0.00	0.00	0.00	0.00	0.00	0.00	0.00	0.34	0.00	0.00	0.00
												AEP (kwh)		12866.3

		EPM - CCDL - COPPE WEC - Cx = 5												
		Tp (s)												
		4	5	6	7	8	9	10	11	12	13	14	15	16
Hs (m)	0.25	0.03	0.41	0.09	0.17	0.20	0.24	0.40	0.33	0.41	0.50	0.46	0.70	0.41
	0.75	2.40	3.67	3.92	4.43	4.32	3.93	4.33	3.42	4.50	4.87	3.23	2.70	2.31
	1.25	6.30	6.30	6.30	0.00	1.06	0.00	0.72	0.39	2.92	3.77	1.77	2.82	1.08
	1.75	0.00	6.30	0.00	0.00	0.00	0.48	1.00	0.14	1.17	0.39	0.84	0.05	0.71
	2.25	0.00	0.00	0.00	0.00	0.00	0.00	0.49	0.00	0.00	1.67	0.00	0.00	0.04
	2.75	0.00	0.00	0.00	0.00	0.00	0.00	0.00	0.00	0.00	0.00	0.00	0.00	1.22
	3.25	0.00	0.00	0.00	0.00	0.00	0.00	0.00	0.13	0.00	0.00	0.00	0.00	0.00
	3.75	0.00	0.00	0.00	0.00	0.00	0.00	0.00	0.00	0.00	0.00	0.00	0.00	0.26
	4.25	0.00	0.00	0.00	0.00	0.00	0.00	0.00	0.00	0.00	0.00	0.00	0.00	0.00
	4.75	0.00	0.00	0.00	0.00	0.00	0.00	0.00	0.00	0.00	0.28	0.00	0.00	0.00
												Rated Power (kW)		6.3

a)

		AMPM - CCDL - COPPE WEC - Cx = 10												
		Tp (s)												
		4	5	6	7	8	9	10	11	12	13	14	15	16
Hs (m)	0.25	0.16	0.84	4.28	48.79	50.08	19.69	10.44	8.15	2.46	0.51	0.92	0.57	0.57
	0.75	14.40	64.28	408.54	2600.41	4040.90	2042.65	1564.79	1174.46	418.44	220.36	115.81	51.86	8.94
	1.25	3.79	86.68	530.83	0.00	0.00	0.00	0.00	0.00	0.00	19.35	0.00	0.00	6.40
	1.75	0.00	0.00	0.00	0.00	0.00	0.00	0.00	0.00	0.00	0.00	0.00	0.00	0.00
	2.25	0.00	0.00	0.00	0.00	0.00	0.00	0.00	0.00	0.00	0.00	0.00	0.00	0.00
	2.75	0.00	0.00	0.00	0.00	0.00	0.00	0.00	0.00	0.00	0.00	0.00	0.00	0.00
	3.25	0.00	0.00	0.00	0.00	0.00	0.00	0.00	0.00	0.00	0.00	0.00	0.00	0.00
	3.75	0.00	0.00	0.00	0.00	0.00	0.00	0.00	0.00	0.00	0.00	0.00	0.00	0.00
	4.25	0.00	0.00	0.00	0.00	0.00	0.00	0.00	0.00	0.00	0.00	0.00	0.00	0.00
	4.75	0.00	0.00	0.00	0.00	0.00	0.00	0.00	0.00	0.00	0.00	0.00	0.00	0.00
												AEP (kwh)		10288.39

		EPM - CCDL - COPPE WEC - Cx = 10												
		Tp (s)												
		4	5	6	7	8	9	10	11	12	13	14	15	16
Hs (m)	0.25	0.26	0.42	0.51	0.58	0.63	0.56	0.54	0.45	0.42	0.42	0.31	0.29	0.36
	0.75	1.89	2.70	4.04	4.32	4.66	4.48	4.16	4.18	2.47	2.62	3.53	4.25	2.63
	1.25	4.74	5.00	5.00	0.00	0.00	0.00	0.00	0.00	0.00	0.14	0.00	0.00	0.63
	1.75	0.00	0.00	0.00	0.00	0.00	0.00	0.00	0.00	0.00	0.00	0.00	0.00	0.00
	2.25	0.00	0.00	0.00	0.00	0.00	0.00	0.00	0.00	0.00	0.00	0.00	0.00	0.00
	2.75	0.00	0.00	0.00	0.00	0.00	0.00	0.00	0.00	0.00	0.00	0.00	0.00	0.00
	3.25	0.00	0.00	0.00	0.00	0.00	0.00	0.00	0.00	0.00	0.00	0.00	0.00	0.00
	3.75	0.00	0.00	0.00	0.00	0.00	0.00	0.00	0.00	0.00	0.00	0.00	0.00	0.00
	4.25	0.00	0.00	0.00	0.00	0.00	0.00	0.00	0.00	0.00	0.00	0.00	0.00	0.00
	4.75	0.00	0.00	0.00	0.00	0.00	0.00	0.00	0.00	0.00	0.00	0.00	0.00	0.00
												Rated Power (kW)		5

b)

		AMPM - CCDL - COPPE WEC - Cx = 20												
		Tp (s)												
		4	5	6	7	8	9	10	11	12	13	14	15	16
Hs (m)	0.25	0.12	0.47	2.45	24.41	22.68	9.35	4.39	4.46	1.18	0.24	0.68	0.40	0.30
	0.75	6.75	28.80	158.09	1000.58	1436.08	670.21	577.43	426.98	275.62	132.68	56.65	13.04	4.84
	1.25	1.61	36.68	192.74	801.64	1874.80	1700.95	1808.45	1539.62	1153.68	0.00	0.00	0.00	0.00
	1.75	0.00	0.00	0.00	0.00	0.00	0.00	0.00	0.00	0.00	0.00	0.00	0.00	2.08
	2.25	0.00	0.00	0.00	0.00	0.00	0.00	0.00	0.00	0.00	0.00	0.00	0.00	0.00
	2.75	0.00	0.00	0.00	0.00	0.00	0.00	0.00	0.00	0.00	0.00	0.00	0.00	0.00
	3.25	0.00	0.00	0.00	0.00	0.00	0.00	0.00	0.00	0.00	0.00	0.00	0.00	0.00
	3.75	0.00	0.00	0.00	0.00	0.00	0.00	0.00	0.00	0.00	0.00	0.00	0.00	0.00
	4.25	0.00	0.00	0.00	0.00	0.00	0.00	0.00	0.00	0.00	0.00	0.00	0.00	0.00
	4.75	0.00	0.00	0.00	0.00	0.00	0.00	0.00	0.00	0.00	0.00	0.00	0.00	0.00
												AEP (kwh)		10631.43

		EPM - CCDL - COPPE WEC - Cx = 20												
		Tp (s)												
		4	5	6	7	8	9	10	11	12	13	14	15	16
Hs (m)	0.25	0.19	0.23	0.29	0.29	0.28	0.27	0.23	0.25	0.20	0.20	0.23	0.20	0.19
	0.75	0.89	1.21	1.57	1.66	1.66	1.47	1.53	1.52	1.63	1.58	1.73	1.07	1.42
	1.25	2.01	2.87	3.79	4.02	3.88	3.54	3.67	3.81	4.14	0.00	0.00	0.00	0.00
	1.75	0.00	0.00	0.00	0.00	0.00	0.00	0.00	0.00	0.00	0.00	0.00	0.00	0.52
	2.25	0.00	0.00	0.00	0.00	0.00	0.00	0.00	0.00	0.00	0.00	0.00	0.00	0.00
	2.75	0.00	0.00	0.00	0.00	0.00	0.00	0.00	0.00	0.00	0.00	0.00	0.00	0.00
	3.25	0.00	0.00	0.00	0.00	0.00	0.00	0.00	0.00	0.00	0.00	0.00	0.00	0.00
	3.75	0.00	0.00	0.00	0.00	0.00	0.00	0.00	0.00	0.00	0.00	0.00	0.00	0.00
	4.25	0.00	0.00	0.00	0.00	0.00	0.00	0.00	0.00	0.00	0.00	0.00	0.00	0.00
	4.75	0.00	0.00	0.00	0.00	0.00	0.00	0.00	0.00	0.00	0.00	0.00	0.00	0.00
												Rated Power (kW)		5.32

c)

Figure 6-36 - The annual mechanical power and electrical power matrices of the COPPE nearshore WEC - CCDL model for three speed multiplier coefficients of $C_x = a)\ 5, b)\ 10$ and $c)\ 20$.

		AMPM - ACCDL - COPPE WEC - Cx = 5												
		Tp (s)												
		4	5	6	7	8	9	10	11	12	13	14	15	16
Hs (m)	0.25	0.02	0.78	1.13	19.10	19.40	11.82	8.51	4.60	2.52	0.52	0.96	1.11	0.48
	0.75	17.79	85.46	408.24	2736.55	4006.53	1978.62	1633.14	946.58	684.66	329.73	78.17	30.50	7.77
	1.25	5.31	122.69	598.68	2463.77	4033.50	3948.13	3370.37	2063.43	1182.64	639.29	176.03	43.66	28.12
	1.75	0.00	7.16	272.25	648.62	1033.81	1072.80	1339.27	1683.11	939.67	618.06	177.31	24.20	11.25
	2.25	0.00	0.00	6.35	109.23	330.05	584.05	848.20	590.60	600.31	320.14	78.27	29.92	30.69
	2.75	0.00	0.00	0.00	9.75	80.88	124.08	227.09	306.15	333.89	192.47	74.16	14.90	21.82
	3.25	0.00	0.00	0.00	0.00	1.27	34.31	32.82	44.14	129.68	55.96	51.97	14.97	3.62
	3.75	0.00	0.00	0.00	0.00	0.00	0.00	17.61	10.00	21.04	33.24	6.22	2.67	0.42
	4.25	0.00	0.00	0.00	0.00	0.00	0.00	0.00	0.48	9.92	8.01	1.05	0.00	0.95
	4.75	0.00	0.00	0.00	0.00	0.00	0.00	0.00	0.00	0.00	1.80	1.30	1.16	0.00
												AEP (kWh)		34178.56

		EPM - ACCDL - COPPE WEC - Cx = 5												
		Tp (s)												
		4	5	6	7	8	9	10	11	12	13	14	15	16
Hs (m)	0.25	0.03	0.39	0.13	0.23	0.24	0.34	0.44	0.26	0.43	0.43	0.32	0.55	0.30
	0.75	2.34	3.59	4.04	4.54	4.62	4.34	4.34	3.37	4.04	3.93	2.38	2.50	2.28
	1.25	6.64	9.58	11.79	12.37	8.34	8.21	6.85	5.10	4.24	4.67	3.40	2.91	2.76
	1.75	0.00	17.10	14.03	9.24	6.68	5.32	4.67	4.81	4.37	4.38	4.16	2.47	2.81
	2.25	0.00	0.00	10.59	7.80	5.19	6.00	5.77	3.39	3.71	3.87	3.43	3.05	2.74
	2.75	0.00	0.00	0.00	6.96	4.54	4.19	4.58	4.44	3.41	2.64	2.90	2.19	2.60
	3.25	0.00	0.00	0.00	0.00	3.16	3.43	3.04	2.21	3.27	1.81	2.00	2.14	2.01
	3.75	0.00	0.00	0.00	0.00	0.00	0.00	3.52	2.27	1.99	2.16	1.41	2.23	2.08
	4.25	0.00	0.00	0.00	0.00	0.00	0.00	0.00	2.38	2.07	2.11	1.75	0.00	1.58
	4.75	0.00	0.00	0.00	0.00	0.00	0.00	0.00	0.00	0.00	1.50	2.16	1.45	0.00
												Rated power (kw)		17.10

a)

		AMPM - ACCDL - COPPE WEC - Cx = 10												
		Tp (s)												
		4	5	6	7	8	9	10	11	12	13	14	15	16
Hs (m)	0.25	0.16	0.83	4.15	47.04	46.06	18.93	9.76	7.24	2.05	0.52	0.70	0.45	0.44
	0.75	14.25	63.41	391.57	2484.64	3679.19	1742.33	1363.78	856.62	489.07	173.71	85.27	32.43	7.23
	1.25	3.75	85.84	499.88	1757.69	3145.52	2347.35	2467.54	1772.67	1277.12	574.15	208.52	43.47	27.03
	1.75	0.00	4.97	188.32	624.90	790.37	1275.41	1113.82	1464.47	846.91	514.05	117.51	27.07	9.52
	2.25	0.00	0.00	1.19	74.86	324.81	433.43	737.31	730.88	447.43	282.96	48.63	21.78	24.39
	2.75	0.00	0.00	0.00	1.97	57.83	56.10	134.51	157.99	247.83	175.18	61.56	14.65	14.87
	3.25	0.00	0.00	0.00	0.00	0.49	21.47	28.64	45.86	54.08	67.36	54.54	11.94	2.34
	3.75	0.00	0.00	0.00	0.00	0.00	0.00	6.15	6.53	17.43	22.95	5.90	1.64	0.18
	4.25	0.00	0.00	0.00	0.00	0.00	0.00	0.00	0.25	5.75	6.13	0.54	0.00	0.71
	4.75	0.00	0.00	0.00	0.00	0.00	0.00	0.00	0.00	0.00	1.22	0.72	0.55	0.00
												AEP (kWh)		28249

		EPM - ACCDL - COPPE WEC - Cx = 10												
		Tp (s)												
		4	5	6	7	8	9	10	11	12	13	14	15	16
Hs (m)	0.25	0.26	0.41	0.49	0.56	0.58	0.54	0.50	0.40	0.35	0.43	0.23	0.23	0.28
	0.75	1.87	2.66	3.88	4.13	4.25	3.82	3.62	3.05	2.89	2.07	2.60	2.66	2.13
	1.25	4.69	6.71	9.84	8.82	6.50	4.88	5.01	4.38	4.58	4.19	4.03	2.90	2.65
	1.75	0.00	12.42	9.71	8.90	5.11	6.32	3.89	4.18	3.94	3.64	2.76	2.76	2.38
	2.25	0.00	0.00	1.98	5.35	5.11	4.45	5.02	4.20	2.76	3.42	2.13	2.22	2.18
	2.75	0.00	0.00	0.00	1.41	3.25	1.90	2.71	2.29	2.53	2.41	2.40	2.15	1.77
	3.25	0.00	0.00	0.00	0.00	1.23	2.15	2.65	2.29	1.37	2.17	2.10	1.71	1.30
	3.75	0.00	0.00	0.00	0.00	0.00	0.00	1.23	1.48	1.64	1.49	1.34	1.37	0.92
	4.25	0.00	0.00	0.00	0.00	0.00	0.00	0.00	1.25	1.20	1.61	0.90	0.00	1.18
	4.75	0.00	0.00	0.00	0.00	0.00	0.00	0.00	0.00	0.00	1.02	1.20	0.69	0.00
												Rated power (kw)		14.13

b)

		AMPM - ACCDL - COPPE WEC - Cx = 20												
		Tp (s)												
		4	5	6	7	8	9	10	11	12	13	14	15	16
Hs (m)	0.25	0.12	0.47	2.45	24.41	22.68	9.35	4.39	4.46	1.18	0.24	0.68	0.40	0.30
	0.75	6.75	28.80	160.28	1111.03	1712.42	826.16	651.07	484.91	248.39	116.72	48.75	15.80	5.32
	1.25	1.61	40.85	233.99	1010.47	2486.25	2554.05	2372.30	1696.25	1008.40	518.21	184.37	49.76	35.58
	1.75	0.00	2.69	176.88	429.39	1067.38	1191.93	1906.68	960.60	973.03	710.13	163.40	35.22	10.39
	2.25	0.00	0.00	0.00	0.00	0.00	0.00	305.89	357.57	534.87	270.90	66.82	31.71	25.09
	2.75	0.00	0.00	0.00	0.00	0.00	0.00	0.00	35.58	217.62	145.46	70.95	17.31	22.14
	3.25	0.00	0.00	0.00	0.00	0.00	0.00	0.00	0.00	30.29	39.35	74.83	19.95	3.75
	3.75	0.00	0.00	0.00	0.00	0.00	0.00	0.00	0.00	0.00	8.94	7.88	2.07	0.34
	4.25	0.00	0.00	0.00	0.00	0.00	0.00	0.00	0.00	0.00	0.00	0.14	0.00	0.43
	4.75	0.00	0.00	0.00	0.00	0.00	0.00	0.00	0.00	0.00	0.00	0.00	0.19	0.00
												AEP (kWh)		21000.41

		EPM - ACCDL - COPPE WEC - Cx = 20												
		Tp (s)												
		4	5	6	7	8	9	10	11	12	13	14	15	16
Hs (m)	0.25	0.19	0.23	0.29	0.29	0.28	0.27	0.23	0.25	0.20	0.20	0.23	0.20	0.19
	0.75	0.89	1.21	1.59	1.84	1.98	1.81	1.73	1.73	1.47	1.39	1.49	1.30	1.57
	1.25	2.01	3.19	4.61	5.07	5.14	5.31	4.82	4.19	3.61	3.78	3.56	3.32	3.49
	1.75	0.00	6.72	9.12	6.12	6.90	5.91	6.65	2.74	4.52	5.03	3.84	3.59	2.60
	2.25	0.00	0.00	0.00	0.00	0.00	0.00	2.08	2.05	3.30	3.27	2.93	3.24	2.24
	2.75	0.00	0.00	0.00	0.00	0.00	0.00	0.00	0.52	2.23	2.00	2.77	2.55	2.64
	3.25	0.00	0.00	0.00	0.00	0.00	0.00	0.00	0.00	0.76	1.27	2.88	2.85	2.08
	3.75	0.00	0.00	0.00	0.00	0.00	0.00	0.00	0.00	0.00	0.58	1.79	1.73	1.72
	4.25	0.00	0.00	0.00	0.00	0.00	0.00	0.00	0.00	0.00	0.00	0.23	0.00	0.72
	4.75	0.00	0.00	0.00	0.00	0.00	0.00	0.00	0.00	0.00	0.00	0.00	0.24	0.00
												Rated power (kw)		10.51

c)

Figure 6-37 - The annual mechanical power and electrical power matrices of the COPPE nearshore WEC - ACCDL model for three speed multiplier coefficients of $C_x = a)\ 5, b)\ 10$ and $c)\ 20$.

		AMPM - COOPE WEC buoy - CDL - pure damper PTO												
		Tp (s)												
		4	5	6	7	8	9	10	11	12	13	14	15	16
Hs (m)	0.25	0.17	0.77	4.39	45.88	46.54	18.81	9.69	7.58	3.44	0.47	1.04	0.82	0.47
	0.75	19.39	82.95	475.28	2960.10	4548.40	2206.11	1704.43	1063.68	901.17	299.32	103.57	45.82	9.29
	1.25	5.67	123.92	664.32	2775.92	7491.52	7877.42	8058.19	5262.22	6085.59	2217.11	602.76	251.64	221.98
	1.75	0.00	7.52	561.05	3145.91	6934.77	8065.31	9827.65	10722.79	7607.53	2803.48	1506.72	102.51	162.10
	2.25	0.00	0.00	34.81	771.01	3272.40	4392.10	5609.49	8651.09	8337.13	3884.80	663.53	207.74	638.12
	2.75	0.00	0.00	0.00	87.21	1032.13	1751.01	3003.75	4568.46	4765.47	4260.00	3215.38	432.94	634.04
	3.25	0.00	0.00	0.00	0.00	24.77	716.59	677.17	1280.57	4471.24	2768.88	2023.41	551.45	142.98
	3.75	0.00	0.00	0.00	0.00	0.00	0.00	441.20	363.61	941.63	1490.55	314.39	72.17	17.71
	4.25	0.00	0.00	0.00	0.00	0.00	0.00	0.00	21.28	333.81	497.38	48.59	0.00	58.53
	4.75	0.00	0.00	0.00	0.00	0.00	0.00	0.00	0.00	0.00	181.07	50.00	54.05	0.00
												AEP (kWh)		141081.7

	EPM - COOPE WEC buoy - CDL - pure damper PTO												
	Tp (s)												
	4	5	6	7	8	9	10	11	12	13	14	15	16
0.25	0.28	0.39	0.52	0.55	0.58	0.54	0.50	0.42	0.59	0.39	0.35	0.41	0.29
0.75	2.55	3.49	4.71	4.92	5.25	4.84	4.53	3.79	5.32	3.56	3.16	3.76	2.73
1.25	7.09	9.68	13.08	13.94	15.49	16.38	16.37	13.01	21.81	16.18	11.64	16.78	21.76
1.75	0.00	18.80	28.92	44.81	44.80	39.97	34.29	30.64	35.35	19.85	35.37	10.46	40.53
2.25	0.00	0.00	58.02	55.07	51.45	45.09	38.16	49.72	51.46	46.92	29.10	21.20	56.98
2.75	0.00	0.00	0.00	62.29	57.98	59.16	60.56	66.21	48.73	58.52	68.50	63.67	68.50
3.25	0.00	0.00	0.00	0.00	61.93	68.50	62.70	64.03	68.50	68.50	68.50	68.50	68.50
3.75	0.00	0.00	0.00	0.00	0.00	0.00	68.50	68.50	68.50	68.50	68.50	60.14	68.50
4.25	0.00	0.00	0.00	0.00	0.00	0.00	0.00	68.50	68.50	68.50	68.50	0.00	68.50
4.75	0.00	0.00	0.00	0.00	0.00	0.00	0.00	0.00	0.00	68.50	68.50	67.56	0.00
											Rated power (kw)		68.5

Figure 6-38 - The annual mechanical power and electrical power matrices of the COPPE nearshore WEC applying a tuned constant-delay latching (CDL) control and a pure damper as PTO system.

Figure 6-39 shows the bar graph of the AEP values of the wave converter device.

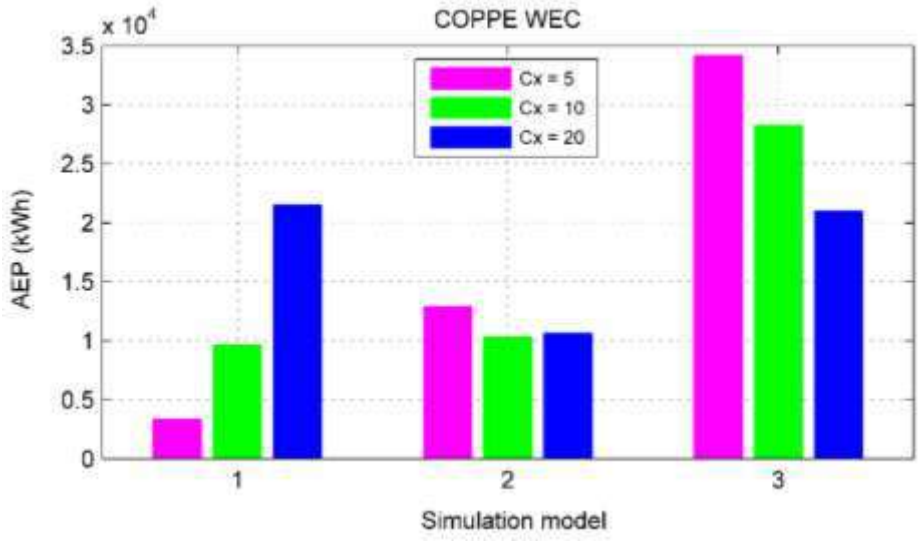

Figure 6-39 – The bar graph of the AEP values of the COPPE nearshore WEC applying the; 1) CCF, 2) CCDL and 3) ACCDL models. The simulations are performed for three speed multiplier coefficients of $C_x = 5, 10$ and 20.

The horizontal axis represents the simulated models of the COPPE nearshore WEC. The numbers 1, 2 and 3 correspond to the constrained control-free (CCF), constrained constant-delay latching (CCDL) and the adapted constrained constant-delay latching (ACCDL), respectively. The vertical axis shows the calculated AEP in kilowatt hour.

It can be observed that the ACCDL model (case 3) significantly improves the energy production of the device. However, this model does not have the same performance in the case of $C_x = 20$. As it is explained in the previous section, it is due to the high damping force of the PTO system that overdamps the buoy motion. The CCDL model increases the AEP for the PTO of $C_x = 5$ while does not enhance the WEC performance in other cases. This is more evident for the system of $C_x = 20$, where applying the CCDL control decreases the device AEP. It can be explained that the CCDL control increases the buoy velocity and displacement by providing an approximate optimum phase condition. This leads to an excessive amplification of the generator speed that increases the "No operational PTO" moments. Additionally, it can be seen that, in some cases the power generation is zero for the sea states that are in the range of the predominant waves of the local sea. For instance, the sea states ($T_p = 8\,s,\ H_s = 1.75\,m$) and ($T_p = 9\,s,\ H_s = 1.75\,m$) for the CCDL model of $C_x = 10$ and 20, or ($T_p = 8\,s, H_s = 2.25\,m$) and ($T_p = 9\,s, H_s = 2.25\,m$) for the ACCDL model of $C_x = 20$. To explain the reason, the power generation and the generator speed of the CCDL - $C_x = 10$ and ACCDL - $C_x = 20$ models are plotted in figure 6-40, for the irregular waves of ($T_p = 8\,s, H_s = 1.75\,m$) and ($T_p = 8\,s, H_s = 2.25\,m$) respectively.

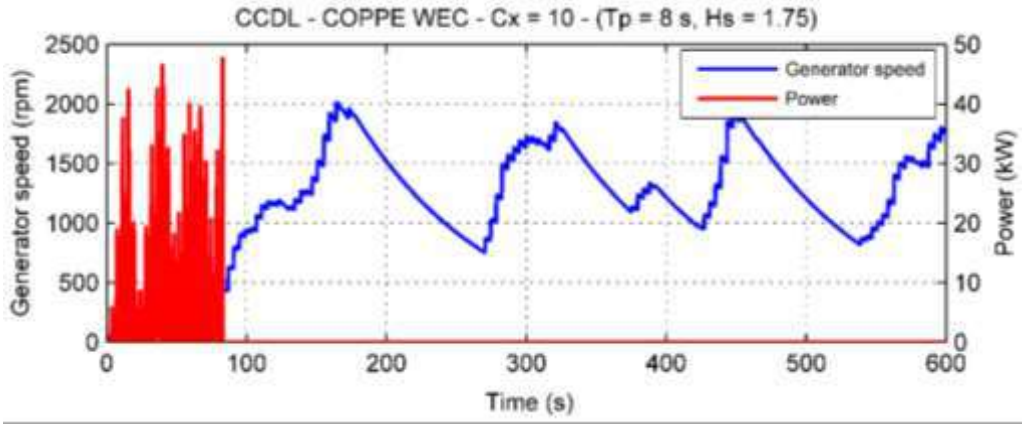

a)

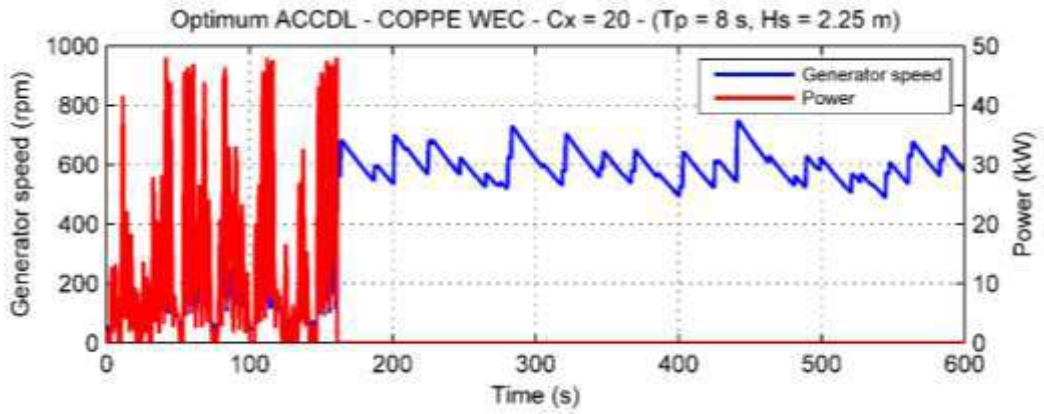

b)

Figure 6-40 – The instantaneous power generation and generator speed of the COPPE nearshore WEC for the CCDL - $C_x = 10$ and the optimum ACCDL - $C_x = 20$ ($GST = 50\ rpm$) models in an irregular wave of ($T_p = 8\ s, H_s = 1.75\ m$) and ($T_p = 8\ s, H_s = 2.25\ m$) respectively.

It can be seen that the PTO generates electrical power up to the moment that the generator speed exceeds the upper bound of the PTO operational range ($400\ rpm$). This condition occurs some time intervals earlier for the CCDL comparing to the ACCDL model. Because of the application of the threshold control in the ACCDL model, it takes more time to PTO reaches to its upper bound limit. Mathematically, in this situation, the power generation of such systems is equal to the summation of the instantaneous generated power divided by the simulation time. Calculating the power generation in this way gives a mean power of about 3.5 kW for each system. However, and if there is no control system to prevents the excessive increase of the generator speed the power production of the system is zero after some initial time intervals (here is about 100 seconds). It implies that, in practice, considering a real sea in which each sea state may last at least one or two hours, the power production of the WEC is zero. Because of this, in the annual energy production section, the mean power calculation of the devices are performed only for the simulation time greater than $200\ s$. It helps us to have more realistic results by taking into account the "fake" power generation values. It can be seen that the sea states with the "No operational PTO" condition are more in the case of CCDL comparing to ACCDL model. Figure 6-38 shows the annual energy calculation of the COPPE nearshore WEC buoy applying a pure damper as the PTO system. An efficiency coefficient of 0.8 is considered for power generation. An AEP value of about $141\ kWh$ is calculated that is very large comparing to the $39\ kWh$ for the ACCDL - $C_x = 5$ model. Moreover, in some cases the

COPPE WEC cannot reaches its rated power, which is calculated numerically using the mechanical power matrix and the capacity factor. These differences results from the restrictions imposed through the PTO device on the power generation.

6.6 Conclusion

This chapter addresses the performance of the COPPE nearshore WEC considering a sea site that is located 14 km far from the Rio de Janeiro coast. The system is a surface point absorber WEC type that consists of an oscillating buoy and a bottom-mounted support structure. The oscillating part is a semisubmersible conical cylinder allowed to move only in heave direction. The PTO device includes a combination of a gearbox (mechanical system) and a rotational generator (electrical system) located on the topside deck. The vertical motion of the buoy is transformed into a rotational motion of high angular velocity that drive the electrical generator. The velocity of the generator can be controlled by the speed multiplier coefficient, C_x. However, the PTO system is able to produce electrical power only in a specific range of generator speed (50 to 400 rpm). This range is called the "PTO operational range". A wave-to-wire model assuming the hydrodynamic linear theory is developed to analyze the COPPE WEC.

The power generation of the device in regular waves shows that increasing the C_x leads to a larger PTO damping. Because of this, a higher level of power is obtained for the buoy with largest C_x in the range of wave periods higher than 6 seconds. It is observed that applying a constant-delay latching (CDL) cannot fully satisfy the optimum phase condition, however, in this situation, applying the optimum speed multiplier coefficients may increase the power generation by providing the optimum amplitude condition. Nevertheless, it should be noted that the optimum term here refers to a variable value (amplitude, C_x etc.) that results in the maximum power production.

The irregular wave analysis show that, the constrained control-free (CCF) device of $C_x = 20$ has a better performance comparing to the others. It is because of the high PTO damping that provides the optimum amplitude condition (see chapter 5). The application of the CDL improves the power generation, however the excessively amplified speed of the generator is observed as a practical challenge. It is seen that as the wave period becomes larger the power production decreases. It occurs because the generator speed is out of the PTO operational range. Consequently, the PTO device loses a significant

portion of the absorbed energy performing in the "no operational PTO" condition during a large fraction of the simulation time. An adapted constraint constant-delay latching (ACCDL) is proposed, to eliminate or at least diminish the exaggerated amplification of the generator speed. To achieve this goal, a threshold generator speed in which the latching does not apply on the system should be determined for the PTO. It means that the latching mechanism keeps the buoy at its heave extremum only if the generator speed is less than the threshold value at that moment. As the result, for the rotations larger than the threshold, the velocity of the buoy is not amplified due to the no latching control situation and this prevents the excessive growth of the generator speed. A series of time domain simulation in irregular waves are performed to find the optimum threshold value in which the power production is maximum. The range of the predominant wave periods of the nearshore Rio de Janeiro is considered for the simulations. Additionally, the mean power of the device is calculated applying twenty series of wave random phase for each sea states. Considering a significant wave height of $H_s = 1.33$ meter and nine peak periods of $T_p = 5$ to 13 seconds, 7020 simulations, which takes about 60 minutes, are performed by the computer. The results show that, applying the ACCDL control strategy improves significantly the power generation of the COPPE WEC specifically in the range of the predominant sea waves. Moreover, it keeps the average generator speed in the PTO operational range that decreases the moments of "no operational PTO". It is observed that the mean power decreases by increasing the sea state peak period. The maximum latching force is calculated for each model and it is shown that applying the ACCDL control significantly decreases the latching force. This advantage may facilitate the implementation of the latching mechanism in a real sea. The annual energy production matrices of the COPPE WEC applying three models CCF, CCDL and ACCDL is calculated. Except the case of $C_x = 20$, the ACCDL model produces higher AEP comparing to the other two models. The same level of AEP are obtained for the CCF and ACCDL model of $C_x = 20$. It is because that the speed multiplier coefficient highly amplifies the PTO force, which overdamps the buoy displacements and leaves it less sensitive to the control system. Considering the electrical power matrices (EPM) of the ACCDL - $C_x = 5$ and 10, it can be seen that although a significant improvement is obtained, the maximum power generation occurs in a sea state close to the buoy natural period, which is out of the predominant range of the wave periods.

Chapter 7

7. Conclusions and future works

7.1 Conclusions

This thesis work can be divided into three parts. The first part (chapter four) includes the optimization of a control-free point absorber wave energy converter in frequency domain. In the second part (chapter five) a series of time domain simulations are performed to analyze the application of a constant-delay latching (CDL) control on a point absorber and its effect on the optimum dimensions of the system. The last part (chapter six) addresses the performance of the COPPE nearshore WEC considering the application of a CDL control. Additionally, an alternative CDL control adapted to the device PTO system is proposed in order to improve the power generation.

In chapter four, the objective is to present a methodology for the geometric optimization of WECs based on a series of frequency domain analyses and a statistical analysis method known as Design of Experiments (DOE). The optimization process is applied to the preliminary design of a one-body point absorber with an axisymmetric floating cylinder for the nearshore region of Rio de Janeiro. An ideal pure damper is considered as PTO and the energy absorption is calculated for different wave frequencies. The local sea characteristics has been described through a five-year wave hindcast (2006-2010) based on a third generation wind wave model WAVEWATCH III. The results indicated a predominant wave period range between 7 and 13 s with an energy period $T_e = 9.7$ s , as well as an average significant height of $H_s = 1.33$ m. At first, the lower and upper bounds of the geometrical parameters are determined (immature determination), and then after performing a set of frequency domain analyses and the design of experiments method, the WEC's geometrical parameters (diameter and draft) are determined to achieve a system that absorbs the maximum energy over a wide range of wave periods (mature determination). The results show that the tuning the WEC buoy to absorb the maximum power in the range of the predominant wave period of the local sea (7 to 13 seconds) leads to a prohibitively large dimensions. Additionally, even the largest buoy in the range of the upper and lower bound, which determines in the immature determination step, cannot provide a natural period close to the sea site predominant wave. Finally, it is inferred that an extremely large buoy is required to tune a control-free heaving point absorber to the local sea wave periods. As the result, it is observed as a primary challenge of designing a point absorber for the nearshore Rio de Janeiro.

Chapter five addresses the application of a constant-delay latching (CDL) control, presented by Sheng et al [77], on a point absorber WEC. The objective is to reduce the

buoy size while maintaining its performance in the range of the sea predominant wave periods. The latching control tunes the buoy natural period to the larger wave periods. Therefore, a buoy with a natural period below the sea wave range ($T_p = 5$ seconds which is the lower bound of the sea local wave period) should be selected. Using the results of the preliminary optimization (chapter 4), four buoys of different diameter and drafts, with the natural period of 5 seconds are selected to be analyzed. A wave-to-wire model is developed through a FORTRAN code to simulate the unconstrained buoys through the linear hydrodynamic theory. The term "unconstraint" means that there is no restriction on the buoy heave motion and it can freely oscillate in the vertical direction. An ideal (100% conversion efficiency) power take-off (PTO) system that works as a pure damper (stiffness is equal to zero) is considered for the energy conversion. The analyses are performed for twenty different wave random phases for each sea states and the average value of the mean power is considered as the mean power generated by the buoy. In the control-free case, the maximum mean power values in each sea state are slightly different for each buoy, while the corresponding optimum PTO damping values increase with sea state modal period. In contrast, for the buoys controlled by a CDL control, the optimum PTO damping values are independent of the wave period and approximately the same for all sea states. This value is equal to the hydrodynamic damping of the buoy at its natural frequency. The results show that, applying the CDL control, the larger buoys require larger optimum PTO damping. For instance, the optimum PTO damping value is about 2 and 156 $kN/(m/s)$ for the buoys, b1 (4, 5) and b4 (11.5, 3) respectively. It plays a significant role on the implementation of the PTO system in a real sea. It is observed that applying the CDL control significantly increases the power production. This power growth is very sensitive to the buoy dimension and is larger for the smaller buoys. However, part of this amplification may be due to the unrealistic buoy displacement which occurs at the resonance frequency of the smaller buoys. Calculation of the capture width of the buoys in the irregular waves show that the largest buoy can absorb more energy, nevertheless, it is seen that using a large size buoy brings some practical challenges besides the economic issues. Additionally, it is observed that the smaller buoys produce smoother power output representing a less expressive ratio of the instantaneous power to the mean power. The power-to-volume ratio, which affects the estimation of the WEC cost, are calculated for each buoy to evaluate their performance. This ratio, in contrast to the capture width, shows the power generation of the buoy relative to its

volume rather than the available energy at sea. It is observed that this ratio decreases with the increase of the buoy size. In other words, the smallest buoy produces more energy in one cubic meter of its volume comparing to the larger ones.

Thus, it can be inferred that although the smallest buoy generates the lower power comparing to the others, has the best performance in terms of power-to-volume ratio and smooth power production. Additionally, a small buoy requires a lower PTO damping level to maximize the mean power which facilitates its practical implementation. The AEP of the buoys are calculated applying two latching strategies. In the first method, the latching duration is tuned to each sea states. The other method proposes that the buoy is tuned only to one sea state corresponding to the peak period of the wave spectrum of the local sea. The results show that applying the first latching strategy results in an increase of about 50% in AEP and rated power values.

As a case study, chapter six is dedicated to the performance analysis of the wave energy converter proposed by the COPPE/ Federal University of Rio de Janeiro. It is the second generation of the Brazilian WEC that is going to be installed near to the Rio de Janeiro coastline and in this thesis, it is called "COPPE WEC". The system is a surface point absorber WEC type that consists of an oscillating buoy and a bottom-mounted support structure. The oscillating part is a semisubmerged conical cylinder allowed to move only in heave direction. The PTO device includes a combination of a gearbox (mechanical system) and a rotational generator (electrical system) located on the topside deck. The vertical motion of the buoy is transformed into a rotational motion of high angular velocity that drive the electrical generator. The velocity of the generator can be controlled by the speed multiplier coefficient, C_x. However, the PTO system is able to produce electrical power only in a specific range of generator speed (50 to 400 rpm). This range is called the "PTO operational range". The wave-to-wire model developed in chapter five is adapted to simulate the COPPE WEC performance. The regular wave analyses show that the larger value of C_x impose higher PTO forces on the WEC buoy. Therefore, a better power production is obtained by the system with the largest C_x in the range of predominant wave periods. It is observed that although the application of the CDL control does not fully satisfy the optimum phase condition, power generation improvement can be obtained by applying an optimum value of the speed multiplier coefficient. The results show that applying a CDL control results in an excessive amplification of the generator speed leading to the "no operational PTO" condition in which the power generation is

zero. This results a decline in mean power level for the sea states with a peak period larger than 6 seconds, specifically for the systems of $C_x = 5$ and 10. It implies that the PTO device loses a significant portion of the absorbed energy performing in the "no operational PTO" condition during a large fraction of the simulation time. An adapted constraint constant-delay latching (ACCDL) is proposed, to eliminate or at least diminish the exaggerated amplification of the generator speed. To achieve this goal, a threshold generator speed in which the latching does not apply on the system should be determined for the PTO. It means that the latching mechanism keeps the buoy at its heave extremum only if the generator speed is less than the threshold value at that moment. As the result, for the rotations larger than the threshold, the velocity of the buoy is not amplified due to the no latching control situation and this prevents the excessive growth of the generator speed. The results of the COPPE WEC simulation in irregular waves show that, applying the ACCDL control strategy improves significantly the power generation of the COPPE WEC specifically in the range of the predominant sea waves. Moreover, it keeps the average generator speed in the PTO operational range that decreases the moments of "no operational PTO". The maximum latching force is calculated for each model and it is shown that applying the ACCDL control significantly decreases the latching force. This advantage may facilitate the implementation of the latching mechanism in a real sea. The AEP analysis of the COPPE WEC shows that applying the ACCDL control strategy can significantly improve the device performance. However, it is seen that applying a high value of the speed multiplier coefficient, C_x leaves the WEC less sensitive to the control system. It should be noted that although a significant improvement is obtained, the maximum power generation occurs in a sea state close to the buoy natural period, which is out of the predominant range of the wave periods.

7.2 Future works

To enhance the results of this thesis, there are some ideas that can be pursued is future studies.

I. Application of the constant-delay latching control considering the effect of viscosity and the constrained motion through the end-stop control.

In this thesis, the simulations are based on the linear hydrodynamic neglecting the effect of viscosity. Considering the viscous forces can result in more realistic buoy responses

specifically for the buoy with small diameters and large draft. It is because that in such buoys the hydrodynamic damping at the resonance frequency is too low leading to high amplitudes of heave motion. In this situation, considering the viscous force may results in a diminution in the buoy heave motion. Additionally, applying the latching control amplified the buoy displacement in heave direction. This may leads to excessively amplified heave amplitudes that are not feasible in a real system due to the practical limits of the device. Therefore, an end-stop control should be added to the wave-to-wire model to control the maximum heave amplitude of the buoy. Then, the WEC performance can be addressed considering the couple effect of the latching and end-stop control strategies.

II. Experimental tests to verify the wave-to-wire model results

A series of experimental tests can be adapted to verify the numerical results. For the case study model, the coupled WEC-PTO system should be modeled in laboratory to observe its performance. Moreover, the proposed ACCDL control strategy can be verified through the experimental tests in irregular waves.

III. Control of the electrical generator to improve the power production of the COPPE WEC

In this thesis, the objective of the control strategies (CCDL and ACCDL) that applied on the COPPE WEC is to improve the delivered energy to the PTO system. This mechanical power is received by the mechanical part of the PTO and transmitted to the electrical generator to produce electrical power. Since the force magnitude varies in time, the electrical generator characteristics should be tuned to improve its power generation.

References

[1] Edenhofer O, Pichs Madruga R, Sokona Y et al. Renewable Energy Sources and Climate Change Mitigation (Special Report of the Intergovernmental Panel on Climate Change). vol. 6. 2012. doi:10.5860/CHOICE.49-6309.

[2] Mørk G, Barstow S, Kabuth A, Pontes MT. Assessing the global wave energy potential. ASME 2010 29th Int Conf Ocean Offshore Arct Eng 2010:447–54.

[3] Mertz B, Davidson O, Bosch P, Dave R, Meyer L. Mitigation of climate change: Contribution of working group III to the fourth assessment report of the Intergovernmental Panel on Climate Change. 2007.

[4] Estefen SF, Garcia Rosa PB, Beserra ER, Costa PR, Pinheiro M, Lourenco MI, et al. Wave energy hyperbaric converter: Small scale models, prototype and control strategies. Proc. ASME 2012 31 st Int. Conf. Ocean. Offshore Arct. Eng. Julay 1-6, 2012, Rio Janeiro, Brazil, 2012.

[5] Falcão AF de O. Wave energy utilization: A review of the technologies. Renew Sustain Energy Rev 2010;14:899–918. doi:10.1016/j.rser.2009.11.003.

[6] Journée JMJ, Massie W. W. Offshore hydromechanics 2001:570. doi:10.1016/S0013-4686(01)00879-9.

[7] Chakrabarti S. Hydrodynamics of offshore structures. Springer; 1987.

[8] Krewitt W, Nienhaus K, Kleßmann C, Capone C, Stricker E, Graus W, et al. Role and potential of renewable energy and energy efficiency for global energy supply. vol. 2009,18. 2009.

[9] United Nations Development Programme. World Energy Assessment. Energy and the challenge of Sustainability. 2000.

[10] Sims REH, Schock RN, Torres-Martínez J, Adegbululgbe A, Fenhann J, Konstantinaviciute I, et al. Energy Supply. Clim Chang 2007 Mitigation Contrib Work Gr III to Fourth Assess Rep Intergov Panel Clim Chang 2007:72.

[11] Charlier RH, Justus JR. Ocean Energies. Environmental, Economic and

Technological Aspects of Alternative. 1th Eidtio. n.d.

[12] Nihous GC. Apreliminary assessment of ocean thermal energy conversion resources. J Energy Resour Technol 2007;127:328. doi:10.1115/1.1949624.

[13] Skråmestø ØS, Skilhagen SE, Nielsen WK. Power Production based on Osmotic Pressure . Proc. 16th waterpower, Spokane, WA, USA: 2009.

[14] Barber N., Ursell F. the generation and propagation of ocean waves and swell. Philos Trans R Soc London 1948;240.

[15] Lighthill J. Waves in Fluids. 2nd ed. cambridge university press; 1978.

[16] Pelc R, Fujita RM. Renewable energy from the ocean. Mar Policy 2002;26:471–9. doi:10.1016/S0308-597X(02)00045-3.

[17] OES. An International Vision for Ocean Energy 2011.

[18] Khan J, Moshref A, Bhuyan G. A Generic Outline for Dynamic Modeling of Ocean Wave and Tidal Current Energy Conversion Systems. Power Energy Soc. Gen. Meet. 2009, IEEE; 2009. doi:10.1109/PES.2009.5275177.

[19] Falcão A. Modelling and control of oscillating-body wave energy converters with hydraulic power take-off and gas accumulator. Ocean Eng 2007;34:2021–32. doi:10.1016/j.oceaneng.2007.02.006.

[20] Garcia-Rosa PB, Cunha JPVS, Lizarralde F, Estefen SF, Machado IR, Watanabe EH. Wave-to-Wire Model and Energy Storage Analysis of an Ocean Wave Energy Hyperbaric Converter. IEEE J Ocean Eng 2013;39:386–97. doi:10.1109/JOE.2013.2260916.

[21] Kempener R, Neumann F. Wave energy, IRENA ocean energy technology brief 4. Int Renew Energy Agency 2014.

[22] James V. Marine renewable energy: A global review of the extent of marine renewable energy developments, the developing technologies and possible conservation implications for cetaceans. whale and dolphin conservation, WDC; 2013.

[23] US DOE. Energy Efficiency and Renewable Energy Marine and Hydrokinetic Database. Energy Efficiency and Renewable Energy, US Department of Energy. Washington DC, USA; 2010.

[24] Drew B, Plummer A., Sahinkaya MN. A review of wave energy converter technology. J Power Energy 2009;223:887–902. doi:10.1243/09576509JPE782.

[25] Falcão AF de O. The shoreline OWC wave power plant at the Azores. 4th Eur. Wave Energy Conf. Aalborg, Denmark, 2000, p. 42–7.

[26] Augustine, C.; Bain, R.; Chapman, J.; Denholm, P.; Drury, E.; Hall, D.G.; Lantz, E.; Margolis, R.; Thresher, R.; Sandor, D.; Bishop, N.A.; Brown, S.R.; Cada, G.F.; Felker, F.; Fernandez, S.J.; Goodrich, A.C.; Hagerman, G.; Heath, G.; O'Neil, S.; Paquette, K. Renewable electricity futures study; Vol2: Renewable electricity generation and storage technologies. NREL/TP-6A20-52409-2. Golden; CO: National Renewable Energy Laboratory; 2012.

[27] Falnes J, Lillebekken PM. Budal's latching-controlled-buoy type wave-power plant. Proc. Fifth Eur. Wave Energy Conf., 2003, p. 233–44.

[28] ITTC. Specialist Committee on Hydrodynamic Testing of Marine Renewable Energy Devices. Proc 27th Int Towing Tank Conf 2017;I:680–725.

[29] Mofor L, Goldsmith J, Jones F. Ocean Energy:Techmology Readiness, Patents, Deployment Status and Outlook. Int Renew Energy Agency IRENA 2014:76. doi:10.1007/978-3-540-77932-2.

[30] Pérez C, Iglesias G. Integration of Wave Energy Converters and Offshore Windmills. 4th Int Conf Ocean Energy 2012:1–6.

[31] Waters R, Stålberg M, Danielsson O, Svensson O, Gustafsson S, Strömstedt E, et al. Experimental results from sea trials of an offshore wave energy system. Appl Phys Lett 2007;90. doi:10.1063/1.2432168.

[32] Hotta H, Washio Y, Yokozawa H, Miyazaki T. R&D on wave power device "Mighty Whale." Renew Energy 1996;9:1223–6. doi:10.1016/0960-1481(96)88497-7.

[33] Lavelle J, Kofoed JP. Power Production Analysis of the OE Buoy WEC for the

CORES Project. CORES EU Proj DCE Tech Rep No 119 2011.

[34] Dti. Near Shore Floating Oscillating Wave Column: Prototype Development and Evaluation. Urn 05/581 2004.

[35] Healt T, Whittaker TJ., Boake C. The design, construction and operation of the LIMPET wave energy converter (Islay, Scotland). 4th Eur. Wave Energy Conf. Aalborg, Denmark, 2000, p. 49–55.

[36] JRC European Commision. 2011 Technology Map of the European Strategic Energy Technology Plan (SET-Plan): Technology Description. 2011. doi:10.2790/37519.

[37] Whittaker T, Collier D, Folley M, Osterried M, Henry A. The development of Oyster - A shallow water surging wave energy converter . 7th Eur Wave Tidal Energy Conf 2007.

[38] Estefen S, Costa PR, Ricarte E, Pinheiro M. Wave energy hyperbaric device for electricity production. Proc. 26th Int. Conf. Offshore Mech. Arct. Eng. , June 10-15 , 2007, San Diego, California, USA, n.d.

[39] Fernandez H, Iglesias G, Carballo R, Castro A, Sánchez M, Taveira-Pinto F. Optimization of the Wavecat Wave Energy Converter. Coast Eng 2012 2012;1:1–8.

[40] Falnes J, Budal K. Wave - power conversion by point absorbers. Nor Marit Res 1978;6:1–11.

[41] Evans D V. A theory for wave-power absorption by two independently oscillating bodies. J Fluid Mech 1979;90:337. doi:10.1017/S0022112079002251.

[42] Newman JN. The interaction of stationary vessels with regular waves. Proc. 11th Symp. Nav. Hydrodyn. London, 1976, p. 491–501.

[43] Mei CC. Power extraction for water waves. J Sh Res 1976;21:248–53.

[44] Salter SH. Wave Power. Nature 1974;249:720–4.

[45] Budal K, Falnes J. A resonant point absorber of ocean-wave power. Nature

1975;256:478–9. doi:(With corrigendum in Vol.257, p.626).

[46] Falnes J. A review of wave-energy extraction. Mar Struct 2007;20:185–201. doi:10.1016/j.marstruc.2007.09.001.

[47] Salter S. Power conversion systems for ducks. Proc. Int. Conf. Futur. Energy Concepts, London, Inst. Electr. Eng., London: 1979, p. 100–8.

[48] Budal K, Falnes J. Optimum operation of wave power converter. 1976.

[49] Budal K, Falnes J. A system for conversion of sea wave energy, 1978. doi:United States Patent US4203294 (year of patent 1975).

[50] Nebel P. Maximizing the Efficiency of Wave-Energy Plant Using Complex-Conjugate Control. Proc Inst Mech Eng Part I J Syst Control Eng 1992;206:225–36. doi:10.1243/PIME_PROC_1992_206_338_02.

[51] Perdigão JNM, Sarmento AJN. A phase control strategy for OWC devices in irregular seas. Int. Work. Water Waves Float. Bodies, 1989, p. 205–9.

[52] Beirão P. Modelling and control of a wave energy converter: Archimedes wave Swing, Phd thesis. Mechanical engineering department, Universidade Técnica de Lisboa, Instituto Superior Técnico, 2007.

[53] Gieske P. Model Predictive Control of a Wave Energy Converter: Archimedes Wave Swing, Master thesis. Faculty of Electrical enginerrring, Mathematics and Computer Science, EPP department, TUDelft, 2007.

[54] Budal K, Falnes J. Apparatus for utilising or absorbing wave energy. British patent 1587344 1981.

[55] Budal K, Falnes J. Interacting point absorbers with controlled motion. Power from Sea Wave, Academic Press, London; 1980, p. 381–99.

[56] Hals J, Falnes J, Moan T. A Comparison of Selected Strategies for Adaptive Control of Wave Energy Converters. J Offshore Mech Arct Eng 2011;133:31101. doi:10.1115/1.4002735.

[57] Hoskin R, Nichols N. Optimal strategies for phase control of wave energy

devices, In: McCormick, M. E. and Kim, Y. C. (eds) Utilization of ocean waves-wave to energy conversion, ASCE:American Society of Civil Engineering, New York, ISBN:978-0-87262-624-9; 1987, p. 184–99.

[58] Guenther DA, Jones D, Brown DG. An investigative study of a wave-energy device. Energy 1979;4:299–306. doi:10.1016/0360-5442(79)90129-4.

[59] French M. A Generalized View of Resonant Energy Transfer. J Mech Eng Sci 1979;21:299–300.

[60] Budal K, Falnes J, Iversen L., Lillebekken PM, Oltedal G, Hals T, et al. The Norwagian wave power buoy project.pdf. Second Int. Symp. wave energy Util. trondheim, 22-24 June 1982, 1982.

[61] Greenhow MJL, Rosen JH, Reed M. Control strategies for the Clam Wave Energy Device. Appl Ocean Res 1984;6:197–206. doi:10.1016/0141-1187(84)90058-0.

[62] Greenhow M, White SP. Optimal heave motion of some axisymmetric wave energy devices in sinusoidal waves. Appl Ocean Res 1997;19:141–59. doi:10.1016/S0141-1187(97)00020-5.

[63] Eidsmoen H. Simulation of a tight-moored amplitude-limited heaving-buoy wave-energy converter with Phase Control, PhD thesis, Division of Physics, Norwegian University of science and technology, N-7034 Torendheim, Norway, http://folk.ntnu.no/falnes/web_arkiv/InstFysikk/simconve.pdf; 1996.

[64] Eidsmoen H. Simulation of a slack-moored heaving-buoy wave-energy converter, Division of Physics, Norwegian University of science and technology, N-7034 Torendheim, Norway, https://brage.bibsys.no/xmlui/bitstream/handle/11250/246703/550031_FULLTEXT01.pdf?sequence=1; 1996.

[65] Korde U a. Latching control of deep water wave energy devices using an active reference. Ocean Eng 2002;29:1343–55. doi:10.1016/S0029-8018(01)00093-2.

[66] Hals J, Bjarte-Larsson T, Falnes J. Optimum reactive control and control by latching of a wave-absorbing semi-submerged heaving sphere. Proc. OMAE2002,

21st Int. Conf. Offshore Mech. Artic Eng., 2002.

[67] Bjarte-Larsson T, Lillbekken per M, Hals J, Falnes J. Model experiment on an OWC-type wave-energy converter with hydraulic power take-off. Proc. OMAE´02 21st Int. Conf. offshore Mech. Arct. Eng., 2002.

[68] Lillebekken PM, Aakenes UR, Falnes J. The conWEC wave energy device. Third Eur. Wave Energy Conf. Inc. waves tidal Mar. Curr. Proc. an Int. Conf. held Patras, Greece, Patras, 30 Sept. - 2 Oct. 1998, 1998, p. 146–52. doi:(edited and published by Dr.Ing.Wilhelm Dursthoff, University of Hannover, Germany, 2000).

[69] Bjarte-Larsson T, Falnes J. Laboratory experiment on heaving body with hydraulic power take-off and latching control. Ocean Eng 2006;33:847–77. doi:10.1016/j.oceaneng.2005.07.007.

[70] Babarit a., Duclos G, Clément AH. Comparison of latching control strategies for a heaving wave energy device in random sea. Appl Ocean Res 2004;26:227–38. doi:10.1016/j.apor.2005.05.003.

[71] Falcão A. Phase control through load control of oscillating-body wave energy converters with hydraulic PTO system. Ocean Eng 2008;35:358–66. doi:10.1016/j.oceaneng.2007.10.005.

[72] Lopes MFP, Hals J, Gomes RPF, Moan T, Gato LMC, Falcão a. FDO. Experimental and numerical investigation of non-predictive phase-control strategies for a point-absorbing wave energy converter. Ocean Eng 2009;36:386–402. doi:10.1016/j.oceaneng.2009.01.015.

[73] Babarit A, Guglielmi M, Clément AH. Declutching control of a wave energy converter. Ocean Eng 2009;36:1015–24. doi:10.1016/j.oceaneng.2009.05.006.

[74] Babarit a., Clément a. H. Optimal latching control of a wave energy device in regular and irregular waves. Appl Ocean Res 2006;28:77–91. doi:10.1016/j.apor.2006.05.002.

[75] Clement a. H, Babarit a. Discrete control of resonant wave energy devices. Philos Trans R Soc A Math Phys Eng Sci 2012;370:288–314.

doi:10.1098/rsta.2011.0132.

[76] Babarit A, Mouslim H, Guglielmi M, Clement AH. Simulation of the SEAREV wave energy converter with a by-pass control of its hydraulic power-take-off. Proc. World Renew. Energy Congr. Glas. UK, Elsevier; 2008, p. 1004–9.

[77] Sheng W, Alcorn R, Lewis A. On improving wave energy conversion, part I: Optimal and control technologies. Renew Energy 2015;75:922–34. doi:10.1016/j.renene.2014.09.048.

[78] Sheng W, Alcorn R, Lewis A. On improving wave energy conversion, part II: Optimal and control technologies. Renew Energy 2015;75:935–44. doi:10.1016/j.renene.2014.09.049.

[79] Clauss GF, Birk L. Hydrodynamic shape optimization of large offshore structures. Appl Ocean Res 1996;18:157–71. doi:10.1016/S0141-1187(96)00028-4.

[80] Brik L, Clauss G. Automated Hull optimisation of offshore structures based on rational sea keeping criteria. Elev. Int. offshore polar Eng. Conf. Stavanger, Norw., 2001.

[81] Brik L, Clauss G. Parametric hull design and automated optimization of offshore structures. Tenth Congr. Int. Marit. Assoc. Mediterr. (IMAM 2002), n.d.

[82] Brik L. Application of constrained multi-objective optimization to the design of offshore structure hulls. J Offshore Mech Arct Eng 2009;131:11301. doi:10.1115/1.2957919.

[83] Elchahal G, Lafon P, Younes R. Modelling and optimizing floating breakwaters using density distribution. Seventeenth Int Offshore Polar Eng Conf Lisbon , Port 2007.

[84] Vantorre M, Banasiak R, Verhoeven R. Modelling of hydraulic performance and wave energy extraction by a point absorber in heave. Appl Ocean Res 2004;26:61–72. doi:10.1016/j.apor.2004.08.002.

[85] Sjökvist L, Krishna R, Rahm M, Castellucci V, Hagnestål A, Leijon M. On the Optimization of Point Absorber Buoys. J Mar Sci Eng 2014;2:477–92.

doi:10.3390/jmse2020477.

[86] Goggins J, Finnegan W. Shape optimisation of floating wave energy converters for a specified wave energy spectrum. Renew Energy 2014;71:208–20. doi:10.1016/j.renene.2014.05.022.

[87] Kramer MM, Frigaard PB. Efficient wave energy amplification with wave reflectors. Proc. Twelfth Int. Offshore Polar Eng. Conf. Kitakyushu, Japan, 2002.

[88] Babarit A, Clément AH. Shape optimisation of the SEAREV wave energy converter. 9th World Renew Energy Congr 2006.

[89] McCabe AP. Constrained optimization of the shape of a wave energy collector by genetic algorithm. Renew Energy 2013;51:274–84. doi:10.1016/j.renene.2012.09.054.

[90] Ruellan M, Ben Ahmed H, Multon B, Josset C, Babarit A, Clément AH. Design Methodology for a SEAREV Wave Energy Converter. IEEE Trans Energy Convers 2010;25:760–7. doi:10.1109/TEC.2010.2046808.

[91] Kurniawan A, Moan T. Optimal geometries for wave absorbers oscillating about a fixed axis. IEEE J Ocean Eng 2013;38:117–30. doi:10.1109/JOE.2012.2208666.

[92] Garcia-rosa PB, Lizarralde F, Estefen SF. Optimization of the Wave Energy Absorption in Oscillating-Body Systems using Extremum Seeking Approach 2012:1011–6.

[93] Garcia-Rosa PB, Ringwood J V. On the sensitivity of optimal wave energy device geometry to the energy maximizing control system. IEEE Trans Sustain Energy 2016;7:419–26. doi:10.1109/TSTE.2015.2423551.

[94] Hasselmann K, Barnett TP, Bouws E, Carlson H, Cartwright DE, Enke K, et al. Measurements of Wind-Wave Growth and Swell Decay during the Joint North Sea Wave Project (JONSWAP). Ergnzungsh Zur Dtsch Hydrogr Zeitschrift R 1973;A(8):p.95. doi:citeulike-article-id:2710264.

[95] Chakrabarti SK. Handbook of Offshore Engineering (2-volume set). Elsevier Ltd; 2005. doi:10.1016/B978-008044381-2.50007-2.

[96] Cummins W.E. The impulse response function and ship motions. Int. Symp. Sh. Theory, Hamburg, Ger., 1962.

[97] Ogilvie T. Recent Progress Towards the Understanding and Prediction of Ship motions. Proc. 5th Symp. Nav. Hydrodyn., 1964.

[98] http://support.minitab.com/en-us/minitab/17/(last access on 09/02/2017) n.d.

[99] http://148.204.81.206/Ansys/150/Aqwa%20Users%20Manual.pdf (last access on 09/02/2017) n.d.

[100] Falnes J. Ocean Waves and Oscillating Systems: Linear interactions including wave-energy extraction. Appl Mech Rev 2003;56:B3. doi:10.1115/1.1523355.

[101] Chawla A, Spindler DM, Tolman HL. Validation of a thirty year wave hindcast using the Climate Forecast System Reanalysis winds. Ocean Model 2013;70:189–206. doi:10.1016/j.ocemod.2012.07.005.

[102] Waters R, Engström J, Isberg J, Leijon M. Wave climate off the Swedish west coast. Renew Energy 2009;34:1600–6. doi:10.1016/j.renene.2008.11.016.

[103] Ching-Piao T, Ching-Her H, Chien H, Hao-Yuan C. Study on the wave climate variation to the renewable wave energy assessment. Renew Energy 2012;38:50–61. doi:10.1016/j.renene.2011.06.041.

[104] Hiles CE. On the use of computational models for wave climate assessment in support of the wave energy industry (Master thesis). Department of Mechanical Engineering, University of Victoria, 2010.

[105] Beserra ER, Mendes ALT, Estefen SF, Parente CE. Wave climate analysis for a wave energy conversion application in Brazil. ASME 2007 26th Int. Conf. Offshore Mech. Arct. Eng., 2007, p. 897–902. doi:10.1115/OMAE2007-29597.

[106] Contestabile P, Ferrante V, Vicinanza D. Wave energy resource along the coast of Santa Catarina (Brazil). Energies 2015;8:14219–43. doi:10.3390/en81212423.

[107] Estefen SF, Costa PR, Ferreira R, Lourenco MI, Martins M, Castello X, et al. Relatório -7 do projeto de implantação de conversor nearshore para geração de eletricidade pelas ondas do mar - PENO-12754 2014.

[108] Tolman HL. User manual and system documentation of WAVEWATCH-IIITM version 3.14. Tech Note 2009. doi:10.3390/ijerph2006030011.

[109] Saha S, Moorthi S, Pan HL, Wu X, Wang J, Nadiga S, et al. The NCEP climate forecast system reanalysis. Bull Am Meteorol Soc 2010;91:1015–57. doi:10.1175/2010BAMS3001.1.

[110] Hagerman G. Southern England wave energy resource potential. Proc. Build. Energy 2001 ,Boston, Massachusetts, New Engl. Sustain. Energy Assoc., 2001.

[111] Thomas GP. The Theory Behind the Conversion of Ocean Wave Energy: a Review. Ocean Wave Energy Curr Status Futur Prepectives 2008:41–91.

[112] Twidell J, Weir T. Renewable energy resources. Third edit. 2015.

[113] Hooft JP. Oscillatory wave forces on small bodies. Int. Shipbuild. Prog., IOS Press; 1970, p. 127–35.

[114] Paul G. Mathews. Design of Experiments with MINITAB. Am. Stat., vol. 60, 2006, p. 205–205. doi:10.1198/tas.2006.s46.

[115] Falnes J. Principles for Capture of Energy From Ocean Waves. Phase Control and Optimum Oscillation. 1997:1–8.

[116] Alves M, Traylor H, Sarmento A. Hydrodynamic Optimization of a Wave Energy Converter Using a Heave Motion Buoy. EWTEC, Porto, Port 11-13 Sptember 2007:1–8.

[117] McCabe AP, Aggidis GA, Widden MB. Optimizing the shape of a surge-and-pitch wave energy collector using a genetic algorithm. Renew Energy 2010;35:2767–75. doi:10.1016/j.renene.2010.04.029.

[118] Shadman M, Estefen SF, Rodriguez CA, Lourenco MI. Preliminary Design of Floating Point Absorber Offshore Rio de Janeiro. 34th Int. Conf. Ocean. Offshore Arct. Eng. OMAE2015, May 31-June 5, St.John's, Newfoundland, Canada, 2015.

[119] Iversen LC. Numerical method for computing the power absorbed by a phase-controlled point absorber. Appl Ocean Res 1982;4:173–80. doi:10.1016/S0141-1187(82)80054-0.

[120] Falnes J. Small is beatuful: How to make wave energy economic. Eur. Wave Energy Symp. 21-24 July, Edinburgh, Scotl., NEL; 1993.

[121] Celis MA. Análise da Influência da Memória Fluida em Balanço Paramétrica. MSc Diss COPPE/UFRJ, Rio Janeiro, Brazil 2008.

[122] Kurniawan A, Hals J, Moan T. Assessment of Time-Domain Models of Wave Energy Conversion Systems. Proc 9th Eur Wave Tidal Energy Conf 2011:12.

[123] Neary VS, Previsic M, Jepsen RA, Lawson MJ, Yu Y, Copping AE, et al. Methodology for Design and Economic Analysis of Marine Energy Conversion (MEC) Technologies 2014.

[124] IEEE Standard Definitions for Use in Reporting Electric Generating Unit Reliability , Availability , and Productivity. vol. 2006. 2007.